ERDC/CHL TR-22-23

Coastal and Hydraulics Laboratory

US Army Corps
of Engineers®
Engineer Research and
Development Center

ERDC
ENGINEER RESEARCH & DEVELOPMENT CENTER

South Atlantic Coastal Study (SACS)

Coastal Hazards System–Puerto Rico and US Virgin Islands (CHS-PR)

Norberto C. Nadal-Caraballo, Madison C. Yawn, Luke A. Aucoin, Meredith L. Carr, Jeffrey A. Melby, Efrain Ramos-Santiago, Fabian A. Garcia-Moreno, Victor M. Gonzalez, Thomas C. Massey, Margaret B. Owensby, Alexandros A. Taflanidis, Aikaterini P. Kyprioti, Andrew T. Cox, and Juan Gonzalez-Lopez

December 2022

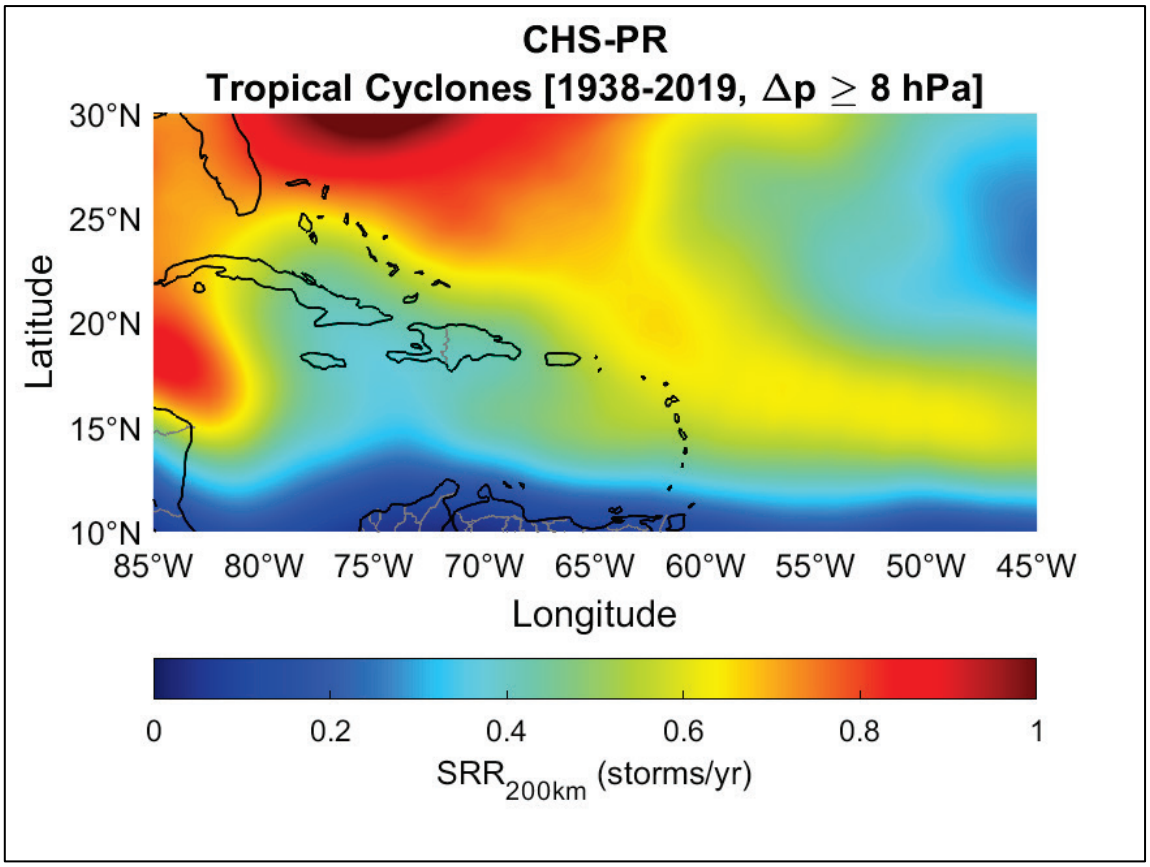

The US Army Engineer Research and Development Center (ERDC) solves the nation's toughest engineering and environmental challenges. ERDC develops innovative solutions in civil and military engineering, geospatial sciences, water resources, and environmental sciences for the Army, the Department of Defense, civilian agencies, and our nation's public good. Find out more at www.erdc.usace.army.mil.

To search for other technical reports published by ERDC, visit the ERDC online library at https://erdclibrary.on.worldcat.org/discovery.

ERDC/CHL TR-22-23
December 2022

Coastal Hazards System–Puerto Rico and US Virgin Islands (CHS-PR)

Norberto C. Nadal-Caraballo, Madison C. Yawn, Luke A. Aucoin, Meredith L. Carr, Jeffrey A. Melby, Efrain Ramos-Santiago, Fabian A. Garcia-Moreno, Victor M. Gonzalez, Thomas C. Massey, and Margaret B. Owensby

Coastal and Hydraulics Laboratory
US Army Engineer Research and Development Center
3909 Halls Ferry Road
Vicksburg, MS 39180-6199

Alexandros A. Taflanidis and Aikaterini P. Kyprioti

University of Notre Dame
Fitzpatrick Hall
Notre Dame, IN 46556

Andrew T. Cox

Oceanweather, Inc.
5 River Road, Suite 1
Cos Cob, CT 06807

Juan Lopez-Gonzalez

Wood Environment & Infrastructure Solutions, Inc.
50 Troop Ave #300
Dartmouth, NS B3B 1Z1, Canada

Final report

Prepared for US Army Corps of Engineers, South Atlantic Division (SAD)
60 Forsyth St. SW
Atlanta GA, 30303-8001

Under US Army Corps of Engineers, Labor Charge Code

Abstract

The South Atlantic Coastal Study (SACS) was completed by the US Army Corps of Engineers to quantify storm surge and wave hazards allowing for the expansion of the Coastal Hazards System (CHS) to the South Atlantic Division (SAD) domain. The goal of the CHS-SACS was to quantify coastal storm hazards for present conditions and future sea level rise (SLR) scenarios to aid in reducing flooding risk and increasing resiliency in coastal environments. CHS-SACS was completed for three regions within the SAD domain, and this report focuses on the Coastal Hazards System–Puerto Rico and US Virgin Islands (CHS-PR). This study applied the CHS Probabilistic Coastal Hazard Analysis (PCHA) framework for quantifying tropical cyclone (TC) responses, leveraging new atmospheric and hydrodynamic numerical model simulations of synthetic TCs developed explicitly for the CHS-PR region. This report focuses on documenting the PCHA conducted for CHS-PR, including the characterization of storm climate, storm sampling, storm recurrence rate estimation, marginal distributions, correlation and dependence structure of TC atmospheric-forcing parameters, development of augmented storm suites, and assignment of discrete storm weights to the synthetic TCs. As part of CHS-PR, coastal hazards were estimated for annual exceedance frequencies over the range of 10 yr^{-1} to 10^{-4} yr^{-1}.

Contents

Figures and Tables

Figures

Tables

Preface

The study summarized in this report was performed for the US Army Corps of Engineers (USACE), South Atlantic Division (SAD). The study was funded by Headquarters, USACE, through the USACE SAD (under a labor charge code) and conducted at the US Army Engineer Research and Development Center (ERDC), Coastal and Hydraulics Laboratory (CHL), Vicksburg, MS, during the period of October 2019–September 2021. Ms. Kelly R. Legault and Mr. Andrew J. Condon, Jacksonville District (SAJ), were the primary engineering points of contact. Ms. Elizabeth S. Godsey, Mobile District, and Mr. Gabriel Todaro, SAJ, were the primary engineering regional points of contact.

This work was performed by the Harbors, Entrances, and Structures Branch of the Navigation Division at CHL; the Coastal Processes Branch of the Flood and Storm Protection Division at CHL; the University of Notre Dame; Oceanweather, Inc.; and Wood Environment & Infrastructure Solutions, Inc.

At the time of publication of this report, Mr. Chad R. Bounds was chief, Harbors, Entrances, and Structures Branch; Ms. Ashley E. Frey, chief, Navigation Division; Mr. Victor M. Gonzalez, chief, Coastal Processes Branch; and Dr. Cary A. Talbot, chief, Flood and Coastal Division. Dr. Ty V. Wamsley was director, CHL, and Mr. Keith W. Flowers was deputy director, CHL.

The commander of ERDC was COL Christian Patterson, and the director was Dr. David W. Pittman.

1 Introduction

1.1 Background

Coastal communities within the US Army Corps of Engineers (USACE) South Atlantic Division (SAD) are highly vulnerable to the threats of tropical cyclones (TCs), with 6 of the ten costliest US hurricanes impacting the SAD directly (NCEI 2022). The devastation caused by recent TCs such as Hurricane Michael and Hurricane Maria have underscored the need for accurate quantification of coastal storm hazards to aid in flood-risk management and resiliency efforts within coastal communities. In response to these needs, the USACE sponsored the South Atlantic Coastal Study (SACS), leading to the expansion of the Coastal Hazards System (CHS) (https://chs.erdc.dren.mil) within the SAD domain. For the CHS-SACS, the main goal was to determine the magnitude of existing and future coastal storm hazards and compute uncertainties to use in areas such as coastal planning and engineering related to flood-risk reduction and increased resiliency.

The domain considered within this study includes coastal areas from Mississippi to North Carolina as well as Puerto Rico and the US Virgin Islands. The CHS-SACS was conducted in three separate phases divided by coastal study region as follows:

- CHS-PR: Puerto Rico and US Virgin Islands
- CHS-SA: South Atlantic–North Carolina to South Florida
- CHS-GoM: Gulf of Mexico–Southwest Florida to Mississippi.

The CHS-SACS was conducted by the US Army Engineer Research and Development Center, Coastal and Hydraulics Laboratory, and the University of Notre Dame in collaboration with the USACE SAD. The work described in this technical report follows the application of the CHS Probabilistic Coastal Hazard Analysis (PCHA) framework (Nadal-Caraballo et al. 2020) for CHS-PR. The application of the PCHA encompassed state-of-the-art models, methods, and technically defensible data for accurate and robust quantification of coastal compound hazards in support of coastal flood risk management efforts.

1.2 Objective

The CHS-SACS sought to quantify hurricane-induced coastal hazards for the USACE SAD domain. This study provides necessary information related to coastal storm-induced hazards to support coastal engineering and planning activities conducted by the USACE and partners. The CHS-SACS takes advantage of the CHS PCHA framework, which has been implemented in other recent USACE regional coastal studies such as the Coastal Hazards System–Louisiana (CHS-LA) study (Nadal-Caraballo et al. 2022) and the Coastal Texas Protection and Restoration Study[1] (CTXS) (Melby et al. 2021), leading to consistency of methodology applied and results obtained for US hurricane-exposed coastlines. The PCHA is a statistical and probabilistic framework that builds upon previous joint probability analysis methodologies while incorporating several statistical and machine-learning advancements for more robust and accurate quantification of coastal storm hazards and uncertainty.

Joint probabilistic analysis of coastal storm hazards requires the evaluation of historical TC data, including the characterization of regional storm climatology and the development of a joint probability model of TC atmospheric-forcing parameters. Standard TC parameters used to describe hurricane and tropical storms are track reference location, track heading direction, central pressure deficit (intensity), radius of maximum winds (size), and forward translation speed. The magnitude and range of storm surge, for example, is primarily a function of storm intensity and size as well as the along-shore location relative to the eye of the storm, as discussed in Toro et al. (2010b). Results from this study include the estimation of annual exceedance frequencies (AEF) of still water level (SWL) and wave climate parameters: significant wave height (H_{mo}) and wave peak period (T_p). The AEF represents the number of times a given event is expected to be equaled or exceeded per year. The inverse of the AEF returns the average recurrence interval (ARI), or $ARI = 1/AEF$. The ARI represents the average time of occurrence between two events of interest and is often referred to as the *return period*. The magnitude of hazards can also be quantified in terms of annual exceedance probability (AEP), which represents the annual probability of an event occurring

[1] Nadal-Caraballo, N. C., A. B. Lewis, V. M. Gonzalez, T. C. Massey, and A. T. Cox. 2019. *Coastal Texas Protection and Restoration Feasibility Study, Probabilistic Modeling of Coastal Storm Hazards*. Report submitted to USACE-SWG. Vicksburg, MS: US Army Engineer Research and Development Center.

within a given year. Equations 1-1 and 1-2 convey the methods for converting between AEF and AEP:

$$AEP = \frac{e^{AEF}-1}{e^{AEF}} \tag{1-1}$$

$$AEF = -\log(1 - AEP) \tag{1-2}$$

The primary results quantified in this study are hazard curves depicting the magnitude of a given coastal hazard (y-axis) as a function of AEF (x-axis). In general, the magnitude of a given hazard and the corresponding AEF are inversely correlated; this is, the magnitude of the hazard increases with decreasing values of AEFs.

1.3 Approach

Accurate estimation of hurricane and extreme storm hazards is particularly challenging given that the occurrence of these events is sparse, both in time and space, and are not well represented in historical observation records. For the quantification of TC hazards, the CHS PCHA framework employs an enhanced methodology based on the joint probability method (JPM). As such, rather than relying on extreme value analysis of hydrodynamic observations (e.g., storm surge and waves) that extrapolate beyond the historical record, the PCHA requires developing a large number of synthetic TCs to efficiently cover a wide range of hurricane atmospheric and hydrodynamic characteristics. Spanning the atmospheric-forcing parameter and probability spaces is necessary to quantify coastal storm hazards accurately over the study area. Building on the results and lessons learned from the North Atlantic Coast Comprehensive Study (NACCS) (Nadal-Caraballo et al. 2015; Cialone et al. 2015) and the CTXS, the PCHA addresses the limitations of previous JPM studies by integrating (1) regional storm climatology characterization, (2) marginal distribution of TC atmospheric-forcing parameters, (3) development of synthetic storms, (4) dependence modeling of storm forcing parameters, (5) joint probability model of atmospheric forcing and hydrodynamic responses, (6) high-resolution numerical simulation, (7) machine learning storm-response prediction, and (8) quantification of uncertainties.

Quantifying storm hazards for this study required expanding the geographical coverage of the CHS and applying the PCHA framework to address coastal flooding relative to the CHS-PR study area. In this study,

sampling of the multivariate TC parameter space yielded an initial TC suite (ITCS) of 300 unique storms covering a wide range of probabilities, from frequent (10 yr^{-1}) to rare (10^{-4} yr^{-1}) coastal events. This ITCS constituted the input to the high-fidelity atmospheric and hydrodynamic numerical models used to simulate the coastal storm responses. To improve the robustness and accuracy of the coastal hazard curves, the ITCS was expanded to develop an augmented TC suite (ATCS) containing two orders of magnitude more storms, thus, increasing the resolution of the parameter and probability spaces used to characterize coastal storm responses. For this study, an ATCS of 348,000 storms was subsequently developed through hyper-discretization of the TC parameter space. The hydrodynamic responses of the ATCS were estimated through the application of Gaussian process metamodeling (GPM), a machine learning technique developed in collaboration with the University of Notre Dame. Hazard curves describing the magnitude of SWL (storm surge + astronomical tide), H_{mo}, and T_p as a function of AEF were developed at 14,891 virtual gauge (VG) locations in the study area.

The following sections describe in detail the PCHA framework and its implementation within CHS-PR study. Section 2 provides context to the probability analysis of TC responses using the JPM, and Section 2.3 describes advancements of the PCHA over the standard JPM approach. A description of the CHS and the stochastic Storm Simulation (StormSim) suite of tools are also provided in Section 2.4. The storm climatology of the study area and storm recurrence analysis performed herein are discussed in Section 3. The joint probability analysis of TC parameters through the development of marginal probability distributions and correlation coefficient matrices, as well as the characteristics of the storm suite applied in this study, are described in Section 4. The development of the synthetic storm suite is discussed in Section 5, including the application of the ITCS in the planetary boundary label (PBL) model. Section 6 provides details on the GPM development, computation of hazards, including the estimation and correction of bias, estimation of uncertainty, methods applied for waves, and the integration of TC responses. Finally, Section 7 summarizes the analysis conducted for Puerto Rico and the US Virgin Islands.

2 Coastal Hazards System (CHS)

The CHS (https://chs.erdc.dren.mil) is a national-scale, multi-agency initiative to quantify coastal storm hazards along US coastlines and other strategic locations critical to national security. Coastal hazards from hurricanes and extratropical storms can include storm surge, waves, wind, rainfall, compound coastal-inland flooding, seiche, and extreme tides. Climate change and sea level rise (SLR), which are expected to significantly exacerbate coastal flooding in the upcoming decades, are also part of the CHS scope. These coastal storm hazards can threaten the lives of millions of people living in coastal regions and devastate coastal communities and infrastructure, resulting in profound adverse social, economic, and environmental impacts. The foundation of the CHS is its PCHA framework.

The PCHA is a comprehensive statistical and probabilistic framework for quantifying coastal storm hazards. The framework encompasses the characterization of regional storm climatology, joint probability analysis of storm forcing and response, high-resolution numerical atmospheric and hydrodynamic modeling, machine learning, and estimation of associated uncertainties. The end goal of the PCHA is to develop a joint probability model linking storm forcing and responses. S*torm forcing* refers to the characteristics of a storm, including atmospheric pressure and wind fields. S*torm response* not only describes a hydrodynamic reaction to storm forcing, such as surge, waves, and currents, but could also include specific atmospheric variables such as maximum wind speed or rainfall. Results from the joint probability analysis are conveyed through hazard curves, which express the magnitude of a given hazard as a function of its AEF. The CHS also features a database hosting dozens of terabytes of coastal data, a web tool for easy access to results, and a website with corresponding documentation and metadata.

In the CHS PCHA framework, past tropical storms and hurricanes are parameterized according to their track (storm path), track heading direction, central pressure deficit, radius of maximum winds, and forward translation speed. Marginal (or conditional) distribution functions are fitted to these TC atmospheric parameters. These parameters' marginal distributions and dependencies form a multivariate probability distribution. Multiple parameter combinations are extracted to efficiently cover the plausible range of the storm parameter and probability spaces. Each of these parameter combinations constitutes a synthetic TC. Discrete

storm weights (DSW) are computed for the resulting synthetic TC suite by discretizing the multivariate probability distribution, which along with the magnitudes of the predicted storm responses, represents the joint probability model. Finally, the DSWs are integrated over the range of storm responses to develop the hazard curves (i.e., response magnitude as a function of AEF).

The CHS database includes PCHA results currently including more than 4,300 synthetic TCs, hundreds of extratropical cyclones (XCs) (for regions of the coast impacted by XCs), and multiple future SLR scenarios, totaling more than 15,000 unique high-resolution numerical hydrodynamic simulations resolving non-linear interactions between storm surge, wind waves, astronomical tide, and SLR. The CHS ensures accurate, robust, and consistent quantification of coastal hazards along all Atlantic, Gulf of Mexico, and Great Lakes coastlines of the United States, thus facilitating nationwide coastal storm risk management and resilience strategies. CHS data also support individual feasibility studies, economic analyses, evaluation of nature-based features, stochastic engineering design, and risk assessments. The CHS PCHA framework's primary goal is to address the limitations of the JPM and derived optimal sampling (OS) approaches, which are discussed in the following sections.

2.1 Joint probability method (JPM)

The joint probability analysis of storm surge and waves from TCs, in most cases, suffers from a lack of historical observations resulting in small sample sizes. Moreover, some of the characteristics of the TCs that impact a particular area may make it necessary to consider them as belonging to different subpopulations, further reducing the already small sample sizes. The JPM addresses these limitations by characterizing the atmospheric forcing of storms instead of their responses. In broad terms, TCs are defined by several forcing parameters and corresponding probability distribution functions (PDFs), which are discretized to generate the wind and pressure fields required to simulate storm surge and waves. Typical TC parameters include track reference location, track heading direction, central pressure deficit, radius of maximum winds, and forward translation speed.

The JPM has become a standard joint probabilistic model for estimating coastal storm hazards in hurricane-prone areas. Gonzalez et al. (2019)

summarized the development and evolution of the JPM, and a brief synopsis is provided here. Early characterization and probabilistic analyses of individual hurricane parameters were performed by Myers (1954). The precursor of the JPM was pioneered in the late 1960s (Russell 1968a, 1968b) using a full Monte Carlo simulation to estimate probabilities of wind, storm surge, and wave loads on offshore structures. In the 1970s, the National Oceanic and Atmospheric Administration (NOAA) further developed and adapted the JPM for hurricane climatology and probabilistic storm surge studies in the US Atlantic and GoM coastal areas (e.g., Myers 1970, 1975; Ho 1974; Ho and Myers 1975). The total annual frequency of a given water level was determined by adding the frequencies of landfalling TCs, bypassing TCs, and XCs. By the late 1980s, the Federal Emergency Management Agency (FEMA) had adopted the JPM (FEMA 1988) as presented in the National Weather Service report NWS-38 (Ho et al. 1987).

Although the JPM approach has been implemented since the 1970s, recent advancements in sampling techniques and the development of the JPM with optimal sampling (JPM-OS) made it possible to reduce the necessary number of synthetic storms, more efficiently characterizing the parameter and probability spaces. Different implementations of the JPM emerged from several studies conducted after 2005 following the devastation caused by Hurricane Katrina. These approaches and their application are discussed in the following sections.

2.2 JPM with optimal sampling (JPM-OS)

The destruction caused by Hurricane Katrina in 2005 led to the proliferation of storm surge hazard studies that brought further improvements to the JPM. Of particular importance was the work done by the IPET (2009) in which JPM-OS approaches were developed for the statistical analysis of extreme water levels to evaluate the performance of the Southeast Louisiana hurricane surge protection system. The IPET provided the basic framework for storm surge modeling approaches used in later works. This effort, led by a team of USACE, FEMA, NOAA, private sector, and academic researchers, was documented in the IPET report. These JPM-OS developments aimed to reduce the number of storms required for populating the parameter space without sacrificing resolution and accuracy relative to the probability space.

JPM variants labeled as "OS" include the JPM by Bayesian Quadrature (JPM-OS-BQ) and the JPM with augmented sampling utilizing a Response Surface (JPM-OS-RS). In practice, the optimal sampling and, thus, the reduction in the number of storms is accomplished by either (1) expert selection of TC parameter combinations (e.g., JPM-OS-RS) or (2) trial-and-error sampling of a storm subset that closely matches target hazard curves produced by a much larger storm set simulated using a low-fidelity hydrodynamic model or a high-fidelity model with a coarse grid (e.g., JPM-OS-BQ). Applying these techniques in practice, the number of sampled storms generally decreases from tens of thousands of storms (denoted as the reference set) to a few hundred.

The JPM-OS-RS approach (Resio et al. 2007), as described in Toro et al. (2010a), requires a careful selection of TC parameter combinations based on expert judgment. This selection should yield a moderate number of synthetic TC simulations used to construct a storm surge response surface. The TC parameter space is filled in by interpolating intermediate surge values from the response surface using a finer discretization, primarily considering the Δp-R_{max} bivariate space. The surge response is assumed to have a small, linear variation along the θ-V_t space in this scheme. Storm surge values interpolated from the response surface have been shown to introduce uncertainty with root-mean-square deviation on the order of 0.70 m (CPRA 2013). The JPM-OS-RS approach was applied to regional studies such as the Louisiana Coastal Protection and Restoration Authority (LACPR) study (USACE 2009a), the Mississippi Coastal Improvements Project (USACE 2009d), and the Flood Insurance Study (FIS) for Coastal Counties in Texas (USACE 2011).

As stated in the Operating Guidance No. 8-12 document (FEMA 2012), FEMA's guidelines focused on the JPM-OS-BQ (Toro 2008) approach "since it is more readily automated than the [JPM-OS-RS] which requires a greater degree of expert judgment in the selection of storms." This acknowledgment made JPM-OS-BQ the de facto JPM approach of FEMA's National Flood Insurance Program Risk Mapping, Assessment, and Planning program. Beginning with the Mississippi Coastal Analysis Project (MCAP) (FEMA 2008), most FEMA studies to date have relied on this approach.

Reliance on choices made based on judgment is not unique to the JPM-OS-RS. The JPM-OS-BQ approach requires the development and

simulation of a JPM storm set consisting of thousands or tens of thousands of TCs to construct a *reference set* of storms and corresponding target hazard curves before conducting the storm sampling. The primary shortcoming of the JPM-OS-BQ approach is that, due to computational constraints, in practice, it must rely on either (1) low-fidelity hydrodynamic models that do not incorporate all physical processes or (2) models with coarse-resolution grids to efficiently simulate the storms that constitute the reference set.

Moreover, the JPM-OS-BQ employs a double-exponential covariance function (Toro et al. 2010a) as a pseudo-dependence structure with correlation distances as inputs that dictate the discretization of TC marginal distributions. As discussed by Niedoroda et al. (2010) and Toro et al. (2010a, 2010b), the Bayesian Quadrature (BQ) correlation distances must be specified based on expert judgment. The JPM-OS-BQ sampling scheme consists of a trial-and-error process where various combinations of these correlation distances yield different storm sets. Each set's storm surge hazard curves are compared to the target hazard curves from the reference set at select locations within the study area. The end goal is to select the storm set that produces storm surge hazard curves with the smallest difference from the reference set. However, the reliability of the target hazard curves is unknown, particularly outside open water domains, and they potentially incorporate significant bias from the low-fidelity or coarse-grid simulations of the storm in the reference set. Another limitation of what is referred to as the OS approach is the lack of an actual joint probability model or consideration of joint probability distribution. In practice, TC parameters have been assumed to be independent, or pairs of TC parameters have been linked through simplified linear relationships.

In summary, the JPM-OS approaches initially adopted by federal agencies (e.g., BQ and response surface [RS]) include some limitations that have not been adequately documented and corrected. This report discusses how the CHS PCHA framework developed by USACE overcomes some of the previous JPM limitations, including the lack of a dependence structure correlating the TC atmospheric-forcing parameters, optimal sampling scheme, dry-node correction of hydrodynamic results, and quantification of the geospatial bias correction and uncertainty.

2.3 The CHS Probabilistic Coastal Hazards Analysis (PCHA)

As part of the CHS, the USACE initially developed a version of the JPM with a hybrid optimal sampling approach for the NACCS and the CTXS. This hybrid JPM approach evolved into the PCHA framework by incorporating significant advancements that will be discussed later in this section.

In addition to CHS-SACS, the advanced PCHA framework has also been implemented in the CHS-LA coastal study. CHS-LA provided critical storm surge and wave hazards data for conducting risk assessment of levees within the Hurricane and Storm Damage Risk Reduction System in the Greater New Orleans metropolitan area. Although the application of the JPM can vary significantly by study, the different approaches typically follow a general methodology, depending on the dominant processes and respective solution strategies. The JPM methodology generally includes the following steps:

- characterization of historical storm climatology
- computation of historical storm recurrence rate (SRR)
- development of PDFs of historical TC atmospheric parameters
- discretization of PDFs of TC parameters
- development of synthetic TC suite
- atmospheric and hydrodynamic modeling of synthetic TC suite
- quantification of uncertainties (e.g., numerical model skill)
- integration of DSWs and responses to compute hazard curves (i.e., magnitude of response vs. AEF).

The AEF of coastal hazards such as storm surge or waves at any given site is a function of three main components: the SRR, the joint probability of characteristic TC parameters, and the storm responses. Recent CHS studies, including CHS-PR, employ the form of the JPM integral without error term as uncertainty is conveyed through non-exceedance confidence limits (CLs), as further discussed in Section 6.4. The AEF is computed from the JPM integral:

$$\lambda_{\tau_{max}>\tau} = \lambda \int P[\tau_{max}(\hat{x}) > \tau|\hat{x}]\, f_{\hat{x}}(\hat{x}) d\hat{x} \tag{2-1a}$$

$$\approx \sum_i^n \hat{\lambda}_i\, P[\tau_{max}(\hat{x}_i) > \tau|\hat{x}_i] \tag{2-1b}$$

where $\lambda_{\tau_{max}>\tau}$ = AEF of TC response τ due to the atmospheric-forcing vector $\hat{x} = f(x_o, \theta, \Delta p, R_{max}, V_t)$; λ = SRR (storms/year/km); and n = number of TCs. The expression $P[\tau_{max}(\hat{x}) > \tau|\hat{x}]$ represents the conditional probability that response $\tau_{max}(\hat{x})$ is greater than τ given $\hat{x}$. In the discrete form of the JPM integral (Equation (2-1b)), $\hat{\lambda}_i$ is defined as the DSW of the i-th synthetic TC, where $\hat{\lambda}_i = \lambda p_i$, and p_i is the product of its discrete joint probability (i.e., normalized probability densities) and the spacing between synthetic TC tracks (in kilometers) defined in the JPM. After multiplying the SRR, TC probability densities, and track spacing, the DSW is defined by units of storms/year. For this study, a track spacing of 60 km[1,2] was applied for developing the synthetic TC suite.

The JPM integral with the error term, which is presented in Nadal-Caraballo et al. (2019a), takes the following form:

$$\lambda_{\tau_{max}>\tau} = \lambda \int P[\tau_{max}(\hat{x}) + \varepsilon > \tau|\hat{x}, \varepsilon] \, f_{\hat{x}}(\hat{x}) f_{\varepsilon}(\varepsilon) d\hat{x} d\varepsilon \quad (2\text{-}2a)$$

$$\approx \sum_i^n \hat{\lambda}_i \, P[\tau_{max}(\hat{x}_i) + \varepsilon > \tau|\hat{x}_i, \varepsilon] \quad (2\text{-}2b)$$

where ε = unbiased error term or uncertainty of TC response and expression $P[\tau_{max}(\hat{x}) + \varepsilon > \tau|\hat{x}, \varepsilon]$ represents the conditional probability that $\tau_{max}(\hat{x}) + \varepsilon$ produces a response greater than τ given $\hat{x}$ and ε.

The TC atmospheric-forcing parameters commonly used in the JPM for the characterization of TCs and included in the forcing vector $\hat{x}$ are the following:

- track reference location (x_o)
- track heading direction (θ)
- central pressure deficit (Δp)
- radius of maximum winds (R_{max})
- forward translation speed (V_t).

[1] For a full list of the spelled-out forms of the units of measure used in this document, please refer to *US Government Publishing Office Style Manual*, 31st ed. (Washington, DC: US Government Publishing Office 2016), 248-52, https://www.govinfo.gov/content/pkg/GPO-STYLEMANUAL-2016/pdf/GPO-STYLEMANUAL-2016.pdf.

[2] For a full list of the unit conversions used in this document, please refer to *US Government Publishing Office Style Manual*, 31st ed. (Washington, DC: US Government Publishing Office 2016), 345-7, https://www.govinfo.gov/content/pkg/GPO-STYLEMANUAL-2016/pdf/GPO-STYLEMANUAL-2016.pdf.

The parameter x_o is characterized through the computation of SRR (Section 3.5). Subsequently, either a marginal or a conditional PDF is fitted to each of the remaining atmospheric-forcing parameters (i.e., θ, Δp, R_{max}, and V_t). This is done to adequately capture the likelihood of occurrence of each of these parameters according to historical hurricane records. The PCHA implements a hybrid approach for discretizing these PDFs. This hybrid sampling approach employs a structured discretization of the θ and Δp distributions to ensure (1) optimal coverage of the probability and parameter spaces, and (2) complete geospatial coverage of the study region. Discretization of R_{max} and V_t is performed by the BQ method. Synthetic TCs are thus developed as likely combinations of the atmospheric-forcing parameters, as sampled from their respective PDFs. The parameters of the synthetic TCs are used as inputs to the PBL model to estimate the time histories of the wind and pressure fields that drive high-fidelity numerical hydrodynamic storm surge and wave models.

In conjunction with the common JPM steps previously listed in this section, the recent PCHA advancements included in this study are summarized as follows:

- characterization of storm climate and TC hazards at over 1,000 coastal reference locations (CRLs) along US hurricane-exposed coastlines
- use of GPM, a machine learning method, to fill in gaps in the HURricane DATa 2nd generation (HURDAT2) database (Landsea and Franklin 2013) and incorporate long-term estimates of R_{max}
- use of GPM for the development of an ATCS to achieve hyper-resolution of the TC forcing parameter space
- computation of an accurate joint probability model of TC forcing parameters through the use of meta-Gaussian copula (MGC) as the dependence structure, explicitly accounting for the correlation between TC parameters
- performance of dry-node correction (DNC) to fill in missing storm surge values
- geospatial bias correction and quantification uncertainty.

The interconnections of the main components of the CHS PCHA framework are illustrated in Figure 2-1. The PCHA-related advancements are represented in the diagram below as red-bordered boxes. In the diagram, processes related to TCs are shown by solid arrows, whereas dashed arrows illustrate XC processes.

The implementation of metamodeling technologies, such as the GPM (Jia et al. 2016; Zhang et al. 2018), is fundamental to the PCHA framework. A metamodel is first trained and applied within the PCHA to perform data imputation, which is a process to estimate missing TC parameter values and fill gaps in the HURDAT2 historical record. The primary function of the GPM, however, is the development of an ATCS of tens of thousands to millions of synthetic TCs that retain the high-fidelity nature of the numerical simulation of the ITCS. The ATCS' finer discretization of the TC atmospheric-forcing parameter space made possible by GPM is coupled with the use of the MGC, which incorporates the dependencies between the TC parameters for a more truthful representation of the historical hurricane climatology. The metamodeling capabilities are then applied to predict storm responses (i.e., storm surge) produced by the ATCS to develop coastal hazard curves. The GPM component of the PCHA framework supersedes the optimum sampling-response surface (OS-RS) approach previously developed by USACE, given the GPM's capability to explicitly use all TC forcing parameters as inputs and the higher accuracy of its predictions.

The PCHA introduced the DNC method to fill in missing storm surge information at dry nodes or VGs. DNC is performed either through the use of a geospatial GPM approach for sparse hydrodynamic data (e.g., at VGs) or through the application of weighted *k*-nearest neighbor regression in cases where hydrodynamic results are available at high spatial resolution (e.g., ADvanced CIRCulation [ADCIRC] model nodes). PCHA also applies a Gaussian kernel function (GKF) to assess geospatial model errors across all point locations in the study to include uncertainty within the hazard curves.

The application of the PCHA components (Figure 2-1) to the CHS-PR study area is detailed in Sections 3 through 6. The *Tropical Cyclone (TC) Climatology* (green box) analysis is documented in Section 3, which describes the storm recurrence analysis and distance adjustment of TC parameters from historical storms before developing the PDFs. The *Joint Probability Analysis* of the TC parameters (purple box), including the application of the MGC and the development of the ATCS, is discussed in Section 4. In Section 5, a detailed description of developing the meteorological *Modeling Components* (navy box) for input into the hydrodynamic models is provided (navy box). Section 6 (navy and light-blue boxes) documents the post-processing of the hydrodynamic modeling results and metamodeling development (navy box) and the

Hazard Quantification (light blue box), including the application of the ATCS storm responses for developing hazard curves.

Figure 2-1. Diagram of the CHS PCHA framework (Nadal-Caraballo et al. 2020).

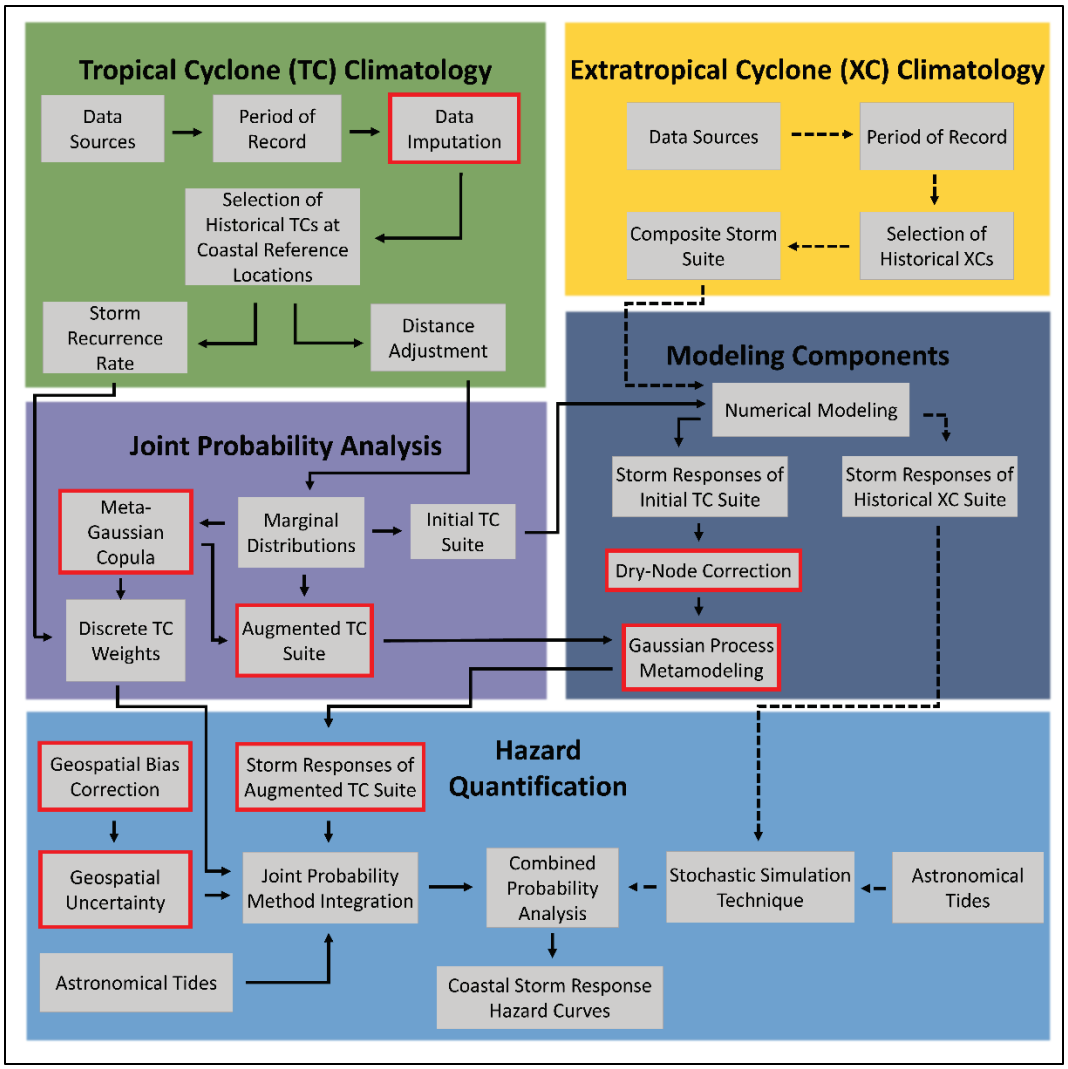

2.4 An integrated coastal hazards platform

The CHS is a national-scale effort for quantifying coastal hazards for US coastlines based on high-fidelity modeling and a cutting-edge statistical framework. Along with this framework, the CHS encompasses multiple components (Figure 2-2), including a webtool for accessing coastal hazards information, a website with documentation and metadata, the StormSim suite of tools for engineering applications, and the Coastal Hazards Rapid Prediction System for real-time probabilistic and deterministic predictions of coastal storm hazards.

Figure 2-2. Components within the Coastal Hazards System (CHS).

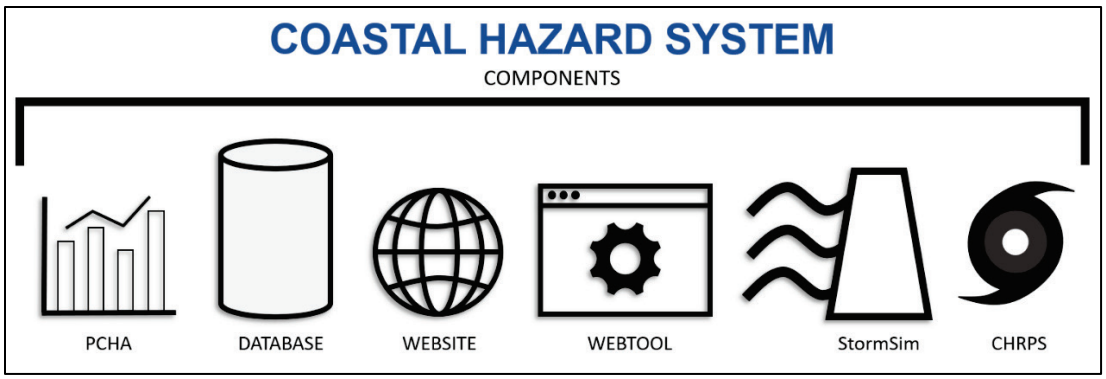

The CHS stores and distributes USACE and FEMA high-fidelity coastal storm data from comprehensive regional studies. Modeling results and probabilistic coastal hazards data derived from the TC and XC simulations are converted into consistent and efficient, standard formats and stored in a centralized system that is relatively easily maintained due to an innovative database architecture. The user-friendly web interface includes a multi-access environment where the user can query data through a map interface or through a text-based navigation window, or some arbitrary combination of the two. As shown in Figure 2-3, the CHS website can be accessed at https://chs.erdc.dren.mil.

The Puerto Rico and US Virgin Islands (CHS-PR) probabilistic analysis and numerical modeling effort generated a large amount of data, including probabilistic analysis and modeling results for the coastal region of Puerto Rico and the US Virgin Islands. These data and data products will serve the coastal engineering and coastal management communities in the USACE SAD for many years. Managing and providing access to this vast quantity of information is made possible via the CHS website and webtool. The data stored include comprehensive, high-fidelity, storm-response computer modeling results, including climatology, storm surge, SWL, wind, currents, and waves. Extremal statistics and uncertainties are also stored, and the data are easily accessed, mined, plotted, and downloaded through a user-friendly web interface (Figure 2-4 and Figure 2-5).

Figure 2-3. Screen capture of the CHS website.

Figure 2-4. Screen capture of the CHS webtool.

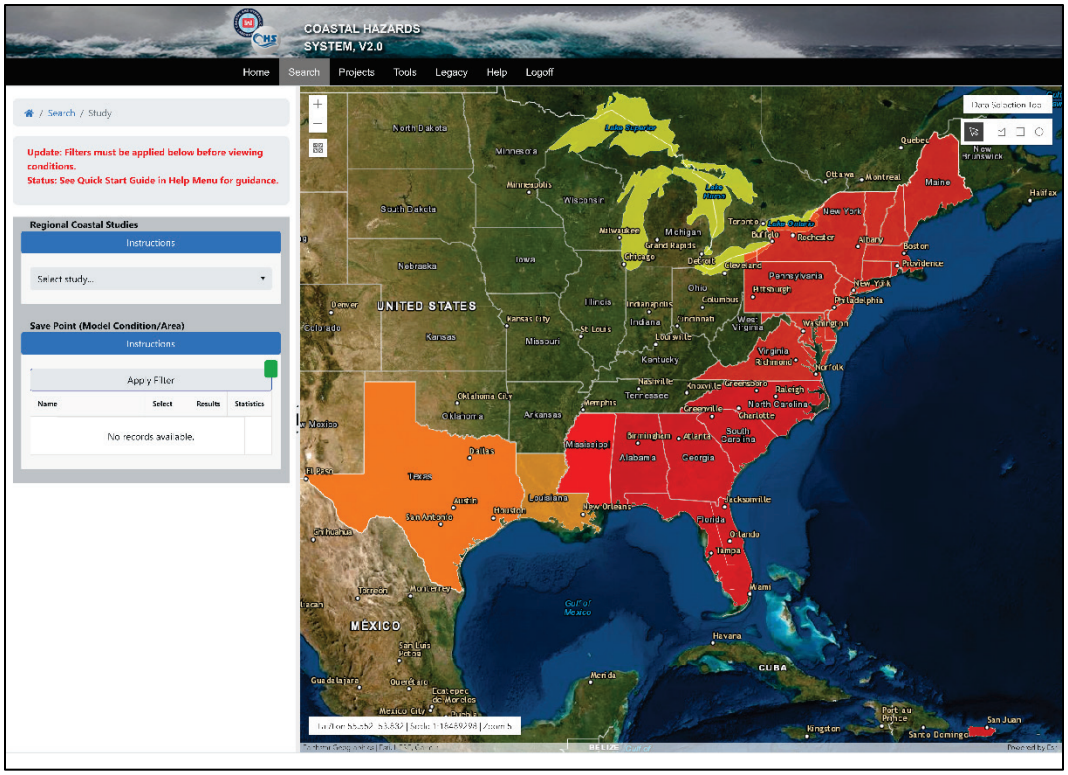

Figure 2-5. Screen capture of save points (virtual gauges) within the CHS webtool.

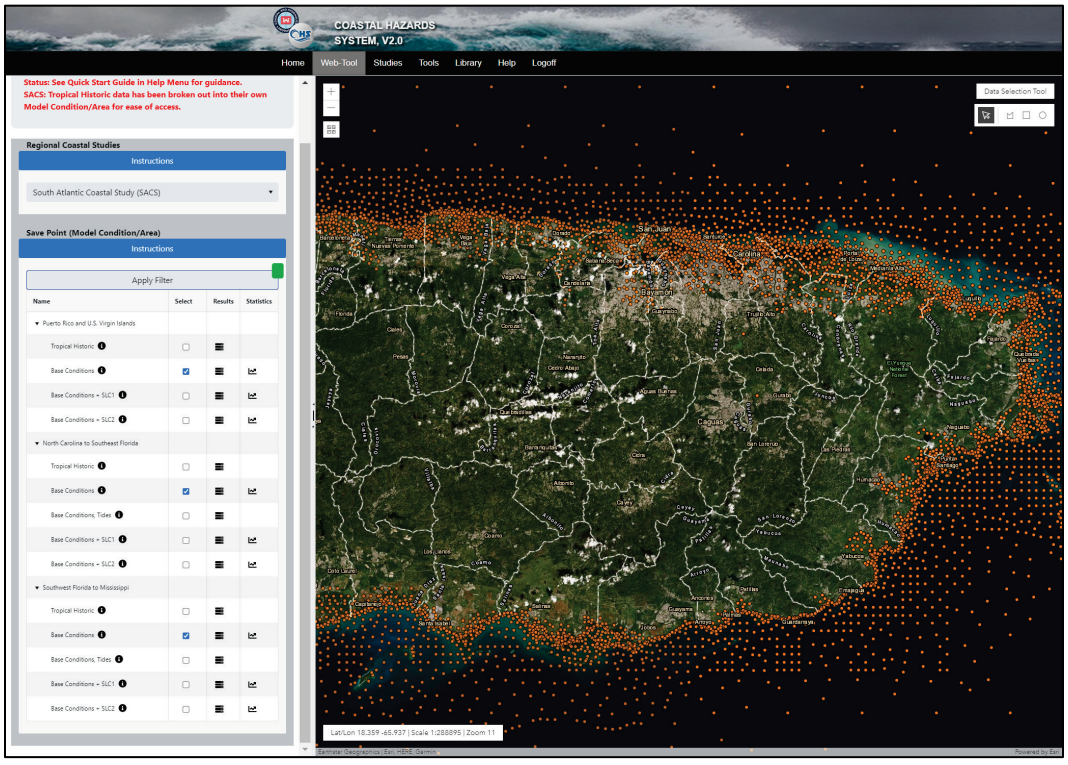

2.4.1 CHS-PR Available Data

As discussed herein, the CHS data are comprehensive and span the practical probability space of the study regions. Following the completion of the hydrodynamic modeling and probabilistic analysis, the final data are stored and accessed by regional study within the CHS webtool. The types of data that are distributed for CHS-PR include the following:

- ADCIRC model output
- STeady-state spectral WAVe (STWAVE) model output
- TC tracks and parameters
- discrete storm weights
- storm recurrence rates
- storm response statistics
- hazard curves
- uncertainty data.

Both time-varying and maxima data from the hydrodynamic models as well as statistics results are stored by VG, or save point, location. For the CHS-PR, data within the CHS database and webtool are available at more than 14,000 save point locations distributed throughout the study area. Responses for all storms for a specific point are stored in a unique file. The CHS native file formats are self-describing compressed HDF5[1]; however, the capability for online conversion to comma-separated values format exists within the CHS web environment.

Uncertainties, computed using the methods discussed in this report, are stored in files containing this data at the save points. Documentation for the system, data, and file formats is contained in easily accessible documents within the CHS library.

2.4.2 Storm Simulation (StormSim) suite of tools

StormSim is a suite of tools that address a wide range of federal needs including applications within coastal research, emergency management, coastal planning, and coastal engineering. The StormSim tool suite is a collection of scripts related to hazard computations, engineering responses, stochastic simulations, and metamodeling, making them

[1] Hierarchical data format version 5

applicable to various research and engineering areas of interest. These tools were developed with the intent of accurately simplifying and automating the complex processes within the PCHA framework. The StormSim tools include the following:

- StormSim-Storm Selection: storm selection methods for developing small-scale storm suites
- StormSim-JPM: quantification of tropical cyclone induced hazards through application of the JPM
- StormSim-SST: quantification of XC-induced hazards using the extreme value analysis based Stochastic Simulation Technique (SST).
- StormSim-MCS/CSR: Monte Carlo simulations (MCS) for coastal structure life-cycle response analyses and coastal structure reliability (CSR)
- StormSim-PROS: response-based assessment of coastal structure threshold responses (e.g., Peaks, Runup, Overtopping, and Stone sizing [PROS]) using peak storm parameters.

The tools readily apply regional study data available through the CHS, such as the AEFs of coastal storm hazards and peak storm responses from the hydrodynamic simulation results. The development of the StormSim software system is an ongoing effort that has been funded through USACE Flood and Coastal Systems Research and Development program.

3 Characterization of Storm Climatology

Puerto Rico and the US Virgin Islands are frequently subjected to coastal hazards due to hurricanes and other extreme storms. As previously discussed, the characterization of historical TCs for purposes of the statistical analysis of coastal storm hazards is based on the primary TC parameters accounted for in the JPM: x_o, θ, Δp, R_{max}, and V_t. In this report, the definition of track and landfall conforms to that used within the HURDAT2 database. The TC track is defined as the center of the eye, which is computed as the location of minimum central pressure within HURDAT2. Landfall occurs when the track crosses the coastline, where the coastline is defined as the interface between the mean-sea-level (MSL) and land. An idealized coastline defined by a series of CRLs was constructed from data obtained from NOAA's National Geophysical Data Center for use in the PCHA workflow

The following sections describe the climatological data sources used in this study, period of record considered, CRLs, selection of historical TCs, and the computation of SRR.

3.1 Data sources

The screening of TCs refers to the identification of historical TCs for the computation of SRR, marginal probability distributions of TC parameters, and correlation of TC parameters. For TC screening, the main data source was HURDAT2. HURDAT2 is a product of NOAA's National Hurricane Center (NHC) Re-Analysis Project and consists of the reanalysis of all *historical* TCs recorded in the North Atlantic basin (i.e., North Atlantic Ocean, GoM, and the Caribbean Sea) from 1851 to 2019 (https://www.aoml.noaa.gov/hrd/hurdat/hurdat2.html).

A major limitation of HURDAT2 is the lack of R_{max} observations prior to 2021. The PCHA framework incorporates R_{max} from the extended best track (EBTRK) database (http://rammb.cira.colostate.edu) (Demuth et al. 2006). This database was created to supplement HURDAT2 best track data with storm structure information, including R_{max}. The EBTRK dataset currently covers the 1988 to 2018 time period. Table 3-1 lists the sources and available record lengths for the primary TC parameters used in this study.

3.2 Period of record for the PCHA

Prior to the selection of historical TCs, the specific period of record to be used for the PCHA was assessed. The SRR and the marginal distributions of TC parameters are sensitive to the historical record length. The 1940s decade marked the dawn of modern aircraft reconnaissance missions to measure hurricane parameters, resulting in much more reliable estimates of storm characteristics, including frequency and intensity.

Prior to 1944, the main data sources were land stations and ship reports, and it was typical for storms to go undetected (Jarvinen et al. 1984). After 1944 and as a consequence of World War II, aerial reconnaissance led to increased data collection incidence and measurement accuracy, including storm position, track, wind speed, and pressure. The use of satellite imagery was introduced during the 1964 hurricane season (Neumann et al. 1985) and was considered one of the most significant advances in TC tracking (Jarvinen et al. 1984).

The undersampling of TCs prior to the 1940s has been well documented. Mann et al. (2007) estimated an undercount in the pre-aircraft reconnaissance era (1870–1943) ranging from 0.5 to 2.0 TC/yr, with a mean of 1.2 TC/yr. Landsea et al. (2010) discussed that the increase in reported TCs during the 1940s and until approximately 1960 had been interpreted as a result of climate change. This increase, however, is likely the result of improved observing and recording of short-lived TCs with the advent of aircraft reconnaissance and satellite imagery.

Worley et al. (2005) identified fewer recorded moderate-track to long-track TCs during the 1910s and 1940s due to reduced ship observations during World War I and World War II, respectively. Vecchi and Knutson (2011), after adjusting HURDAT data for unrecorded TCs, concluded that the mid-twentieth century was a high-activity period that extended from the 1940s to the 1960s.

A review of technical literature indicates that although the 1940s decade saw improvements in the observation and recording of TCs, there was still a significant undercount of events during this period. In recent flood hazard studies where the JPM-OS methodology was used, the period of record that was considered in the analysis started in the early 1940s (FEMA 2008, 2012; Resio et al. 2007). The NACCS conducted by the

USACE for the Virginia-to-Maine coastline used a period of record from 1938 to the present, corresponding to a few years before the dawn of Hurricane Hunter aircraft reconnaissance missions, to capture The Great New England Hurricane of 1938. Therefore, due to concerns of TC undercount prior to the 1940s and climatic non-stationarity, the PCHA framework avoids these issues by using the period of record from 1938 – 2019 for the computation of geospatial SRR (Section 3.5) and directional SRR (DSRR) (Section 4.1.4).

Due to issues with data collection, data gaps are present within the HURDAT2 database. To overcome the limitation of missing data values, GPM is also used in a data imputation process to estimate missing values and fill in the database gaps. The data imputation within the PCHA framework is completed using GPM techniques with two main goals: (1) to fill in central pressure gaps in the HURDAT2 database and (2) to fill in R_{max} gaps in the EBTRK database. The metamodel trained to predict Δp is trained on the following input vector: $\hat{x}_{\Delta p} = f(lat, lon, W_{max}, V_t, \theta)$, where W_{max} = maximum sustained wind speed. Similarly, the metamodel trained to predict R_{max} considered the previous input vector, with the addition of Δp: $\hat{x} = f(lat, lon, W_{max}, \Delta p, V_t, \theta)$.

Examples of the reconstructed values for Δp and R_{max} are shown in Figures 3-1 through 3-4. These figures illustrate the performance of the GPM in filling in missing values of Δp and R_{max} during historical TCs. In each figure, the blue line and associated points indicate the values filled in by the GPM estimates as compared to the observed historical data points (red points).

Figure 3-1. Reconstruction of Δp for a 1938 historical TC using metamodeling techniques.

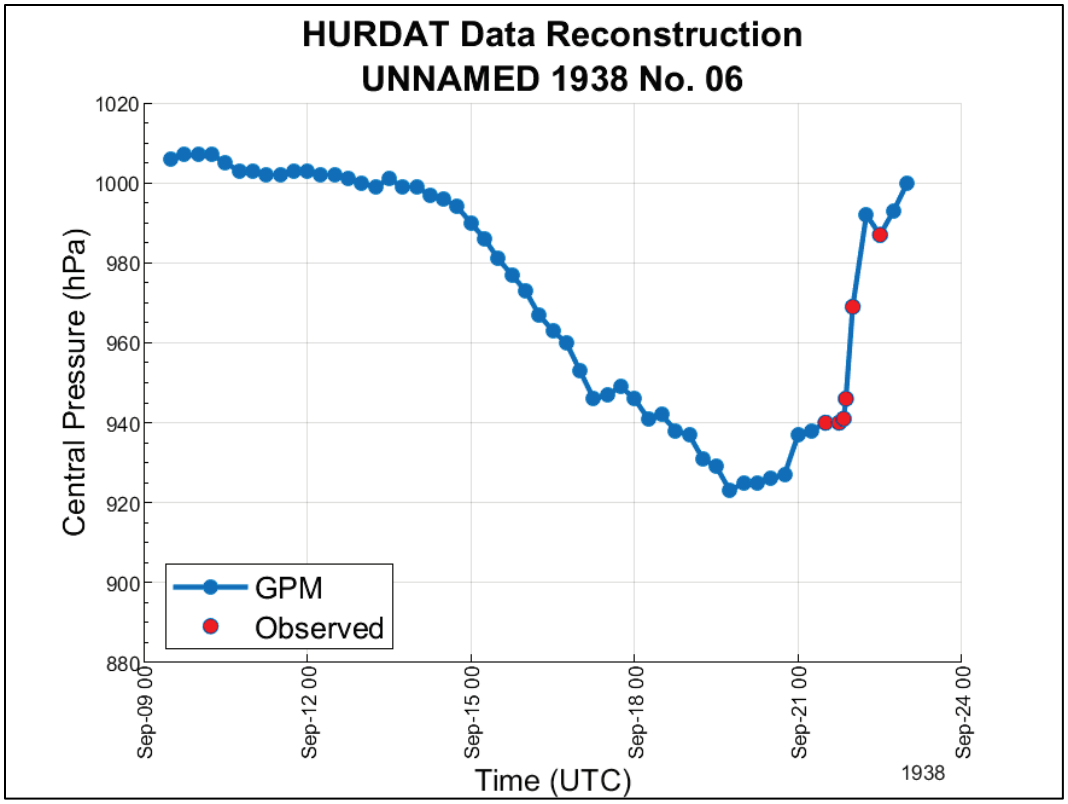

Figure 3-2. Reconstruction of Δp for Hurricane Sandy using metamodeling techniques.

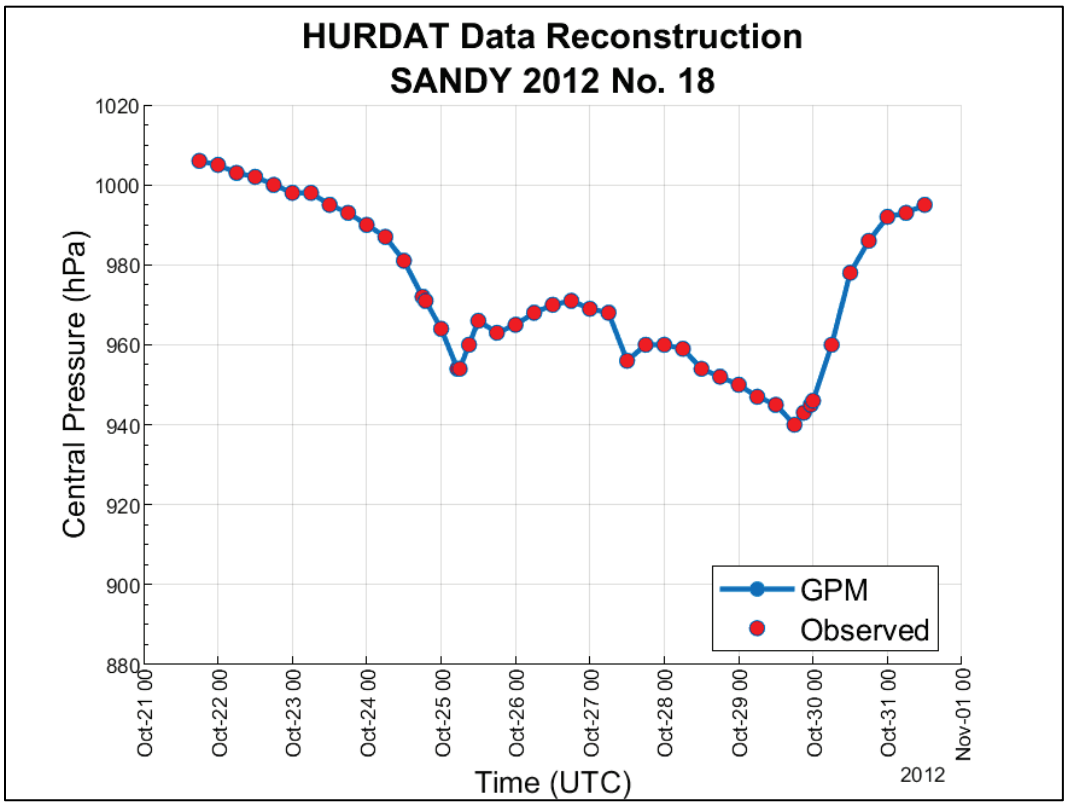

Figure 3-3. Reconstruction of R_{max} for a 1938 historical TC using metamodeling techniques.

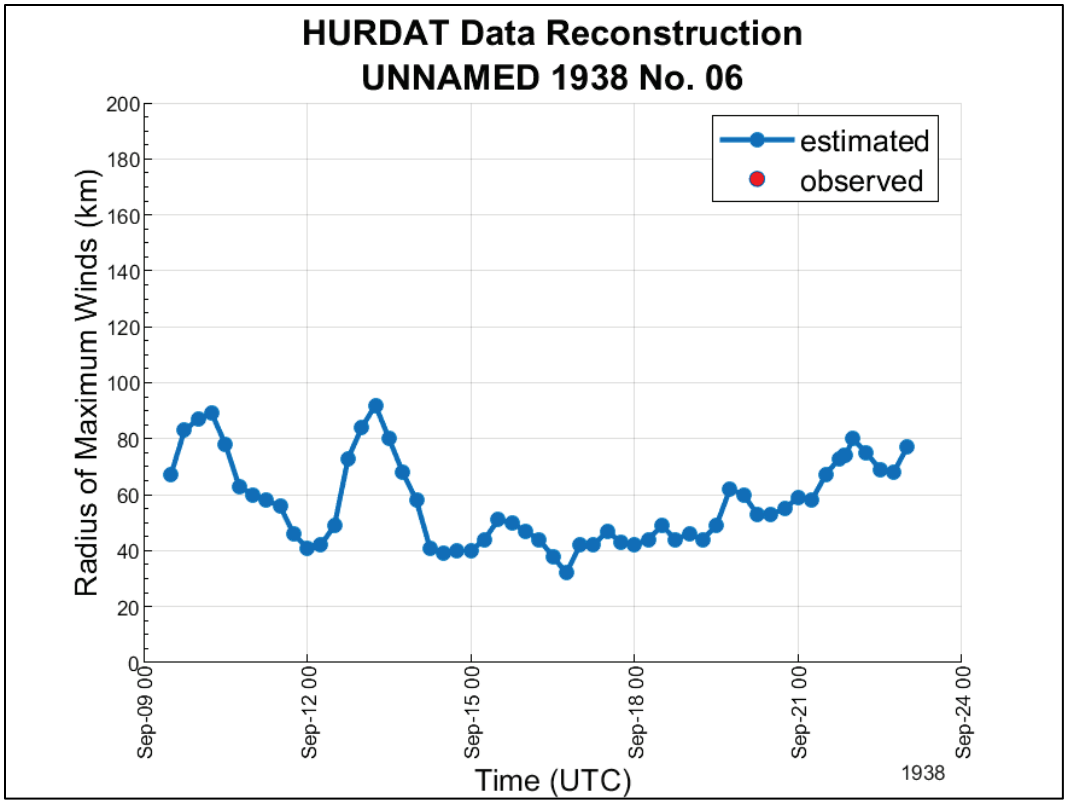

Figure 3-4. Reconstruction of R_{max} for Hurricane Sandy using metamodeling techniques.

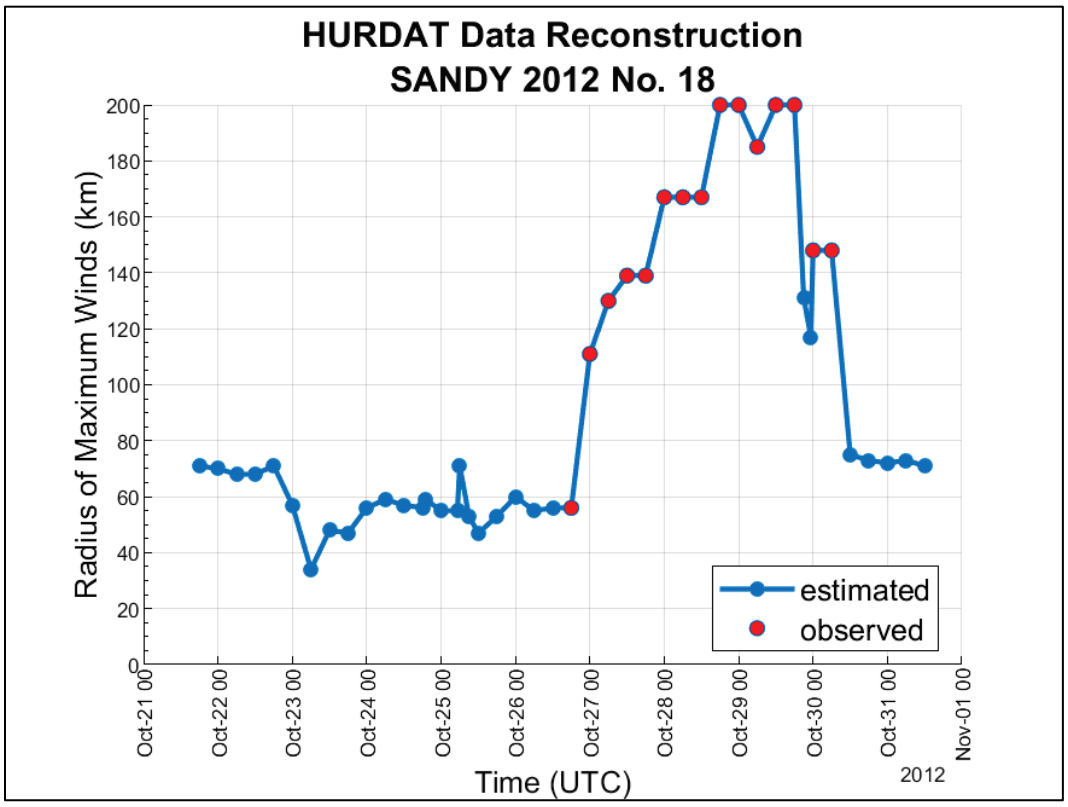

After performing the data assimilation process using GPM, gaps in Δp were filled for the entire HURDAT2 period of record from 1851 to 2019. Likewise, for R_{max}, GPM was used to fill in gaps in the EBTRK data record extending the record length to the 1851 to 2019 period. However, due to concerns of non-stationarity and undercounting of TC occurrences, only TC data during the 1938 to 2019 period was considered in the development of marginal distributions for the following TC parameters: Δp, V_t, θ, and R_{max}. Table 3-1 provides the period of record considered in the development of marginal distributions for each TC parameter.

Table 3-1. Period of record considered for each TC parameter.

Tropical Cyclone Parameter	Source and Availability	Period of Record
Track reference location	HURDAT2 (1851–2019)	1938–2019
Track heading direction	Estimated from HURDAT2 (1851–2019)	1938–2019
Central pressure deficit	HURDAT2 (1851–2019)	1938–2019
Forward translation speed	Estimated from HURDAT2 (1851–2019)	1938–2019
Radius of maximum winds	EBTRK (1988–2018)	1938–2019

3.3 Coastal reference locations (CRLs)

The quantification of coastal hazards performed for the CHS is completed on a national scale for the coverage of all hurricane-prone coastlines of the United States. This requires the consistent characterization of storm climate to be conducted at a high geospatial resolution.

The PCHA characterizes the storm climate at points along an idealized coastline defined by a series CRLs. The average spacing between adjacent CRLs is 10 km. Additional CRLs are also positioned in offshore locations to characterize bypassing TCs in regions like the North Atlantic Coast, Puerto Rico, and the US Virgin Islands. These point locations mark where the (1) SRR, (2) fitting of each TC parameter probability distribution, and (3) computation of the joint probability through the MGC are defined to characterize the storm climate at that given location. The network of over 1,000 CRLs allows for the computation of the DSWs at a high geospatial resolution.

For the contiguous United States, 663 CRLs (IDs 1–663) have been established along an idealized coastline starting south of the Mexico-Texas boundary (23.5°N) and ending in northern Nova Scotia (45.0°N). The idealized coastline was constructed using data obtained from NOAA's National Centers for Environmental Information (https://www.ngdc.noaa.gov/mgg/shorelines). These data can also be accessed directly through the "Global Self-consistent, Hierarchical, High-resolution Geography Database" website (http://www.soest.hawaii.edu/pwessel/gshhg).

For offshore locations established for bypassing storms, 117 CRLs (identifiers [IDs] 664–780) were placed around the North Atlantic Coast region from Virginia to Maine, and 65 CRLs were established off the southern tip of Florida (IDs 961–1,025). These offshore CRLs were explicitly placed to capture bypassing TCs. For the Caribbean, 180 CRLs (IDs 781–960) were established near Puerto Rico and the US Virgin Islands, for a total of 1,025 CRLs along the coastline and offshore. For this study, only the horizontal line of 134 CRLs (781–914) crossing over the CHS-PR study area were used in the PCHA. Additional CRLs might be placed in the future to improve the geospatial resolution of the PCHA at particular locations. Figure 3-5 illustrates the current network of 1,025 CRLs, and Figure 3-6 shows a closer view of the CRLs implemented in the PCHA for CHS-PR. In the following sections, examples of the PCHA framework will be illustrated at CRL 844 as this point is the closest CRL to San Juan, Puerto Rico. The location of CRL 844 relative to the study area is illustrated by the red point in Figure 3-6.

Figure 3-5. Network of CRLs for the CHS.

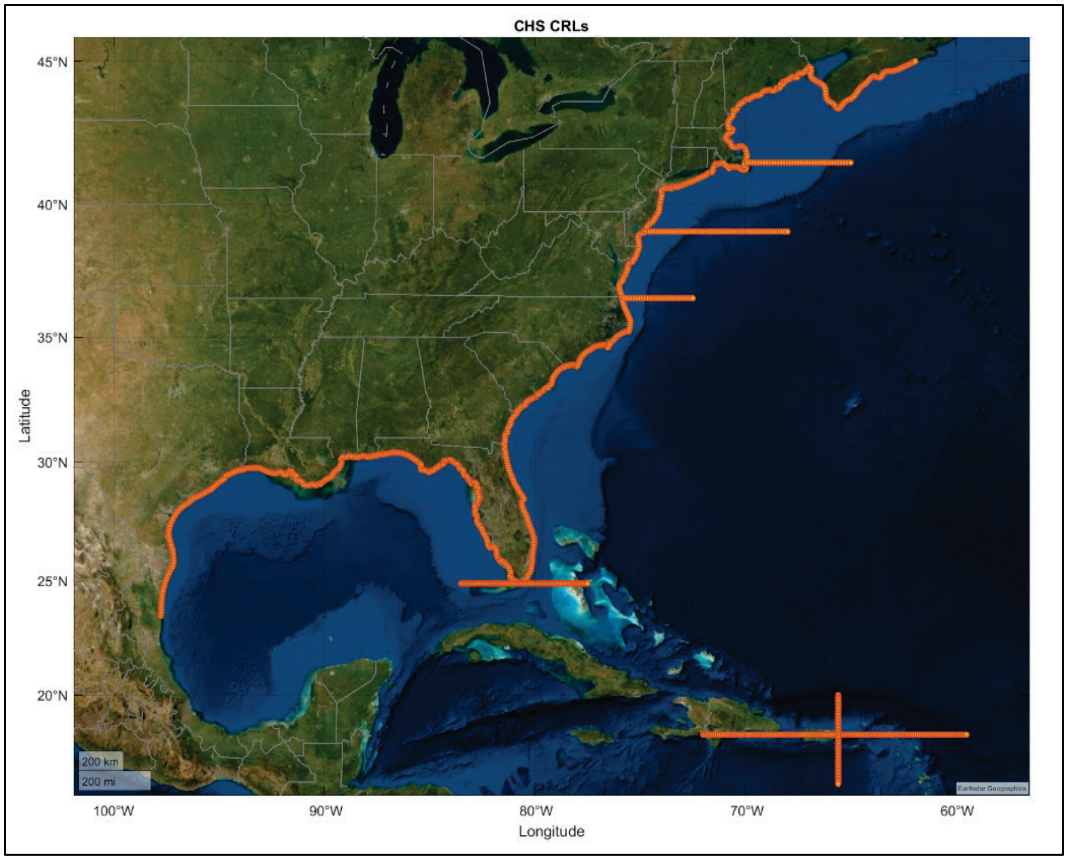

Figure 3-6. CRLs 781–914 (blue) used in the PCHA for the CHS-PR study area.

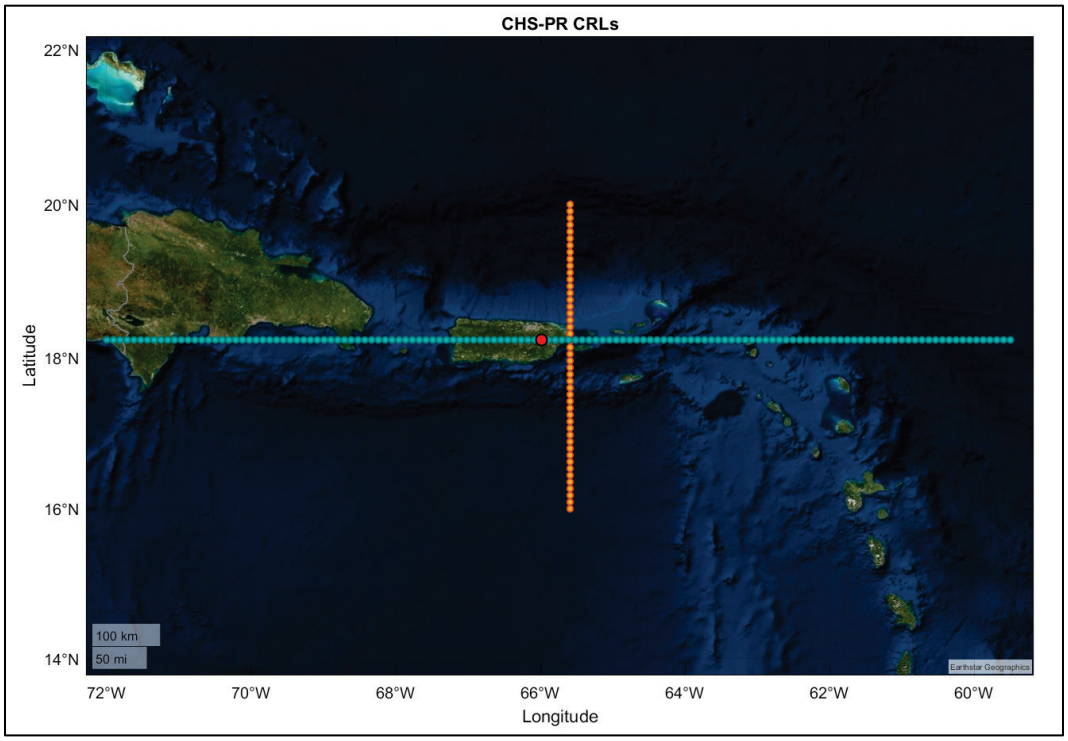

3.4 Selection and stratification of historical tropical cyclones (TCs)

The probabilistic characterization of storm climatology for the CHS-PR region requires sampling a set of storms from the historical record (i.e., HURDAT2, EBTRK). The PCHA is then performed with this set of TCs as its basis, including the computation of SRR, and development of marginal distributions of individual TC parameters. As previously discussed, the sampling of historical TCs for the SRR and the fitting of marginal distributions was limited to the 1938–2019 period.

In the PCHA framework, TCs are sampled on a per CRL basis. TCs with $\Delta p \geq 8$ hPa that are within 600 km of a CRL are selected and assigned to that specific CRL. Note that Δp is computed as the difference between a far-field atmospheric pressure of 1,013 hPa and the TC minimum central pressure (c_p) taken at the center of the TC (FEMA 2008). The sampling process is repeated for each of the 1,025 CRLs. For CHS-PR, the tracks of the 300 synthetic TCs cross the horizontal line (Figure 3-6) defined by CRLs 781 through 914. Therefore, CRLs 781-914 were used for the selection of historical TCs and the characterization of the regional climatology through the PCHA.

For the selected TCs, an assessment of track points is performed to identify the closest point of highest intensity to each CRL using Equation 3-1. For each TC, all track points within the 600 km radius are evaluated to ensure the selection of the most influential track location, considering both TC intensity and distance from the CRL. The intensity index function (Nadal-Caraballo et al. 2015) defined by Equation 3-1 is applied to determine the optimal sampling location along each track:

$$I_{\Delta p_i} = w(d_i)\Delta p_i \tag{3-1}$$

where $I_{\Delta p_i}$ = TC intensity index for a given TC, computed at all track points within 600 km of a particular CRL; Δp_i = central pressure deficit at individual track points; $w(d_i)$ = distance-adjusted Gaussian weights from the GKF method developed by Chouinard and Liu (1997); and d_i = distance from the location of interest (CRL) to a track point (kilometer).

The distance-adjusted Gaussian weights were calculated considering the distance between TC track points and each CRL as follows:

$$w(d_i) = \frac{1}{\sqrt{2\pi}h_d} exp\left[-\frac{1}{2}\left(\frac{d_i}{h_d}\right)^2\right] \quad (3\text{-}2)$$

where h_d = optimal kernel size (kilometer). The optimal kernel size applied in the study was 200 km, consistent with the value selected from numerical experiments described in Nadal-Caraballo et al. (2019). In the PCHA, each CRL within the boundaries of the study area has its own set of sampled storms. For each CRL, the most influential track location is identified in the probabilistic analysis as the point along each TC track with the largest $I_{\Delta p_i}$. This results in a storm sampling approach that is consistent with the GKF method. This approach also balances (1) the distances from historical TC tracks to the study's CRLs and (2) the intensity of the selected TCs. Therefore, it avoids the bias that could be introduced by either sampling TC track points only considering their shortest distance to a CRL or, conversely, by sampling TCs only at their peak of intensity regardless of the distance to the CRL. Considering CRL and TC track pairs, the track point with the shortest distance to the CRL will generally be selected unless one of the next closest track points (with similar distance) has significantly higher intensity, in which case the latter will be selected. The R_{max}, V_t, and θ were identified from this optimal sampling location for the marginal distribution development. Figure 3-7 shows the optimal sampling locations from TCs selected for CRL 844. Further discussion on using a kernel size of 200 km and sampling storms within 600 km as it relates to the computation of SRR of each CRL is provided in Section 3.5.

Figure 3-7. Optimal sampling locations of selected historical TCs within 600 km of CRL 844 (blue point).

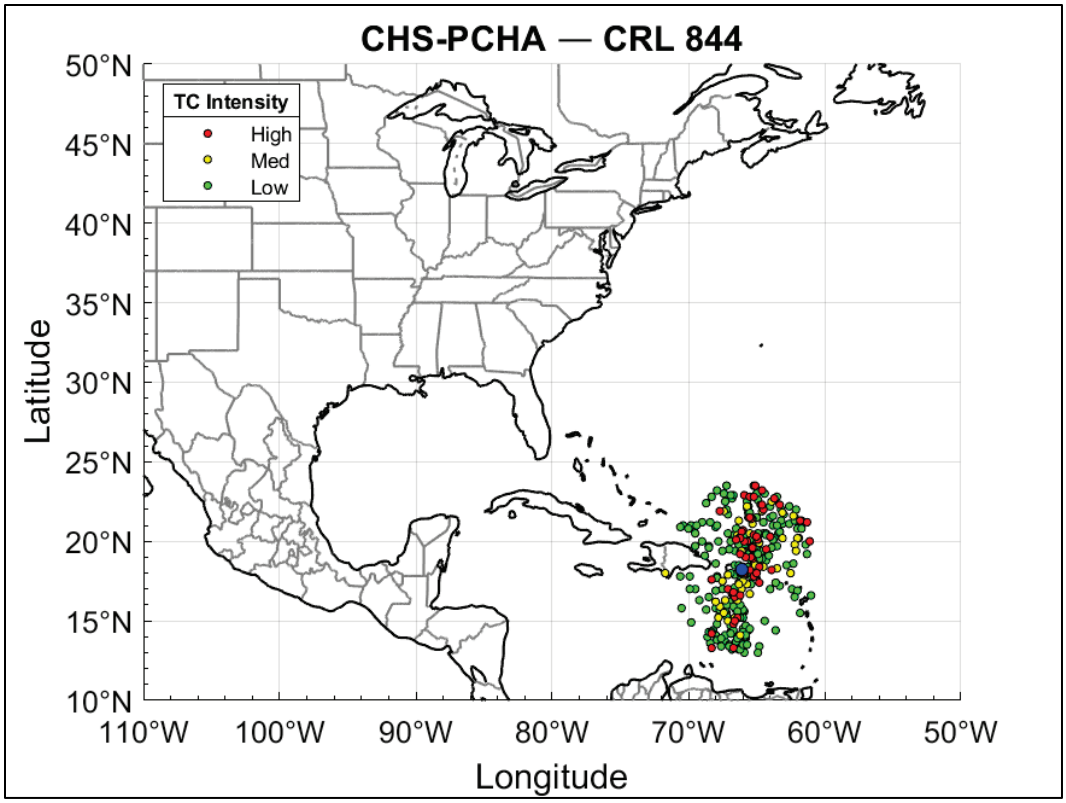

After the historical TCs are selected, they are stratified according to their intensity, as defined by central pressure deficit:

- Low intensity (LI); $8 \le \Delta p < 28$ hPa
- Medium intensity (MI); $28 \le \Delta p < 48$ hPa
- High intensity (HI); $\Delta p \ge 48$ hPa.

Partitioning TCs into low, medium, and high-intensity strata is primarily done to account for potential differences in the correlation of pairs of atmospheric-forcing parameters between intense and weak cyclones. The PCHA seeks to represent the categories defined by the NHC's Saffir-Simpson Hurricane Wind Scale (SSHWS) (NHC 2022) using these three strata. Regarding the maximum sustained wind speed categories established by the SSHWS, generally, the LI stratum represents TCs of tropical-storm intensity, whereas the MI stratum is intended to capture Category 1 and 2 hurricanes. Similarly, Category 3 through 5 hurricanes are covered by the HI stratum. Note that since the correlation between Δp and wind speed is high but less than unity, there is some variability in the SSHWS categories represented by each intensity stratum.

3.5 Geospatial storm recurrence rate (SRR)

TC sampling from the historical records and robust statistical computation of SRR can be achieved through several different approaches. In recent studies, some of the methods used to compute the geospatial variation of SRR have included area-crossing, line-crossing, GKF, and other combined methods. Area-crossing and line-crossing are examples of capture zone methods. In the area-crossing approach, only storms passing through a particular area are counted in the computation of the SRR. The line-crossing approach usually consists of an idealized coastline or a reference line representing a segment of the coastline. Only storms making landfall along the chosen segment of coastline are captured and counted towards the computation of the SRR. The SRR is the single most significant parameter in the JPM (Nadal-Caraballo et al. 2019a) and the PCHA framework, given that it describes the expected annual recurrence of storms at locations of interest or CRLs.

Capture zones can also be defined in other ways, such as a rectangular or circular window or any other finite geospatial region. In past studies, the standard had been to apply any of the capture zone methods to count the storms and to assign uniform weights to all captured storms. The main limitation of the capture zone approach is that, while all storms within the chosen capture zone are given uniform weights, storms outside this zone are given a weight of zero. The conundrum lies in establishing a capture zone large enough to reduce the uncertainty associated with sample size by capturing an adequate number of storms from which significant statistics can be derived but small enough to balance the uncertainty associated with geospatial variability and population heterogeneity.

Nadal-Caraballo et al. (2019) conducted an extensive evaluation of different methods for the computation of SRR, including GKF, uniform kernel function (UKF), and the Epanechnikov kernel function (EKF). The curves of relative distance-adjusted weights for the UKF, GKF, and EKF with a kernel size of 200 km are shown in Figure 3-8. The curves are shown relative to the weight of a TC track point located at the CRL (distance = 0 km). All three kernel functions decrease with distance from the CRL, as expected. The weights of both UKF and EKF decrease to zero when the distance reaches the kernel size of 200 km. On the other hand, the GKF weight decreases following the well-known bell shape,

decreasing almost to zero at a distance of 600 km and extending indefinitely afterward.

Figure 3-8. UKF, GKF, and EKF weights as a function of distance from CRL.

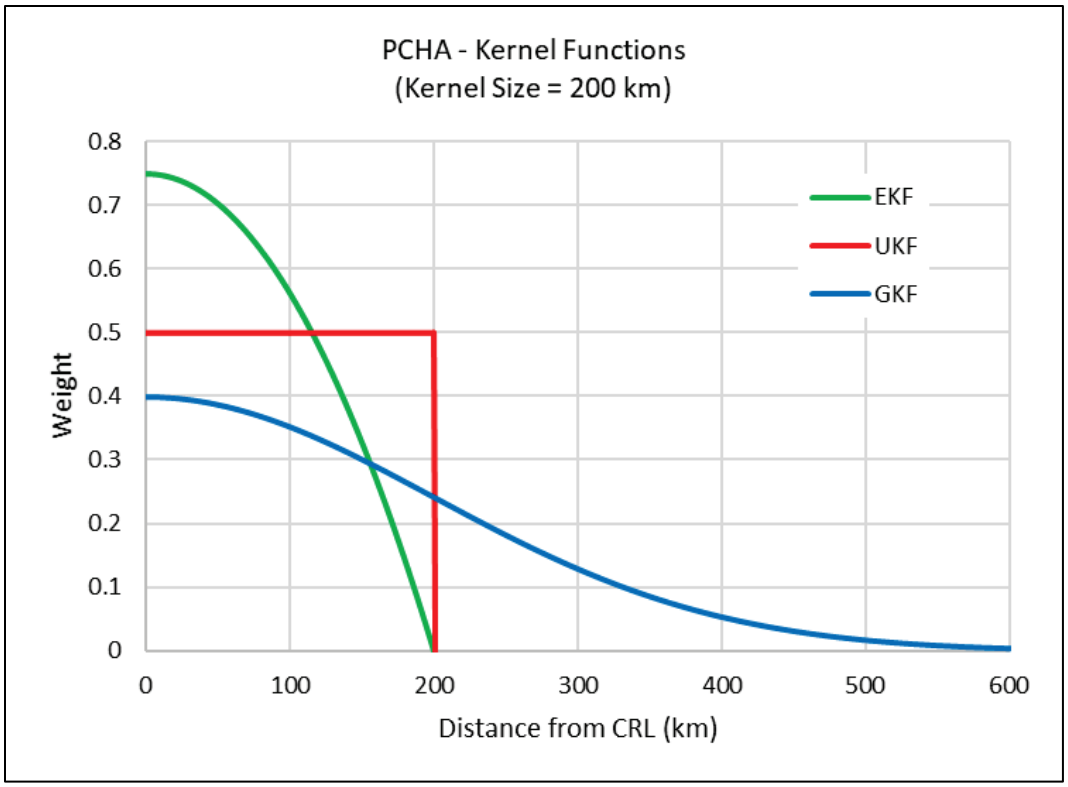

The study by Nadal-Caraballo et al. (2019) also found that the line-crossing approach can lead to underestimating the hazard due to its exclusion of bypassing events. The area-crossing method was treated as a special case of the kernel approach through the application of the UKF. A significant advantage of the GKF is that it can consider a larger number of storms than the capture zone approach and the EKF. For the same ranges of optimal capture zone radii and Gaussian kernel sizes, the GKF SRR estimates exhibited a reduced coefficient of variation when compared to UKF estimates. The GKF was deemed to be the best method to be used for conducting the SRR computational experiments.

As discussed above, the GKF method, developed by Chouinard and Liu (1997), can overcome the main limitations of capture zone approaches. The standard application of the GKF consists of establishing a grid of nodes where estimates of the SRR are sought. All storms within this gridded space can be counted at any given node, but the weight assigned to each storm decreases with increasing distance from storm to node. The

GKF SRR equation, with $w(d_i)$ = Gaussian distance-adjusted weights given by Equation (3-2), has the form:

$$\lambda = \frac{1}{T}\sum_i^n w(d_i) \quad (3\text{-}3)$$

where λ = SRR in storms/yr/km; T = record length in (yr); and d_i = distance from location of interest (e.g., CRL) to a track point (kilometer). Using the GKF weights minimizes sample size uncertainty by taking full advantage of all available storm data while significantly reducing the uncertainty associated with geospatial variability and potentially heterogeneous populations.

The PCHA for CHS-PR adopted an optimal kernel size of 200 km, similar to previous studies such as the CTXS and the CHS-LA study. Since the kernel size is representative of a standard deviation, TCs were sampled at a distance of three standard deviations, or 3*h_d. In previous studies such as NACCS, a distance of 800 km was chosen for sampling landfalling storms. However, further evaluations have shown that no measurable differences in SRR are observed between a sampling radius of 600 km and 800 km. This study subsequently used a sampling distance of 600 km for the calculation of SRR for each CHS-PR CRL. Table 3-2 summarizes the SRR results for All TCs, as well as High, Medium, and Low TC intensities at the 134 CRLs considered for the CHS-PR PCHA. Additionally, Figures 3-9 through 3-12 illustrate the geospatial variance in SRR across the Caribbean for each TC intensity stratum. Note the scale applied to Figures 3-9 through 3-12 varies with the change in the intensity stratum under consideration.

Figure 3-9. Geospatial SRR for All TCs within the CHS-PR study area.

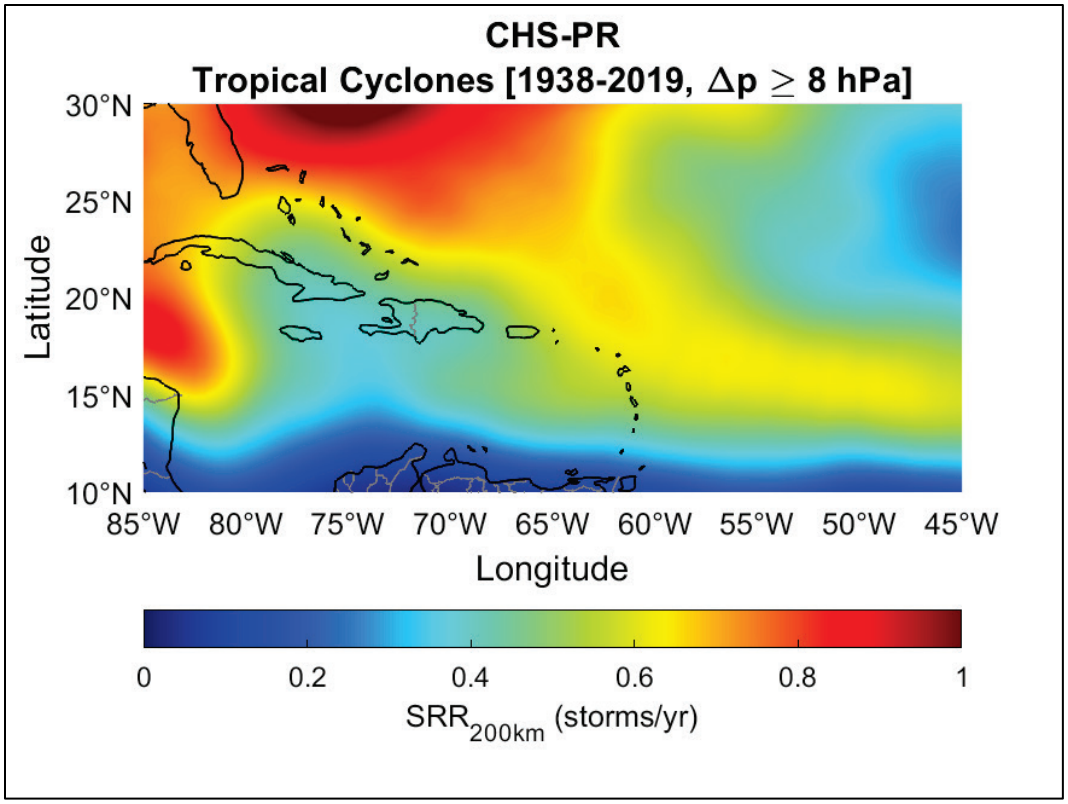

Figure 3-10. Geospatial SRR for HI TCs within the CHS-PR study area.

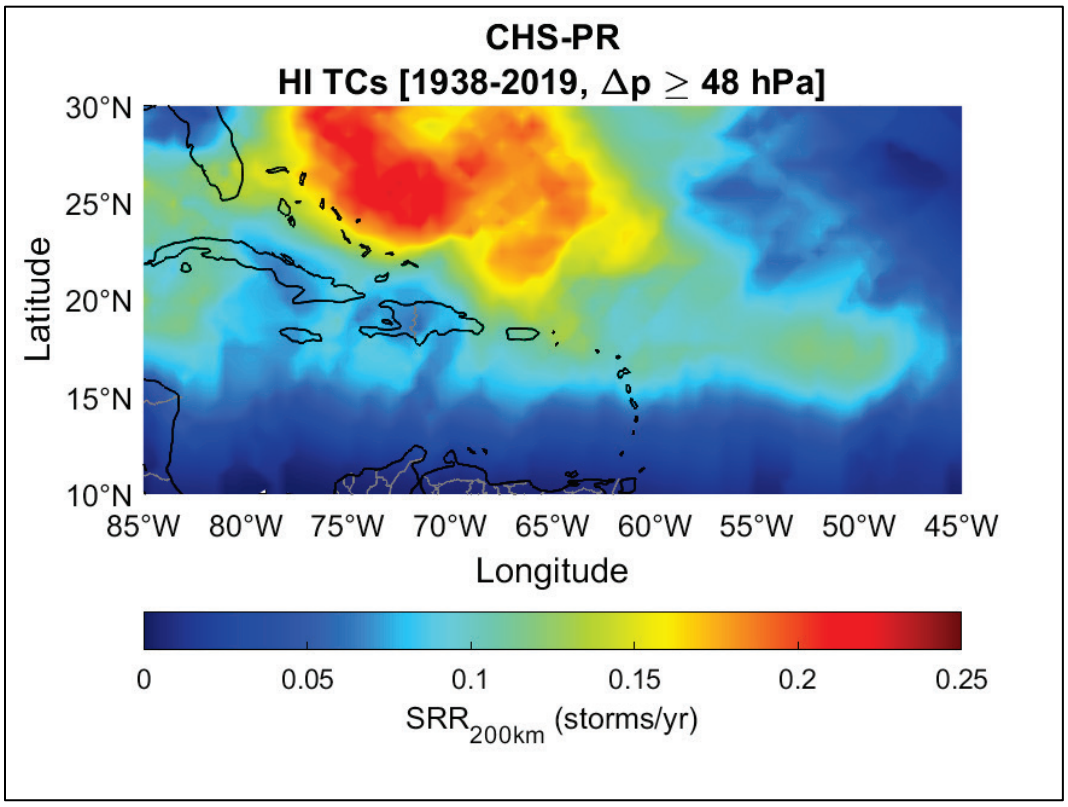

Figure 3-11. Geospatial SRR for MI TCs within the CHS-PR study area.

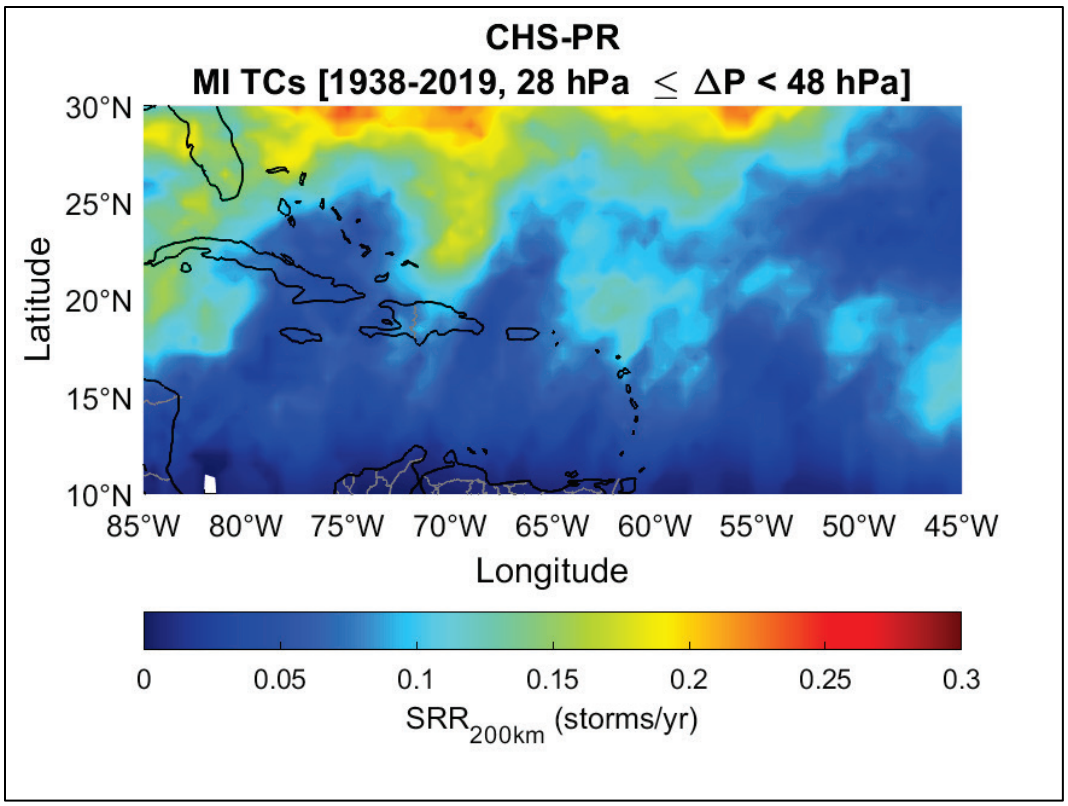

Figure 3-12. Geospatial SRR for LI TCs within the CHS-PR study area.

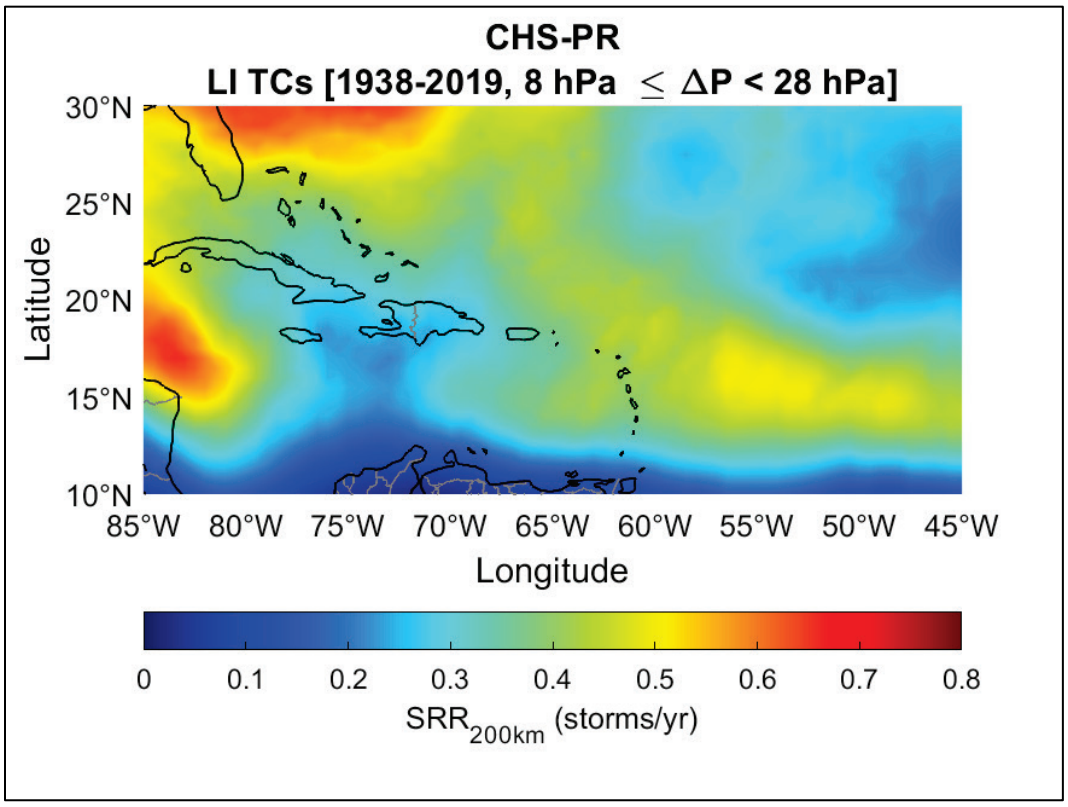

Table 3-2. SRR results for TC intensity strata and CRLs in the CHS-PR study area.

CRL	SRR (storms/yr/km)			
	LI	MI	HI	Total
781	5.65E-04	1.86E-04	2.41E-04	9.92E-04
782	5.69E-04	1.87E-04	2.38E-04	9.94E-04
783	5.72E-04	1.88E-04	2.36E-04	9.96E-04
784	5.76E-04	1.88E-04	2.34E-04	9.98E-04
785	5.79E-04	1.89E-04	2.31E-04	1.00E-03
786	5.82E-04	1.89E-04	2.28E-04	1.00E-03
787	5.84E-04	1.90E-04	2.26E-04	1.00E-03
788	5.86E-04	1.90E-04	2.25E-04	1.00E-03
789	5.88E-04	1.90E-04	2.24E-04	1.00E-03
790	5.89E-04	1.97E-04	2.16E-04	1.00E-03
791	5.89E-04	2.00E-04	2.12E-04	1.00E-03
792	5.90E-04	2.01E-04	2.10E-04	1.00E-03
793	5.92E-04	2.09E-04	2.02E-04	1.00E-03
794	5.94E-04	2.10E-04	2.01E-04	1.00E-03
795	5.97E-04	2.11E-04	2.01E-04	1.01E-03
796	6.00E-04	2.11E-04	2.00E-04	1.01E-03
797	6.03E-04	1.89E-04	2.23E-04	1.01E-03
798	6.18E-04	1.85E-04	2.14E-04	1.02E-03
799	6.19E-04	1.86E-04	2.15E-04	1.02E-03
800	6.25E-04	1.81E-04	2.15E-04	1.02E-03
801	6.28E-04	1.78E-04	2.18E-04	1.02E-03
802	6.22E-04	1.98E-04	2.07E-04	1.03E-03
803	6.01E-04	2.19E-04	2.09E-04	1.03E-03
804	6.00E-04	1.98E-04	2.34E-04	1.03E-03
805	6.00E-04	2.00E-04	2.35E-04	1.03E-03
806	6.00E-04	1.94E-04	2.44E-04	1.04E-03
807	5.99E-04	1.95E-04	2.46E-04	1.04E-03
808	6.00E-04	1.89E-04	2.55E-04	1.04E-03
809	6.00E-04	1.90E-04	2.57E-04	1.05E-03
810	6.02E-04	1.89E-04	2.58E-04	1.05E-03

Table 3-2. (cont.) SRR results for TC intensity strata and CRLs in the CHS-PR study area.

CRL	SRR (storms/yr/km)			
	LI	MI	HI	Total
811	6.03E-04	1.92E-04	2.59E-04	1.05E-03
812	6.10E-04	1.87E-04	2.60E-04	1.06E-03
813	6.12E-04	1.88E-04	2.62E-04	1.06E-03
814	6.16E-04	1.90E-04	2.62E-04	1.07E-03
815	6.33E-04	1.78E-04	2.64E-04	1.07E-03
816	6.36E-04	1.80E-04	2.67E-04	1.08E-03
817	6.62E-04	1.58E-04	2.69E-04	1.09E-03
818	6.64E-04	1.59E-04	2.71E-04	1.09E-03
819	6.66E-04	1.61E-04	2.74E-04	1.10E-03
820	6.67E-04	1.62E-04	2.78E-04	1.11E-03
821	6.93E-04	1.40E-04	2.81E-04	1.11E-03
822	6.95E-04	1.40E-04	2.83E-04	1.12E-03
823	6.98E-04	1.41E-04	2.85E-04	1.12E-03
824	7.22E-04	1.23E-04	2.85E-04	1.13E-03
825	7.27E-04	1.24E-04	2.88E-04	1.14E-03
826	7.32E-04	1.24E-04	2.91E-04	1.15E-03
827	7.38E-04	1.25E-04	2.94E-04	1.16E-03
828	7.45E-04	1.27E-04	2.97E-04	1.17E-03
829	7.52E-04	1.28E-04	3.01E-04	1.18E-03
830	7.61E-04	1.42E-04	2.89E-04	1.19E-03
831	7.67E-04	1.67E-04	2.69E-04	1.20E-03
832	7.74E-04	1.69E-04	2.72E-04	1.21E-03
833	7.79E-04	1.70E-04	2.75E-04	1.22E-03
834	7.83E-04	1.71E-04	2.79E-04	1.23E-03
835	7.87E-04	1.71E-04	2.82E-04	1.24E-03
836	8.15E-04	1.48E-04	2.84E-04	1.25E-03
837	8.18E-04	1.49E-04	2.87E-04	1.25E-03
838	8.22E-04	1.51E-04	2.89E-04	1.26E-03
839	8.27E-04	1.52E-04	2.92E-04	1.27E-03
840	8.32E-04	1.62E-04	2.87E-04	1.28E-03

Table 3-2. (cont.) SRR results for TC intensity strata and CRLs in the CHS-PR study area.

CRL	SRR (storms/yr/km)			
	LI	MI	HI	Total
841	8.37E-04	1.63E-04	2.90E-04	1.29E-03
842	8.42E-04	1.65E-04	2.93E-04	1.30E-03
843	8.48E-04	1.51E-04	3.11E-04	1.31E-03
844	8.53E-04	1.51E-04	3.16E-04	1.32E-03
845	8.68E-04	1.43E-04	3.20E-04	1.33E-03
846	8.81E-04	1.36E-04	3.25E-04	1.34E-03
847	8.85E-04	1.36E-04	3.29E-04	1.35E-03
848	8.80E-04	1.46E-04	3.33E-04	1.36E-03
849	8.84E-04	1.61E-04	3.21E-04	1.37E-03
850	8.87E-04	1.62E-04	3.25E-04	1.37E-03
851	8.91E-04	1.63E-04	3.29E-04	1.38E-03
852	8.77E-04	1.81E-04	3.32E-04	1.39E-03
853	8.82E-04	1.83E-04	3.36E-04	1.40E-03
854	8.86E-04	1.98E-04	3.24E-04	1.41E-03
855	8.91E-04	2.00E-04	3.27E-04	1.42E-03
856	8.96E-04	2.02E-04	3.29E-04	1.43E-03
857	8.83E-04	2.21E-04	3.31E-04	1.43E-03
858	8.71E-04	2.38E-04	3.34E-04	1.44E-03
859	8.74E-04	2.40E-04	3.36E-04	1.45E-03
860	8.78E-04	2.50E-04	3.31E-04	1.46E-03
861	8.81E-04	2.52E-04	3.33E-04	1.47E-03
862	8.84E-04	2.54E-04	3.34E-04	1.47E-03
863	8.87E-04	2.56E-04	3.36E-04	1.48E-03
864	8.90E-04	2.58E-04	3.38E-04	1.49E-03
865	9.04E-04	2.50E-04	3.39E-04	1.49E-03
866	9.09E-04	2.65E-04	3.29E-04	1.50E-03
867	9.14E-04	2.68E-04	3.30E-04	1.51E-03
868	9.22E-04	2.68E-04	3.31E-04	1.52E-03
869	9.27E-04	2.70E-04	3.32E-04	1.53E-03
870	9.32E-04	2.72E-04	3.33E-04	1.54E-03

Table 3-2. (cont.) SRR results for TC intensity strata and CRLs in the CHS-PR study area.

CRL	SRR (storms/yr/km)			
	LI	MI	HI	Total
871	9.35E-04	2.74E-04	3.34E-04	1.54E-03
872	9.38E-04	2.75E-04	3.35E-04	1.55E-03
873	9.52E-04	2.65E-04	3.35E-04	1.55E-03
874	9.72E-04	2.47E-04	3.35E-04	1.55E-03
875	9.52E-04	2.71E-04	3.35E-04	1.56E-03
876	9.54E-04	2.73E-04	3.34E-04	1.56E-03
877	9.62E-04	2.68E-04	3.34E-04	1.56E-03
878	9.67E-04	2.68E-04	3.34E-04	1.57E-03
879	9.69E-04	2.70E-04	3.33E-04	1.57E-03
880	9.46E-04	3.11E-04	3.16E-04	1.57E-03
881	9.22E-04	3.40E-04	3.12E-04	1.57E-03
882	9.21E-04	3.43E-04	3.11E-04	1.58E-03
883	9.22E-04	3.45E-04	3.11E-04	1.58E-03
884	9.45E-04	3.48E-04	2.89E-04	1.58E-03
885	9.47E-04	3.50E-04	2.90E-04	1.59E-03
886	9.50E-04	3.50E-04	2.90E-04	1.59E-03
887	9.50E-04	3.52E-04	2.91E-04	1.59E-03
888	9.53E-04	3.52E-04	2.91E-04	1.60E-03
889	9.79E-04	3.29E-04	2.92E-04	1.60E-03
890	9.81E-04	3.32E-04	2.90E-04	1.60E-03
891	9.86E-04	3.50E-04	2.69E-04	1.61E-03
892	9.87E-04	3.51E-04	2.70E-04	1.61E-03
893	9.87E-04	3.55E-04	2.67E-04	1.61E-03
894	1.01E-03	3.36E-04	2.68E-04	1.61E-03
895	9.86E-04	3.59E-04	2.68E-04	1.61E-03
896	9.85E-04	3.59E-04	2.68E-04	1.61E-03
897	9.83E-04	3.60E-04	2.68E-04	1.61E-03
898	9.79E-04	3.62E-04	2.69E-04	1.61E-03
899	9.77E-04	3.44E-04	2.87E-04	1.61E-03
900	9.74E-04	3.45E-04	2.88E-04	1.61E-03

Table 3-2. (cont.) SRR results for TC intensity strata and CRLs in the CHS-PR study area.

CRL	SRR (storms/yr/km)			
	LI	MI	HI	Total
901	9.75E-04	3.43E-04	2.88E-04	1.61E-03
902	9.75E-04	3.61E-04	2.70E-04	1.61E-03
903	9.75E-04	3.61E-04	2.71E-04	1.61E-03
904	9.74E-04	3.61E-04	2.72E-04	1.61E-03
905	9.92E-04	3.41E-04	2.71E-04	1.60E-03
906	1.01E-03	3.24E-04	2.72E-04	1.60E-03
907	1.00E-03	3.23E-04	2.73E-04	1.60E-03
908	9.98E-04	3.23E-04	2.74E-04	1.59E-03
909	1.04E-03	2.79E-04	2.70E-04	1.59E-03
910	1.04E-03	2.71E-04	2.71E-04	1.59E-03
911	1.04E-03	2.80E-04	2.61E-04	1.58E-03
912	1.04E-03	2.78E-04	2.62E-04	1.58E-03
913	1.06E-03	2.60E-04	2.62E-04	1.58E-03
914	1.04E-03	2.68E-04	2.63E-04	1.58E-03

3.6 Distance adjustment of historical TCs

JPM-OS studies have often sampled TCs that are hundreds of kilometers away from the areas of interest simply because its track crossed an idealized coastline. In previous studies, for example, TCs making landfall near the Florida Keys have been sampled for study areas as far away as Alabama or Mississippi. The geospatial and temporal occurrence of TCs is a natural stochastic process. As such, it is difficult to justify that a TC making landfall 500 km away from the study area is more relevant to the area's climatology than a bypassing TC just 250 km away.

For this reason, the PCHA framework has adopted a normalization and distance-adjustment approach for the sampled historical TCs. As discussed in Section 3.4, all TCs within 600 km from each CRL are sampled and assigned to that particular CRL. Continuing with the example above, and analogous to the computation of SRR, a bypassing TC just offshore of a CRL in Puerto Rico should carry more weight relative to that CRL than a TC making landfall in Florida. Therefore, the concept of computing geospatial SRR through the application of GKF and distance weights is extended to the selected TCs. The GKF is employed to generate distance weights required for the normalization of the TC parameters. The goal is to transform the TC parameters so the sampled population reflects distance-weighted mean and standard deviation.

Z-score normalization is a common technique used by machine learning practitioners to adjust population parameters even if the populations are not normally distributed. The first step in the normalization of a TC parameter (x_i) (e.g., one set of values per TC taken at the optimal sampling location relative to a CRL) is the computation of the mean (μ) and standard deviation (σ) of the parameter for the i-th sampled TC:

$$\mu = \frac{\sum_{i=1}^{N} x_i}{N} \tag{3-4}$$

$$\sigma = \sqrt{\frac{\sum_{i=1}^{N} (x_i - \mu)^2}{N-1}} \tag{3-5}$$

The normalized TC parameters (z_i) are determined through the basic z-score formula:

$$z_i = \frac{x_i - \mu}{\sigma} \tag{3-6}$$

The next step is the computation of distance-weighted mean (μ_{DW}) and standard deviation (σ_{DW}) for each TC parameter:

$$\mu_{DW} = \frac{\sum_{i=1}^{N} w(d_i) x_i}{\sum_{i=1}^{N} w(d_i)} \tag{3-7}$$

$$\sigma_{DW} = \sqrt{\frac{\sum_{i=1}^{N} w(d_i)(x_i - \mu_{DW})^2}{\left(\frac{\acute{N}-1}{\acute{N}}\right)\sum_{i=1}^{N} w(d_i)}} \tag{3-8}$$

where $w(d_i)$ = distance weights computed using the GKF (Equation 3-2); x_i = individual parameter values of sampled TCs (i.e., one set of parameters per TC taken at the optimal sampling location relative to a CRL); and N = number of sampled TCs, and $\acute{N}$= number of sampled TCs with non-zero weights. Finally, the adjusted TC parameters (x'_i) are obtained from the following equation:

$$x'_i = z_i \sigma_{DW} + \mu_{DW} \tag{3-9}$$

The historical TCs sampled from the HURDAT2 data set within 600 km of CRL 844 (1938–2019 period) and their distance-adjusted atmospheric parameters are listed in Appendix A.

4 Joint Probability Analysis of Coastal Storm Hazards

Most joint probability analyses of coastal storm hazards in hurricane-prone regions, including the PCHA, require the development of synthetic TC suites to effectively cover the TC parameter and probability spaces. Given that the PCHA framework builds upon the JPM approach, it employs the same primary TC atmospheric-forcing parameters: track reference location (x_o); track heading direction (θ); central pressure deficit (Δp); radius of maximum winds (R_{max}); and forward translation speed (V_t). These TC parameters are required as inputs to the PBL model used to generate wind and pressure fields for each storm. The work described here consists of fitting TC parameter probability distributions and the correlation analysis. The selection of a parametric or non-parametric probability distribution to characterize the likelihood of a given TC parameter is ultimately based on expert judgment. There is no single best solution.

Sections 4.1 and 4.2 describe the development of marginal probability distributions and correlation coefficients used in the joint probability model needed for estimating AEFs. The ITCS and ATCS developed for this study, and the computation of DSWs are documented in Sections 4.3 and 4.4.

4.1 Marginal distributions of TC parameters

The development of probability distributions was required to characterize the storm climatology for constructing the CHS-PR synthetic storm suite. These distributions were developed from the HURDAT2 1938–2019 data record, which were used to assess the historical maxima and variances of the individual TC atmospheric-forcing parameters. This section discusses the PCHA steps to develop marginal distributions at the 134 CRLs specific to the CHS-PR and provides examples of plots and marginal distributions at CRL 844.

As discussed in Section 3.4, for each TC track, the forcing parameters were selected at an optimal location, balancing intensity and distance from a given CRL. Marginal probability distributions were then fit to the distance-adjusted TC parameters. The historical TCs sampled from the HURDAT2 database within 600 km from CRL 844 (1938–2019 period) and their distance-adjusted atmospheric parameters are listed in

Appendix A. Sections 4.1.1 through 4.1.4 discuss the distribution fitted to each parameter.

4.1.1 Central pressure deficit (Δp)

The central pressure, c_p, is an inversely proportional measurement of TC intensity, meaning that as TC intensity increases, the value of c_p decreases. However, for convenience and to facilitate statistical analyses, hurricane intensity is usually expressed in terms of Δp. It is common practice to use these parameters interchangeably. In most JPM studies, the Δp has been computed from an assumed far-field atmospheric pressure of 1,013 hPa, known as the standard atmospheric pressure.

Past JPM studies have typically chosen either the Weibull or the Gumbel distribution to fit Δp, resulting in very similar storm surge hazard curves (USACE 2009b, 2011). The probabilistic model of Δp is represented in the PCHA by the Weibull distribution:

$$F[\Delta p > x] = 1 - exp\left[-\left(\frac{x}{U}\right)^k\right] \quad (4\text{-}1)$$

where U = scale parameter and k = shape parameter. The Weibull best fit is shown in Figures 4-1 and 4-2. Since the PCHA employs TC intensity stratification (i.e., LI, MI, and HI), a doubly-truncated Weibull distribution (DTWD) is used to characterize the data from these strata. Figure 4-1 illustrates the Weibull best fit for Δp values ranging from $8 \leq x < 28$ hPa. In Figure 4-2, the Weibull is fit to Δp values truncated at 28 and 148 hPa. Note that in Figures 4-1 through 4-14, the legend "Emp" refers to historical data plotted using the Weibull plotting position formula.

Figure 4-1. The doubly truncated Weibull distribution (DTWD) for sampled Δp ranging from 8 to less than 28 hPa at CRL 844.

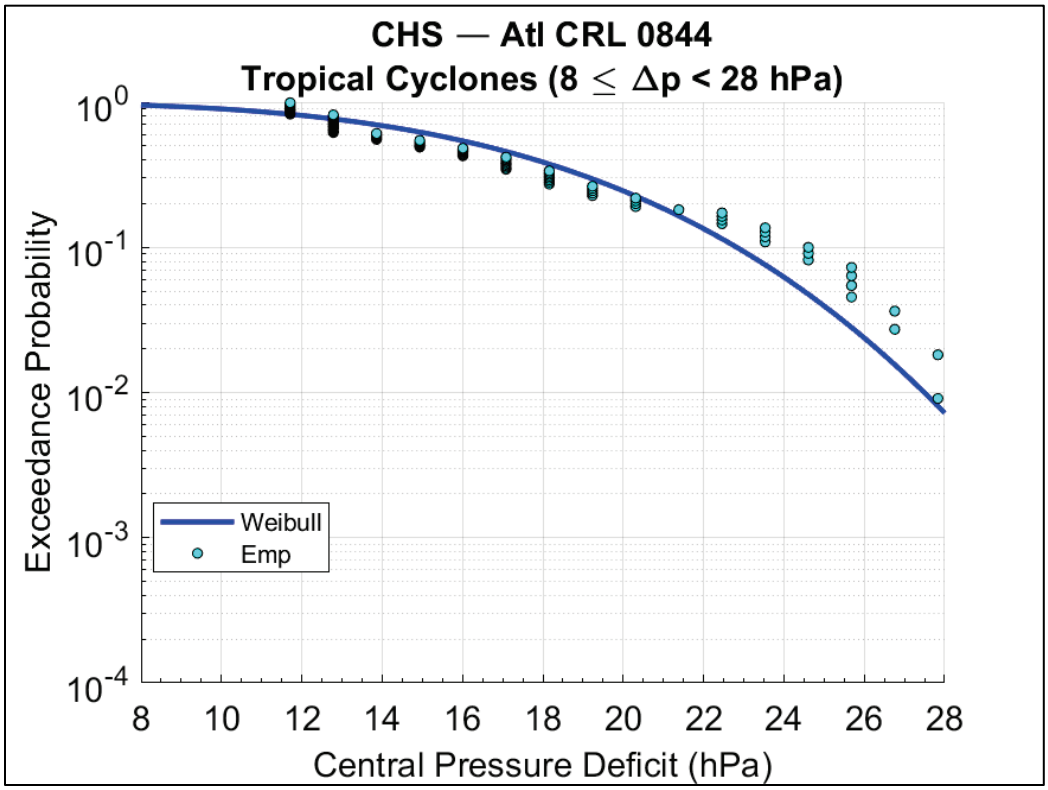

Figure 4-2. DTWD for all sampled Δp of 28 to 148 hPa at CRL 844.

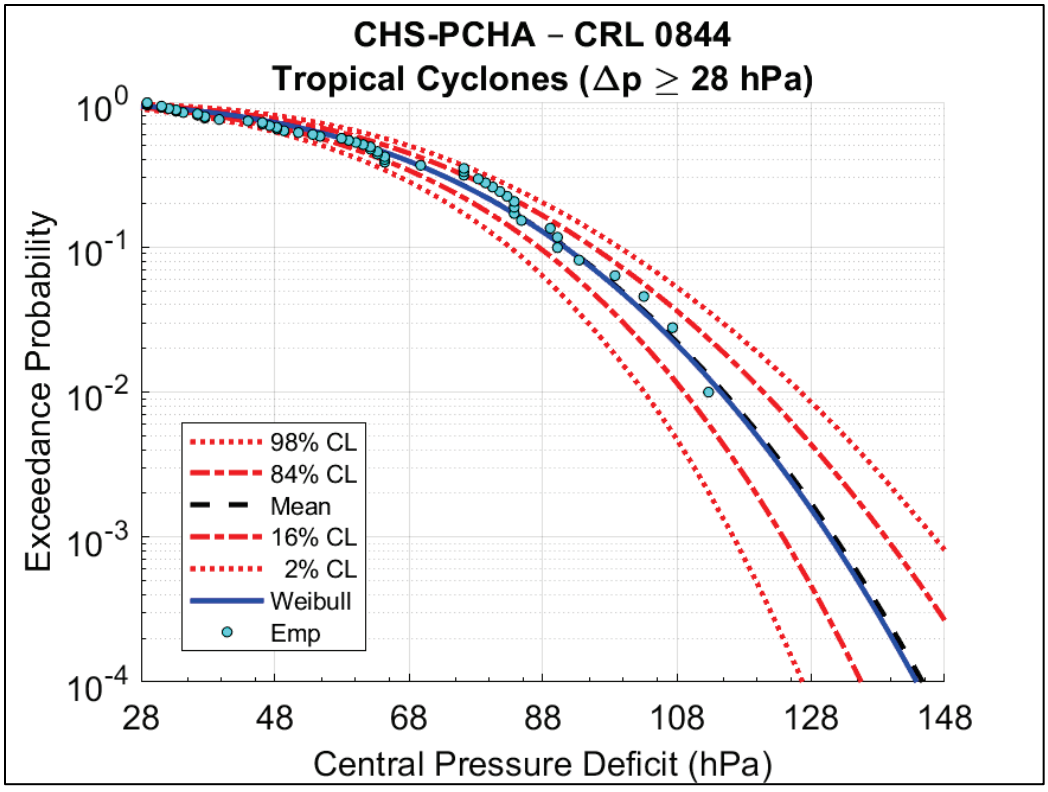

The scale parameter, shape parameter, and truncation limits of the Δp for CRL 844 are listed in Table 4-1. The Weibull distribution fits corresponding to each intensity group are shown in Figures 4-3, 4-4, and 4-5.

Table 4-1. Marginal distribution parameters of Δp at CRL 844.

TC Intensity	U	k	Δp_1	Δp_2
High (DTWD)	69.4	3.04	48	148
Medium (DTWD)	69.4	3.04	28	48
Low (DTWD)	18.2	3.73	8	28

Figure 4-3. Marginal distribution (DTWD) of Δp for HI TCs at CRL 844.

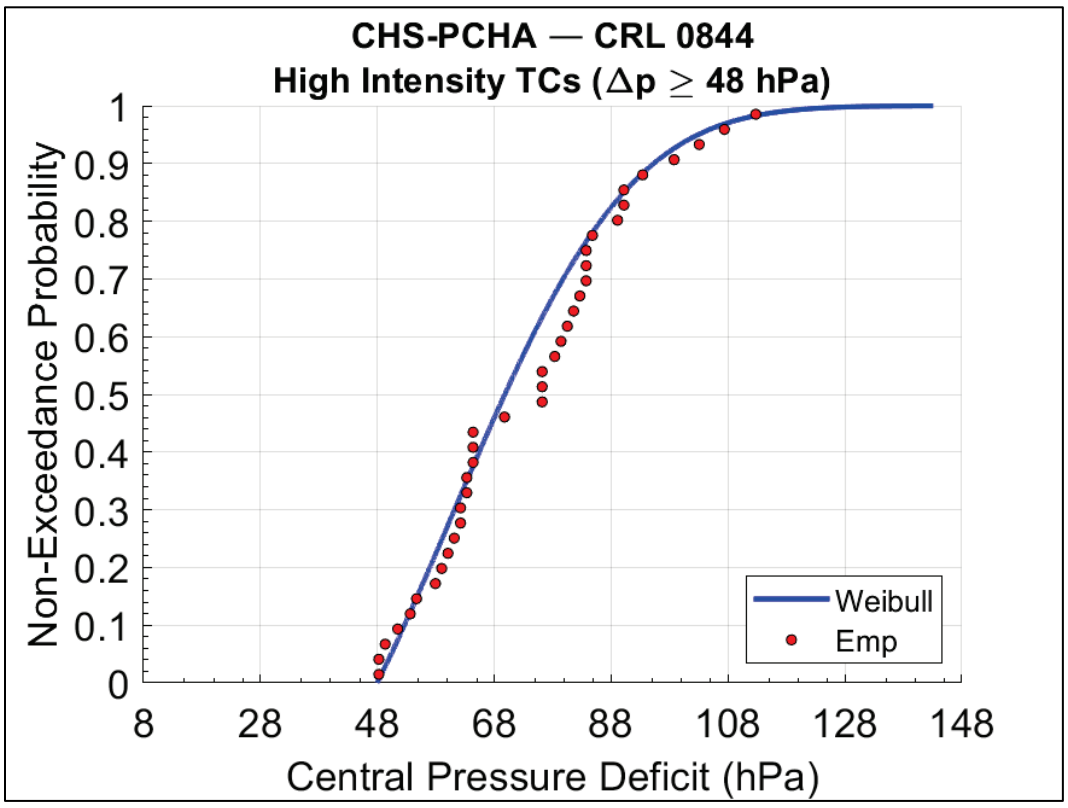

Figure 4-4. Marginal distribution (DTWD) of Δp for MI TCs at CRL 844.

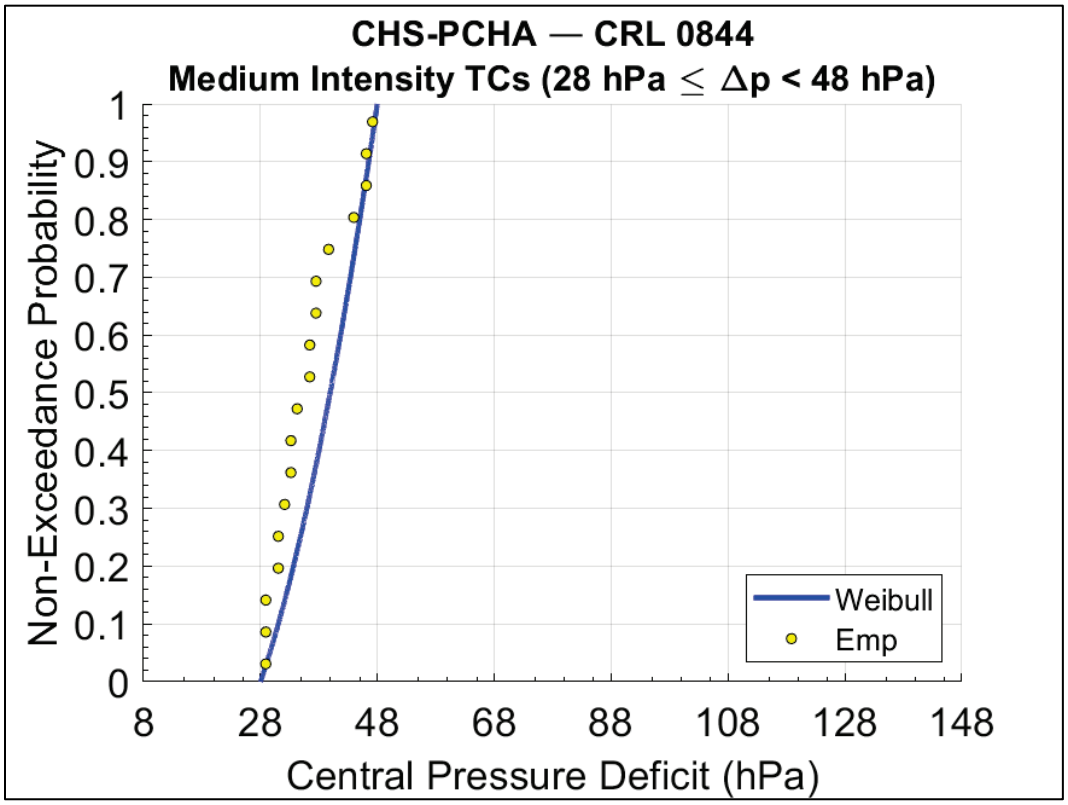

Figure 4-5. Marginal distribution (DTWD) of Δp for LI TCs at CRL 844.

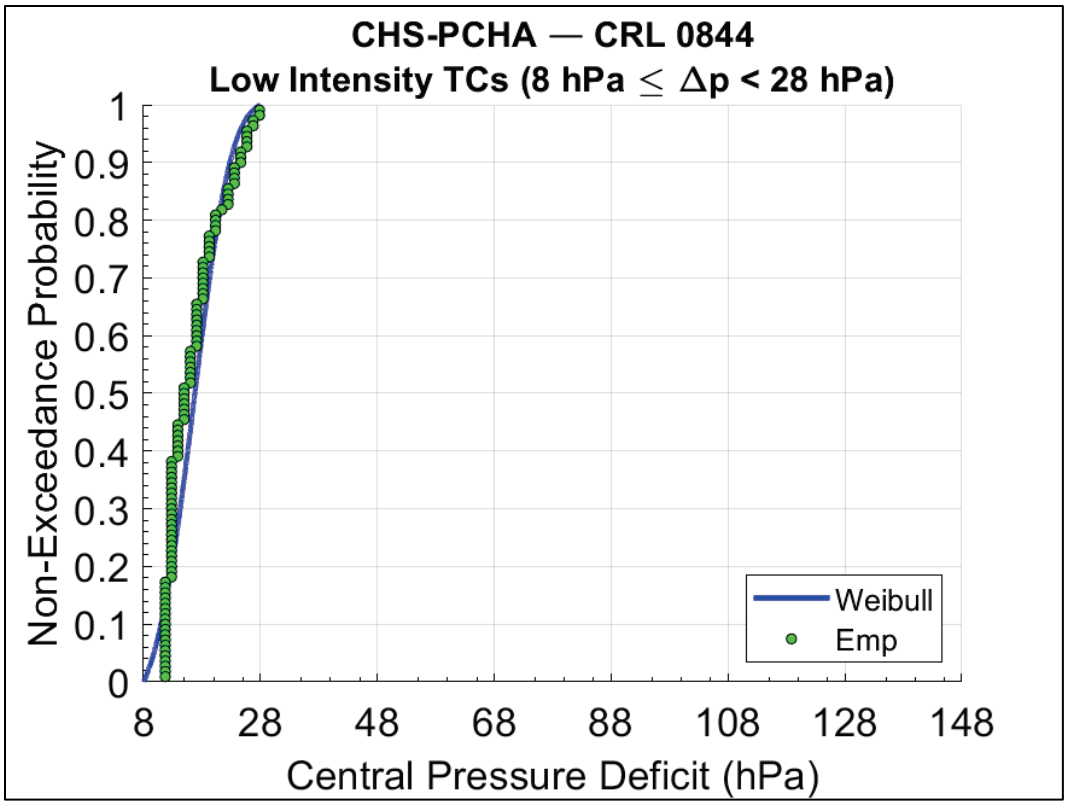

4.1.2 Radius of maximum winds (R_{max})

In this study, the parameter R_{max} is represented by the lognormal distribution, which has the form

$$f(x) = \frac{1}{x\sigma\sqrt{2\pi}} exp\left[-\frac{1}{2}\left(\frac{ln(x)-\mu}{\sigma}\right)^2\right] \quad (4\text{-}2)$$

where μ = mean of $ln(x)$ and σ= standard deviation of $ln(x)$. The main difference between the normal and lognormal distribution is that in the latter, $ln(x)$ is the normally distributed variable rather than x itself. The R_{max} lognormal distribution parameters corresponding to CRL 844 are listed in Table 4-2. Figures 4-6, 4-7, and 4-8 show the marginal distribution fitted to R_{max} for each TC intensity stratum.

Table 4-2. Marginal distribution parameters of R_{max} at CRL 844.

TC Intensity	$\mu_{ln(x)}$	$\sigma_{ln(x)}$
High	3.45	0.72
Medium	3.72	0.44
Low	4.35	0.51

Figure 4-6. Marginal distribution (lognormal) of R_{max} for HI TCs at CRL 844.

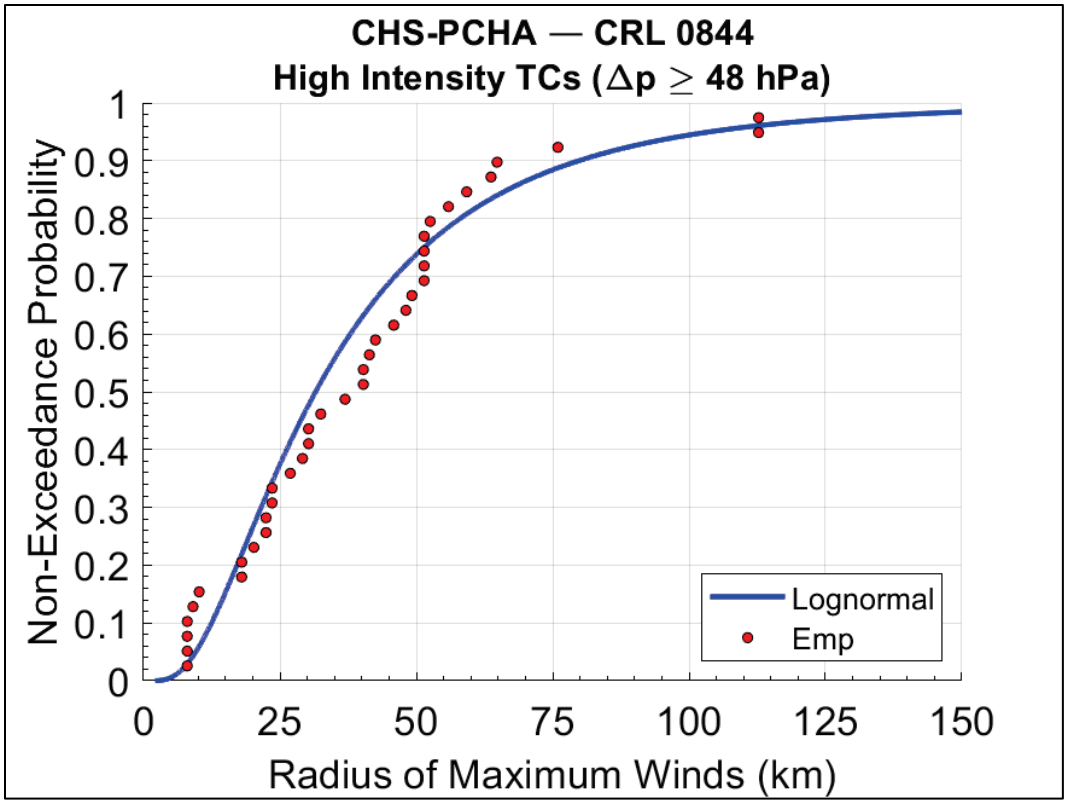

Figure 4-7. Marginal distribution (lognormal) of R_{max} for MI TCs at CRL 844.

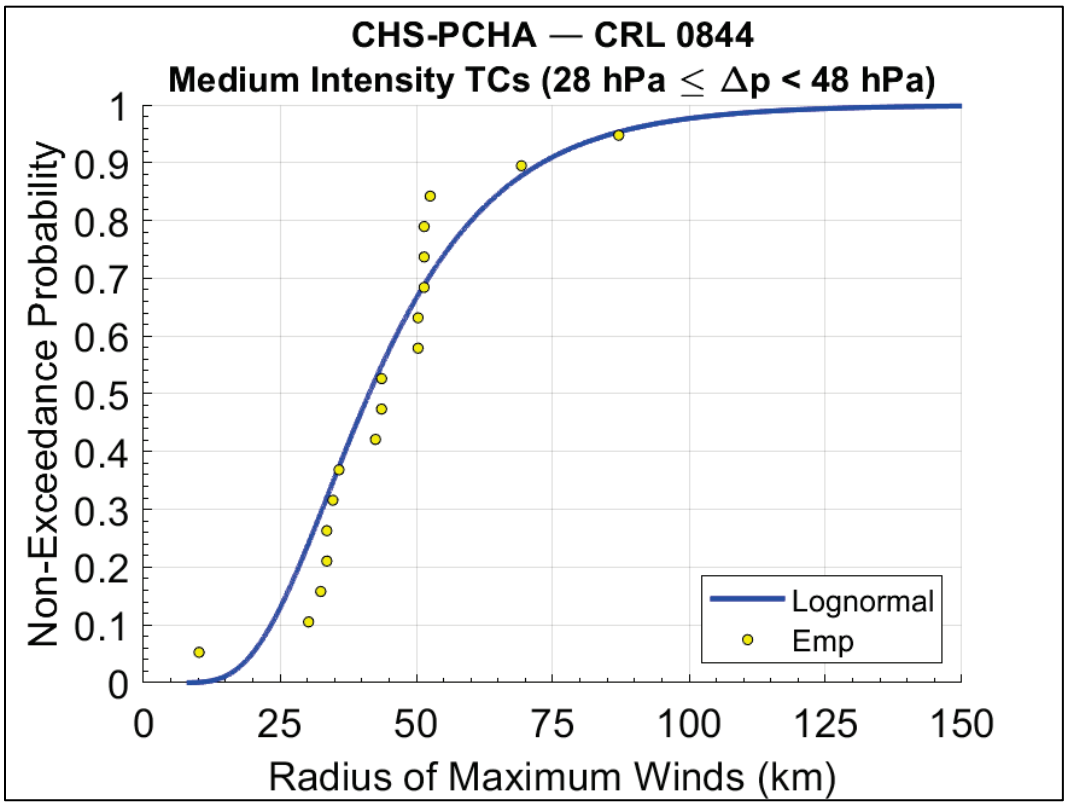

Figure 4-8. Marginal distribution (lognormal) of R_{max} for LI TCs at CRL 844.

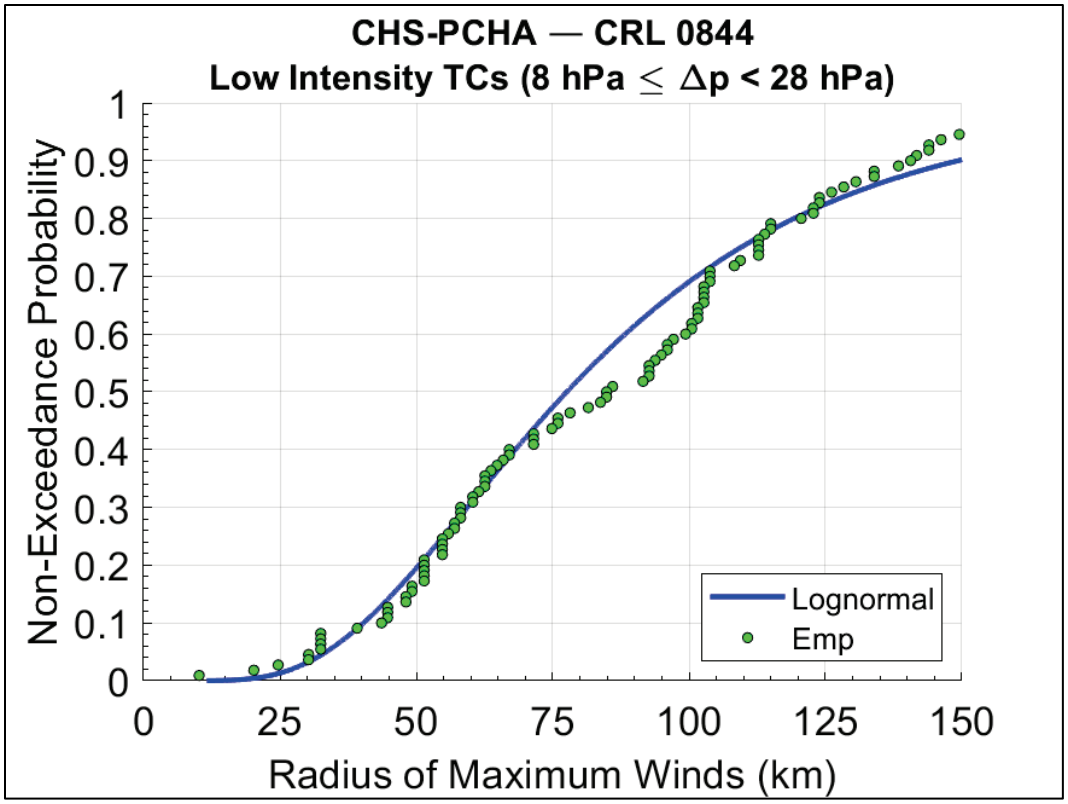

4.1.3 Forward translation speed (V_t)

The V_t data requires two different parametric distributions. The lognormal distribution, discussed in the previous section (Equation 4-2), is used to fit LI TCs in an effort to capture the variability which exists within the empirical data for this intensity stratum. The V_t of MI and HI TCs exhibits less variability and is represented by the normal distribution with the form:

$$f(x) = \frac{1}{\sigma\sqrt{2\pi}} exp\left[-\frac{1}{2}\left(\frac{x-\mu}{\sigma}\right)^2\right] \quad (4\text{-}3)$$

where μ = mean of random variable x and σ= standard deviation of x.

The marginal distribution of V_t for HI, MI, and LI TCs corresponding to CRL 844 are listed in Table 4-3. Figures 4-9, 4-10, and 4-11 show the marginal distribution fitted to V_t at CRL 844 or each intensity stratum.

Table 4-3. Marginal distribution parameters of V_t at CRL 844.

TC Intensity (Normal)	μ	σ
High	22.8	5.99
Medium	18.9	5.58
TC Intensity (Lognormal)	$\mu_{ln(x)}$	$\sigma_{ln(x)}$
Low	3.09	0.31

Figure 4-9. Marginal distribution (normal) of V_t for HI TCs at CRL 844.

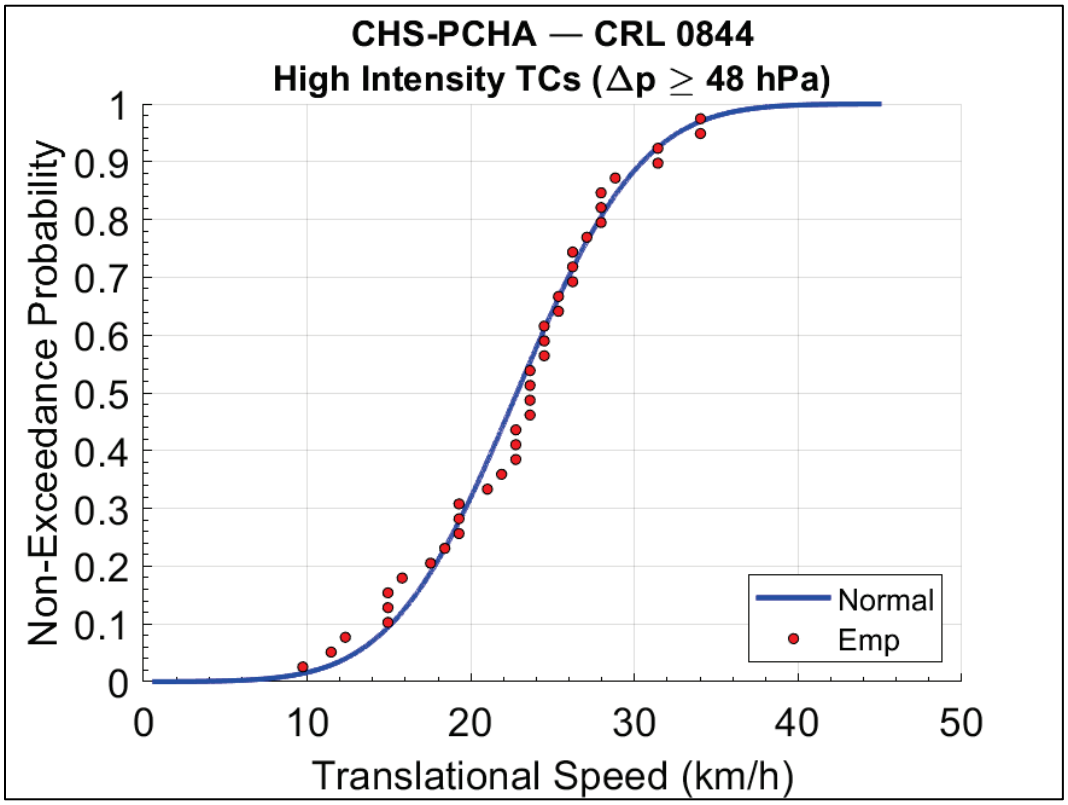

Figure 4-10. Marginal distribution (normal) of V_t for MI TCs at CRL 844.

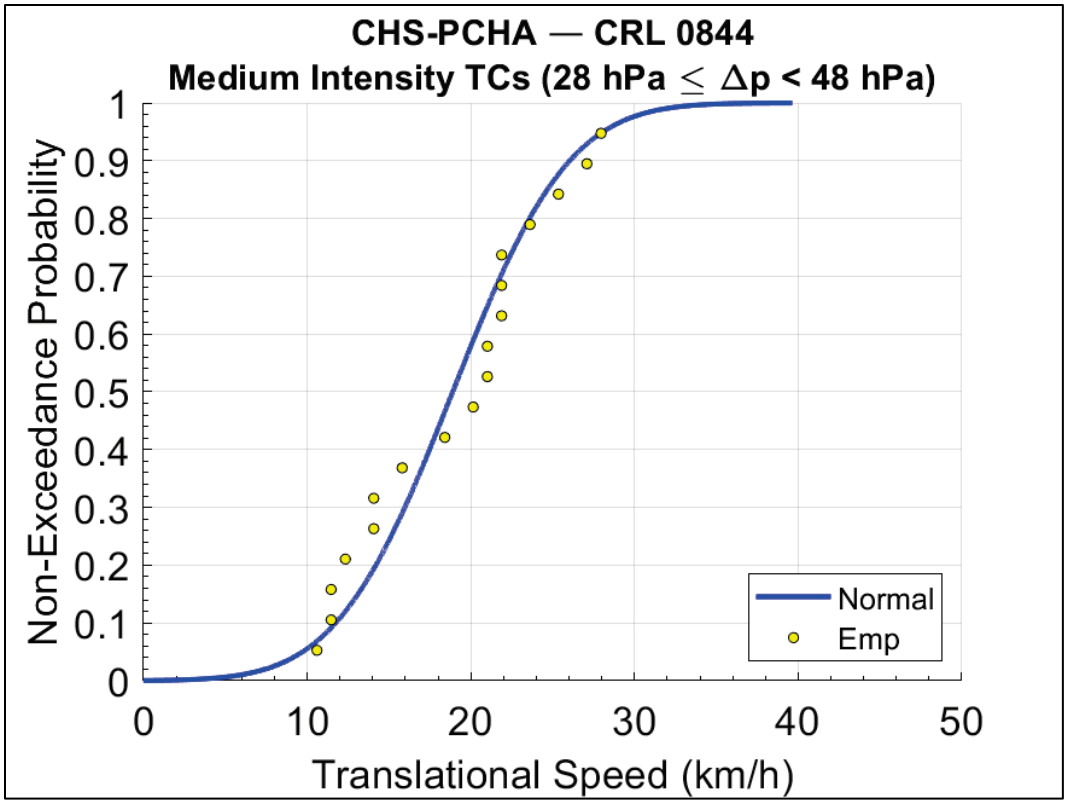

Figure 4-11. Marginal distribution (lognormal) of V_t for LI TCs at CRL 844.

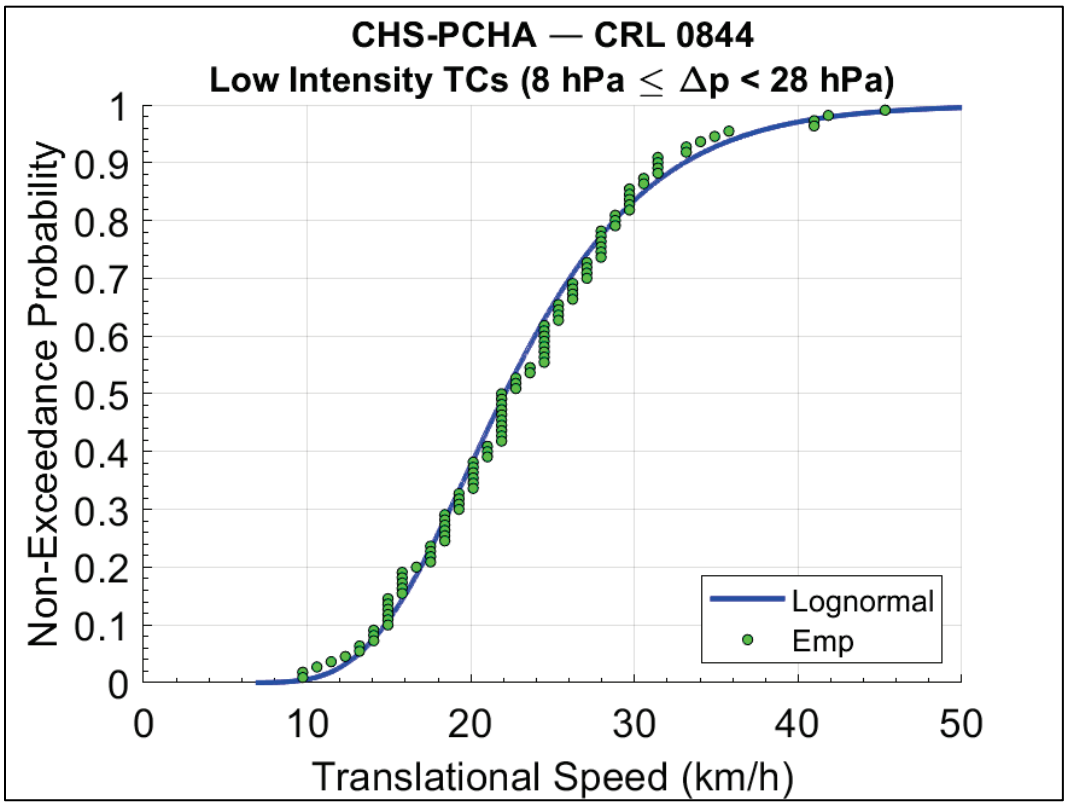

4.1.4 Track heading direction

In the PCHA, the θ marginal distribution is taken as the directional SRR (DSRR) estimated from the GKF model (Chouinard and Liu 1997). The DSRR is given by

$$\lambda_\theta = \frac{1}{T}\sum_i^n w(d_i)\, w(\theta_i - \theta) \tag{4-4}$$

$$w(\theta_i - \theta) = \frac{1}{\sqrt{2\pi}h_\theta}\exp\left(-\frac{1}{2}\left(\frac{\theta_i-\theta}{h_d}\right)^2\right) \tag{4-5}$$

where λ_θ = the DSRR in storms/yr/km; T = record length in (yr); d_i = distance from location of interest to a storm data point (km); h_d = optimal kernel size (km); $w(\theta_i)$ = distance weights from the track heading direction GKF (deg^{-1}); θ_i = track heading direction (deg); h_θ = optimal directional kernel size (e.g., 30 deg); and $w(d_i)$ = distance weights computed using the GKF (Equation 3-2). Figures 4-12, 4-13, and 4-14 show the marginal distribution of θ derived from the DSSR for HI, MI, and LI TCs, respectively.

Figure 4-12. Marginal distribution (DSRR) of θ for HI TCs at CRL 844.

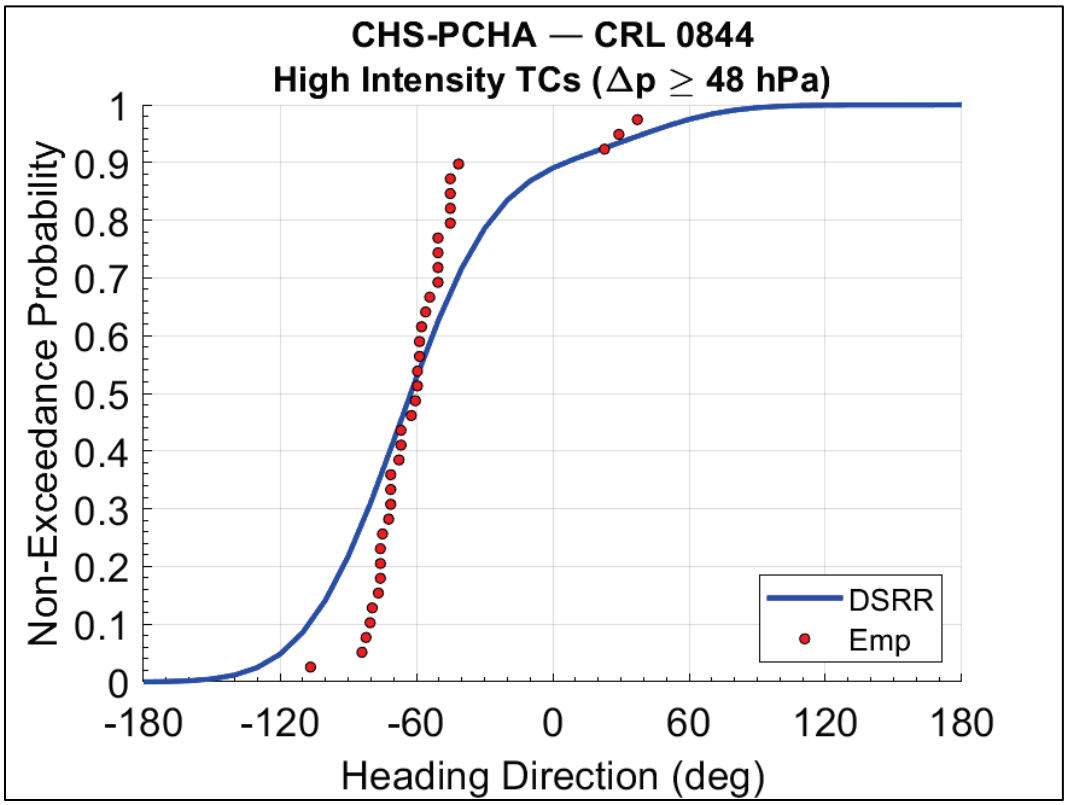

Figure 4-13. Marginal distribution (DSRR) of θ for MI TCs at CRL 844.

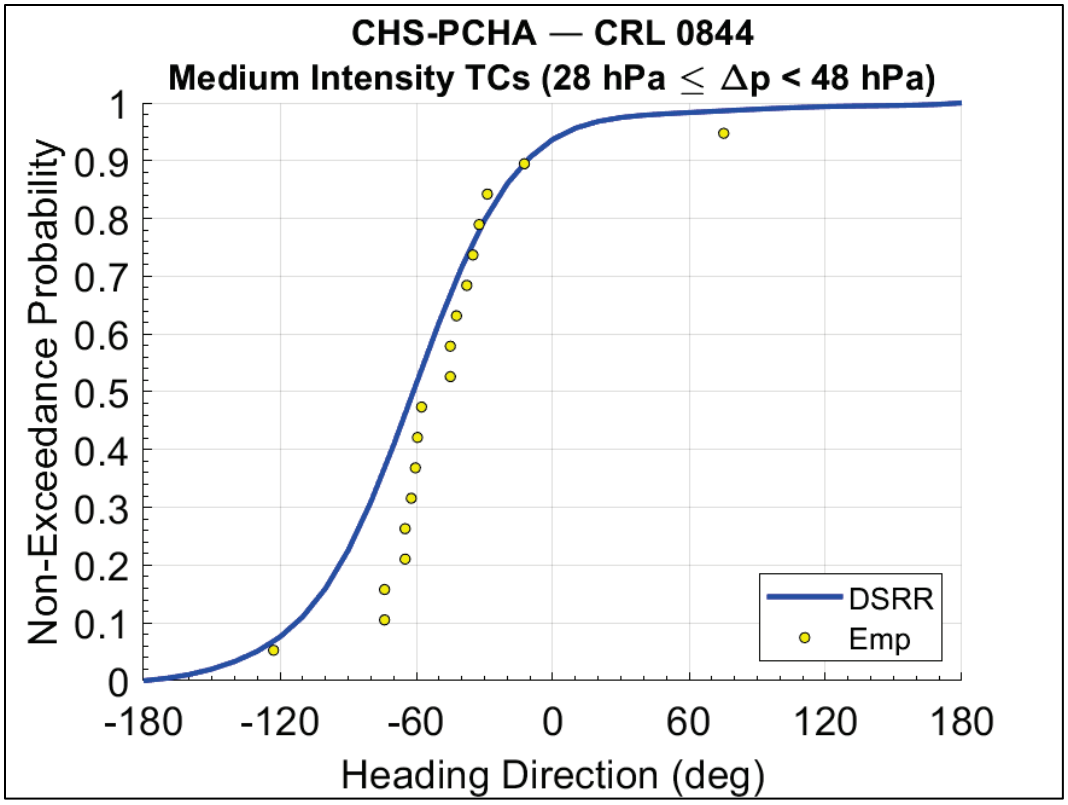

Figure 4-14. Marginal distribution (DSRR) of θ for LI TCs at CRL 844.

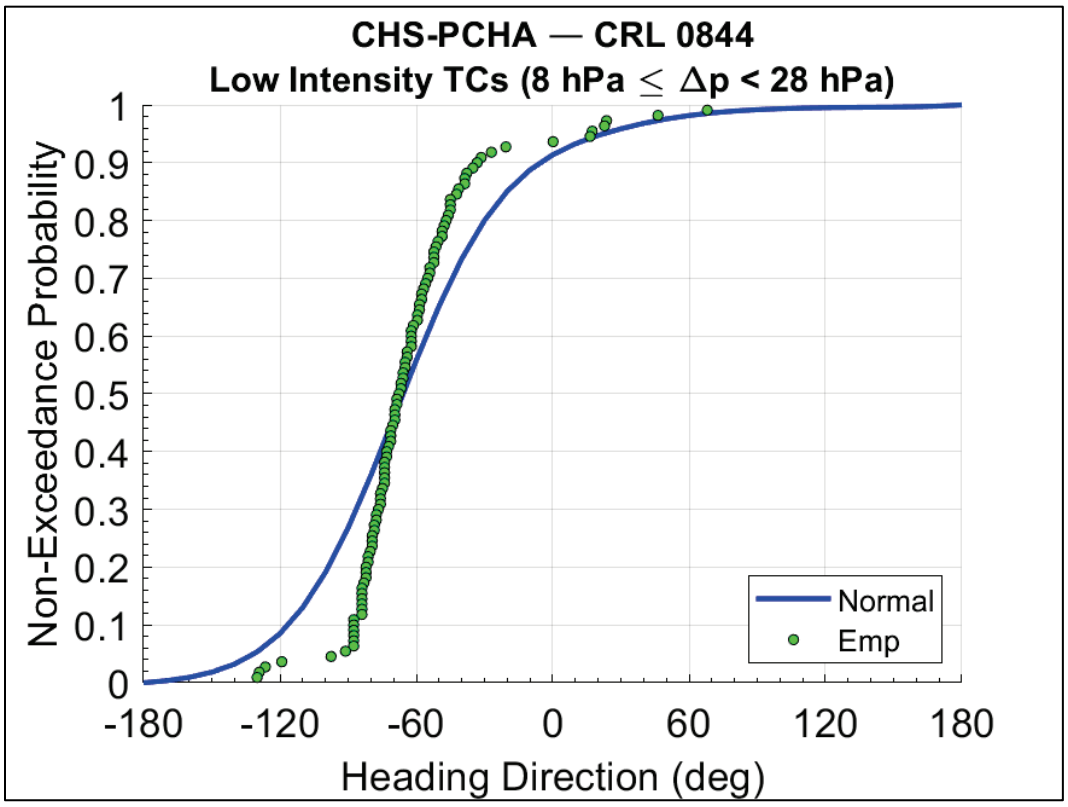

4.2 Joint probability analysis using the meta-Gaussian copula (MGC)

The main limitation in JPM studies as applied to date is the lack of an actual joint probability model. Typical joint probability approaches often involve unrealistic assumptions that either (1) all random variables are independent of one another or (2) that variables follow a joint normal distribution. TC parameters have some level of correlation between them (FEMA 2012). The correlation of TC parameters with location is implicitly considered since the analysis is centered on a CRL; therefore, the SRR and the TC parameters used for fitting the probability distributions are a function of that specific location. The dependence between Δp and R_{max} is often considered in JPM studies, particularly if the latter is computed using a statistical model such as Vickery and Wadhera (2008), which explicitly uses Δp as input.

The JPM-OS-BQ, for example, uses a double-exponential covariance function (Toro et al. 2010b) as a pseudo dependence structure. Instead of computing the correlation between pairs of JPM atmospheric-forcing parameters, this approach relies on expert judgment to set correlation distances that dictate the discretization of marginal distributions of JPM parameters. Previous studies have either assumed independence between the parameters (Equation 2-1) or used a correlation tree with 1:1 dependence, as seen in the diagram in Figure 4-15. The latter approach was described by Resio et al. (2007):

$$P(x_0, \Delta p, R_{max}, V_f, \theta) = P(x_0) \cdot P(\Delta p) \cdot P(R_{max}) \cdot P(V_f) \cdot P(\theta) \quad (4\text{-}6)$$

Figure 4-15. TC parameter correlation tree with 1:1 dependence.

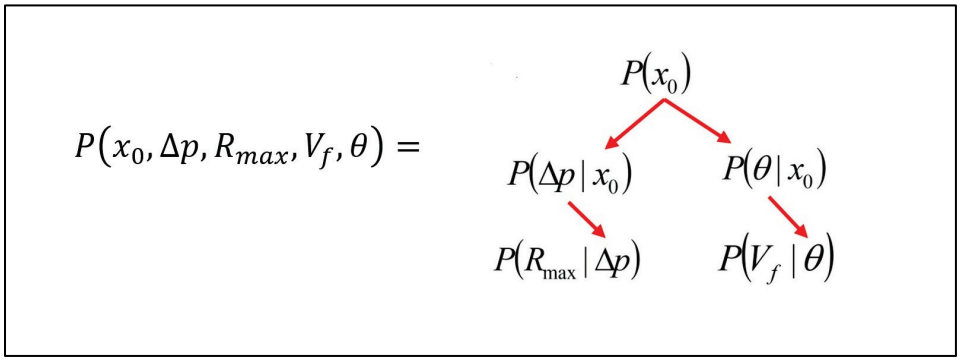

Other approaches have proposed using conditional distributions linking pairs of random variables, but in practice, variables are often interconnected through simplified linear relationships.

The PCHA framework uses copula theory to overcome the aforementioned limitations. A copula is a dependence function that links a set of marginal distributions to form a unique joint probability distribution. According to the seminal Sklar's (1959) theorem, any joint (multivariate) distribution, H, can be deconstructed into marginal distributions, $F_{1,\ldots,n}$, and a copula, C, as follows:

$$H(x_1, \ldots, x_n) = C\big(F_1(x_1), \ldots, F_n(x_n)\big) \tag{4-7}$$

where n is the number of dimensions of the cumulative distribution function (CDF).

A copula must be expressed in terms of uniform marginal distributions (u_n) defined on the interval [0, 1]. The general formulation is

$$C(u_1, \ldots, u_n) = H\big(F_1^{-1}(x_1), \ldots, F_n^{-1}(x_n)\big) \tag{4-8}$$

where $F^{-1}(\,)$ is the inverse of the marginal distribution.

Zhang and Singh (2019) recommend the use of meta-elliptical copulas since this family frequently outperforms other multivariate copulas in capturing the full range of dependence while also excelling due to simplicity of construction and ease of parameter estimation, particularly in the case of the MGC.

The MGC consists of a multivariate CDF constructed by linking a set of marginal probability distributions with a multivariate Gaussian copula as the dependence structure. The CDF of the Gaussian copula is expressed as

$$C_R^{Gauss}(u) = \Phi_R\big(\Phi^{-1}(u_1), \ldots, \Phi^{-1}(u_n)\big) \tag{4-9}$$

where $\Phi^{-1}(\,)$ is the inverse of the standard Gaussian distribution and Φ_R is the multivariate distribution of n Gaussian distributions with correlation matrix R, given by

$$R = \begin{pmatrix} 1 & \rho_{1,2} & \cdots & \rho_{1,n} \\ \rho_{2,1} & 1 & \cdots & \rho_{2,n} \\ \vdots & \vdots & \ddots & \vdots \\ \rho_{n,1} & \rho_{n,2} & \cdots & 1 \end{pmatrix} \tag{4-10}$$

The dependence between pairs of random variables is given by correlation coefficients (ρ). In the case of JPM, ρ must be computed for all pairs of TC forcing parameters. The correlation is accounted for by first computing the rank correlation between the TC atmospheric-forcing parameters using Kendall's Tau (Kendall 1970). By computing the rank correlation, the correlation between TC parameters is preserved following the non-linear transformations required for the MGC. The rank correlation is then transformed to Pearson's rho (Fang et al. 1990, 2002), a linear correlation, using the following form for application in the MGC approach:

$$\rho = \sin\left(\frac{\tau\pi}{2}\right) \tag{4-11}$$

Below are the correlation matrices (R) constructed for All, HI, MI, and LI TCs from Equation 4-10. For each TC intensity stratum, Figures 4-16 through 4-19 illustrate the correlation between the JPM parameters computed as both the rank correlation and Pearson's correlation. In each correlation matrix plot, the first reported correlation corresponds to Kendall's rank correlation and the second value (shown in parentheses) corresponds to Pearson's correlation.

Figure 4-16. Correlation matrix for All TCs at CRL 844.

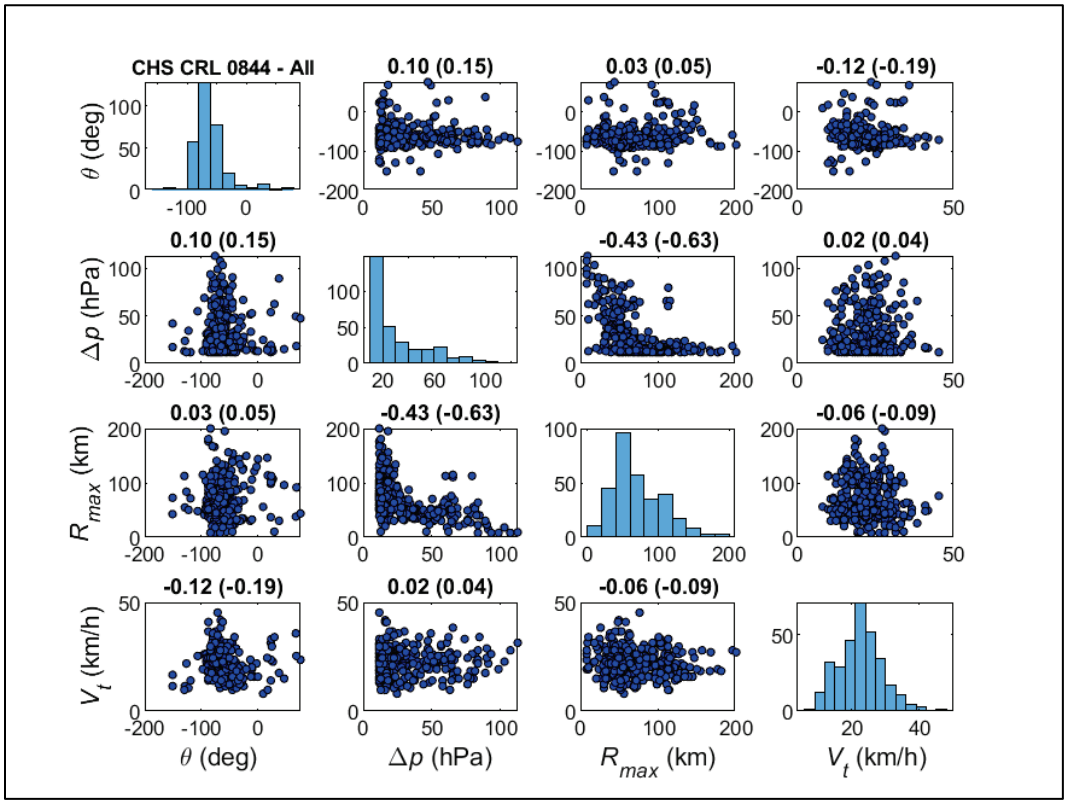

Figure 4-17. Correlation matrix for HI TCs at CRL 844.

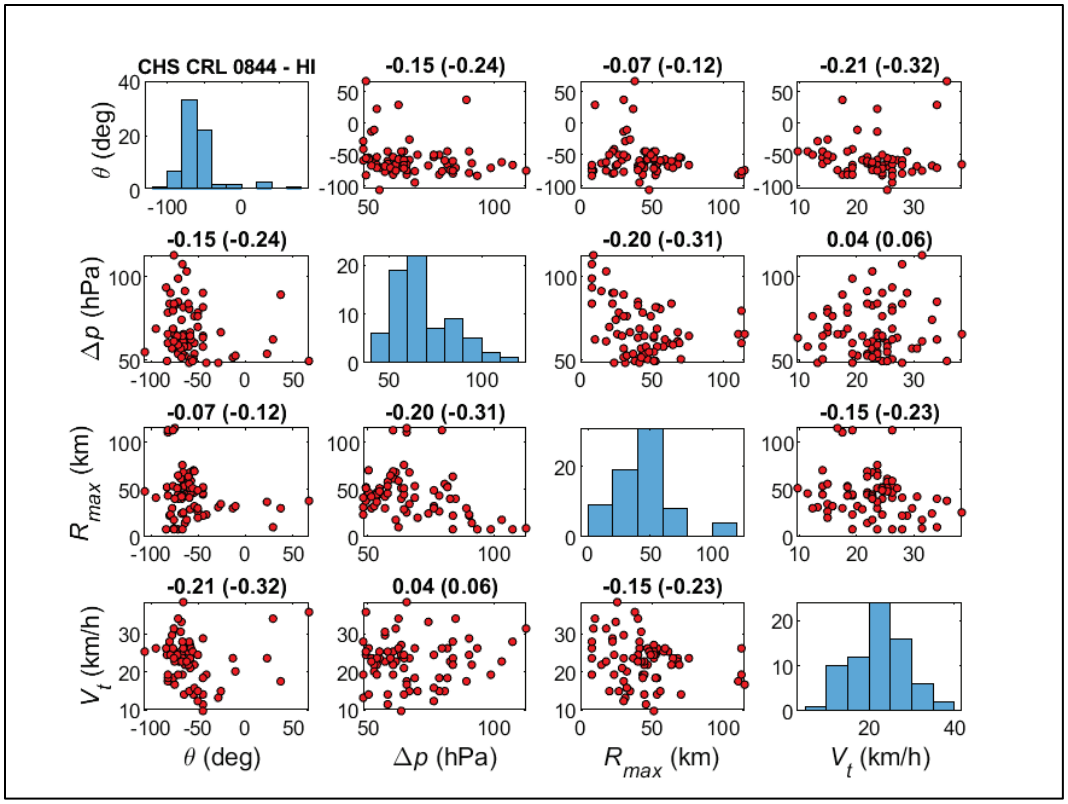

Figure 4-18. Correlation matrix for MI TCs at CRL 844.

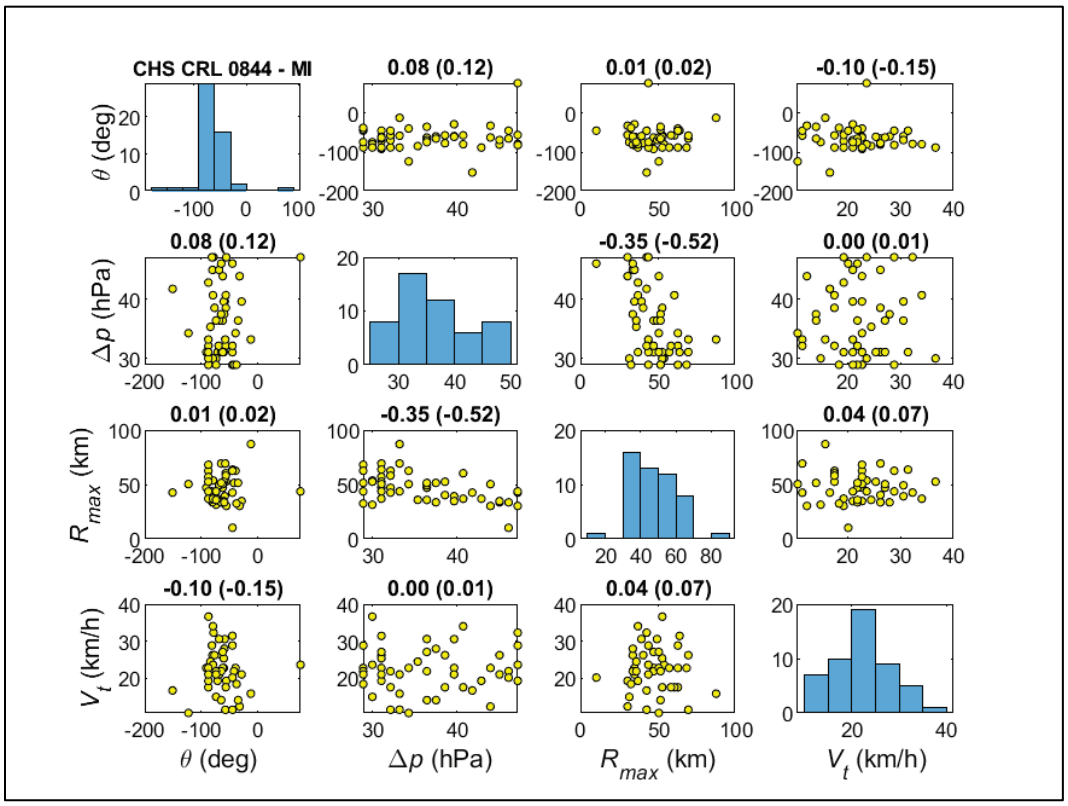

Figure 4-19. Correlation matrix for LI TCs at CRL 844.

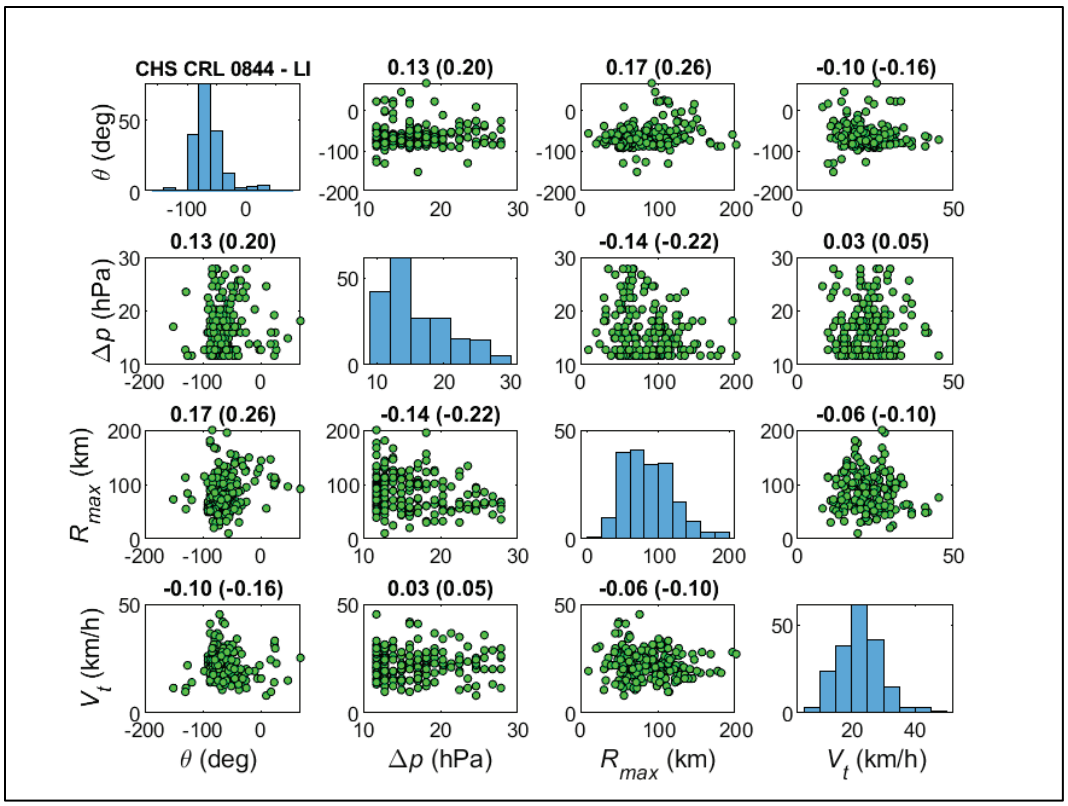

4.3 Discretization of marginal distributions

A hybrid optimal sampling method was employed to discretize the marginal distributions of TC parameters. It is termed *hybrid* because it combines uniform discretization procedures evolved from those used in the LACPR study (USACE 2009a) with the BQ optimization approach developed for FEMA (2012). To ensure optimal coverage of the TC probability and parameter spaces and ensure adequate geospatial coverage of the study area, a structured discretization approach was used for the Δp and θ marginal distributions. The discretization of the R_{max} and V_t marginal distributions was performed using the BQ approach. The range of values resulting from the discretization of marginal distributions is provided in Table 4-4. Combining storm tracks and TC parameter permutations resulted in an ITCS of 300 synthetic storms. Section 5 discusses the along-track variation of these parameters for implementation in the PBL model.

Table 4-4. Atmospheric-forcing parameters from the CHS-PR ITCS.

TC Parameter	Range
θ	-140°, -100°, -60°, -20°, +20°, +60° (clockwise from North)
Δp	8, 18, 28, 38, 48, 58, 68, 78, 88, 98, 108, 118, 128, 138, 148 hPa
R_{max}	8 to 143.6 km (from BQ sampling)
V_t	8 to 40 km/h (from BQ sampling)

4.4 Augmented synthetic TC suite (ATCS) and discrete storm weights (DSWs)

The PCHA methodology includes the development of an ATCS to fully cover the parameter and probability spaces for the study area. This requires the simulation of hundreds of TCs (up to several thousands in regional studies) from the ITCS to ensure high-resolution, high-fidelity hydrodynamic results. After the ITCS is defined, the ATCS is developed using the discretized marginal distributions to create a higher density of synthetic TCs. Metamodeling is then introduced to predict the responses of an augmented suite of tens of thousands to millions of TCs that retain the high-fidelity nature of the initial suite. As described by Jia et al. (2016) and Zhang et al. (2018), the GPM establishes the relationship between the input atmospheric-forcing vector $\hat{x} = f(x_o, \theta, \Delta p, R_{max}, V_t)$ and output TC responses (e.g., storm surge, wave parameters). However, to avoid an excessive computational cost, the size of the ATCS needs to be balanced with the number of point locations where the JPM integral is solved.

For the CHS-PR study, the first step in defining the ATCS was to discretize the distributions of the TC atmospheric-forcing parameters at a much higher resolution than the ITCS. The discretization of the TC parameter space used in the definition of the ATCS is shown in Table 4-5. Multiplying the number of discrete values for Δp (29), R_{max} (30), and V_t (10) resulted in 8,700 TCs per master track. The resulting ATCS developed for this study consisted of 348,000 synthetic TCs with an average of 8,700 storms per track. Using the high-fidelity hydrodynamic modeling results produced by simulating the ITCS, GPMs were trained to predict storm responses produced by storms within the ATCS. The GPM training for the SWL and H_{mo} responses is discussed in Section 6.1.

Table 4-5. Atmospheric-forcing parameters from the CHS-PR ATCS.

TC Parameter	Range	Discretization	Number of Discrete Values
Δp	8 to 148 hPa	5 hPa	29
R_{max}	10 to 155 km	5 km	30
V_t	5 to 50 km/h	5 km/h	10
Master Tracks	θ = -140°, -100°, -60°, -20°, +20°, +60° (clockwise from North)		40
Total number of TCs			348,000

Following the development of the ATCS, the DSWs were computed for each storm as defined by Equation 2-1b and 2-2b, where $\hat{\lambda}_i$ is a product of the SRR, the joint probability densities of the TC parameters, and the track spacing. In this formulation, the SRR is the most important factor for quantifying hazards because it represents the average number of storms that a specific location is likely to experience in any given 1 yr period. Each TC in the synthetic suite constitutes a partition of this SRR and is represented by its DSW. Increasing the number of storms in the synthetic TC suite (e.g., upgrading from ITCS to ATCS) also increases the resolution of both the probability and physical parameter spaces while decreasing the DSW of each TC. The computation of DSWs relies on historical TC datasets established at each CRL to assign a realistic relative likelihood to each synthetic storm. As shown by the diagram in Figure 4-20, the workflow for computing DSWs begins by generating the ATCS and identifying the unique combinations of TC forcing parameters that exist within the augmented suite. This is necessary as some TC parameter combinations are identical and are replicated across different master tracks to constitute different synthetic storms.

The 5 steps illustrated by the teal-colored boxes are repeated across all CRLs within the study area to compute DSWs for all storms in the ATCS. These steps take advantage of the copula-based joint probability model and TC intensity stratification for the computation of joint probability densities. The probability densities are determined by discretizing the joint distribution with multivariate copula given by Equation (4-9) but in PDF form. These probability densities are then normalized to produce a total probability density sum equal to 1.0 for all unique TC parameter combinations at a given CRL. The local DSWs are computed for the different TC parameter combinations, as previously described, and

assigned back to the storms in the ATCS based on each storm's specific parameter combination and intensity stratum. The result is a local DSW value for each storm in the ATCS specific to each CRL considered in the storm climatology analysis (Section 3.3). The last step in computing the final set of global DSWs for the ATCS is geospatially interpolating the local DSW for each storm based on the proximity of its track to the CRLs. As a result, the global DSWs computed for the ATCS account for the joint probability of the TC parameters with respect to geographical location and intensity stratification, which is important for accurate quantification of coastal hazards.

Figure 4-20. PCHA workflow for computing the ATCS DSWs.

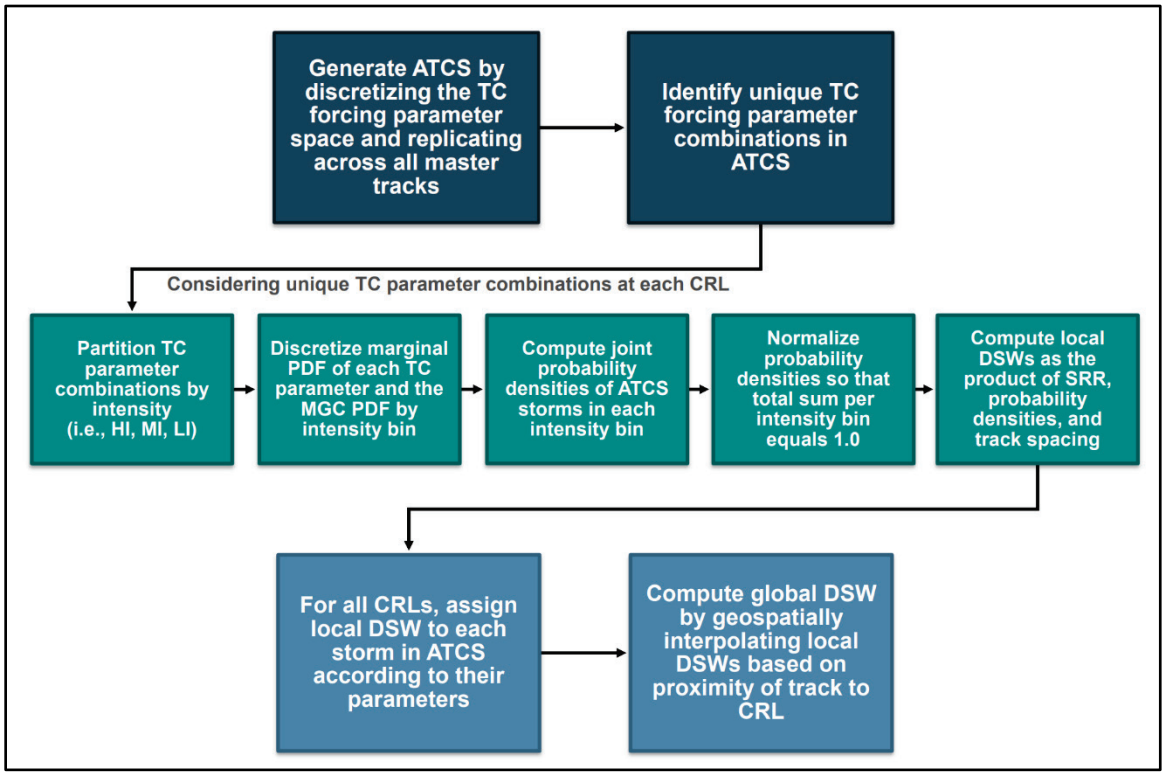

5 Development of Synthetic TC Suite

This section describes the generation of the synthetic TC track paths and the along-track variation of TC parameters for application in the PBL model. The wind and pressure fields generated by this model constitutes the forcing needed to drive the hydrodynamic models. Section 5.1 presents the generation of the synthetic TC tracks. Section 5.2 describes how TC parameters defined in Table 4-4 were used and how the storm parameters were modified for pre-landfall and post-landfall changes. Section 5.3 summarizes the tropical wind and pressure forcing inputs. Section 5.4 discusses the application of the PBL model.

5.1 TC master tracks

For the CHS-PR study, six landfalling track headings of -140°, -100°, -60°, -20°, 20°, 60° (clockwise from north) were applied in the JPM. Generation of the landfall locations applied linear tracks with parallel track spacing of 60 km. These linear tracks are referred to as master tracks as they define the path along which parameter sets representing the synthetic TCs propagate. The master tracks, and their associated headings, were defined by analyzing historical TC tracks from the HURDAT2 database to determine the climatological track paths affecting CHS-PR.

All tracks apply a constant track heading from an offshore reference point (ORP) 250 km prior to and post-landfall or bypassing reference point. A smoothed bearing path is used prior to the 250 km offshore reference location to result in track paths consistent with climatological TC tracks. Analysis of historical TC tracks resulted in the definition of 40 master tracks along which TC parameter sets were altered. The master tracks defined provide adequate coverage of the probable and practical TC parameter space for the CHS-PR region. The resulting 40 master tracks are listed in Appendix B. Track paths for all 40 master tracks are depicted in Figure 5-1, with tracks by heading in Figures 5-2 to 5-7.

Figure 5-1. All JPM track paths (blue) with landfall/closest approach location (red) and historical TC tracks (gray). Inset image shows zoomed view of all tracks and their reference locations relative to Puerto Rico.

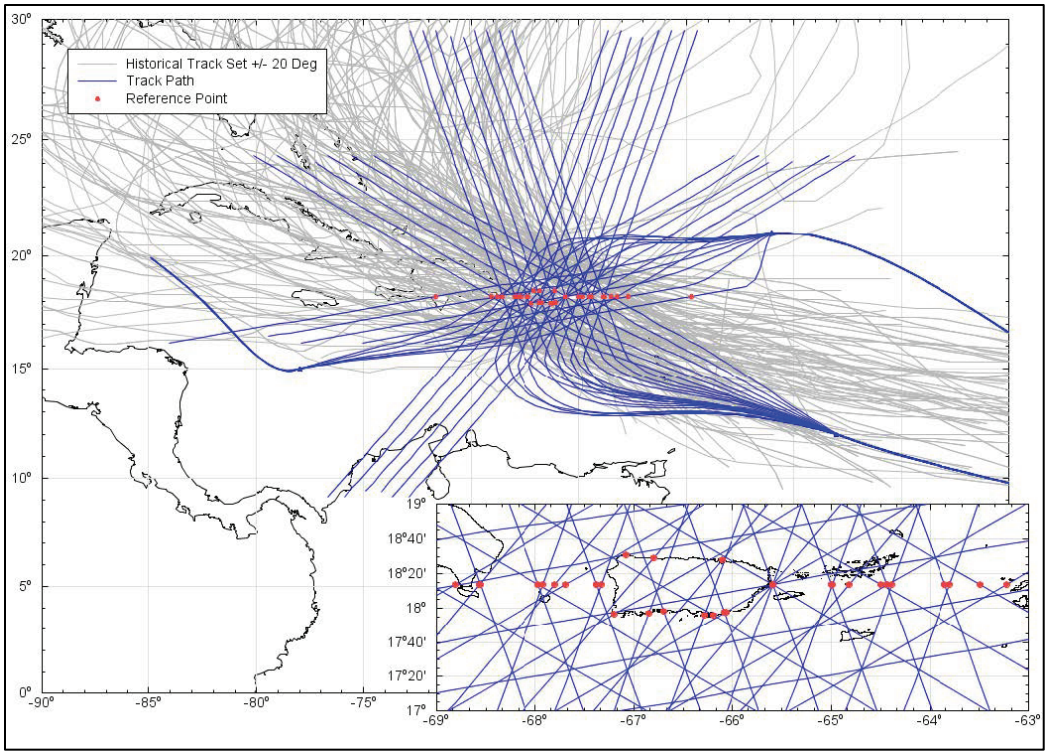

Figure 5-2. JPM heading -140° track paths (blue) with historical tracks (gray). Inset image shows zoomed view of tracks and their reference locations relative to Puerto Rico.

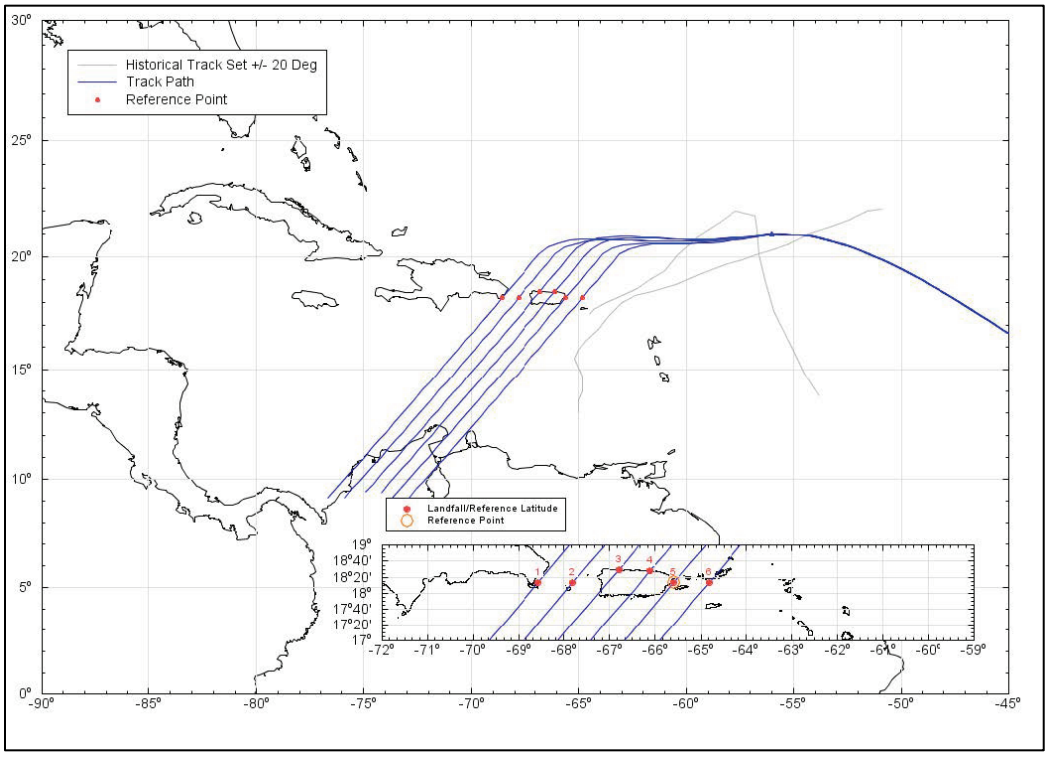

Figure 5-3. JPM heading -100° track paths (blue) with historical tracks (gray). Inset image shows zoomed view of tracks and their reference locations relative to Puerto Rico.

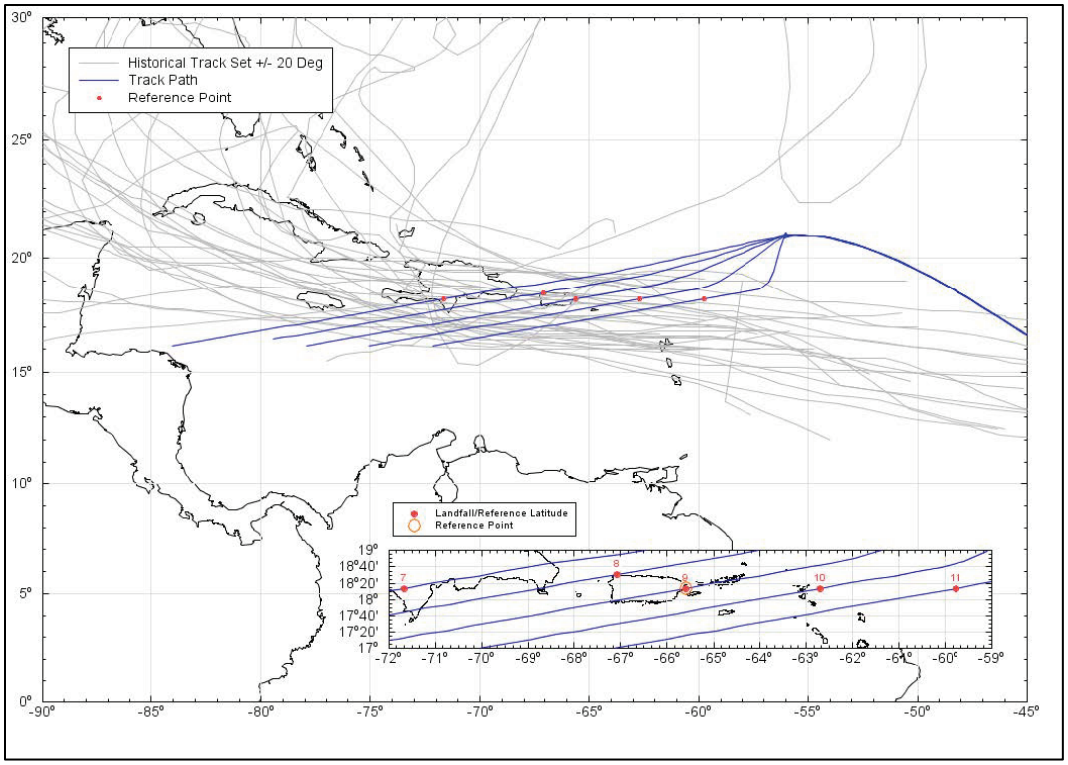

Figure 5-4. JPM heading -60° track paths (blue) with historical tracks (gray). Inset image shows zoomed view of tracks and their reference locations relative to Puerto Rico.

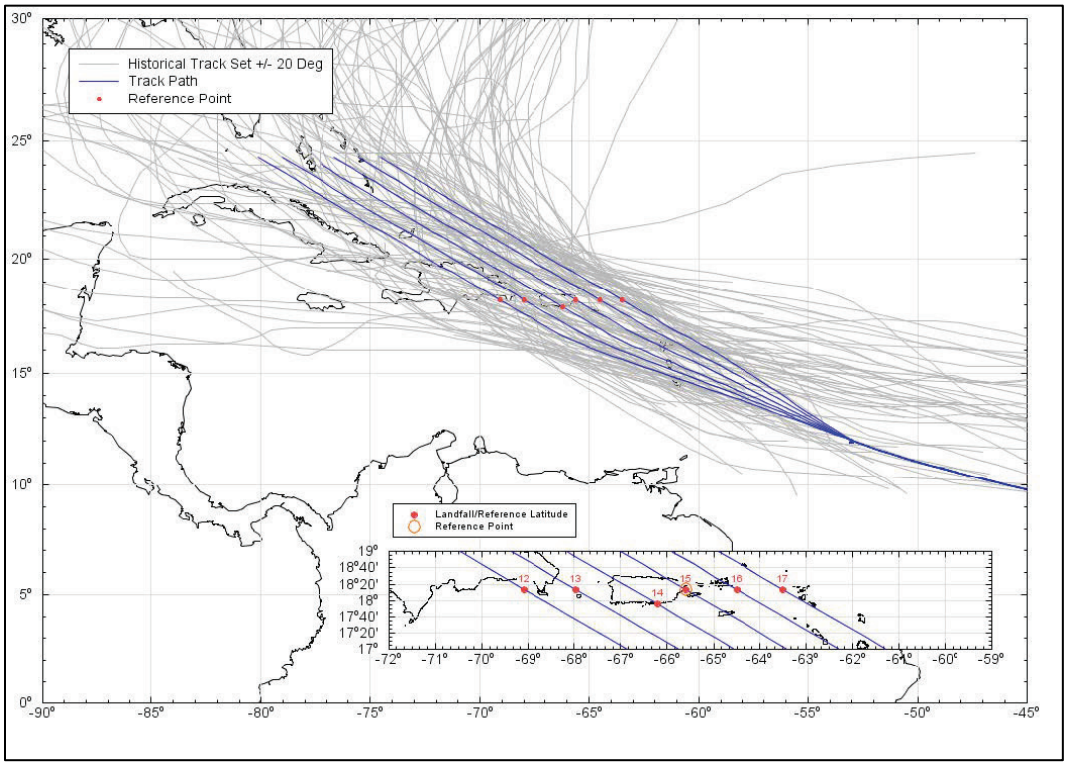

Figure 5-5. JPM heading -20° track paths (blue) with historical tracks (gray). Inset image shows zoomed view of tracks and their reference locations relative to Puerto Rico.

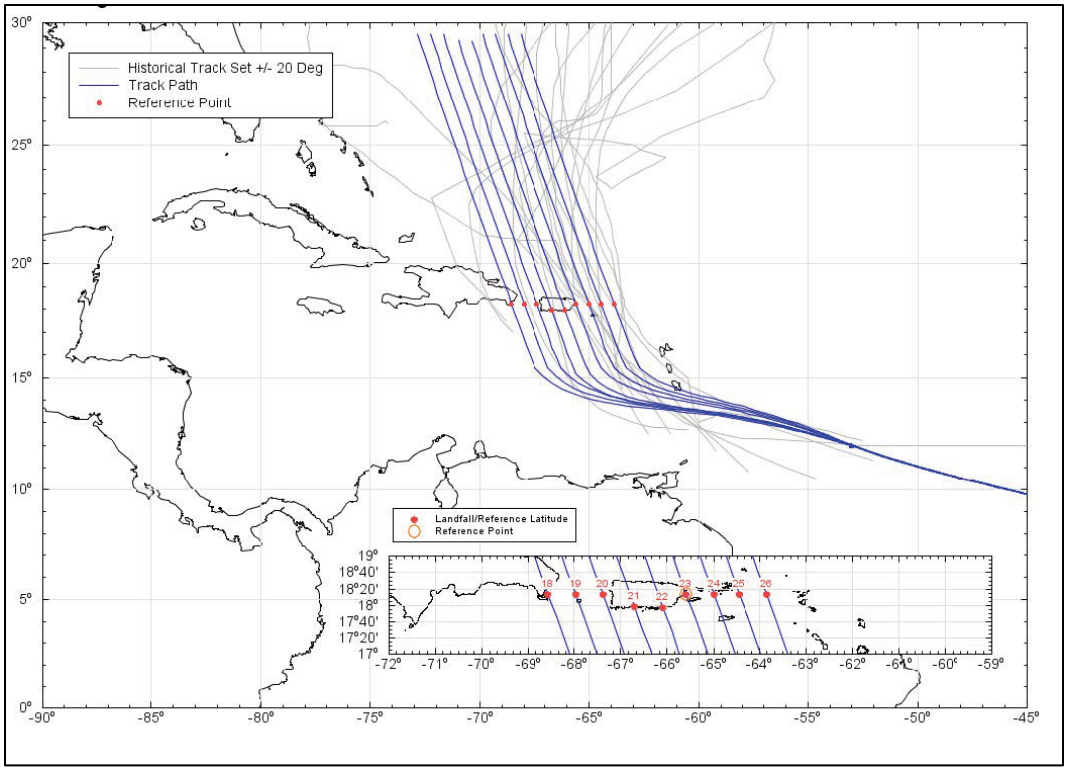

Figure 5-6. JPM heading 20° track paths (blue) with historical tracks (gray). Inset image shows zoomed view of tracks and their reference locations relative to Puerto Rico.

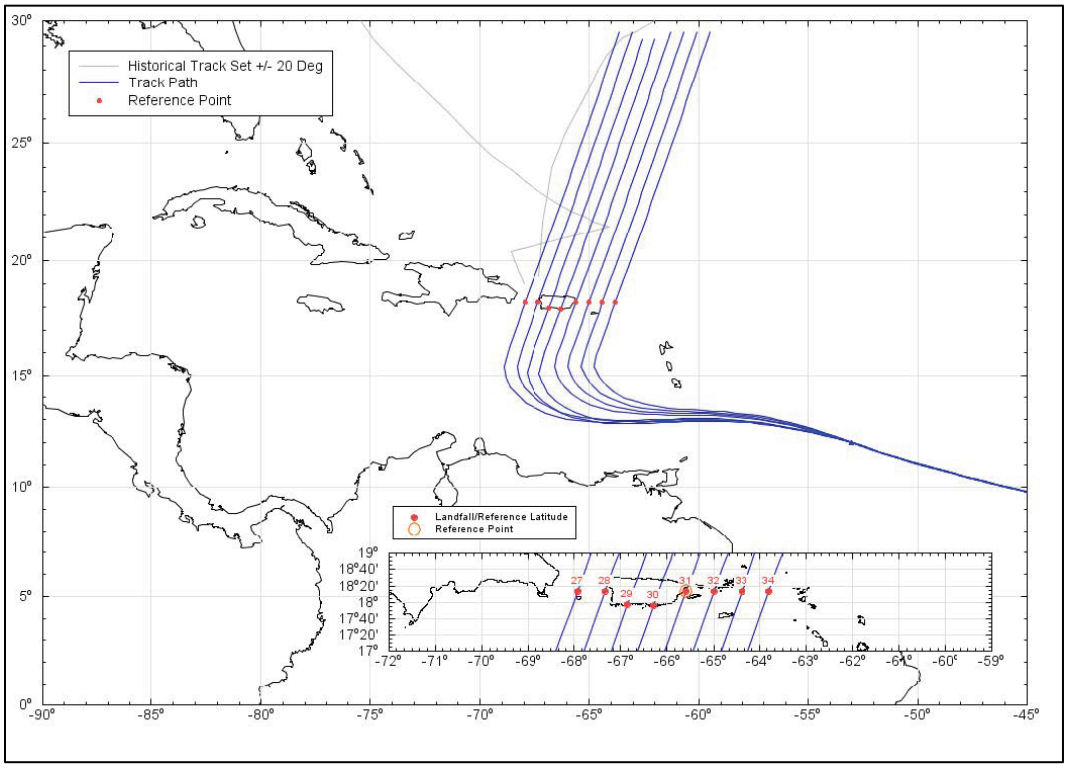

Figure 5-7. JPM heading 60° track paths (blue) with historical tracks (gray). Inset image shows zoomed view of tracks and their reference locations relative to Puerto Rico.

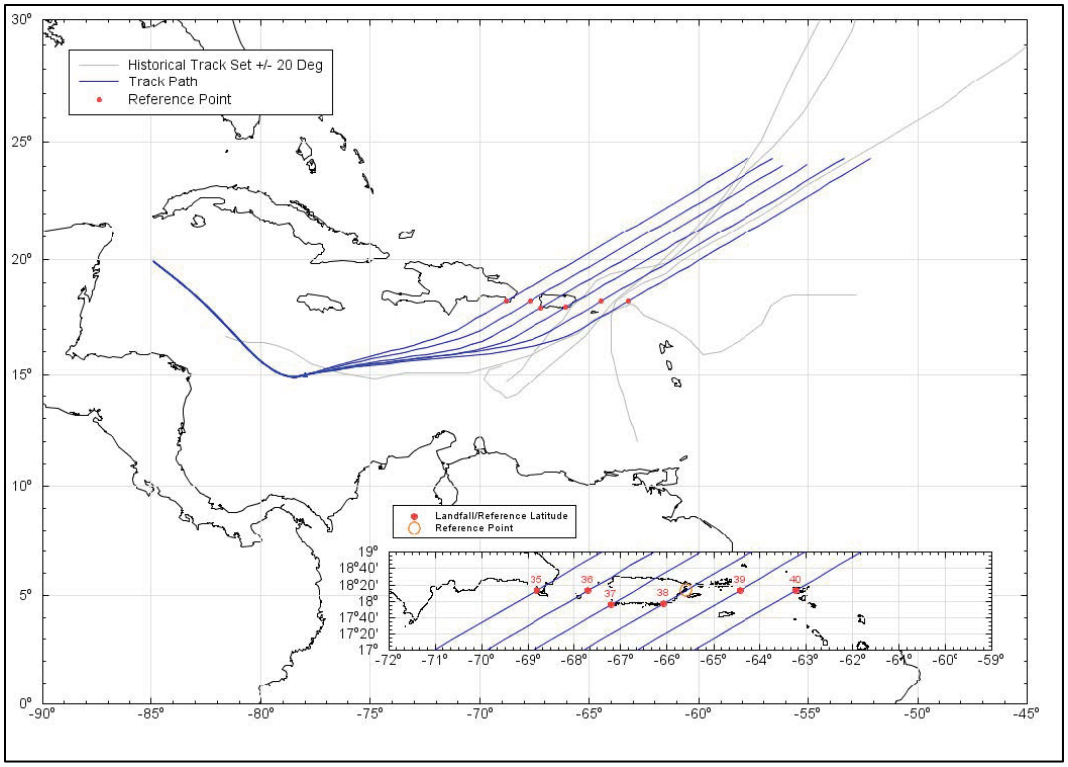

5.2 Along-track variations of TC parameters

Varying combinations of the discrete x_o and θ values resulted in a total of 40 master tracks (Appendix B) for CHS-PR. To complete the synthetic storm set, combinations of the remaining parameters, Δp, R_{max}, V_t, are assigned to each of the master tracks. In Section 4.3, it was discussed that structured discretization was used for Δp and θ. Discretization of the marginal distributions through BQ optimization was used for the remaining parameters R_{max} and V_t. This process resulted in 300 synthetic TCs for the CHS-PR with the number of storms per track varying between 7 and 8 TCs. The final suite of synthetic TCs is listed in Appendix B: CHS-PR Synthetic Tropical Cyclone Master Tracks.

The JPM parameters Δp, R_{max}, and V_t defined for each TC are valid at the ORP. As described in Section 5.2.1, these parameters are allowed for pre-landfall filling of the storm, or weakening, prior to landfall. The pre-landfall filling analysis performed for CHS-PR is described in Section 5.2.1. All track sets apply the post-landfall filling model described in Section 5.2.2. Overall storm duration was determined by V_t, as shown in Table 5-1.

Table 5-1. Forward translation speeds and segment durations of JPM TCs.

Forward Translation Speed (knot)	Hours Prior to ORP (Spin Up)	Hours Post ORP (Spin Down)	Model Time-step (min)
$V_t \leq 5.0$	144	60	15
$V_t \leq 7.5$	132	54	15
$V_t \leq 10.0$	120	48	5
$V_t \leq 12.5$	108	42	5
$V_t \leq 15.0$	96	36	5
$V_t \leq 17.5$	84	30	5
$V_t \leq 20$	72	24	5

All storms applied a far-field pressure of 1,013 hPa to be consistent with the value used to determine the central pressure deficit in the JPM development. The Holland B parameter, which controls the peakedness of the wind profile, was based on Equation 5-1.

$$B = 1.7642 - 1.2098\sqrt{A} \tag{5-1}$$

$$\sigma_B = 0.226$$

$$A = \frac{R_{max} \cdot f_c}{\sqrt{2R_d T_s \cdot \ln\left(1 + \frac{\Delta p}{c_{p \cdot e}}\right)}} \tag{5-2}$$

where

R_d = gas constant for dry air (287 N m $^{k-1}$ kg^{-1})
C_p = central pressure (mb or hPa)
T_s = sea surface temperature (˚C)
Δp = central pressure difference (mb or hPa)
f_c = 0.00001454 sin θ, where θ is the latitude
R$_{max}$ = radius of maximum winds (m).

A mean sea surface temperature of 27.1°C was applied based on the annual mean of National Center for Environmental Prediction/National Center for Atmospheric Research reanalysis sea surface temperature data. To avoid unrealistic B values with weak storms, central pressure was capped to a maximum of 980 hPa when applied in Vickery and Wadhera (2008)

Equation 22 to match the development of the statistical model described in Vickery and Wadhera (2008). Strong storms with c_p <= 930 hPa and R_{max} >= 40 km at the JPM reference point applied a mean B of 1.01 with σ_B = 0.082. A randomly generated standard deviation of +/-1 was generated for each storm and applied in the B calculations on a per storm basis.

The following subsections (5.2.1–5.2.3) describe the work done to develop synthetic TC time series by varying the JPM parameter sets along the TC master tracks. The along-track variations in TC parameters were based on climatological analysis of historical storms near CHS-PR.

5.2.1 Determination of pre-landfall filling/closest approach filling

A set of 88 historical storm reference landfalls in the study area from the 1938–2016 period were used to determine any pre-landfall modifications to be applied from the reference point 250 km offshore to the landfall/latitude reference location. This period of record was applied since this pre-landfall filling analysis for the storm suite development was performed near the beginning of the study. Since very few of the historical storms make landfall on CHS-PR, the storm set applied an analysis of pre- and post-intensities from a reference point at the closest approach from the track reference location at 18.23°N, 65.59°W to increase the available population. Storm locations and central pressures were obtained from the IBTracs (International Best Track Archive for Climate Stewardship) (Knapp et al. 2010, 2018) archive which is based on HURDAT2. Storm parameters at the closest approach applied in the analysis are detailed in Appendix C for storms within the CHS-PR region.

Given the landfall time/location specified in Appendix C, over-water estimates of central pressure within 500 km from landfall or for the time period 48 hr prior to the closest approach (for bypassing storms) were extracted from the IBTracs archive. Pressure estimates are sparse for early twentieth century storms and typically specified at 3–6 hr intervals for modern storms. Figure 5-8 depicts the pre-landfall and post-landfall pressures and pressure deficit for Hurricane Irene (2011) expressed in hours and in distance relative to landfall for Puerto Rico locations. Figure 5-9 shows all track segments within 500 km of landfall for the closest approach location.

When the ratio of pressure deficit offshore to the landfall pressure deficit ($\Delta p/\Delta p$(Ref)) is expressed as a function of distance (Figure 5-10), the storm data shows the storm both weakening ($\Delta p/\Delta p$(Ref) > 1) and strengthening ($\Delta p/\Delta p$(Ref) < 1) as a function of distance to the closest approach point. On average, there appears to be very little change in storm intensity prior to the closest approach.

To explore the effect of storm strength on pre-landfall filling, a series of linear fits were made on a per storm basis to determine the pressure deficit at 250 km prior to the closest approach. Figure 5-11 depicts the linear fit applied to all storms analyzed with at least three pressure estimates in the IBTracs dataset. In general, the linear fit describes the pre-landfall conditions well for most storms. Based on the fits by storm, the pressure deficit at 250 km prior to the closest approach was determined, and a summary of 250 km pressure deficits is shown in Appendix C.

The relationship of the pressure deficit ratio $\Delta p(250)/\Delta p$(Ref) is expressed as a function of pressure in Figure 5-12. Unlike the GoM analysis performed for the CTXS, there is not a strong relationship between the pressure deficit and changes prior to the closest approach. The slope of the fit was highly dependent on the exact reference location selected, search radius of the storm population, and fit threshold criteria for determining Δp at 250 km for individual storms. Pre-landfall filling in the GoM is suspected to be linked to the location of the loop current and is not applicable to the Puerto Rico region. Thus, it was recommended that no pre-landfall filling be applied in the JPM analysis.

Figure 5-8. Hurricane Irene (2011) track with pre-landfall (blue) and post-landfall (green) estimates from HURDAT expressed as central pressure (mb) and pressure deficit (mb) by time (hours) and distance (km) from landfall reference location (red).

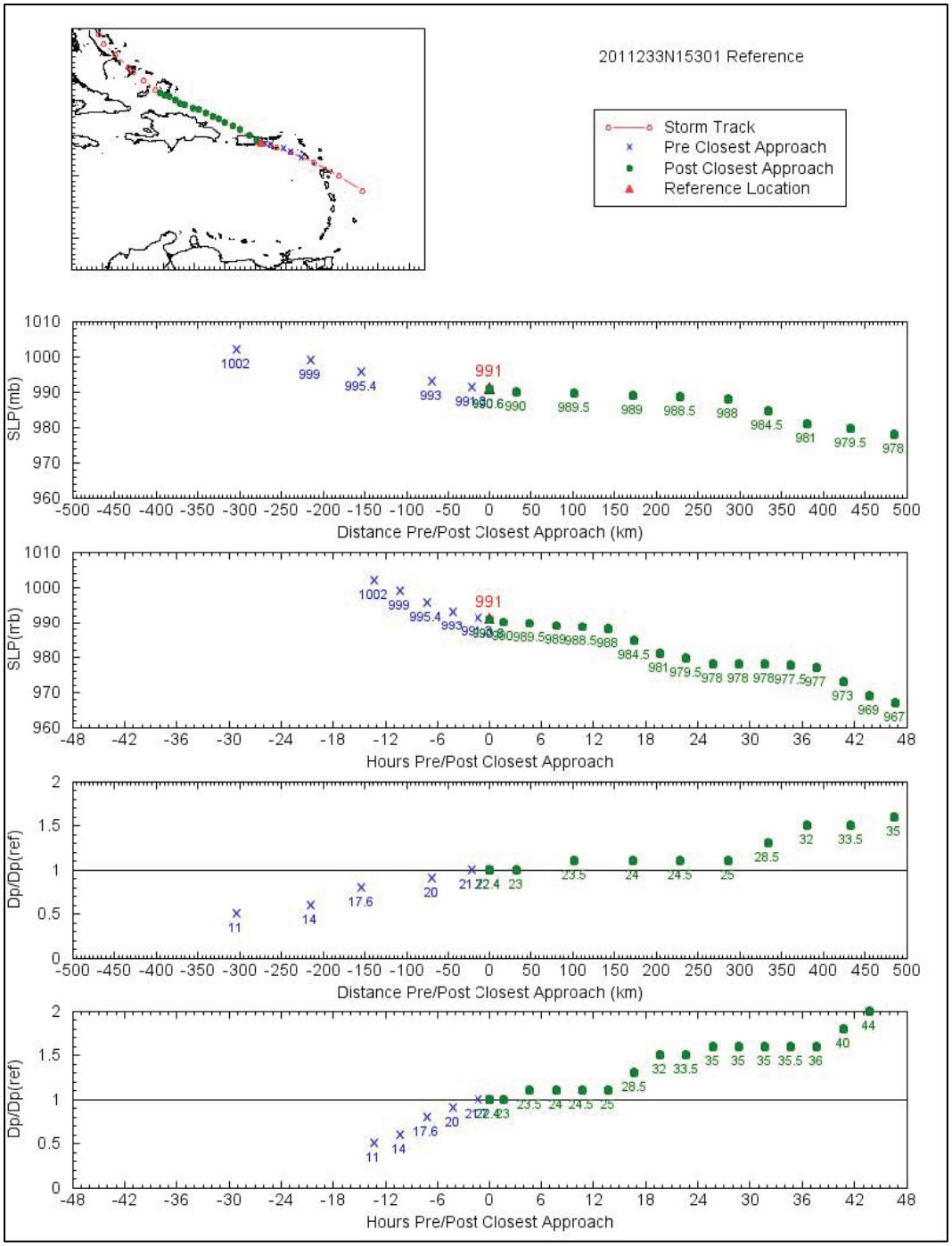

Figure 5-9. Tracks 1938-2016 with CHS-PR area landfall location (red) with track location pre-landfall (blue) and post-landfall (green) within 500 km of Puerto Rico.

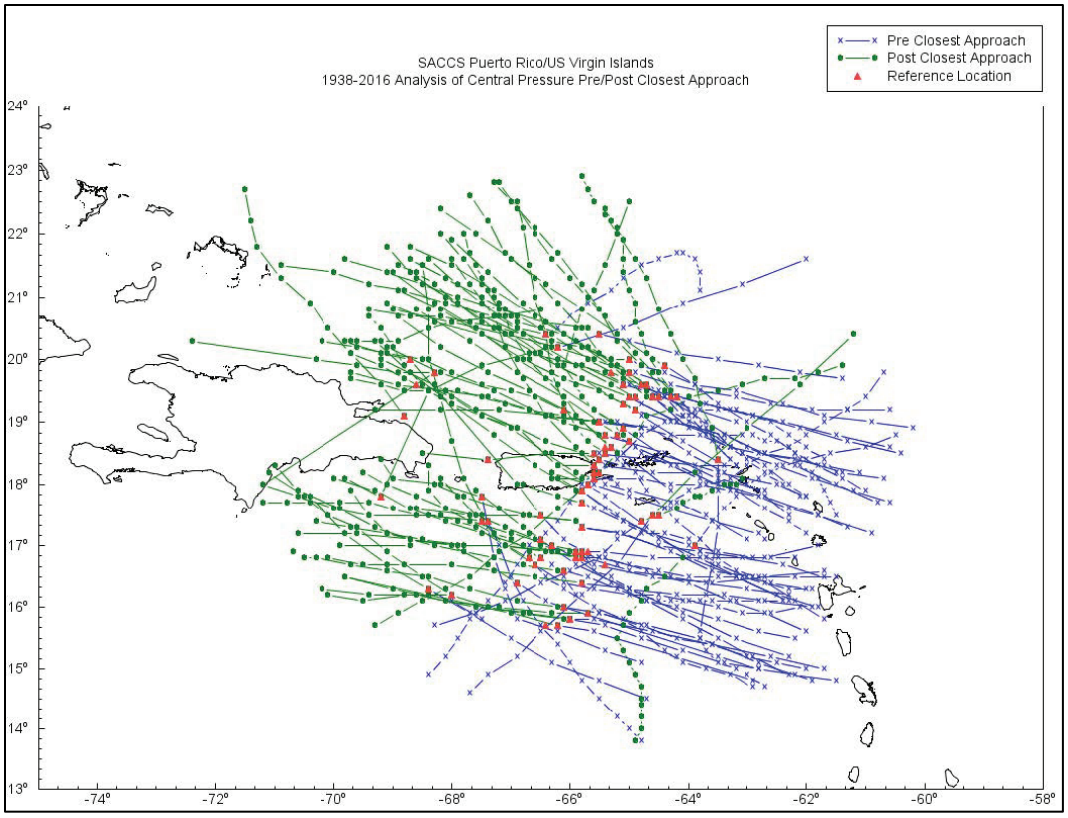

Figure 5-10. Linear fit to the ratio of pressure deficit offshore to pressure deficit at closest approach as a function of distance (km) for Puerto Rico storms 1938–2016.

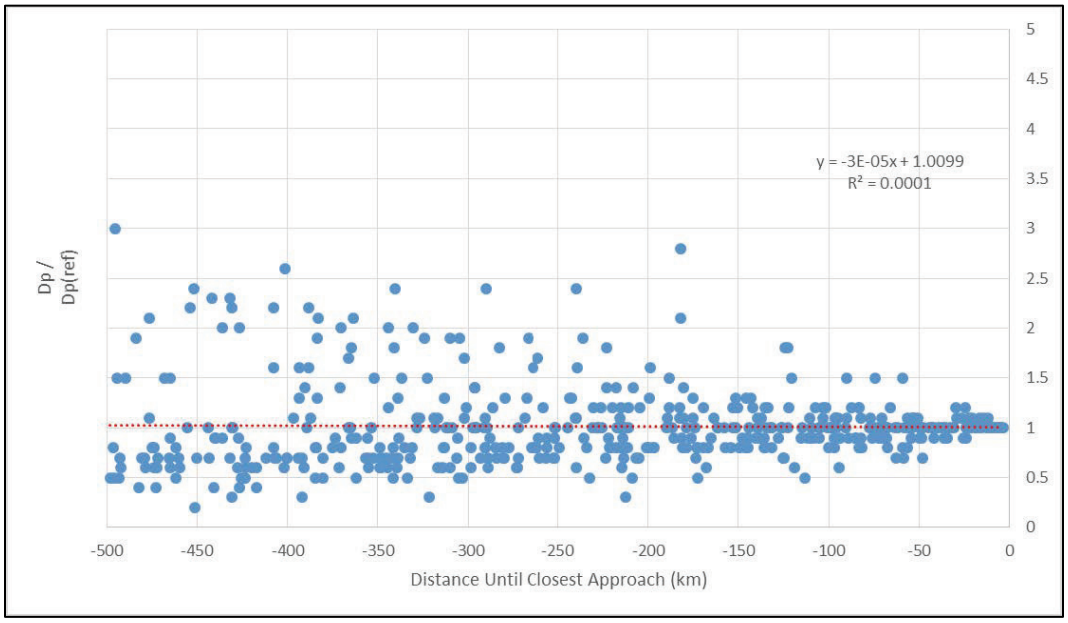

Figure 5-11. Example of linear fits for 12 historical CHS-PR storms showing the ratio of pressure deficit offshore to pressure deficit at landfall by distance offshore (km).

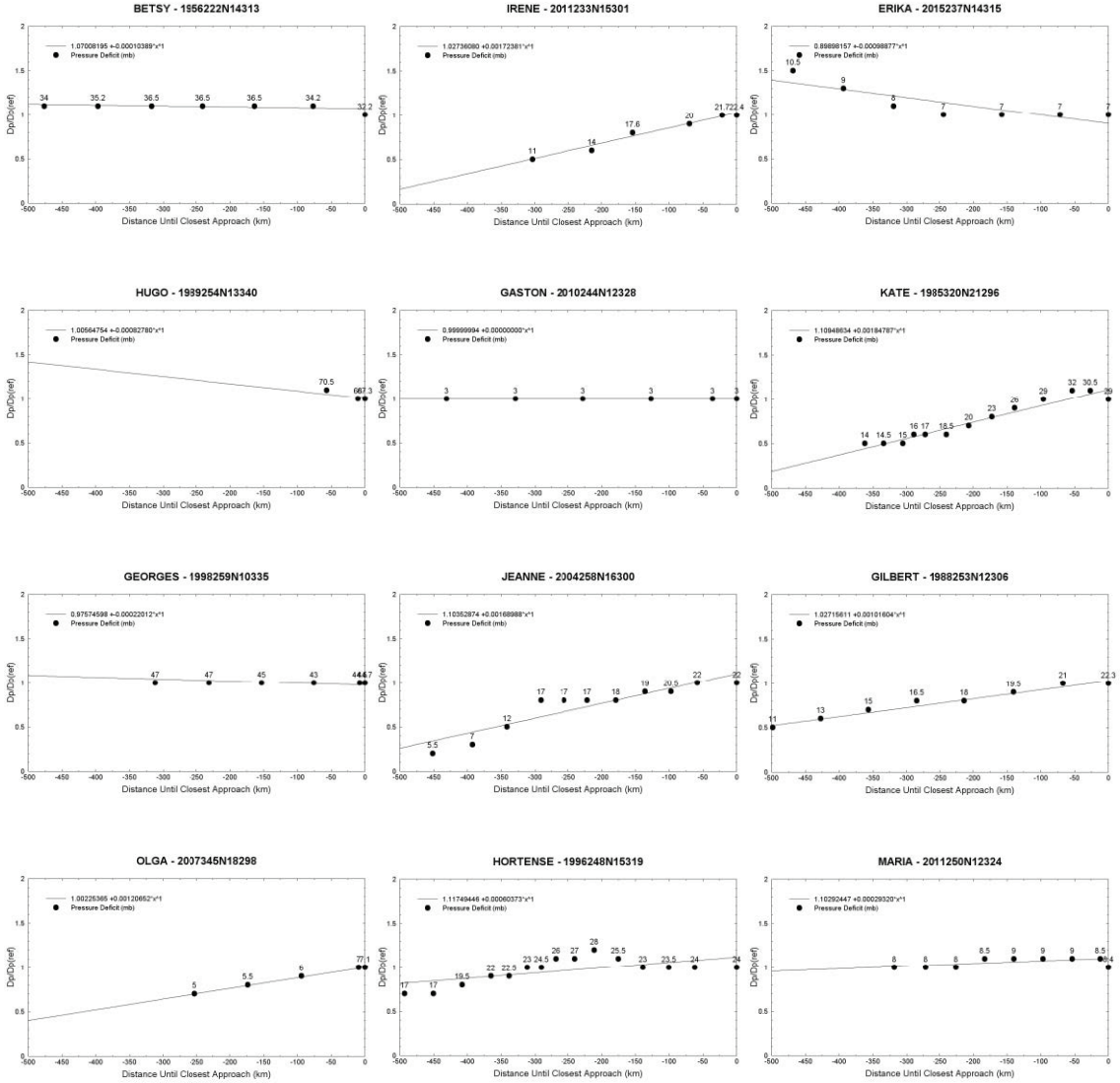

Figure 5-12. Linear fit to the ratio of pressure deficit at 250 km and landfall (*y*-axis) as a function of pressure deficit at 250 km (*x*-axis).

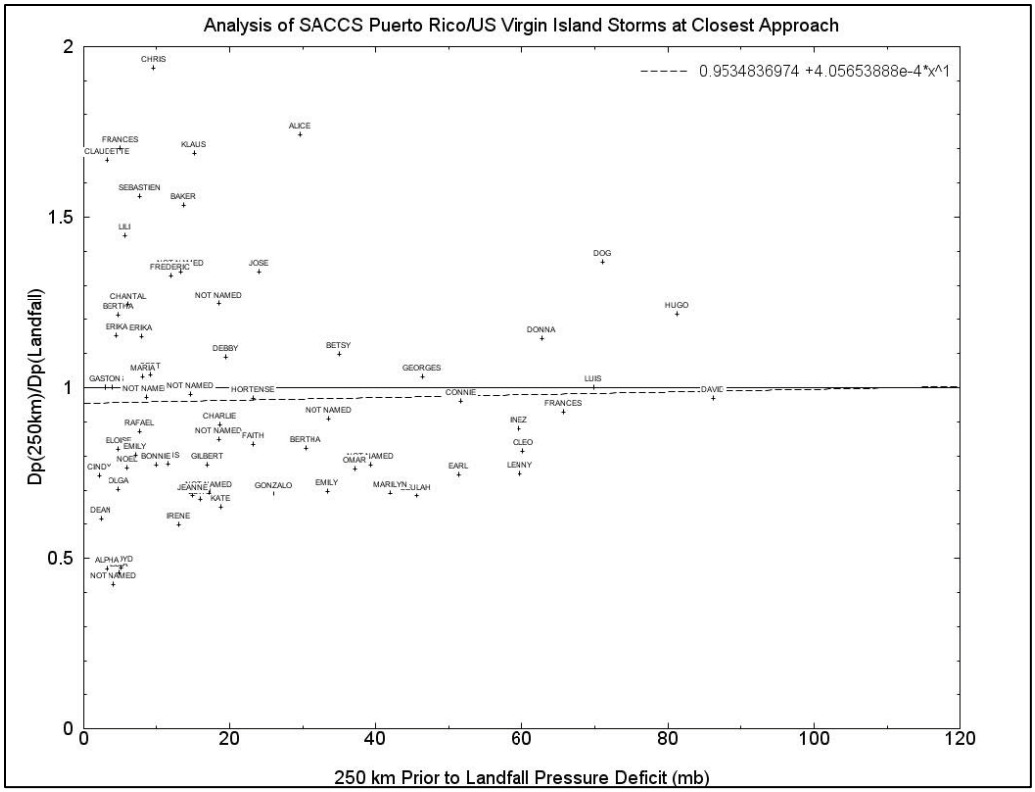

5.2.2 Determination of landfall filling

In the period from 1852 to 2016, only nine storms made landfall on Puerto Rico (Appendix C) that contain central pressure estimates both at landfall and after the storm exits the island. Figure 5-13 depicts the locations of the landfall data set with storm tracks. When the data are expressed as the difference in pressure relative to landfall pressure deficit (Figure 5-14), a clear relationship is present where stronger storms experience more weakening after landfall. Landfall filling models (Ho et al. 1987; Vickery 2005) historically take the form of

$$\Delta p(t) = \Delta p_0 \exp(-at) \tag{5-3}$$

where a is a decay constant applied with pressure deficit at landfall (Δp_o) and time (t) to result in the pressure deficit on land $\Delta p(t)$ at time t. Ho et al. (1987) expressed a as a function of pressure deficit at landfall while Vickery expanded on the analysis by introducing an a decay term that was also dependent on the radius of maximum wind and forward speed by region on the US East Coast and the GoM.

Given the sparse data available, an analysis of the decay term was explored as a function of pressure deficit at landfall (Δp_o). The analysis was formed using the raw data (Figure 5-15, top) as well as using the central pressure/pressure change relationship described above (Figure 5-15, bottom). Use of Figure 5-14 relationship to determine a increases the fit r_2 from 0.0013 to 0.5704 and retains a more positive slope with Δp_o. When the a decay function is applied back to the storm data Δp_o and compared back to the post-landfall value (Figure 5-16), the use of the fit function (Figure 5-16, bottom) results in a better representation across all values of Δp_o with a similar r_2 value. Thus, the adopted decay coefficient applied in the JPM became

$$a = 0.002\Delta p_0 + 0.0034 \tag{5-4}$$

Compared to decay values for the US regions detailed in Vickery (2005), the adopted a results in less landfall weakening for Puerto Rico storms.

Figure 5-13. Storms making landfall in Puerto Rico 1938–2016 with landfall intensity (blue, mb) and post-storm exit (red, mb).

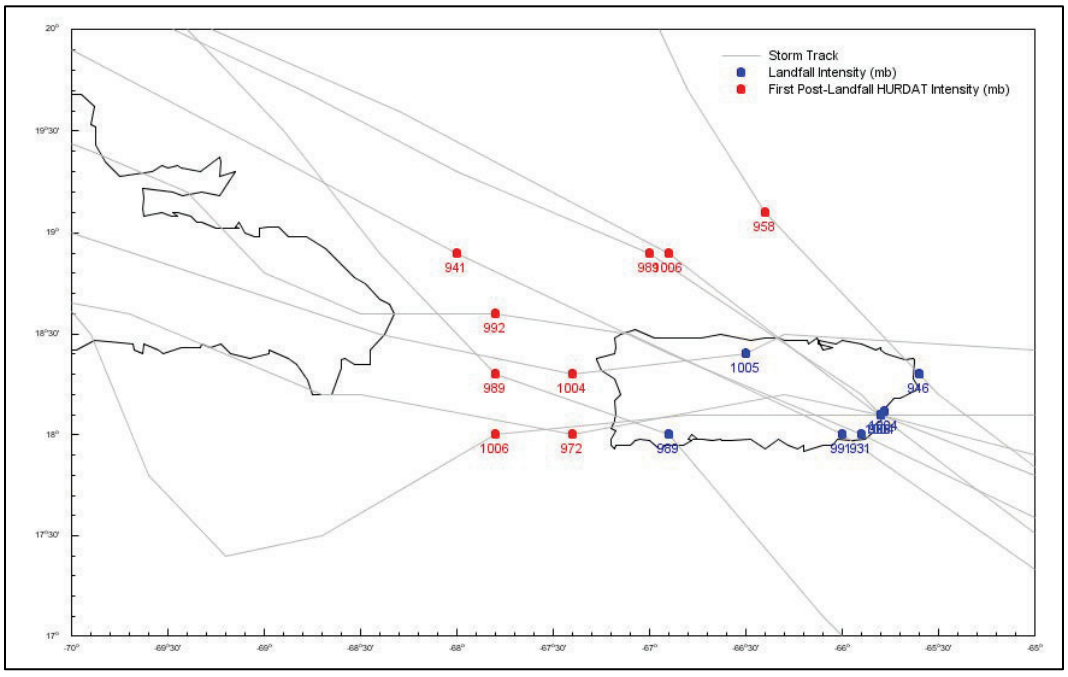

Figure 5-14. Change in central pressure as a function of landfall central pressure deficit (hPa).

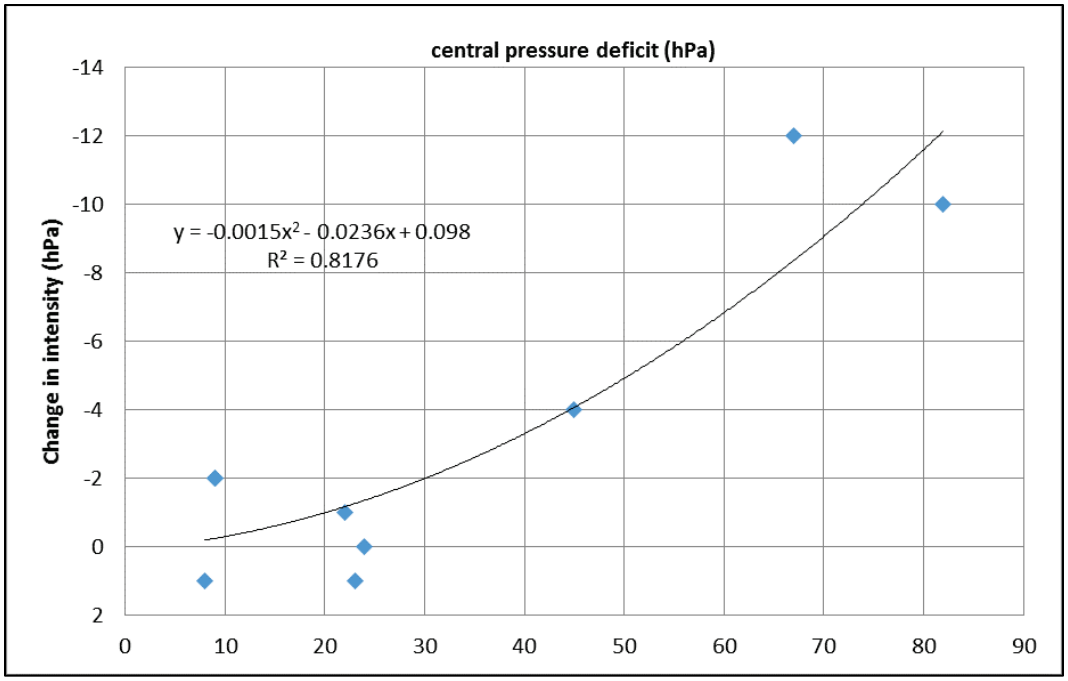

Figure 5-15. Fit of exponential decay function to central pressure deficit using historical data (top) and fit developed from Figure 5-14's pressure change relationship (bottom).

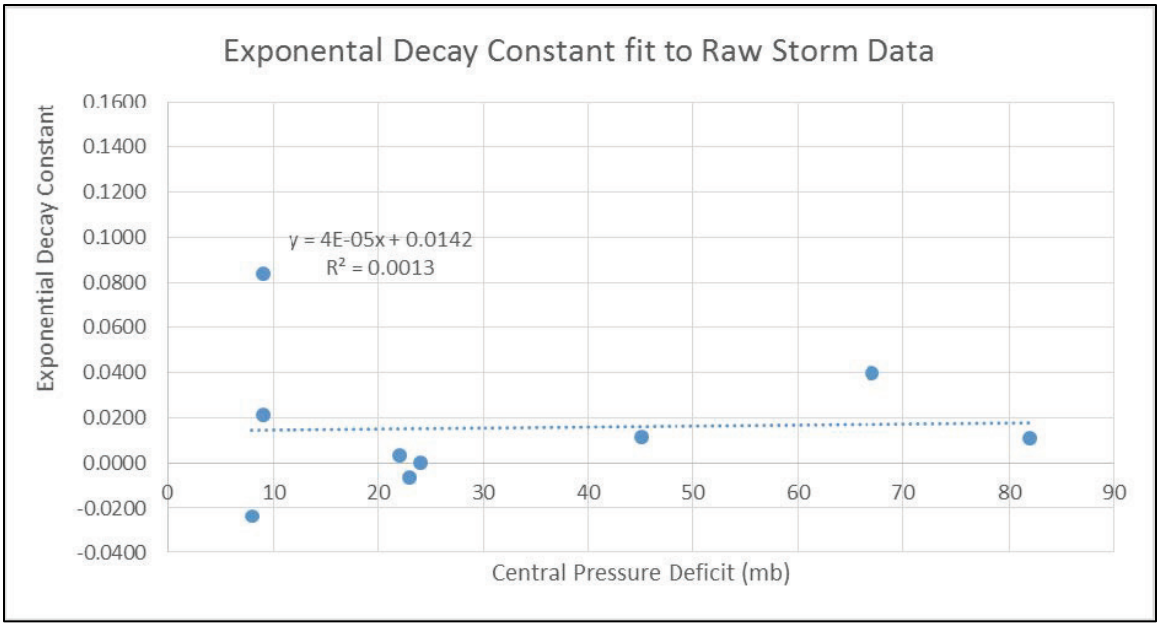

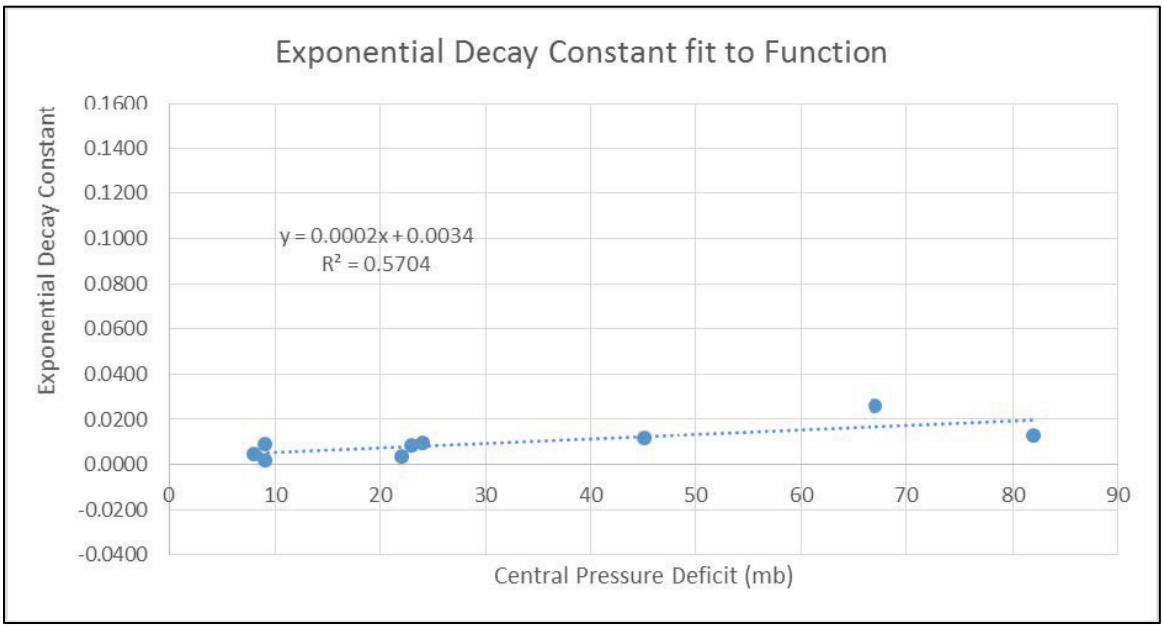

Figure 5-16. Comparison of post-landfall central pressure (mb) and predicted value using decay constant based on data (top) and decay constant based on fitted pressure relationship (bottom) from Figure 5-14.

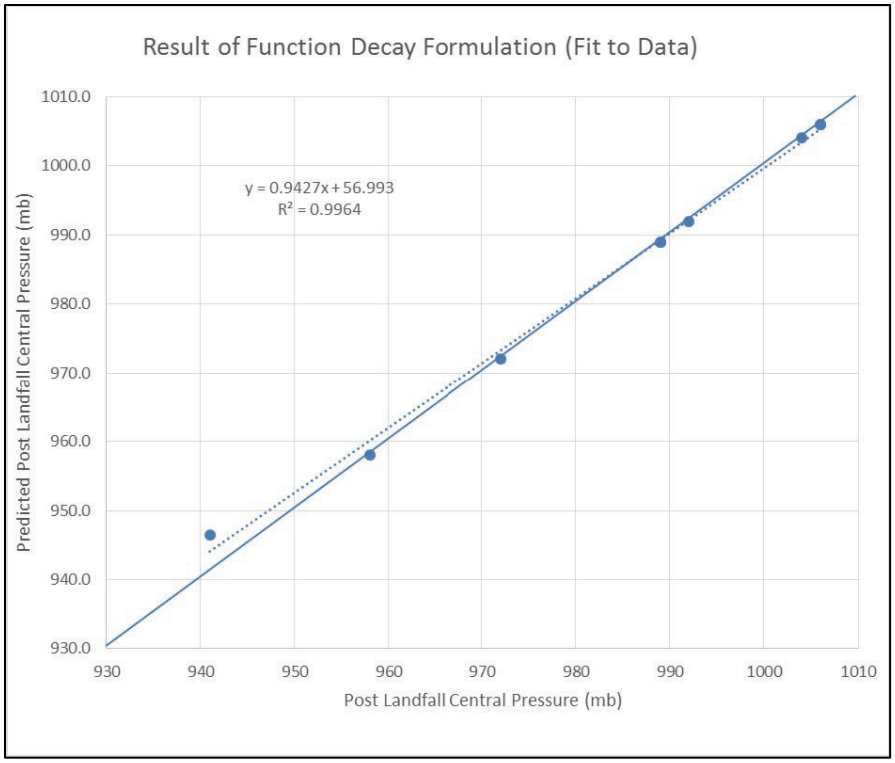

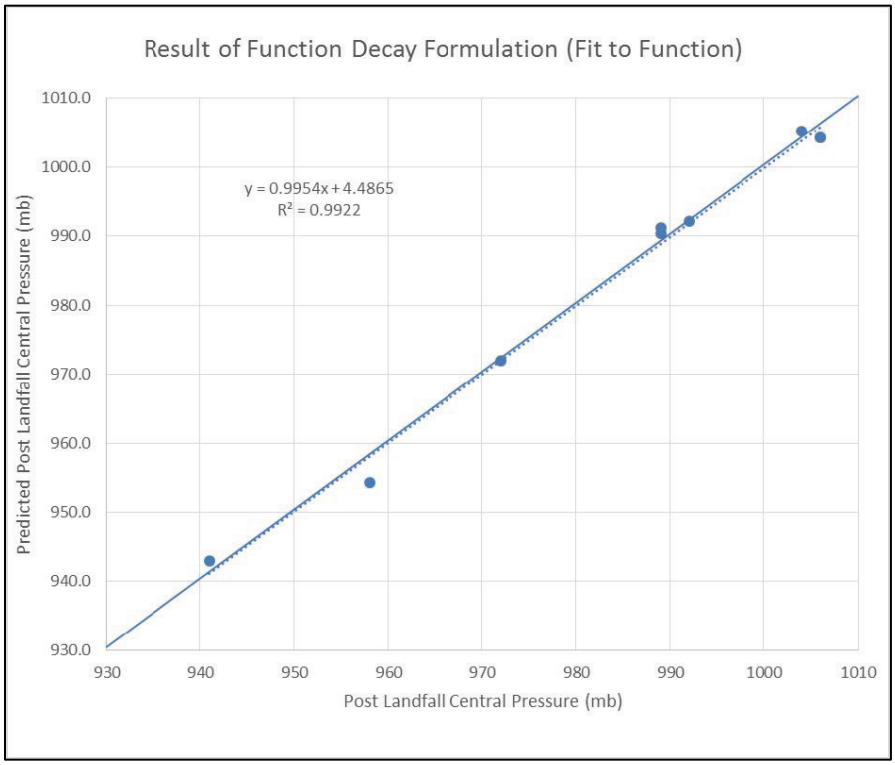

5.2.3 Scale pressure radius

In both the JPM development and in the pre-landfall/post-region filling application, the R_{max} was used as a parameter to describe each storm. In the PBL model, the R_{max} is not an input value but rather the end result of running the model with the prescribed inputs. The radius of the storm in the PBL model is primarily controlled by the scale pressure radius (R_p). Therefore, a function (Equation 5-5) to convert R_{max} to R_p is required for executing the model. This function was developed by Oceanweather, Inc., (OWI) as part of the Modeling of Relevant Physics of Sedimentation (MORPHOS) (MORPHOS 2009) project. It was based on a series of real historical storms of various radii, forward speeds, and latitudes. To test if the R_{max} to R_p conversion would be appropriate for use in this study, the PBL model was run, and the R_{max} output by the model was extracted at landfall for the entire 1,700 storm set established for the SACS. Figure 5-17 depicts the input JPM R_{max} and output model R_{max}, which shows excellent agreement across the entire range of R_{max} required.

$$R_p(Nmi) = -1.964089822 + 1.0833507089 * R_{max}(Nmi) + .00697299296 * R_{max}(Nmi)^2 \quad (5\text{-}5)$$

Figure 5-17. Comparison of JPM-specified R_{max} (nmi) and model result.

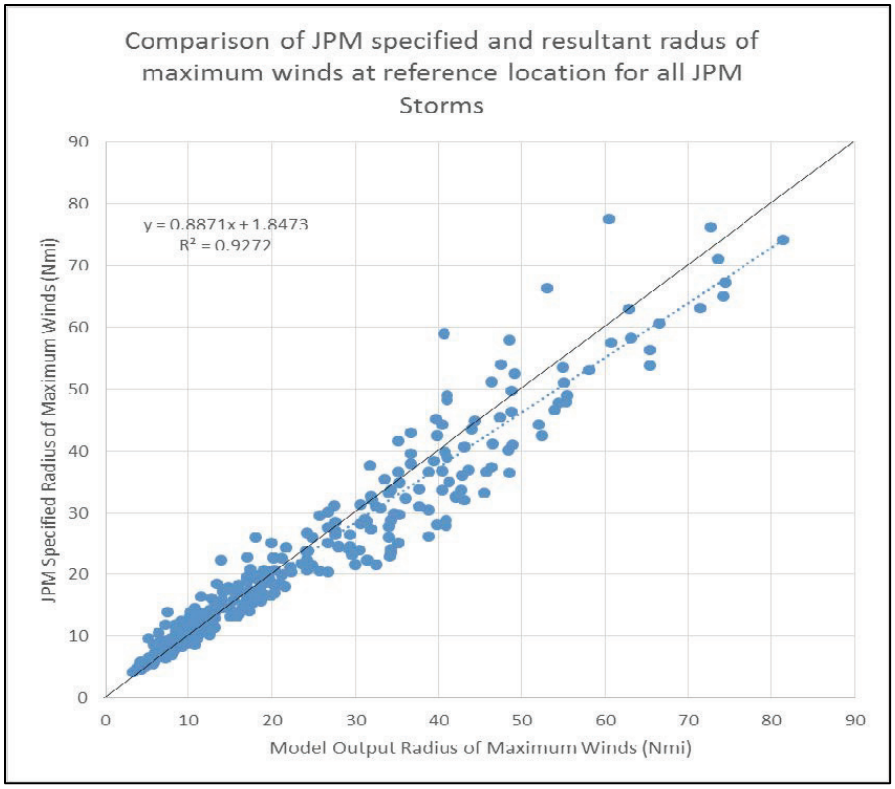

5.3 Planetary boundary layer (PBL) model

The OWI Tropical Model, also known as the PBL model, was first developed into a practical tool in the Ocean Data Gathering Program (ODGP) (Cardone et al. 1976), which can provide a fairly complete description of the time-space evolution of the surface winds in the boundary layer of a tropical cyclone from the simple model parameters available in historical storms. The model is an application of a theoretical description of the horizontal airflow in the boundary layer of a moving vortex. That model solves, by numerical integration, the vertically averaged equations of motion that govern a boundary layer subjected to horizontal and vertical shear stresses. The equations are resolved in a Cartesian coordinate system whose origin translates at constant velocity, V_t, with the storm center of the pressure field associated with the cyclone. Variations in storm intensity and motion are represented by a series of quasi-steady-state solutions. The original theoretical formulation of the model is given by Chow (1971). A similar model was described more recently in the open literature by Shapiro (1983).

The present version of the model is the result of three major upgrades. The first upgrade involved mainly replacement of the empirical scaling law by a similar boundary layer formulation to link the surface drag, surface wind, and the model vertically averaged velocity components (Cardone et al. 1992). The second upgrade (Cardone et al. 1994) added spatial resolution and generalized the pressure field specification. A more complete description of the theoretical development of the model as upgraded is given by Thompson and Cardone (1996). Last and most recently, modifications to the model PBL physics allowed for the introduction of a saturation roughness formulation (a capped drag coefficient) consistent with that found by Powell (2007) for the MORPHOS project (MORPHOS 2009).

The model pressure field is described as the sum of an axially symmetric part and a large-scale pressure field of constant gradient. The symmetric part is described in terms of an exponential pressure profile, which has the following parameters:

$$P(r) = P_o + \sum_i^n dp_i e^{-\left(\frac{Rp_i}{r}\right)^{B_i}} \quad (5\text{-}6)$$

where P_o = minimum central pressure; dp_i = total pressure deficit; R_{p_i} = scale radius of exponential pressure profile; B_i = profile peakedness parameter (Holland B); and r = radius. Holland B is an additional scaling parameter whose significance was discussed by Holland (1980). This analytical form is also used to explicitly model the storm pressure field for use in the hydrodynamic model. The model may be prescribed with a single profile (1 combination of Δp, B, R_p) for storm systems with simple wind profiles. More complex wind profiles, such as those which display wind maxima at two radii or those with a shelf structure to the wind profile, are described with a double profile. Cox and Cardone (2007) describe the methodology applied in the analysis of historical tropical cyclones, while Cardone and Cox (2009) discusses the impact of complex wind profiles on the ocean response.

The PBL model is driven from parameters that are derived from data in historical meteorological records and the ambient pressure field. The entire wind field history is computed from knowledge of the variation of those parameters along the storm track by computing solutions, or so-called *snapshots* on the nested grid as often as is necessary to describe different stages of intensity, and then interpolating the entire time history from the snapshots.

As presently formulated, the wind model is free of arbitrary calibration constants, which might link the model to a particular storm type or region. For example, differences in latitude are appropriately handled in the primitive equation formulation through the Coriolis parameter. The variations in structure between tropical storm types manifest themselves basically in the characteristics of the pressure field of the vortex itself and of the surrounding region. Therefore, the interaction of a tropical cyclone and its environment can be accounted for by a proper specification of the input parameters. The assignable parameters of the PBL formulation, namely PBL depth and stability, and of the sea surface roughness formulation, are taken from studies performed in the GoM.

The model was originally validated against winds measured in several ODGP storms. It has since been applied to nearly every recent hurricane to impact the US offshore area, to all major storms impacting the South China Sea since 1945, and to storms impacting many other foreign basins, including the Northwest Shelf of Australia, Tasman Sea of New Zealand, Bay of Bengal, Arabian Sea, and the Caribbean Sea. Many comparisons

have been published (e.g., Ross and Cardone 1978; Cardone and Ross 1979; Forristall et al. 1977, 1978; Forristall 1980; Forristall and Greenwood 1998; Cardone et al. 1992; Cardone and Grant 1994). More recent publications on the application of the PBL model in driving the ADCIRC and coupled ADCIRC/Simulating WAves Nearshore modeling system can be found in Hope et al. *(*2013) (Hurricane Ike 2008), Dietrich et al. *(*2011) (Hurricane Gustav 2008), Bacopoulos et al. *(*2011) (Hurricane Jeanne 2004), and Bunya et al. *(*2010) (Hurricanes Katrina and Rita 2005). Application in Hurricane Harvey (2017) is presented in Cox et al. (2017).

5.4 Summary of tropical wind and pressure forcing inputs

Following the development of along-track variation of the TC parameters, post-landfall filling, and estimation of scale pressure radius, the 300-storm set was run through the PBL model for the development of wind and pressure fields on two working grids. The large-scale Western North Atlantic Domain is a latitude-longitude grid covering the domain 5°-47°N 99°-55°W at a 0.2° resolution. The more refined grid, referred to as the Puerto Rico Domain grid, is a 0.02° latitude-longitude grid centered at the landfall location which extends +/- 1.5°.

The output time-step is 15 or 5 min, depending on the forward speed of the storm (see Table 5-1). Data files generated from this process are denoted with the file extensions WIN and PRE, which are standard preprocessor input file extensions to ADCIRC for wind and pressure fields, respectively. Wind fields represent a 30 min average wind at a 10 m height designated for marine exposure. Pressures are at sea level in millibars.

Figure 5-18 depicts an overall summary of the track paths and model inputs in terms of scale pressure radius, Holland's B, and forward speed versus storm intensity for the entire 300 storm set.

Figure 5-18. Summary of JPM track path and derived parameters for the entire 300 storm set.

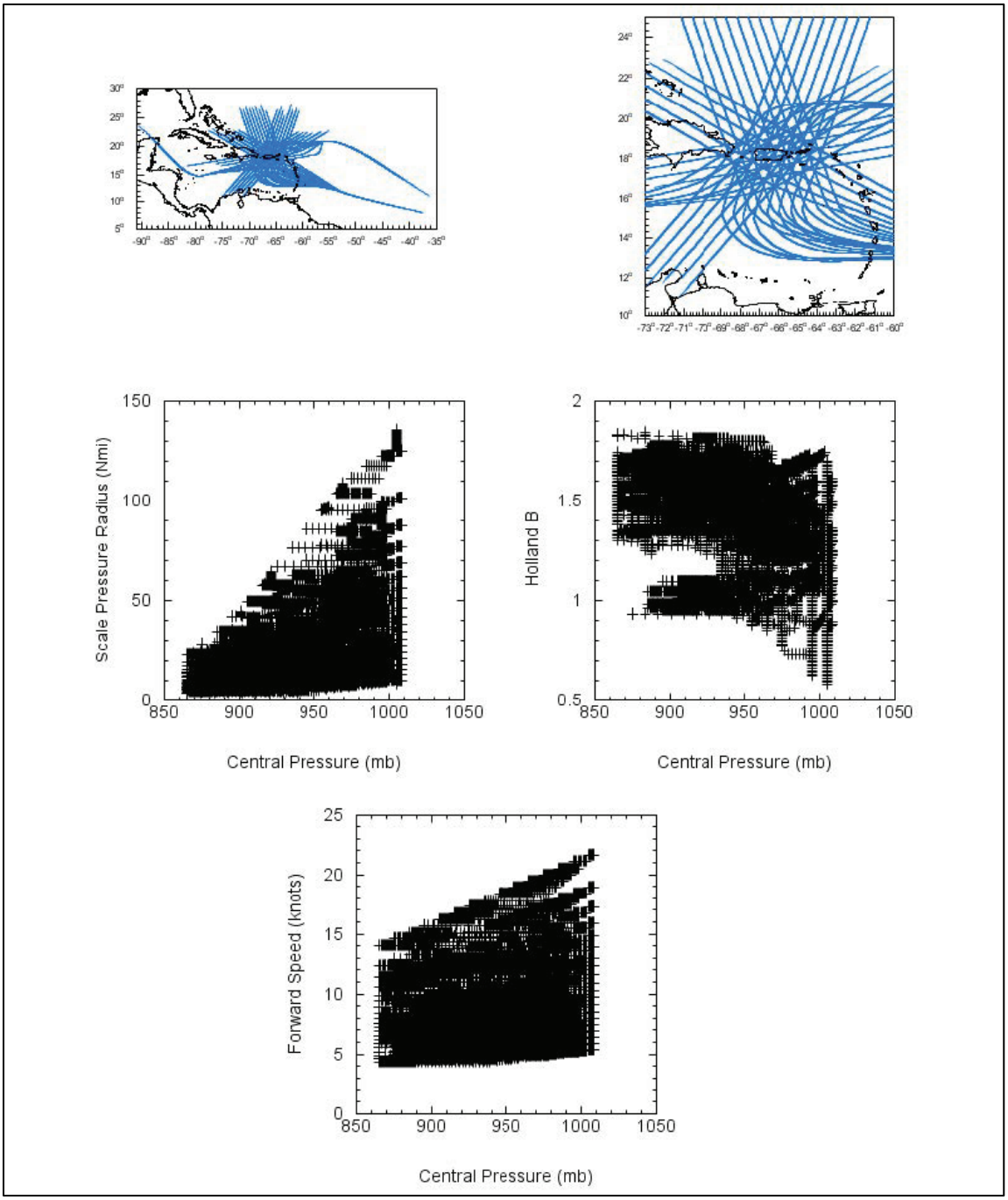

6 Quantification of Coastal Storm Hazards

The following subsections describe the PCHA methodology applied to quantify coastal storm hazards and develop SWL, H_{m0}, and T_p hazard curves for the CHS-PR study area. Details related to the hydrodynamic modeling, including DNC and training of the GPMs, are provided in Section 6.1. Section 6.2 describes the correction of bias and the estimation of uncertainty associated with TC responses. The methods applied to account for the effects of astronomical tides are detailed in Section 6.3. The joint probability analysis of the TC responses for SWL and the wave parameters is discussed in Sections 6.4 and 6.5, respectively.

6.1 Hydrodynamic modeling considerations

For the CHS-PR region, the ITCS was simulated under multiple sea level change (SLC) scenarios using the ADCIRC and STWAVE models. The values selected for the SLC 1 and SLC 2 scenarios were determined from the USACE high and intermediate SLC curves in the year 2120. For the synthetic TCs, the hydrodynamic model simulations of each SLC scenario also included a steric water level adjustment of +0.0485 m, which was determined using the 1983–2001 tidal epoch. In the case of the historical TCs, the steric water level adjustment was based on the mean water level during the month of the event as determined by data from NOAA gauges. The modeling cases and SLC scenarios considered for the ITCS are documented in Table 6-1. Additionally, the modeling completed for the CHS-PR study area considered a vertical datum relative to MSL.

Table 6-1. Description of scenarios considered for the hydrodynamic model simulations.

Scenario	Description	Sea Level Change (m)	Considered for Storm Type
SLC 0, Tides 0	Base Conditions modeled on mean sea level with wave effects and without astronomical tides.	0.00	TC
SLC 0, Tides 1	Base Conditions modeled on mean sea level with wave effects and the historical tides timed with the winds. This scenario was considered for the historical TC simulations.		Historical TCs
SLC 1, Tides 0	Base Conditions modeled with waves and without astronomical tides while considering the effects of sea level change.	0.7102	TC
SLC 2, Tides 0	Base Conditions modeled with waves and without astronomical tides while considering the effects of sea level change.	2.1184	TC

6.1.1 Dry-node correction (DNC)

When considering storm surge results for any given study area, some locations are not inundated (remain dry) for some TCs. The occurrence of these dry computational point locations (nodes or VGs), if left uncorrected, can adversely affect the reliability of the GPM and the accuracy of hazard estimates due to both the reduced number of support points for training a metamodel and the loss of DSWs associated with TCs that do not inundate a given VG. To avoid this potential inaccuracy, the PCHA performs DNC through the application of a geospatial GPM, which interpolates the missing storm surge at the dry VGs.

For the geospatial GPM, the input data applied in the optimization of the kriging parameters was the storm surge recorded at VGs that were inundated during all simulations of the ITCS. These locations are referenced as always-wet VGs. Maximum Likelihood Estimation was used to optimize the parameters in the kriging equation, which was evaluated at the dry VGs to fill in the missing data with pseudo-surges (Shisler and Johnson 2022). The forcing vector for each of the always-wet VGs and the dry VGs was the latitude and longitude of each location. To fill in the missing information at the dry VGs, the geospatial GPM completes the SWL surface over the project domain, on a per-storm basis. Figure 6-1 shows an idealized cross section to demonstrate the implementation of the DNC.

Figure 6-1. Idealized across-shore sketch illustrating the dry-node correction.

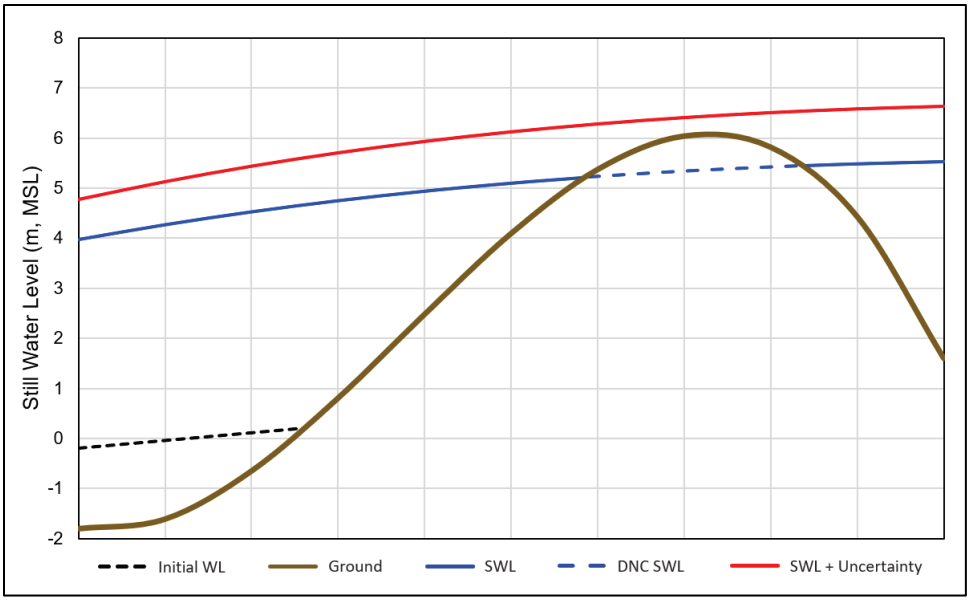

The dashed black curve and solid-brown curve represent the initial water level and ground elevation, respectively. The SWL surface (solid blue curve) is interrupted by a section of high ground elevation (e.g., coastal bluff, dune, or barrier island). In typical JPM applications, VGs within this high ground area are inundated by only the most extreme TCs, leaving an incomplete representation of the SWL at this location, which can result in significant underestimation of the storm surge hazard at these locations. For these uncorrected locations, the DNC completes the SWL surface over the entire domain and across the high ground sections (dashed blue curve) to provide an accurate estimate along the entire blue line. Extending the SWL surface, even below ground, allows for proper integration of JPM uncertainty (per Equation 2-2). As a result, the SWL + uncertainty surface (red curve) may exceed the elevation of the high ground section. For CHS-PR, the DNC was completed for all SLCs prior to training a GPM for the prediction of the ATCS storm responses.

When the DNC is applied to perform imputation of storm surge values at point locations apart from ADCIRC nodes, such as VGs, it is important to note that the SWL hazard computation is not adjusted for topographic elevation. Therefore, some of the resulting SWL hazard curves might reflect values below ground level. It is not recommended to use the ground elevation of a VG to adjust the corresponding SWL hazard curve given that VG elevation (i.e., -1×depth) is determined by interpolating the depth from the triangulated computational grid nodes surrounding the VG. As such, interpolated VG depths can be inconsistent when the triangulated nodes are located in areas of rapidly varying topography/bathymetry, such as flood risk reduction structures or riverbanks. The recommendation is to instead rely on high-resolution elevation data and limit the application of hazard curves to SWL values above ground level.

6.1.2 Metamodel training

The CHS-PR ITCS was defined by a five-parameter set: $x = [x_o, \theta, \Delta p, v_t, R_{max}]$. For the GPM training, the number of input parameters increased to six to consider both the latitude and longitude of the landfall locations; thus, $x = [Latitude, Longitude, \theta, \Delta p, v_t, R_{max}]$. To fully capture the probability space and to improve the hazard estimates of the AEFs, an ATCS consisting of 348,000 TCs was created by discretizing the existing parameter range of the ITCS (Section 4.4). Predicting the storm responses of the ATCS required the development of separate metamodels for SWL

and H_{mo}. Following the DNC, a GPM was trained on the ITCS storm surge responses at all 14,891 VGs (Figure 6-2). Since no correction is available for missing wave data, a total of 915 VGs were removed from the training database, and a second GPM was trained on the ITCS H_{mo} responses at 13,976 VGs.

The GPM estimates the hydrodynamic responses with a kriging prediction equation (Zhang et al. 2018). Prior to the kriging development, the surge values in the ITCS were normalized to facilitate decreasing the dimensionality of the synthetic TC parameters by Δp. The main requirements of the equation for the metamodel are basis vectors, $f(x)$, and a correlation structure $R(x^i, x^j|s)$, where s is a set of hyper-parameters (Zhang et al. 2018). For this study, linear basis functions were chosen for $f(x)$, and the predictive cross-validation method was utilized to optimize s. The raw predictions generated by the kriging model were transformed to the original, high-dimensional response space with the Principal Component Analysis transformation. The resulting average validation statistics show good accuracy for the storm surge predictions with a root mean squared error ($\overline{RMSE}$) of 10 cm, a coefficient of correlation ($\overline{CC}$) of 97%, and a correlation of determination ($\overline{R^2}$) of 94%. After the metamodels were trained, the surge and H_{mo} responses were calculated for the ATCS.

Figure 6-2. Geospatial distribution of VGs within the CHS-PR study area.

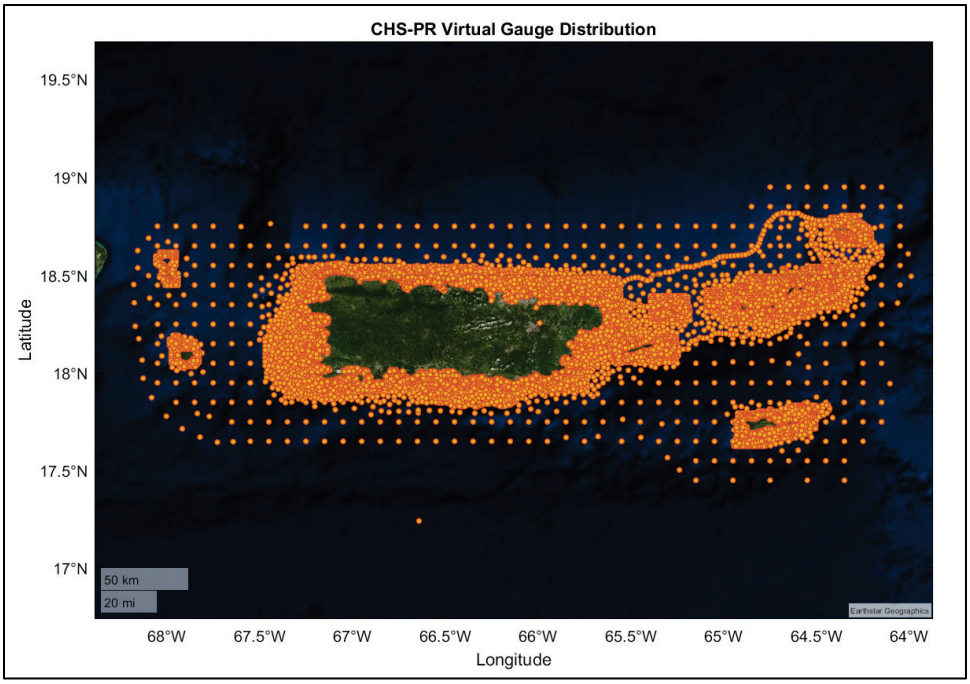

6.2 Estimation of geospatial bias and uncertainty

A natural consequence of the inherent simplification associated with the modeling of complex natural systems is that model outputs will differ to some degree from the actual values of the evaluated phenomena. Quantification of the difference or error is necessary to calibrate model parameters, validate the results, and characterize the model performance. Errors in hydrodynamic modeling may originate from the idealization of wind fields, discretized approximation of the bathymetry and topography, shallow water approximations of the governing hydrodynamic equations, simplified wave model equations, or assumptions related to boundary conditions. As shown in Figure 6-3, the two main error components are systematic error (bias) and spread (uncertainty), which relate to model accuracy and precision. In the JPM approach, it has been typically assumed that the error is unbiased, and the uncertainty has been addressed by using an error term within the JPM integral. Bias correction is required before the JPM integration if found in the assessment of model error. Generally, errors in SWL and H_{mo} are evaluated by comparing the validation storm simulation results to observations. For SWL, the comparison is primarily made with water level gauge measurements and high-water marks (HWM). While gauge measurements are typically reliable, HWMs often include wave effects as well as some degree of human interpretation of the HWM that limit their usefulness for SWLs. As a result, HWM data are carefully screened to remove HWMs that could include significant wave effects. For the CHS-PR study, the validation Hurricanes considered were Georges (1998), Irene (2011), Irma (2017), and Maria (2019)[1]. These validation TCs were simulated under the SLC 0 Tides 1 scenario considering the effect of historical tides. The sources of error considered in this study are documented in Section 6.2.1 whereas the methods for quantifying these errors are discussed in detail in Sections 6.2.2 through 6.2.4.

[1] Owensby, M., M. Bryant, T. Hesser, L. Provost, T. C. Massey, and Y. Ding. 2019. *Calibration and Validation of the Puerto Rico/US Virgin Island Domain Model Setup for the South Atlantic Coastal Study (SACS)*. ERDC/CHL LR-19-9. Vicksburg, MS: US Army Engineer Research and Development Center.

Figure 6-3. Illustration of bias and uncertainty in model prediction.

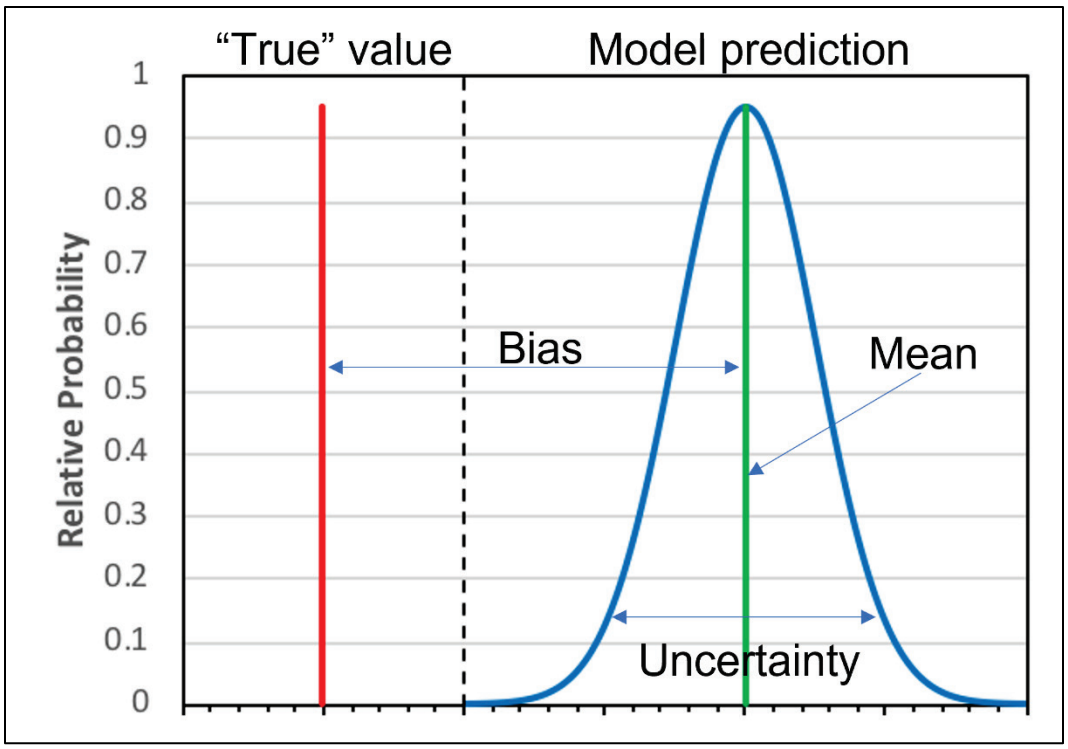

6.2.1 Aleatory and epistemic uncertainties

As discussed by Gonzalez et al. (2019), uncertainties associated with coastal storm hazards are generally classified as either aleatory or epistemic. *Aleatory* uncertainty, also called aleatory variability, describes the stochastic (i.e., random) nature of hazard events and processes. *Epistemic* uncertainty refers to the scientific uncertainty associated with the modeling of natural processes and arises due to a lack of data, information, or knowledge about the physical world. This form of uncertainty is often called subjective or reducible uncertainty since it can theoretically be reduced through further research and additional data collection efforts. In practice, this possibility of reduction is also present for aleatory uncertainty and is not exclusive to epistemic uncertainty (Vrouwenvelder 2003). Estimates of stochastic processes that are characterized as aleatory uncertainty cannot be significantly reduced in the short-term, but they can be improved. Therefore, differentiating between aleatory and epistemic uncertainties can be challenging, depending on the nature of the model (USNRC 1997; IPET 2009). Furthermore, Brun et al. (2011) contend that aleatory and epistemic uncertainties are not mutually exclusive. Der Kiureghian and Ditlevsen (2009) state that the characterization of uncertainty as either epistemic

or aleatory is a pragmatic choice that depends on the application; uncertainty can be defined as epistemic in one model and as aleatory in another. The distinction between epistemic and aleatory uncertainty should serve the practical purpose of acknowledging the sources of uncertainty that could be reduced at present, without demanding major scientific or engineering advances.

In coastal storm hazard applications, aleatory uncertainty arises due to the prevalence of geospatial and temporal variability in atmospheric, hydrodynamic, and other natural physical processes that cannot be exactly replicated by current models. Aleatory coastal storm events are characterized by their likelihood of occurrence and by probability distribution functions describing their intensity, size, forward translation speed, and track direction in the case of TCs. As discussed by Bensi and Kanney (2015), accounting for aleatory uncertainty results in a hazard curve. In contrast, the standard for quantifying and propagating epistemic uncertainty in general probabilistic hazard analysis is the use of logic trees to consider alternative data, methods, and models necessary to perform the analysis (USNRC 1997; Bommer and Scherbaum 2008; IPET 2009; Kammerer and Ake 2012; Kammerer 2013; Gonzalez et al. 2019). Bensi and Kanney (2015) describe various examples of epistemic uncertainty specific to coastal storm hazards analysis, including (1) the selection of probability distribution functions for characterizing aleatory uncertainty associated with storm parameters, (2) the selection of storm sampling technique, (3) the appropriateness of atmospheric and hydrodynamic simulation model applications, and (4) the choice of parameters used in these models. Epistemic uncertainty reflects the lack of understanding in the validity of models and corresponding numerical parameters employed in the quantification of these hazards. The logic tree approach yields a family of hazard curves where each individual curve represents a unique set (i.e., branch) of alternative data, methods, and models, and the range of uncertainty is conveyed through fractile hazard curves.

The use of logic trees is one alternative for quantifying epistemic uncertainty associated with coastal hazards. However, the implementation of logic trees has fallen outside the scope of JPM-based studies to date due to computational burdens and complexity. In logic tree hazard analysis, differences between the observed and modeled outcomes of coastal storm events are attributed to aleatory uncertainty. Specific sources of model

error accounted for in the PCHA framework include (1) hydrodynamic modeling errors potentially arising from unresolved physical processes, inadequate resolution, and bathymetry/topography inaccuracy and (2) atmospheric modeling errors due to idealized wind and pressure fields and wind variations not captured by the PBL model. In practice, even after proper model verification and validation, estimates of hydrodynamic and atmospheric model errors can be improved, but they cannot be significantly reduced in the near-term due to the prevalent spatiotemporal randomness of natural processes. Therefore, these model errors are characterized as aleatory uncertainty following the logic tree paradigm.

6.2.2 Sources of modeling error

The sources of bias and uncertainty errors accounted for in this study include hydrodynamic modeling errors and atmospheric modeling errors. Quantifying coastal storm hazards requires correcting bias and estimating uncertainty across all point locations where hazard curves are developed. Storm surge, wave, and atmospheric modeling errors are discussed below.

6.2.2.1 Storm surge modeling error

Hydrodynamic modeling errors have been estimated as part of several recent JPM-based studies. For example, in the MCAP study (FEMA 2008), the hydrodynamic modeling or calibration error was computed from the differences between simulated and measured storm surge elevations, or HWMs. However, the uncertainty associated with this error was estimated based on the difference between the standard deviations of the calibration and measurement errors. The measurement error was calculated as a standard deviation representing the variability in HWMs from the actual maximum water level. The hydrodynamic modeling uncertainty resulting from the MCAP analysis of these errors was 0.23 m. The hydrodynamic modeling uncertainty calculated in the Coastal Texas FIS (USACE 2011) for the GoM region was estimated to be in the range of 0.53–0.76 m. For NACCS, the hydrodynamic modeling uncertainty was computed based on the differences between ADCIRC results and HWMs and was estimated to be 0.48 m. For CHS-PR, ADCIRC modeling results were compared with HWM data for the validation storm simulations. As a result of this effort, relative and absolute forms of bias and uncertainty were computed at all 14,891 VGs in the study area.

6.2.2.2 Nearshore wave modeling error

For the estimation of uncertainty associated with the skill of the wave model, a global H_{mo} uncertainty was estimated as an average across all VGs due to the sparse availability of buoy measurements for the validation storms. The H_{mo} global uncertainty was assessed by comparing model simulations of validation Hurricanes Irma, Irene, and Maria to measurements recorded at buoys within the study.

6.2.2.3 Atmospheric modeling error

Errors in atmospheric modeling were estimated from the variability in water levels when comparing levels simulated using PBL winds to those simulated using handcrafted best-winds. The wind and pressure fields derived from best-winds employ techniques that combine inputs from various meteorological sources. In previous studies such as the MCAP, the Coastal Texas FIS, and the NACCS (FEMA 2008; USACE 2011; and Nadal-Caraballo et al. 2015), a range of uncertainty of 0.30–0.75 m was determined from the validation efforts. In particular, the MCAP study, which was completed in parallel with LACPR (USACE 2009a), documented a standard deviation of 0.36 m.

6.2.3 Absolute and relative forms of bias and uncertainty

As shown in this section, uncertainty can be characterized as an absolute quantity (e.g., 0.60 m) or a relative quantity (e.g., 20%). Exclusively accounting for absolute uncertainty is problematic when applied to small surges. For example, a storm surge and uncertainty of equal magnitudes would superimpose 0.60 m of uncertainty on a 0.60 m surge. Conversely, accounting for relative uncertainty alone could yield unrealistic uncertainty values for extreme surge elevations. The quantified relative uncertainty can be considerable if based on relatively small surge values. The dynamics of applying either an absolute or relative uncertainty are illustrated in Figure 6-4. The horizontal green line represents an example of absolute uncertainty of 0.6 m. Relative uncertainties of 20% and 40% are shown as the solid red and blue lines, respectively.

The PCHA framework overcomes these limitations by quantifying and combining both the absolute and the relative forms of uncertainty. Combining both forms of uncertainty is performed based on statistical

data assimilation methods. Quantification of SWL hazard, for example, requires estimating the components of uncertainty introduced by ADCIRC and the PBL model. Absolute and relative uncertainties are first estimated separately for each of these numerical models. The total absolute model uncertainty is then computed by aggregating the absolute uncertainties of the ADCIRC and PBL models. Likewise, aggregating the relative uncertainties for both models results in the total absolute model uncertainty. Finally, to combine the absolute and relative forms of the total model uncertainty, the equation corresponding to the scalar case of the data assimilation error statistics described in Gao et al. (2012) is applied across the VGs:

$$\frac{1}{{\sigma_c}^2} = \frac{1}{{\sigma_{a_{Total}}}^2} + \frac{1}{(\sigma_{r_{Total}} \cdot \tau)^2} \tag{6-1a}$$

or

$$\sigma_c = \frac{1}{\sqrt{\frac{1}{{\sigma_{a_{Total}}}^2} + \frac{1}{(\sigma_{r_{Total}} \cdot \tau)^2}}} \tag{6-1b}$$

where σ_c = total combined uncertainty (m); $\sigma_{a_{Total}}$ = total absolute model uncertainty (m); $\sigma_{r_{Total}}$ = total relative model uncertainty (m/m); and τ = storm response (m) (e.g., SWL, H_{mo}).

Using Equation 6-1b, $\sigma_{a_{Total}}$ and $\sigma_{r_{Total}}$ are combined in a manner that prevents the overestimation of uncertainty and limits the overprediction of both low- and high-magnitude SWL values. The effects of this application are shown in the example combined uncertainty curves shown in Figure 6-4. These examples of combined uncertainty curves apply an absolute uncertainty of 0.6 m to relative uncertainties of 20% and 40%. As seen in the red and blue dashed lines, the combined uncertainty increases as a function of the SWL, but the rate of growth follows an asymptotic behavior and diminishes upon approaching the absolute uncertainty.

Figure 6-4. Comparison of methods for characterizing uncertainty.

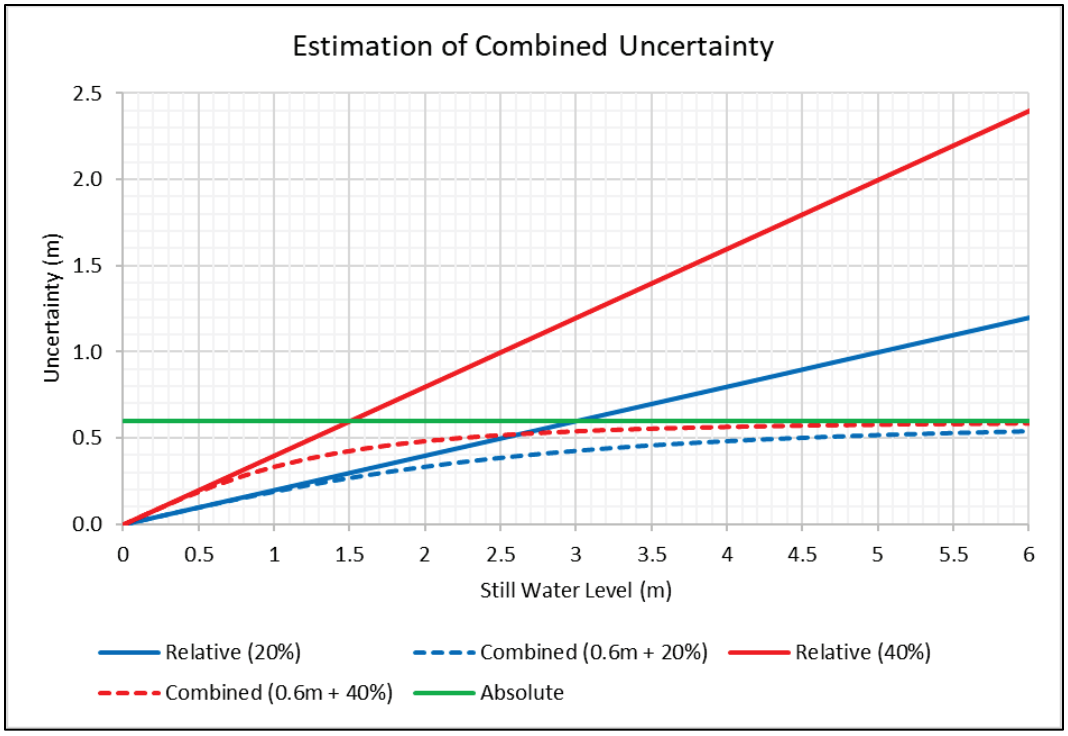

Numerical model bias is also estimated in absolute and relative forms. The total absolute and relative model biases are calculated individually and subsequently aggregated. The total combined model bias (μ_c) is determined at each VG using the following equation:

$$\mu_c = \frac{\mu_{a_{Total}}}{\left\|\mu_{a_{Total}}\right\|} \frac{1}{\sqrt{\frac{1}{\mu_{a_{Total}}{}^2} + \frac{1}{\left(\mu_{r_{Total}} \cdot \tau\right)^2}}} \tag{6-2}$$

where μ_c = total combined bias (m); $\mu_{a_{Total}}$ = total absolute model bias (m); and $\mu_{r_{Total}}$ = total relative model bias (m/m). Note that differently from Equation (6-1b), a non-dimensional factor $\frac{\mu_{a_{Total}}}{\left\|\mu_{a_{Total}}\right\|}$ is incorporated into Equation (6-2) to retain the sign of the bias, which is necessary for the bias correction before estimating uncertainty. The estimation of the total model bias and uncertainties is documented in Sections 6.2.4 and 6.2.5, respectively.

6.2.4 Geospatial bias estimation and correction

In hydrodynamic numerical model simulations, there is bias if the output tends to either over-predict or under-predict the magnitude of observed

responses. The bias associated with the ADCIRC and PBL models was assessed by comparing historical measurement data with simulation results of the validation hurricanes. Due to the geospatial and temporal spareness of the wave buoy measurements, bias associated with the STWAVE simulations was not evaluated as part of this study. Relying on the sparse observational data available for the validation storms to perform bias correction could in turn introduce bias in the simulations; therefore, bias was not corrected for the STWAVE simulations. In the case of SWL, the bias is estimated as the mean difference between simulated and observed water levels at the location of a water level gauge or HWM. The bias generally has units of length, but non-dimensional bias can also be quantified. In cases where the bias is negligible, the hydrodynamic predictions are considered unbiased. This dimensional bias is referred to as the weighted absolute form of the bias (μ_a) and is defined at each VG as follows:

$$\mu_a = \frac{\sum_{i=1}^{N} w_i(\varepsilon_a)_i}{\sum_{i=1}^{N} w_i} = \frac{\sum_{i=1}^{N} w_i(\tau_{sim}-\tau_{obs})_i}{\sum_{i=1}^{N} w_i} \quad (6\text{-}3)$$

where: $(\varepsilon_a)_i$= absolute model error (m); $(\tau_{sim} - \tau_{obs})_i$ = simulated storm response (m) minus observed response (m); w_i = weight assigned to each error value i based on the GKF Equation (3-2) with d_i computed as the distance from validation data point i to each VG; and N = is the number of validation data points (i.e., simulation-observation pairs considered in model validation). A positive bias indicates over-prediction of the observations by the numerical model, whereas a negative bias represents under-prediction of the observations.

Bias that varies as a function of hydrodynamic response magnitude is considered to be a weighted relative bias (μ_r). This form of bias is estimated by normalizing each simulated-observed difference by the simulated value:

$$\mu_r = \frac{\sum_{i=1}^{N} w_i(\varepsilon_r/\tau_{sim})_i}{\sum_{i=1}^{N} w_i} = \frac{\sum_{i=1}^{N} w_i[(\tau_{sim}-\tau_{obs})/\tau_{sim}]_i}{\sum_{i=1}^{N} w_i} \quad (6\text{-}4)$$

where ε_r = relative model error (m/m). In the PCHA framework, both the geospatial bias and uncertainty are estimated by applying a Gaussian kernel surface (GKS). The GKS method takes advantage of the available validation information to characterize the local variability of numerical model biases within the study area. Evidence-based correction of these biases, even when considering a small subset of storms, is crucial to avoid

underestimation of coastal hazards and risk. The data assimilation approach utilized to perform bias correction minimizes the potential for over-correction in relation to the development of the storm response hazard curves.

This method results in two-dimensional (2D) surfaces of the relative and absolute forms of bias and uncertainty for the study area. These quantities' relative and absolute forms are later combined to create 2D surfaces of total bias and uncertainty, respectively. The GKS approach was applied to create 2D surfaces of the biases introduced by the ADCIRC and PBL models covering all VGs considered in this study. In this approach, weights are assigned to each validation data point. From the perspective of each VG, the weights in Equations (6-3) and (6-4) were assigned to the validation data points based on their distance from the VG. These weights are calculated from Equation (3-2), while the optimal kernel size (h_d) for estimating normal densities (Bowman and Azzalini 1997) is determined as a function of the number of validation points and distance to the VGs.

The GKS method for bias leads to the generation of four 2D bias surfaces: (1) ADCIRC absolute bias; (2) ADCIRC relative bias; (3) PBL absolute bias; and (4) PBL relative bias. The next step in this process is to aggregate the absolute forms of the ADCIRC and PBL biases and, separately, aggregate the relative forms of these model biases, resulting in two new quantities: total absolute model bias and total relative model bias. The same workflow is also later implemented for estimating geospatial uncertainty. The total absolute bias and total relative model bias are computed for each VG as the summation of individual model biases (e.g., ADCIRC, PBL):

$$\mu_{a_{Total}} = \mu_{a_1} + \mu_{a_2} + \cdots + \mu_{a_n} \quad \text{(6-5a)}$$

$$\mu_{r_{Total}} = \mu_{r_1} + \mu_{r_2} + \cdots + \mu_{r_n} \quad \text{(6-5b)}$$

where $\mu_{a_{Total}}$ = total absolute model bias (m) and $\mu_{r_{Total}}$ = total relative model bias (m/m). Following the computation of the $\mu_{a_{Total}}$ and $\mu_{r_{Total}}$ forms of the bias, these values are input using Equation 6-2 to estimate a combined bias μ_c at each VG. The average values of the absolute and relative forms of bias estimated in this study are provided in Table 6-2. Plots (2D) of the geospatial ADCIRC and PBL biases are shown in Appendix D.

Table 6-2. Average values of absolute and relative bias estimated in CHS-PR.

Numerical Model	Average Bias	
	Absolute (m)	Relative (m/m)
ADCIRC	-0.01	-0.02
PBL	0.01	0.00
Total (ADCIRC and PBL)	0.00	-0.02

As previously discussed, uncertainty is estimated from unbiased error quantities. In cases where model bias is non-negligible, bias correction is necessary before uncertainty quantification. Bias is removed from the storm responses (i.e., model output) by subtracting the total combined model bias (μ_c) from each simulated storm response (τ_{sim}). The corrected storm response (τ_{cor}) is given by

$$t_{cor} = \tau_{sim} - \mu_c \tag{6-6}$$

Bias correction was only conducted for storm surge estimates based on ADCIRC and PBL model validations. Bias correction of wave results was not performed due to sparse data availability.

6.2.5 Estimation of geospatial uncertainty

Numerical model uncertainty is estimated based on three assumptions routinely made in JPM-based studies: (1) the uncertainty terms are independent; (2) their effects can be combined by addition; and (3) the aggregated uncertainties can be represented as a Gaussian distribution with a mean of zero. After quantifying and correcting any bias, two forms of model uncertainty are evaluated: (1) absolute, which retains the dimensions of the hydrodynamic responses and (2) relative, which is a non-dimensional quantity.

The weighted absolute form of the uncertainty (σ_a) and the relative form (σ_r) are estimated through the following equations:

$$\sigma_a = \sqrt{\frac{\sum_{i=1}^{n} w_i (\varepsilon_a)_i^2}{\frac{(n-1)\sum_{i=1}^{n} w_i}{n}}} = \sqrt{\frac{\sum_{i=1}^{n} w_i (\tau_{sim} - \tau_{obs})_i^2}{\frac{(n-1)\sum_{i=1}^{n} w_i}{n}}} \tag{6-7}$$

$$\sigma_r = \sqrt{\frac{\sum_{i=1}^{N} w_i (\varepsilon_a / \tau_{sim})_i^2}{\frac{(N-1)}{N}\sum_{i=1}^{n} w_i}} = \sqrt{\frac{\sum_{i=1}^{n} w_i [(\tau_{sim} - \tau_{obs})/\tau_{sim}]_i^2}{\frac{(N-1)}{N}\sum_{i=1}^{n} w_i}} \quad (6\text{-}8)$$

The application of the GKS method also results in the generation of four 2D uncertainty surfaces for storm surge: (1) ADCIRC absolute uncertainty; (2) ADCIRC relative uncertainty; (3) PBL absolute uncertainty; and (4) PBL relative uncertainty. The next step in this process is to aggregate the absolute forms of the ADCIRC and PBL uncertainties and, separately, aggregate the relative forms of these model uncertainties. Similar to the case of bias, this approach results in two new quantities: total absolute model uncertainty and total relative model uncertainty. The total absolute and relative uncertainties for each VG are estimated as the summation of individual numerical model uncertainties:

$$\sigma_{a_{Total}} = \sqrt{\left(\sigma_{a_1}\right)^2 + \left(\sigma_{a_2}\right)^2 + \cdots + \left(\sigma_{a_n}\right)^2} \quad (6\text{-}9a)$$

$$\sigma_{r_{Total}} = \sqrt{\left(\sigma_{r_1}\right)^2 + \left(\sigma_{r_2}\right)^2 + \cdots + \left(\sigma_{r_n}\right)^2} \quad (6\text{-}9b)$$

where $\sigma_{a_{Total}}$ = total absolute model uncertainty (m) and $\sigma_{r_{Total}}$ = total relative model uncertainty (m/m). The $\sigma_{a_{Total}}$ and $\sigma_{r_{Total}}$ are then input into Equation 6-1 to estimate a total combined uncertainty (σ_c) for each VG in the CHS-PR study area. The average values of the total relative and absolute uncertainties estimated in this study are provided in Table 6-3. Additional 2D plots of the geospatial ADCIRC and PBL uncertainties are shown in Appendix D.

In the case of H_{mo}, only a global uncertainty value is estimated. The absolute (σ_a) and relative (σ_r) forms of the STWAVE uncertainty are determined as follows

$$\sigma_a = \sqrt{\frac{\sum_{i=1}^{N} (\varepsilon_a)_i^2}{N-1}} = \sqrt{\frac{\sum_{i=1}^{N} (\tau_{sim} - \tau_{obs})_i^2}{N-1}} \quad (6\text{-}10)$$

$$\sigma_r = \sqrt{\frac{\sum_{i=1}^{N} (\varepsilon_a / \tau_{sim})_i^2}{N-1}} = \sqrt{\frac{\sum_{i=1}^{N} [(\tau_{sim} - \tau_{obs})/\tau_{sim}]_i^2}{N-1}} \quad (6\text{-}11)$$

By taking the average σ_a and σ_r across all validation points i, the uncertainties are input into Equation 6-1 to estimate the global STWAVE uncertainty used to compute the CLs for the H_{mo} hazard curves.

Table 6-3. Average values of absolute and relative uncertainty estimated in CHS-PR.

Numerical Model	Average Uncertainty	
	Absolute (m)	Relative (m/m)
ADCIRC	0.22	0.29
PBL	0.08	0.12
Total (ADCIRC & PBL)	0.24	0.32
Numerical Model	**Absolute (m)**	**Relative (m/m)**
STWAVE (H_{m0})	0.69	0.15

6.3 Astronomical tides

The astronomical tides within the CHS-PR study area have a mean range on the order of .33 m (1 ft), which minimally contribute to the SWL produced by TCs affecting the region. Similar to FEMA (2008), the hydrodynamic modeling was completed without the influence of tides for CHS-PR due to the minimal tidal range. Instead, the astronomical tide was characterized as a stochastic quantity in an effort to capture the aleatory variability of a TC occurring at any given tidal phase. The standard deviation of the astronomical tide was calculated and linearly added to the storm surge as a random component, thus considering the effect of the random phasing of the astronomical tide and maximum storm surge.

To estimate the influence of the tide at each VG, an analysis of 14 NOAA tide gauges (Table 6-4) surrounding the study area was completed using the entire record length available for each gauge. The first step in the analysis was to compute a standard deviation of the predicted tides recorded at the NOAA gauges. A nearest-neighbor interpolation of these values was then implemented to assign a standard deviation of the tide to all 14,891 VGs within the CHS-PR study area. After computing the standard deviation of the astronomical tide for each VG, the tides are incorporated into the hazard computation to develop SWL hazard curves. For each storm in the ATCS, a random normal (Gaussian) number is drawn and used as a multiplier to the standard deviation of the tide at a

given VG to represent the random tide phasing. These values are then linearly added to the storm surge of each storm to represent SWL values corresponding to the ATCS.

Table 6-4. NOAA Tide and Currents gauges used for the estimation of tidal variability.

Gauge ID	Name	Latitude	Longitude	Standard Deviation (m)
9755371	San Juan, La Puntilla, San Juan Bay	18.46	-66.12	0.15
9757809	Arecibo	18.48	-66.70	0.15
9759394	Mayaguez	18.22	-67.16	0.16
9759110	Magueyes Island	17.97	-67.05	0.16
9754228	Yabucoa Harbor	18.06	-65.83	0.13
9753216	Fajardo	18.34	-65.63	0.13
9759938	Mona Island	18.09	-67.94	0.08
9752235	Culebra	18.30	-65.30	0.08
9752695	Esperanza, Vieques Island	18.09	-65.47	0.08
9752619	Isabel Segunda, Vieques Island	18.15	-65.44	0.08
9751639	Charlotte Amalie	18.35	-64.93	0.14
9751381	Lameshur Bay, St John	18.32	-64.72	0.14
9751401	Lime Tree Bay	17.69	-64.75	0.08
9751364	Christiansted Harbor, St Croix	17.75	-64.71	0.08

6.4 Quantification of SWL hazards

In the CHS-PR study, hazard curves representing the magnitude of SWL (storm surge + astronomical tide), H_{mo}, and T_p as a function of AEF were developed at 14,891 point locations across Puerto Rico and the US Virgin Islands. To develop the hazard curves, the peak storm responses resulting from the hydrodynamic simulation of each synthetic TC at any given point-location are assigned the DSW of the corresponding TC, as discussed in Section 4.4. For example, estimating the AEF of SWL requires establishing a range of water elevation bins encompassing the entire hazard range. The response's complementary cumulative distribution function is then developed by aggregating the probabilities of all water

levels that exceed each of the established bins applying Equation 2-1b. This form of the JPM integral was used since unbiased uncertainty was instead conveyed through non-exceedance CLs. It is standard practice to represent uncertainty as a Gaussian distribution process with mean zero (Resio et al. 2007; Toro 2008; FEMA 2012). The CL curves are computed from the following equation:

$$CL = \bar{\tau} + z\sigma_c \quad (6\text{-}12)$$

where CL = confidence limit; $\bar{\tau}$ = mean value of a given TC response τ; z = Z-score or number of standard deviations the CL is above $\bar{\tau}$; and σ_c = total combined model uncertainty associated with τ. This study considered CLs of 10%, 16%, 84%, and 90%; however, only the 10% and 90% CLs are illustrated in the hazard curve plots.

For CHS-PR, the TC responses were computed for AEFs ranging from 10 yr^{-1} to 10^{-4} yr^{-1}. Examples of the SWL hazard curves developed are provided in Figures 6-5 and 6-6, which show the best estimate and the CLs as discussed in this section. These figures provide the SWL estimates from FEMA (2009) compared to the SWL hazard curves produced by the PCHA at VGs 102 and 435. The example hazard curves are shown at VGs near San Juan Bay (VG 102) and Magueyes Island (VG 435). Additional details describing the methods employed to characterize the wave parameters are discussed in Section 6.5.

Figure 6-5. SWL hazard curve for SLC 0 at VG 102 compared to FEMA (2009) SWL estimates.

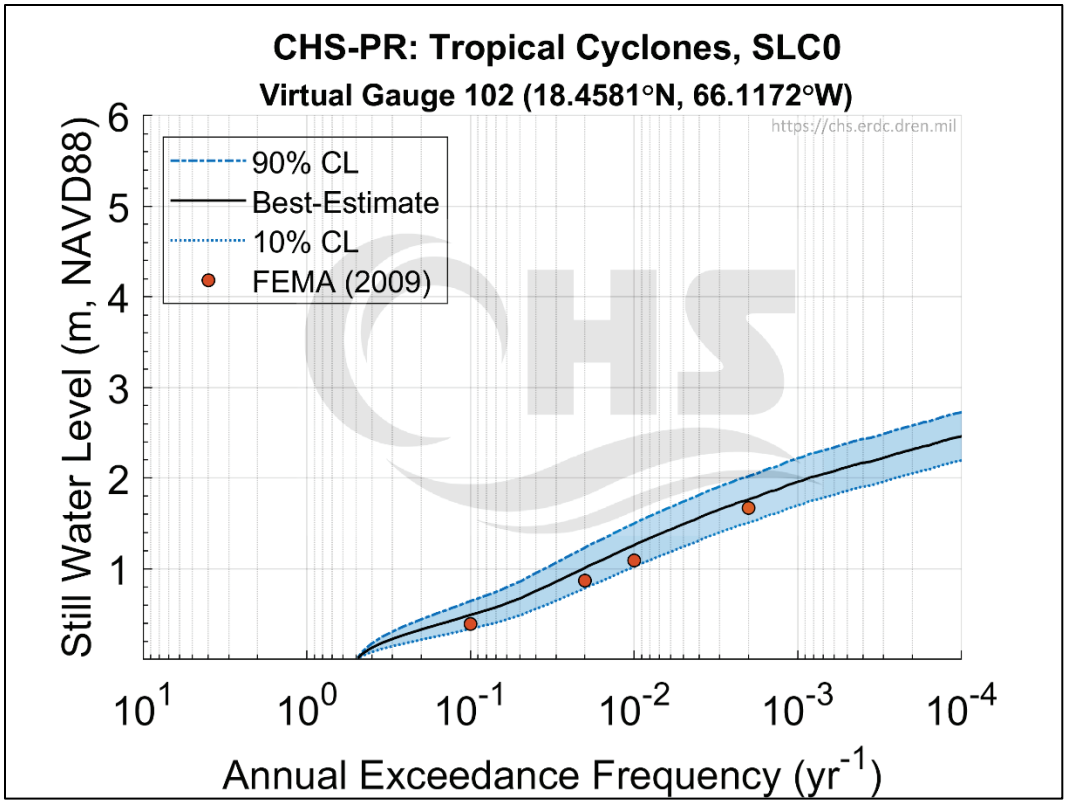

Figure 6-6. SWL hazard curve for SLC 0 at VG 435 compared to FEMA (2009) SWL estimates.

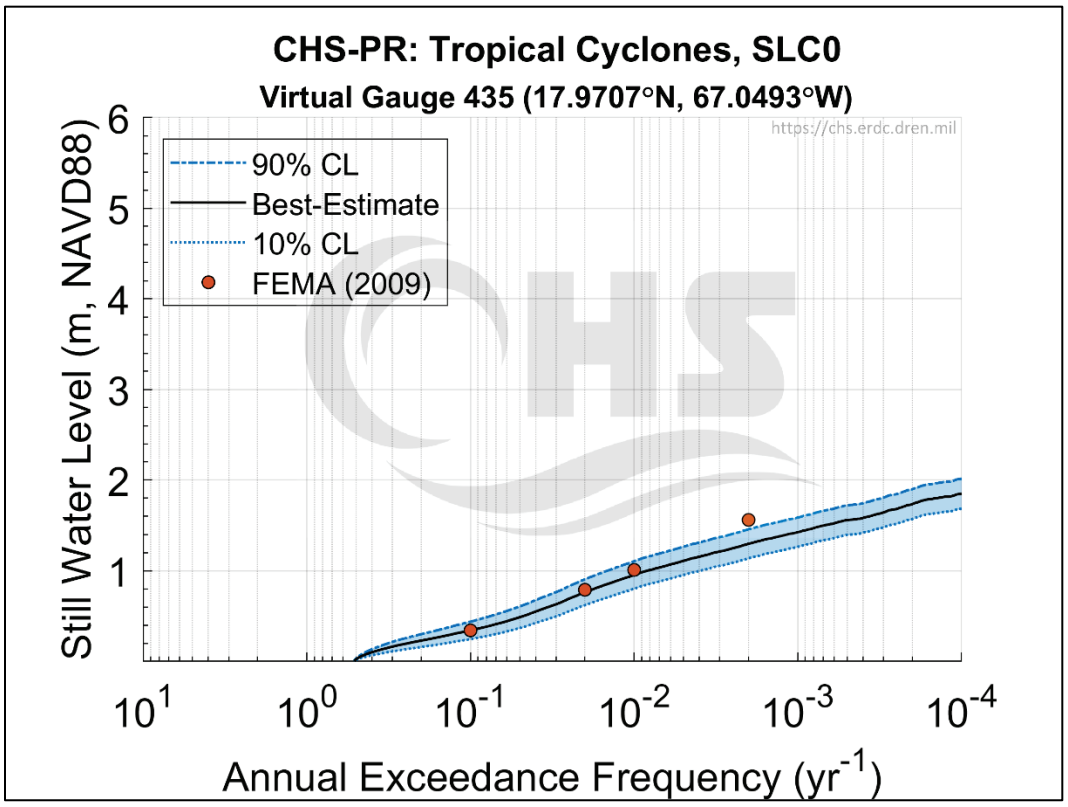

6.5 Quantification of wave hazards

Quantifying TC wave hazards in the study area included a multistep analysis of the H_{mo} and T_p output of the STWAVE model, including spatially correlating H_{mo} to the SWL simulated by ADCIRC on a point-by-point basis. The following section discusses the methodology employed within the PCHA to develop H_{mo} and T_p hazard curves, including AEF estimates of H_{mo} and T_p conditional to SWL.

6.5.1 Significant wave height

The first step in the probabilistic analysis of waves was the development of marginal hazard curves for all CHS-PR VGs. The development of the marginal H_{mo} hazard curves followed the same PCHA methodology as described in Section 6.4, including accounting for uncertainty within the STWAVE simulations (Section 6.2.2.2). The resulting H_{mo} hazard curves from this initial step are considered marginal probability distributions as shown in Figures 6-7 and 6-8 and in the context of the SWL-H_{mo} joint probability, strictly apply when the correlation between SWL and H_{mo} is close to 1.0. In other words, from a stochastic standpoint, the $1x10^{-2}$ yr^{-1} AEF, or 1%, SWL coincides with the 1% H_{mo} when the correlation between both storm responses is 1.0. On the other hand, at locations where H_{mo} is independent of SWL (i.e., correlation of zero), the likelihood of the 1% SWL coinciding with the 1% H_{mo} would be close to 0.01%; in this case, pairing the 1% SWL and 1% H_{mo} would significantly overstate the wave hazard.

Therefore, to properly account for the SWL-H_{mo} joint probability, the process of estimating the wave hazard included quantifying the correlation which exists between SWL and H_{mo}. The H_{mo} hazard curves derived from this second step are conditional probability distributions (i.e., P(H_{mo}|SWL)). The correlation coefficients for SWL and H_{mo} were determined at every VG within the study area based on pairwise ADCIRC and STWAVE simulation results. The SWL-H_{mo} correlation was then employed to compute conditional H_{mo} AEFs using a bivariate Gaussian (or Normal) probability distribution model. The bivariate normal distribution (BND) provided a fitted surface to the joint probability analysis relations between the parameters. The BND probability density function is given as

$$f(x,y) = \frac{1}{2\pi\sigma_x\sigma_y\sqrt{1-\rho^2}}$$

$$\exp\left[-\frac{1}{2(1-\rho^2)}\left(\frac{(x-\mu_x)^2}{\sigma_x^2} - \frac{2\rho(x-\mu_x)(y-\mu_y)}{\sigma_x\sigma_y} - \frac{(y-\mu_y)^2}{\sigma_y^2}\right)\right] \quad (6\text{-}13)$$

where μ_x and μ_y = marginal means, σ_x and σ_y = marginal standard distributions, and ρ = correlation between x and y.

In the case of the BND, the conditional probability distribution for either x (SWL) or y (H_{mo}) is also normally distributed. For example, the conditional probability of x, given a known value of y, can be computed using Equation 6-13. The conditional mean and variance of x are given by

$$\mu_{x/y} = \mu_x + \rho\mu_x\frac{(y-\mu_y)}{\sigma_y} \quad (6\text{-}14)$$

$$\sigma_{x/y} = \sigma_x\sqrt{1-\rho^2} \quad (6\text{-}15)$$

The conditional H_{mo} results, P(H_{mo}|SWL), derived from this model correspond to the expected (mean) H_{mo} associated with each SWL AEF.

Assessing only the 1% SWL AEF and associated 1% H_{mo} AEF to estimate the wave hazard may produce inaccurate estimations of the hazard by not considering the correlation which exists between H_{mo} and SWL. Calculating the correlation between H_{mo} and SWL is a significant step in the development of conditional H_{mo} AEFs. For any given SWL AEF, such as the 1% at VGs where the correlation between H_{mo} and SWL is 1, the marginal and conditional H_{mo} are the same. As the SWL-H_{mo} correlation decreases, the magnitude of the conditional H_{mo} also decreases.

Figure 6-7. Significant wave height (H_{m0}) hazard curve produced for SLC 0 at VG 102.

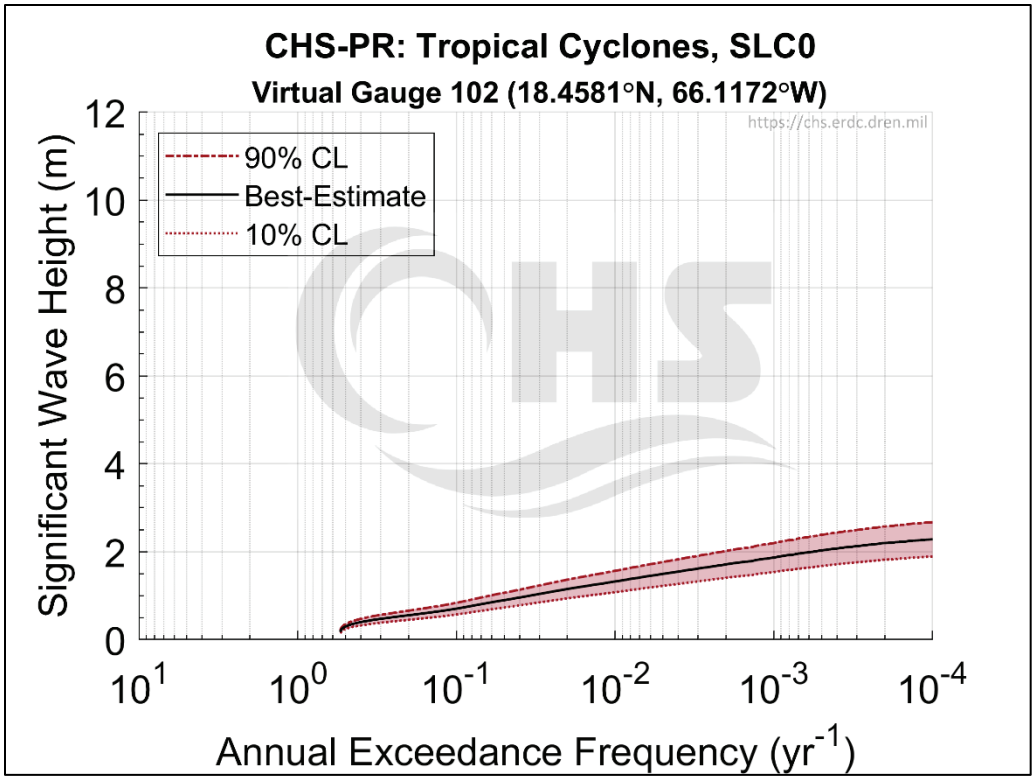

Figure 6-8. Significant wave height (H_{m0}) hazard curve produced for SLC 0 at VG 435.

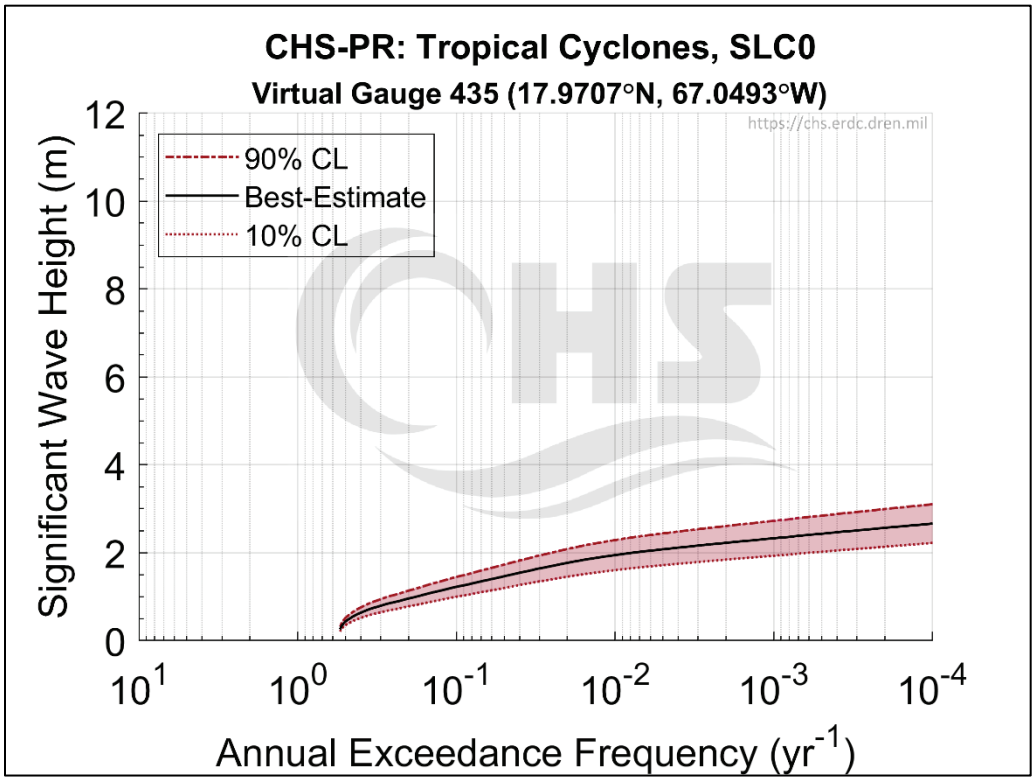

6.5.2 Wave peak period

Probabilistic analysis of the wave hazards within the CHS-PR study area required characterizing the magnitude and frequency of T_p as a marginal probability distribution, while preserving the physical dependence between T_p and H_{mo} through a conditional probability distribution. In this approach, the T_p-H_{mo} relationship at each VG was modeled using a two-parameter power function (Chun and Suh 2018) with the form

$$T_p = \alpha\left(H_{m0}{}^{\beta}\right) \tag{6-16}$$

where coefficients α and β were estimated in this study with the least absolute residual robust linear least-squares fitting method.

Equation 6-16 was applied to estimate the expected values of T_p corresponding to each H_{mo} AEF value for both the marginal and conditional H_{mo} hazard curves at 13,976 VGs (Section 6.1.2) within the CHS-PR study area. Figures 6-9 through 6-10 illustrate the marginal T_p hazard curves produced for select locations within the CHS-PR study area.

Figure 6-9. Wave peak period (T_p) hazard curve produced for SLC 0 at VG 102.

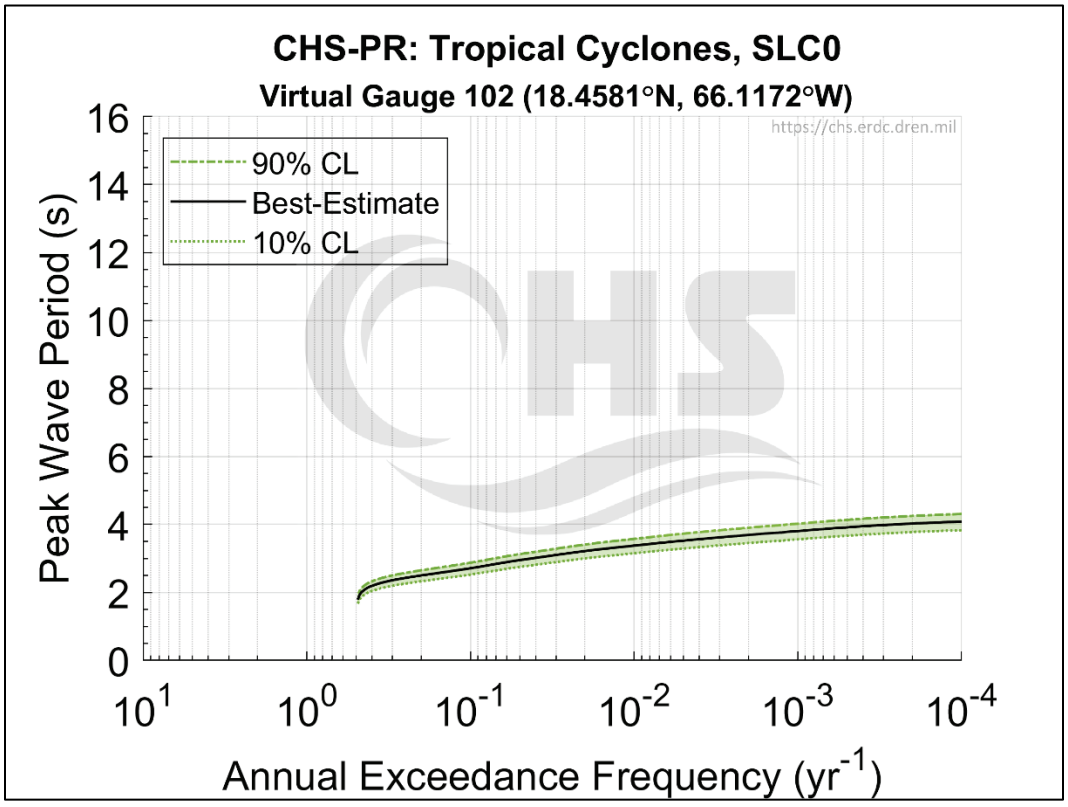

Figure 6-10. Wave peak period (T_p) hazard curve produced for SLC 0 at VG 435.

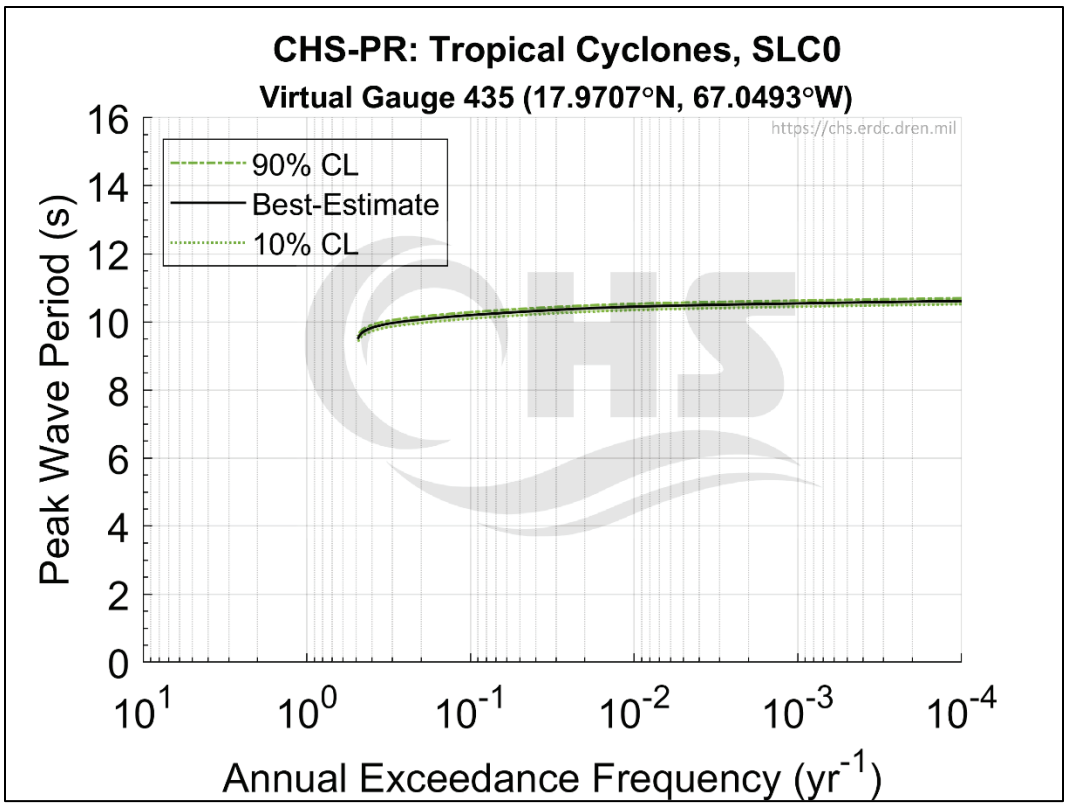

7 Conclusions

The Coastal Hazards System–Puerto Rico (CHS-PR) study was conducted to quantify coastal storm hazards in Puerto Rico and the US Virgin Islands as part of the South Atlantic Coastal Study (SACS). This study applied the CHS Probabilistic Coastal Hazard Analysis (PCHA) framework developed by the US Army Engineer Research and Development Center, Coastal and Hydraulics Laboratory, which integrates (1) regional storm climatology characterization, (2) marginal distributions of tropical cyclone (TC) atmospheric-forcing parameters, (3) development of synthetic TCs, (4) dependence modeling of TC parameters, (5) joint probability analysis of atmospheric forcing and hydrodynamic responses, (6) high-resolution numerical model simulation, (7) metamodeling prediction of storm responses, and (8) quantification of bias and uncertainty.

Following the PCHA framework, the CHS-PR study incorporated several advancements over standard joint probability method approaches such as Gaussian process metamodeling (GPM), meta-Gaussian copula, and geospatial estimation of storm recurrence rates, numerical model bias, and uncertainty. A suite of 300 synthetic TCs was developed for CHS-PR as part of the SACS storm suite, covering the practical probability and parameter spaces for TCs affecting the study area. The storm suite was simulated in high-fidelity hydrodynamic models, and the results of these simulations were applied in training a GPM to predict coastal storm responses. By further discretizing the parameter space covered by the initial suite of 300 TCs, an augmented suite of 348,000 synthetic TCs was developed to cover the parameter and probability spaces more fully. After estimating storm responses for the augmented TC suite through the application of the GPM, hazards curves of hurricane-induced still water level (SWL), significant wave height (H_{mo}), and wave peak period (T_p) for annual exceedance frequencies ranging from 10 yr^{-1} to 10^{-4} yr^{-1} were developed at 14,891 virtual gauges (VGs) within the CHS-PR study area.

Results from the CHS-PR study, including SWL, H_{mo}, and T_p hazard curves, synthetic TC suite, and hydrodynamic modeling output at the VGs, are available through the CHS website (https://chs.erdc.dren.mil). CHS results support US Army Corps of Engineers planning and feasibility studies, economic analyses, flood and coastal storm risk management, climate change adaptation and resilience including evaluations of nonstructural, structural, and nature-based features and stochastic engineering designs.

References

Bacopoulos, P., W. R. Dally, S. C. Hagen, and A. T. Cox. 2011. "Observations and Simulation of Winds, Surge, and Currents on Florida's East Coast During Hurricane Jeanne (2004)." *Coastal Engineering* 60 (February 2012): 84–94.

Bensi, M., and J. Kanney. 2015. "Development of a Framework for Probabilistic Storm Surge Hazard Assessment for United States Nuclear Power Plants." *Transactions, SMiRT-23*, Manchester, United Kingdom, August 10–14.

Bommer, J. J., and F. Scherbaum. 2008. "The Use and Misuse of Logic Trees in Probabilistic Seismic Hazard Analysis." *Earthquake Spectra* 24 (4): 997–1009.

Bowman, A. W., and A. Azzalini. 1997. *Applied Smoothing Techniques for Data Analysis*. New York: Oxford University Press Inc.

Brun, W., G. B. Keren, G. Kirkebøen, and H. Montogomery. 2011. *Perspectives on Thinking, Judging, and Decisions Making*. Oslo: Universitetsforlaget.

Bunya, S., J. Dietrich, J. Westerink, B. Ebersole, J. Smith, J. Atkinson, R. Jensen, D. Resio, R. Luettich, Jr., C. Dawson, V. Cardone, and A. Cox. 2010. "A High-Resolution Coupled Riverine Flow, Tide, Wind, Wind Wave, and Storm Surge Model for Southern Louisiana and Mississippi. Part I: Model Development and Validation." *Monthly Weather Review* 138:345–377.

Cardone, V. J., A. T. Cox, J. A. Greenwood, and E. F. Thompson. 1994. *Upgrade of Tropical Cyclone Surface Wind Field Model*. Miscellaneous Paper CERC-94-14. Vicksburg, MS: US Army Corps of Engineers Waterways Experiment Station.

Cardone, V. J., and A. T. Cox 2009. "Tropical Cyclone Wind Field Forcing for Surge Models: Critical Issues and Sensitivities." *Natural Hazards* 1:29.

Cardone, V. J., and C. K. Grant. 1994. "Southeast Asia Meteorological and Oceanographic Hindcast Study (SEAMOS)." *OSEA 94132. 10th Offshore Southeast Asia Conference*, 6–9 December, Singapore. https://www.oceanweather.com/about/papers/index.html.

Cardone, V. J., C. V. Greenwood, and J. A. Greenwood. 1992. *Unified Program for the Specification of Tropical Cyclone Boundary Layer Winds over Surfaces of Specified Roughness*. Contract Report CERC 92-1. Vicksburg, MS: US Army Corps of Engineers Waterways Experiment Station.

Cardone, V. J., W. J. Pierson, and E. G. Ward. 1976. "Hindcasting the Directional Spectra of Hurricane Generated Waves." *Journal of Petroleum Technology* 28:385–394.

Cardone, V. J., and D. B. Ross. 1979. "State-of-the-Art Wave Prediction Methods and Data Requirements." In *Ocean Wave Climate*, Vol. 8, edited by M. D. Earle and A. Malahoff. New York, NY: Plenum Publishing Corporation.

Chouinard, L. M., and C. Liu. 1997. "Model for Recurrence Rate of Hurricanes in Gulf of Mexico." *Journal of Waterway, Port, Coastal and Ocean Engineering* 123:113–119.

Chow, S. H. 1971. *A Study of the Wind Field in the Planetary Boundary Layer of a Moving Tropical Cyclone*. Master of Science thesis in meteorology, School of Engineering and Science, New York University.

Chun, H., and Kyung-Duck Suh. 2018. "Estimation of Significant Wave Period from Wave Spectrum." Ocean Engineering 163:609–616.

Cialone, M. A., T. C. Massey, M. E. Anderson, A. S. Grzegorzewski, R. E. Jensen, A. Cialone, D. J. Mark, K. C. Peavey, B. L. Gunkel, T. O. McAlpin, N. C. Nadal-Caraballo, J. A. Melby, and J. J. Ratcliff. 2015. *North Atlantic Coast Comprehensive Study (NACCS) Coastal Storm Model Simulations: Waves and Water Levels*. ERDC/CHL TR-15-14. Vicksburg, MS: US Army Engineer Research and Development Center.

Cox, A. T., and V. J. Cardone. 2007. "Specification of Tropical Cyclone Parameters from Aircraft Reconnaissance." *10th International Wind and Wave Workshop*. Oahu, Hawaii, November 11–16, 2007.

Cox, A. T., B. T. Callahan, M. Ferguson, and M. A. Morrone. 2017. "Tropical Cyclone Wind Field Analysis for Ocean Response Modeling: Hurricane Harvey (2017)." *1st International Workshop on Waves, Storm Surges and Coastal Hazards*. Liverpool, UK, 10–15 September 2017.

CPRA (Coastal Protection and Restoration Authority). 2013. *Greater New Orleans Flood Protection System Notice of Construction Completion–Design Assessment by Nonfederal Sponsor*. Bell City, LA: Lonnie G. Harper & Associates.

Demuth, J., M. DeMaria, and J. A. Knaff. 2006. "Improvement of Advanced Microwave Sounder Unit Tropical Cyclone Intensity and Size Estimation Algorithms." *Journal of Applied Meteorology and Climatology* 45:1573–1581.

Der Kiureghian, A., and O. Ditlevsen. 2009. "Aleatory or Epistemic? Does It Matter?" *Structural Safety* 31:105–112.

Dietrich, J. C., J. J. Westerink, A. B. Kennedy, J. M. Smith, R. Jensen, M. Zijlema, L. H. Holthuijsen, C. Dawson, R. A. Luettich, Jr., M. D. Powell, V. J. Cardone, A. T. Cox, G. W. Stone, H. Pourtaheri, M. E. Hope, S. Tanaka, L. G. Westerink, H. J. Westerink, and Z. Cobell. 2011. "Hurricane Gustav (2008) Waves and Storm Surge: Hindcast, Synoptic Analysis and Validation in Southern Louisiana." *Monthly Weather Review* 139:2488–2522.

Fang, H. B., K.-T. Fang, and S. Kotz. 2002. "The Meta-Elliptical Distributions with Given Marginals." *Journal of Multivariate Analysis* 82:1–16.

Fang, K. T., S. Kotz, and K. W. Ng. 1990. *Symmetric Multivariate and Related Distributions*. CRC Press: Chapman and Hall.

FEMA (Federal Emergency Management Agency). 1988. *Coastal Flooding Hurricane Storm Surge Model*. Vol. 1 Methodology. Washington, DC: Office of Risk Management, Federal Insurance Administration, FEMA.

FEMA. 2008. *Mississippi Coastal Analysis Project (MCAP)*. Final Report: HMTAP Task Order 18, prepared for the Federal Emergency Management Agency, Department of Homeland Security. Gaithersburg, MD: URS Group, Inc.

FEMA. 2009. *Flood Insurance Study: Commonwealth of Puerto Rico and Municipalities*. Volume 1 of 5. Fairfax, VA: Dewberry.

FEMA. 2012. *Operating Guidance No. 8-12 for Use by FEMA Staff and Flood Mapping Partners: Joint Probability–Optimal Sampling Method for Tropical Storm Surge*. Washington, DC: Federal Emergency Management Agency, Department of Homeland Security.

Forristall, G. Z. 1980. "A Two-Layer Model for Hurricane Driven Currents on an Irregular Grid." *Journal of Physical Oceanography* 10:1417–1438.

Forristall, G. Z., R. C. Hamilton, and V. J. Cardone. 1977. "Continental Shelf Currents in Tropical Storm Delia: Observations and Theory." *Journal of Physical Oceanography* 7:532–546.

Forristall, G. Z., E. G. Ward, V. J. Cardone, and L. E. Borgman. 1978. "The Directional Spectra and Kinematics of Surface Waves in Tropical Storm Delia." *Journal of Physical Oceanography* 8:888–909.

Forristall, G. Z., and J. A. Greenwood. 1998. "Directional Spreading of Measured and Hindcasted Wave Spectra." *In Proceedings 5th International Workshop on Wave Hindcasting and Forecasting*. Melbourne, FL. January 26-30. Downsview, Ontario: Environment Canada Atmospheric Environment Service.

Gao, F., X. Zhang, N. A. Jacobs, X.-Y. Huang, X. Zhang, and P. P. Childs. 2012. "Estimation of TAMDAR Observational Error and Assimilation Experiments." *Weather and Forecasting* 27:856–877.

Gonzalez, V. M., N. C. Nadal-Caraballo, J. A. Melby, and M. A. Cialone. 2019. *Quantification of Uncertainty in Probabilistic Storm Surge Models: Literature Review*. ERDC/CHL SR-19-1. Vicksburg, MS: US Army Engineer Research and Development Center.

Ho, F. P. 1974. *Storm Tide Frequency Analysis for the Coast of Georgia*. NOAA Technical Memorandum NWS HYDRO-19. Silver Spring, MD: US Department of Commerce.

Ho, F. P., and V. A. Myers. 1975. *Joint Probability Method of Tide Frequency Analysis Applied to Apalachicola Bay and St. George Sound, Florida*. NOAA Technical Report NWS 18. Silver Spring, MD: National Weather Service, National Oceanic and Atmospheric Administration.

Ho, F. P., J. C. Su, K. L. Hanevich, R. J. Smith, and F. P. Richards. 1987. *Hurricane climatology for the Atlantic and Gulf Coasts of the United States*. NOAA Technical Report NWS 38. Silver Spring, MD: National Weather Service, National Oceanic and Atmospheric Administration.

Holland, G. J. 1980. "An Analytic Model of the Wind and Pressure Profiles in Hurricanes." *Monthly Weather Review* 108:1212–1218.

Hope, M. E., J. J. Westerink, A. B. Kennedy, P. C. Kerr, J. C. Dietrich, C. Dawson, C. J. Bender, J. M. Smith, R. E. Jensen, M. Zijlema, L. H. Holthuijsen, R. A. Luettich Jr., M. D. Powell, V. J. Cardone, A. T. Cox, H. Pourtaheri, H. J. Roberts, J. H. Atkinson, S. Tanaka, H. J. Westerink, and L. G. Westerink. 2013. "Hindcast and Validation of Hurricane Ike (2008) Waves, Forerunner, and Storm Surge." *Journal of Geophysical Research* 118:4424–4460.

IPET (Interagency Performance Evaluation Task Force). 2009. *Performance Evaluation of the New Orleans and Southeast Louisiana Hurricane Protection System*. Final Report of the Interagency Performance Evaluation Task Force. Washington, DC: US Army Corps of Engineers, Department of the Army.

Jarvinen, B. R., C. J. Neumann, and M. A. S. Davis. 1984. *A Tropical Cyclone Data Tape for the North Atlantic Basin, 1886–1983: Contents, Limitations, and Uses*. NOAA Tech. Memo 22. Miami, FL: National Hurricane Center, National Weather Service.

Jia, G., A. A. Taflanidis, N. C. Nadal-Caraballo, J. A. Melby, A. B. Kennedy, and J.M. Smith. 2016. "Surrogate Modeling for Peak or Time-Dependent Storm Surge Prediction over an Extended Coastal Region Using an Existing Database of Synthetic Storms." *Natural Hazards* 81:909–938.

Kammerer, A. M. 2013. "Probabilistic Hazard Assessment Approaches: Transferable Methods from Seismic Hazard." In *Proceedings of the Workshop on Probabilistic Flood Hazard Assessment (PFHA) at the US Nuclear Regulatory Commission Headquarters*. NUREG/CP-0302.Rockville, MD: US Nuclear Regulatory Commission.

Kammerer, A. M., and J. P. Ake. 2012. *Practical Implementation Guidelines for SSHAC Level 3 and 4 Hazard Studies*. NUREG-2117 Rev.1 Washington, DC: US Nuclear Regulatory Commission.

Kendall, M. G. 1970. *Rank Correlation Methods*. Griffin: Charles Griffin and Co. Ltd.

Knapp, K. R., H. J. Diamond, J. P. Kossin, M. C. Kruk, and C. J. Schreck. 2018. *International Best Track Archive for Climate Stewardship (IBTrACS) Project, Version 4*. NOAA National Centers for Environmental Information. https://www.ncei.noaa.gov/access/metadata/landing-page/bin/iso?id=gov.noaa.ncdc:C01552.

Knapp, K. R., M. C. Kruk, D. H. Levinson, H. J. Diamond, and C. J. Neumann. 2010. "The International Best Track Archive for Climate Stewardship (IBTrACS): Unifying Tropical Cyclone Best Track Data." *Bulletin of the American Meteorological Society* 91:363–376.

Landsea, C. W., and J. L. Franklin. 2013. "Atlantic Hurricane Database Uncertainty and Presentation of a New Database Format." *Monthly Weather Review* 141:3576–3592.

Landsea, C. W., G. A. Vecchi, L. Bengtsson, and T. R. Knutson. 2010. "Impact of Duration Thresholds on Atlantic Tropical Cyclone Counts." *Journal of Climate* 23:2508–19.

Mann, M. E., T. A. Sabbatelli, and U. Neu. 2007. "Evidence for a Modest Undercount Bias in Early Historical Atlantic Tropical Cyclone Counts." *Geophysical Research Letters* 34:L22707.

Melby, J. A., T. C. Massey, F. Diop, H. Das, N. C. Nadal-Caraballo, V. Gonzalez, M. Bryant, A. Tritinger, L. Provost. M. Owensby, and A. Stehno. 2021. *Coastal Texas Protection and Restoration Feasibility Study–Coastal Texas Flood Risk Assessment: Hydrodynamic Response and Beach Morphology*. ERDC/CHL TR-21-11. Vicksburg, MS: US Army Engineer Research and Development Center.

MORPHOS. 2009. *Report: Oceanweather Tropical Planetary Boundary Layer Model, 2009*. https://www.oceanweather.com/about/papers/index.html.

Myers, V. A. 1954. *Characteristics of United States Hurricanes Pertinent to Levee Design for Lake Okeechobee, Florida*. Hydrometeorological Report No. 32. Washington, DC: Weather Bureau, US Department of Commerce.

Myers, V. A. 1970. *Joint Probability Method of Tide Frequency Analysis Applied to Atlantic City and Long Beach Island, NJ*. ESSA Technical Memorandum WBTM HYDRO 11. Washington, DC: Weather Bureau, US Department of Commerce.

Myers, V. A. 1975. *Storm Tide Frequencies on the South Carolina Coast*. NOAA Technical Report NWS-16. Washington, DC: National Weather Service, National Oceanic and Atmospheric Administration.

Nadal-Caraballo, N. C., J. A. Melby, V. M. Gonzalez, and A. T. Cox. 2015. *North Atlantic Coast Comprehensive Study–Coastal Storm Hazards from Virginia to Maine*. ERDC/CHL TR-15-5. Vicksburg, MS: US Army Engineer Research and Development Center.

Nadal-Caraballo, N. C., V. M. Gonzalez, and L. Chouinard. 2019. *Storm Recurrence Rate Models for Tropical Cyclones–Report 1 of a series on the Quantification of Uncertainties in Probabilistic Storm Surge Models*. ERDC/CHL TR-19-4. Vicksburg, MS: US Army Engineer Research and Development Center.

Nadal-Caraballo, N. C., M. O. Campbell, V. M. Gonzalez, M. J. Torres, J. A. Melby, and A. A. Taflanidis. 2020. "Coastal Hazards System: A Probabilistic Coastal Hazard Analysis Framework. Global Coastal Issues of 2020." *Journal of Coastal Research Special Issue* 95:1211–1216.

Nadal-Caraballo, N. C., M. C. Yawn, L. A. Aucoin, M. L. Carr, A. A. Taflanidis, A. P. Kyprioti, J. A. Melby, E. Ramos-Santiago, V. M. Gonzalez, T. C. Massey, Z. Cobell, and A. T. Cox. 2022. *Coastal Hazards System–Louisiana (CHS-LA)*. ERDC/CHL TR 22-16. Vicksburg, MS: US Army Engineer Research and Development Center.

NCEI (NOAA National Centers for Environmental Information). 2022. *US Billion-Dollar Weather and Climate Disasters*. Accessed February 08, 2022. https://www.ncdc.noaa.gov/billions/.

Neumann, C. J., G. W. Cry, E. L. Caso, and B. R. Jarvinen. 1985. *Tropical Cyclones of the North Atlantic Ocean, 1871–1980*. Asheville, NC: National Climatic Center.

NHC (National Hurricane Center). 2022. *Saffir-Simpson Hurricane Wind Scale*. Accessed 21 July 2022. https://www.nhc.noaa.gov/pdf/sshws.pdf.

Niedoroda, A. W., D. T. Resio, G. R. Toro, D. Divoky, H. S. Has, and C. W. Reed. 2010. "Analysis of the Coastal Mississippi Storm Surge Hazard." *Ocean Engineering* 37:82–90.

Powell, M. D. 2007. *Drag Coefficient Distribution and Wind Speed Dependence in Tropical Cyclones*. Final report to the Joint Hurricane Testbed, April 2007. https://www.nhc.noaa.gov/jht/05-07reports/final_Powell_JHT07.pdf.

Resio, D. T., S. J. Boc, L. Borgman, V. Cardone, A. T. Cox, W. R. Dally, R. G. Dean, D. Divoky, E. Hirsh, J. L. Irish, D. Levinson, A. Niedoroda, M. D. Powell, J. J. Ratcliff, V. Stutts, J. Suhada, G. R. Toro, and P. J. Vickery. 2007. White Paper on estimating hurricane inundation probabilities. Consulting Report prepared by USACE for FEMA. Vicksburg, MS: US Army Engineer Research and Development Center. http://hdl.handle.net/11681/22643.

Ross, D. B., and V. J. Cardone. 1978. "A Comparison of Parametric and Spectral Hurricane Wave Prediction Products." In *Turbulent Fluxes through the Sea Surface, Wave Dynamics, and Prediction*, edited by A. Favre and K. Hasselmann. New York, NY: Plenum Press.

Russell, L. R. 1968a. *Stochastic Models for Hurricane Prediction for the Texas Gulf Coast*. Master's thesis, Stanford University, Stanford, CA.

Russell, L. R. 1968b. *Probability Distributions for Texas Gulf Coast Hurricane Effects of Engineering Interest*. PhD dissertation, Stanford University, Stanford, CA.

Shapiro, L. J. 1983. "The Asymmetric Boundary Layer Flow under a Translating Hurricane." *Journal of the Atmospheric Sciences* 40:1984–1998.

Shisler, M. P., and D. R. Johnson. 2022. "Comparison of Methods for Imputing Non-Wetting Storm Surge to Improve Hazard Characterization." *Water* 12:1420.

Sklar, A. 1959. "Fonctions de Répartition À N Dimensions Et Leurs Marges." *Publications de Institut Statatistique de I'Universite de Paris* 8:299–331.

Thompson, E. F., and V. J. Cardone. 1996. "Practical Modeling of Hurricane Surface Wind Fields." *ASCE Journal of Waterway, Port, Coastal and Ocean Engineering* 122:195–205.

Toro, G. R. 2008. *Joint Probability Analysis of Hurricane Flood Hazards for Mississippi–Final URS Group Report in Support of the FEMA-HMTAP Flood Study of the State of Mississippi*. Boulder CO: Risk Engineering.

Toro, G. R., A. W. Niedoroda, C. W. Reed, and D. Divoky. 2010a. "Quadrature-Based Approach for Efficient Evaluation of Surge Hazard." *Ocean Engineering* 37:114–124.

Toro, G. R., D. T. Resio, D. Divoky, A.W. Niedoroda, and C. Reed. 2010b. "Efficient Joint-Probability Methods for Hurricane Surge Frequency Analysis." *Ocean Engineering* 37:125–134.

USACE (US Army Corps of Engineers). 2009a. *Louisiana Coastal Protection and Restoration (LACPR)*. Final Technical Report. New Orleans, LA: New Orleans District, Mississippi Valley Division, USACE.

USACE. 2009b. *Mississippi Coastal Improvements Program (MSCIP), Hancock, Harrison, and Jackson Counties, Mississippi*. Mobile, AL: Mobile District, South Atlantic Division, USACE.

USACE. 2011. *Flood Insurance Study: Coastal Counties, Texas: Scoping and Data Review*. Denton, TX: Federal Emergency Management Agency, Region 6.

USNRC (US Nuclear Regulatory Commission). 1997. *Panel on Seismic Hazard Evaluation. Review of Recommendations for Probabilistic Seismic Hazard Analysis: Guidance on Uncertainty and Use of Experts*. (n.d.). Washington, DC: Panel on Seismic Hazard Evaluation, National Research Council.

Vecchi, G. A., and T. R. Knutson. 2011. "Estimating Annual Numbers of Atlantic Hurricanes Missing from the HURDAT Database (1878–1965) Using Ship Track Density." *Journal of Climate* 24:1736–1746.

Vickery, P. J. 2005. "Simple Empirical Models for Estimating the Increase in Central Pressure of Tropical Cyclones after Landfall along the Coastline of the United States." *Journal of Applied Meteorology* 44:1807–1826.

Vickery, P. J., and B. O. Blanton. 2008. *North Carolina Coastal Flood Analysis System Hurricane Parameter Development*. Technical Report TR-08-06. Chapel Hill, NC: RENCI Renaissance Computing Institute.

Vickery, P. J., and D. Wadhera. 2008. "Statistical Models of Holland Pressure Profile Parameter and Radius to Maximum Winds of Hurricanes from Flight-Level Pressure and H*Wind Data." *Journal of Applied Meteorology and Climatology* 47:2497–2517.

Vrouwenvelder, A. C. W. M. 2003. "Uncertainty Analysis for Flood Defense Systems in the Netherland." In *Proceedings of European Safety and Reliability (ESREL) Conference 2003*, Maastricht, the Netherlands, 15–18 June.

Worley, S. J., S. D. Woodruff, R. W. Reynolds, S. J. Lubker, and N. Lott. 2005. "ICOADS Release 2.1 Data and Products." *Journal of Climatology* 25:823–842.

Zhang, J., A. A. Taflanidis, N. C. Nadal-Caraballo, J. A. Melby, and F. Diop. 2018. "Advances in Surrogate Modeling for Storm Surge Prediction: Storm Selection and Addressing Characteristics Related to Climate Change." *Natural Hazards* 94:1225–1253.

Zhang, L., and V. P. Singh. 2019. *Copulas and Their Applications in Water Resources Engineering*. Cambridge: Cambridge University Press.

Appendix A: Historical TC Selection (CRL 844)

The TC parameters implemented for the development of marginal distributions (Section 4.1) at each CRL are reported here. The NHC ID indicates the chronological order the storm occurred in a given year. In Table A-1, the latitude, longitude, and Δp were selected based on the greatest intensity index computed for each storm (Section 3.4). The distance parameter reported indicates the distance from CRL 844 at which the intensity index was recorded. The adjusted Δp and z-score were computed as described in Section 3.6. Tables A-2 and A-3 provide the unadjusted and distance-adjusted TC atmospheric forcing parameters for the historical TCs selected at CRL 844, respectively.

Table A-1. Historical TCs: coordinates, distance from CRL 844, and Δp.

Name	Year	NHC ID	Lat (deg)	Lon (deg)	d (km)	Δp (hPa)	z-score	Adj. Δp (hPa)
UNNAMED	1938	2	18.9	-64.6	173	16	-0.48	20
UNNAMED	1938	3	14.1	-67.3	477	12	-0.67	16
UNNAMED	1938	5	22.5	-65.7	476	9	-0.81	13
UNNAMED	1938	6	22.8	-65.5	512	76	2.35	85
UNNAMED	1939	5	21.9	-67.4	431	28	0.09	33
UNNAMED	1940	3	18.9	-64.8	154	8	-0.86	12
UNNAMED	1940	5	21.5	-65.6	367	14	-0.57	18
UNNAMED	1941	4	13.9	-67.6	508	15	-0.53	19
UNNAMED	1941	5	22.2	-64	492	12	-0.67	16
UNNAMED	1942	5	15.7	-68.7	396	9	-0.81	13
UNNAMED	1943	2	20	-66.9	215	9	-0.81	13
UNNAMED	1943	3	19.8	-62.2	444	42	0.75	48
UNNAMED	1943	9	17.5	-67.5	171	34	0.37	40
UNNAMED	1944	2	15.6	-67.3	320	10	-0.76	14
UNNAMED	1944	4	15.2	-66.6	341	40	0.65	46
UNNAMED	1944	7	23	-65	542	21	-0.24	26
UNNAMED	1944	11	16.6	-61	568	9	-0.81	13
UNNAMED	1945	3	16.9	-66.2	148	12	-0.67	16
UNNAMED	1945	4	19.6	-65	190	10	-0.76	14
UNNAMED	1945	8	21.3	-63.2	455	12	-0.67	16

Table A-1. (cont.) Historical TCs: coordinates, distance from CRL 844, and Δp.

Name	Year	NHC ID	Lat (deg)	Lon (deg)	d (km)	Δp (hPa)	z-score	Adj. Δp (hPa)
UNNAMED	1945	9	20.2	-66.2	219	52	1.22	59
UNNAMED	1947	4	21.4	-65.4	360	56	1.41	63
UNNAMED	1947	10	20	-66.2	197	13	-0.62	17
UNNAMED	1948	3	22.2	-62.6	571	19	-0.34	24
UNNAMED	1949	1	22.6	-64.9	501	19	-0.34	24
UNNAMED	1949	2	19.7	-65.8	166	15	-0.53	19
UNNAMED	1949	3	15	-64.4	401	9	-0.81	13
UNNAMED	1949	4	19.8	-66.3	176	18	-0.38	22
UNNAMED	1949	10	17.1	-66.6	137	26	-0.01	31
UNNAMED	1949	15	20.8	-62	514	8	-0.86	12
ABLE	1950	1	22	-63.2	516	16	-0.48	20
BAKER	1950	2	17	-64	259	8	-0.86	12
DOG	1950	4	19.5	-64.3	234	51	1.17	58
UNNAMED	1951	1	20.2	-63.7	332	13	-0.62	17
CHARLIE	1951	4	15.9	-66.7	267	21	-0.24	26
DOG	1951	5	14.4	-65.8	427	23	-0.15	28
ABLE	1952	2	22.2	-65.6	444	15	-0.53	19
BAKER	1952	4	22	-62.1	590	20	-0.29	25
CAROL	1953	4	21.2	-61.3	599	81	2.59	90
DOLLY	1953	6	19.6	-68.5	297	11	-0.71	15
EDNA	1953	7	19.9	-65.3	203	14	-0.57	18
EDNA	1954	8	20.9	-68	359	8	-0.86	12
ALICE	1954	16	17.4	-63.6	278	19	-0.34	24
CONNIE	1955	2	20.4	-65.2	258	55	1.36	62
IONE	1955	8	20.6	-63.3	393	21	-0.24	26
HILDA	1955	9	19.5	-67	171	8	-0.86	12
JANET	1955	10	13.5	-67	535	14	-0.57	18
KATIE	1955	13	18	-71.7	595	47	0.98	54
BETSY	1956	3	17.9	-65.9	41	32	0.28	38
GRETA	1956	8	22.2	-65.7	443	41	0.70	47
BECKY	1958	2	23	-67.4	548	8	-0.86	12
ELLA	1958	5	16	-67.2	275	22	-0.20	27

Table A-1. (cont.) Historical TCs: coordinates, distance from CRL 844, and Δp.

Name	Year	NHC ID	Lat (deg)	Lon (deg)	d (km)	Δp (hPa)	z-score	Adj. Δp (hPa)
FIFI	1958	6	21.1	-63.1	446	13	-0.62	17
GERDA	1958	7	17.8	-70.6	480	9	-0.81	13
HELENE	1958	8	23.5	-67.2	597	10	-0.76	14
ILSA	1958	9	20	-61.1	559	56	1.41	63
EDITH	1959	6	15.5	-61.8	547	11	-0.71	15
ABBY	1960	2	14.7	-65.8	394	14	-0.57	18
DONNA	1960	5	20.1	-66.5	213	72	2.16	81
FLORENCE	1960	7	21	-67.9	362	9	-0.81	13
FRANCES	1961	7	17.8	-67.9	198	8	-0.86	12
DAISY	1962	4	21.1	-62.6	484	10	-0.76	14
EDITH	1963	6	17.7	-67.9	201	21	-0.24	26
FLORA	1963	7	14.2	-68.3	507	57	1.46	64
HELENA	1963	9	16.9	-62	457	12	-0.67	16
CLEO	1964	5	16.5	-66.6	200	75	2.31	84
BETSY	1965	3	20.5	-64.3	314	14	-0.57	18
ELLA	1966	5	20.2	-61.9	490	9	-0.81	13
FAITH	1966	6	19.7	-65.1	193	26	-0.01	31
GRETA	1966	7	21.3	-61.7	571	11	-0.71	15
INEZ	1966	9	17	-67.1	174	81	2.59	90
BEULAH	1967	13	16.8	-66.7	172	70	2.07	78
EDITH	1967	18	14.5	-65.5	419	8	-0.86	12
DOROTHY	1970	9	15.2	-66	337	8	-0.86	12
UNNAMED	1970	15	14	-65.8	471	8	-0.86	12
CHLOE	1971	8	15.4	-67.7	359	16	-0.48	20
CARMEN	1974	10	17	-69.9	427	12	-0.67	16
ELOISE	1975	13	19.4	-67.5	198	11	-0.71	15
EMMY	1976	10	21.3	-63.2	455	15	-0.53	19
UNNAMED	1976	19	13.5	-66	526	8	-0.86	12
DAVID	1979	9	16.6	-66.2	182	89	2.97	99
FREDERIC	1979	11	18.1	-65.8	33	9	-0.81	13
ALLEN	1980	4	14.8	-66.7	387	102	3.58	113
FLOYD	1981	14	20.1	-65.5	217	13	-0.62	17

Table A-1. (cont.) Historical TCs: coordinates, distance from CRL 844, and Δp.

Name	Year	NHC ID	Lat (deg)	Lon (deg)	d (km)	Δp (hPa)	z-score	Adj. Δp (hPa)
GERT	1981	15	17.8	-65.4	86	9	-0.81	13
KLAUS	1984	18	18	-65.8	39	15	-0.53	19
UNNAMED	1985	7	13.4	-67	546	9	-0.81	13
GLORIA	1985	9	21.5	-65.5	369	57	1.46	64
KATE	1985	13	20.4	-66.4	244	29	0.14	34
DANIELLE	1986	8	13.4	-64.8	554	9	-0.81	13
EMILY	1987	12	15.9	-67.7	311	42	0.75	48
GILBERT	1988	8	16.2	-68	304	31	0.23	36
DEAN	1989	5	20.1	-63.8	317	27	0.04	32
HUGO	1989	11	18.2	-65.5	61	68	1.98	76
IRIS	1989	12	21.3	-62.2	530	8	-0.86	12
ARTHUR	1990	2	14.8	-67.9	428	11	-0.71	15
KLAUS	1990	13	19.2	-64.9	164	9	-0.81	13
NANA	1990	16	22.8	-63.5	575	18	-0.38	22
CHANTAL	1995	3	23.2	-67.9	584	8	-0.86	12
IRIS	1995	10	19.4	-62.1	439	28	0.09	33
LUIS	1995	13	20.1	-64.9	242	73	2.21	82
MARILYN	1995	15	19	-65.8	91	62	1.69	70
SEBASTIEN	1995	20	18.6	-62.3	401	8	-0.86	12
BERTHA	1996	2	19.4	-66.1	130	43	0.80	49
EDOUARD	1996	5	22.3	-64.6	478	57	1.46	64
FRAN	1996	6	22.5	-63.9	526	32	0.28	38
HORTENSE	1996	8	18	-66.9	90	24	-0.10	29
ERIKA	1997	7	20.2	-63.1	382	38	0.56	44
GRACE	1997	9	20.8	-66.5	289	14	-0.57	18
BONNIE	1998	2	20.3	-65.9	231	14	-0.57	18
DANIELLE	1998	4	23	-64.4	558	24	-0.10	29
GEORGES	1998	7	18.1	-65.8	33	45	0.89	51
FLOYD	1999	8	22.8	-65.2	516	53	1.27	60
JOSE	1999	14	19.4	-65.8	133	20	-0.29	25
LENNY	1999	16	17.4	-64.8	164	80	2.54	89
DEBBY	2000	7	18.8	-65.4	96	18	-0.38	22
CHANTAL	2001	4	14.4	-68.2	482	9	-0.81	13

Table A-1. (cont.) Historical TCs: coordinates, distance from CRL 844, and Δp.

Name	Year	NHC ID	Lat (deg)	Lon (deg)	d (km)	Δp (hPa)	z-score	Adj. Δp (hPa)
IRIS	2001	11	15.7	-67.7	330	12	-0.67	16
OLGA	2001	17	22.8	-68.3	558	9	-0.81	13
LILI	2002	13	13	-64.9	595	9	-0.81	13
FABIAN	2003	10	21.3	-61.8	563	68	1.98	76
ISABEL	2003	13	23.2	-64.6	574	74	2.26	83
MINDY	2003	18	19.1	-68.8	303	9	-0.81	13
ODETTE	2003	20	20.5	-69.5	439	10	-0.76	14
CHARLEY	2004	3	14.9	-69.8	543	13	-0.62	17
FRANCES	2004	6	20.3	-65	257	71	2.12	79
IVAN	2004	9	13.3	-68.3	597	75	2.31	84
JEANNE	2004	11	18.1	-66.2	19	22	-0.20	27
DENNIS	2005	4	14.3	-68.5	508	13	-0.62	17
EMILY	2005	5	13.3	-66.7	552	54	1.31	61
ALPHA	2005	26	16.5	-68.5	321	8	-0.86	12
GAMMA	2005	28	14.3	-66	437	9	-0.81	13
CHRIS	2006	4	19.6	-63.9	275	9	-0.81	13
ERNESTO	2006	6	14.3	-68.3	497	11	-0.71	15
DEAN	2007	4	15	-66.6	363	84	2.73	93
NOEL	2007	16	18	-65.7	48	8	-0.86	12
OLGA	2007	17	18.5	-66.3	38	8	-0.86	12
GUSTAV	2008	7	15.8	-70.5	542	17	-0.43	21
HANNA	2008	8	21.8	-65.5	402	13	-0.62	17
IKE	2008	9	21.9	-67.7	442	48	1.03	55
KYLE	2008	11	22.4	-68.7	538	11	-0.71	15
OMAR	2008	15	18.2	-63.9	230	55	1.36	62
EARL	2010	7	19.6	-65.3	173	75	2.31	84
FIONA	2010	8	21	-63.8	390	13	-0.62	17
OTTO	2010	17	22	-67.2	435	13	-0.62	17
TOMAS	2010	21	14.1	-65.8	460	16	-0.48	20
EMILY	2011	5	16	-66.2	248	9	-0.81	13
IRENE	2011	9	18.2	-65.9	19	23	-0.15	28
MARIA	2011	14	19.1	-64.1	230	9	-0.81	13
OPHELIA	2011	16	21.6	-62.3	544	31	0.23	36

Table A-1. (cont.) Historical TCs: coordinates, distance from CRL 844, and Δp.

Name	Year	NHC ID	Lat (deg)	Lon (deg)	d (km)	Δp (hPa)	z-score	Adj. Δp (hPa)
ERNESTO	2012	5	13.9	-66.4	483	8	-0.86	12
ISAAC	2012	9	15.6	-66.4	294	10	-0.76	14
RAFAEL	2012	17	20.4	-64.3	305	19	-0.34	24
GONZALO	2014	8	19.9	-64.8	229	40	0.65	46
ERIKA	2015	5	16.5	-62.2	454	9	-0.81	13
MATTHEW	2016	14	14.2	-66.9	457	20	-0.29	25
HARVEY	2017	9	13.5	-65.7	528	8	-0.86	12
IRMA	2017	11	19.2	-66.2	109	97	3.34	107
JOSE	2017	12	20.3	-64	317	68	1.98	76
MARIA	2017	15	18	-65.9	32	93	3.16	103
ISAAC	2018	9	15.2	-66.2	337	9	-0.81	13
DORIAN	2019	5	19.2	-65.7	115	24	-0.10	29
JERRY	2019	10	21	-63.5	410	18	-0.38	22
KAREN	2019	12	18.5	-65.2	97	10	-0.76	14
SEBASTIEN	2019	20	20.8	-61.7	541	14	-0.57	18

Table A-2. Historical TCs with unadjusted atmospheric parameters for CRL 844.

Name	Year	NHC ID	Δp (hPa)	R_{max} (km)	V_t (km/h)	θ (deg)
UNNAMED	1938	2	16	70	25	-58
UNNAMED	1938	3	12	54	45	-66
UNNAMED	1938	5	9	137	15	-43
UNNAMED	1938	6	76	46	36	-72
UNNAMED	1939	5	28	72	10	-57
UNNAMED	1940	3	8	160	28	-82
UNNAMED	1940	5	14	120	22	-70
UNNAMED	1941	4	15	39	23	-85
UNNAMED	1941	5	12	103	33	-56
UNNAMED	1942	5	9	61	30	-75
UNNAMED	1943	2	9	107	27	-57
UNNAMED	1943	3	42	31	19	-39
UNNAMED	1943	9	34	41	21	-25
UNNAMED	1944	2	10	32	32	-73
UNNAMED	1944	4	40	40	22	-65
UNNAMED	1944	7	21	69	26	-69
UNNAMED	1944	11	9	139	15	7
UNNAMED	1945	3	12	60	27	-78
UNNAMED	1945	4	10	62	31	-76
UNNAMED	1945	8	12	101	33	-47
UNNAMED	1945	9	52	68	24	-72
UNNAMED	1947	4	56	56	28	-58
UNNAMED	1947	10	13	127	28	-70
UNNAMED	1948	3	19	66	24	-46
UNNAMED	1949	1	19	83	32	-66
UNNAMED	1949	2	15	123	31	-65
UNNAMED	1949	3	9	100	22	-75
UNNAMED	1949	4	18	121	18	-23
UNNAMED	1949	10	26	57	26	-60
UNNAMED	1949	15	8	102	35	-81
ABLE	1950	1	16	94	22	-53
BAKER	1950	2	8	99	20	-79
DOG	1950	4	51	51	10	-43
UNNAMED	1951	1	13	61	14	-90
CHARLIE	1951	4	21	66	38	-81

Table A-2. (cont.) Historical TCs with unadjusted atmospheric parameters for CRL 844.

Name	Year	NHC ID	Δp (hPa)	Rmax (km)	Vt (km/h)	θ (deg)
DOG	1951	5	23	64	27	-86
ABLE	1952	2	15	74	18	-72
BAKER	1952	4	20	68	23	-43
CAROL	1953	4	81	30	30	-43
DOLLY	1953	6	11	118	20	-62
EDNA	1953	7	14	150	29	-51
EDNA	1954	8	8	97	17	-64
ALICE	1954	16	19	59	10	-136
CONNIE	1955	2	55	63	27	-57
IONE	1955	8	21	87	30	-36
HILDA	1955	9	8	125	17	-70
JANET	1955	10	14	39	21	-74
KATIE	1955	13	47	43	24	32
BETSY	1956	3	32	40	29	-59
GRETA	1956	8	41	49	24	90
BECKY	1958	2	8	78	49	-72
ELLA	1958	5	22	80	30	-86
FIFI	1958	6	13	77	21	-57
GERDA	1958	7	9	102	22	-75
HELENE	1958	8	10	103	19	-61
ILSA	1958	9	56	56	8	-43
EDITH	1959	6	11	65	29	-67
ABBY	1960	2	14	37	20	-79
DONNA	1960	5	72	60	14	-59
FLORENCE	1960	7	9	113	19	-101
FRANCES	1961	7	8	86	22	-47
DAISY	1962	4	10	144	19	-16
EDITH	1963	6	21	70	20	-32
FLORA	1963	7	57	36	21	-58
HELENA	1963	9	12	112	8	26
CLEO	1964	5	75	30	29	-82
BETSY	1965	3	14	139	28	-30
ELLA	1966	5	9	64	16	-62
FAITH	1966	6	26	55	28	-62

Table A-2. (cont.) Historical TCs with unadjusted atmospheric parameters for CRL 844.

Name	Year	NHC ID	Δp (hPa)	Rmax (km)	Vt (km/h)	θ (deg)
GRETA	1966	7	11	108	15	-68
INEZ	1966	9	81	31	25	-81
BEULAH	1967	13	70	34	14	-49
EDITH	1967	18	8	62	14	-90
DOROTHY	1970	9	8	95	22	-80
UNNAMED	1970	15	8	54	14	-90
CHLOE	1971	8	16	39	23	-71
CARMEN	1974	10	12	62	44	-90
ELOISE	1975	13	11	121	14	-75
EMMY	1976	10	15	120	29	-45
UNNAMED	1976	19	8	59	18	-84
DAVID	1979	9	89	14	19	-72
FREDERIC	1979	11	9	172	18	-90
ALLEN	1980	4	102	18	33	-77
FLOYD	1981	14	13	103	18	-51
GERT	1981	15	9	50	31	-53
KLAUS	1984	18	15	101	13	32
UNNAMED	1985	7	9	78	26	-77
GLORIA	1985	9	57	78	24	-67
KATE	1985	13	29	55	9	-129
DANIELLE	1986	8	9	102	33	-77
EMILY	1987	12	42	47	29	-59
GILBERT	1988	8	31	42	22	-75
DEAN	1989	5	27	48	10	-43
HUGO	1989	11	68	39	15	-53
IRIS	1989	12	8	130	17	-64
ARTHUR	1990	2	11	49	29	-67
KLAUS	1990	13	9	136	20	-74
NANA	1990	16	18	37	9	-35
CHANTAL	1995	3	8	56	12	-36
IRIS	1995	10	28	88	15	-7
LUIS	1995	13	73	57	18	-43
MARILYN	1995	15	62	28	14	-49
SEBASTIEN	1995	20	8	74	13	-125

Table A-2. (cont.) Historical TCs with unadjusted atmospheric parameters for CRL 844.

Name	Year	NHC ID	Δp (hPa)	Rmax (km)	Vt (km/h)	θ (deg)
BERTHA	1996	2	43	56	26	-55
EDOUARD	1996	5	57	56	25	-73
FRAN	1996	6	32	56	13	-65
HORTENSE	1996	8	24	56	22	-40
ERIKA	1997	7	38	37	11	-29
GRACE	1997	9	14	92	26	82
BONNIE	1998	2	14	185	29	-58
DANIELLE	1998	4	24	49	21	-75
GEORGES	1998	7	45	48	23	-68
FLOYD	1999	8	53	111	19	-84
JOSE	1999	14	20	56	11	-50
LENNY	1999	16	80	37	17	48
DEBBY	2000	7	18	67	37	-72
CHANTAL	2001	4	9	93	33	-83
IRIS	2001	11	12	28	31	-83
OLGA	2001	17	9	111	8	-137
LILI	2002	13	9	59	22	-80
FABIAN	2003	10	68	37	11	-49
ISABEL	2003	13	74	46	23	-76
MINDY	2003	18	9	66	24	-40
ODETTE	2003	20	10	111	35	33
CHARLEY	2004	3	13	53	44	-62
FRANCES	2004	6	71	111	27	-78
IVAN	2004	9	75	17	24	-77
JEANNE	2004	11	22	50	12	-62
DENNIS	2005	4	13	53	25	-59
EMILY	2005	5	54	26	33	-77
ALPHA	2005	26	8	45	22	-54
GAMMA	2005	28	9	56	18	-84
CHRIS	2006	4	9	19	19	-55
ERNESTO	2006	6	11	50	22	-75
DEAN	2007	4	84	10	27	-86
NOEL	2007	16	8	85	22	-133
OLGA	2007	17	8	200	28	-86

Table A-2. (cont.) Historical TCs with unadjusted atmospheric parameters for CRL 844.

Name	Year	NHC ID	Δp (hPa)	Rmax (km)	Vt (km/h)	θ (deg)
GUSTAV	2008	7	17	96	21	-51
HANNA	2008	8	13	102	17	-84
IKE	2008	9	48	53	26	-111
KYLE	2008	11	11	96	14	58
OMAR	2008	15	55	19	36	39
EARL	2010	7	75	67	22	-60
FIONA	2010	8	13	100	36	-39
OTTO	2010	17	13	134	15	-43
TOMAS	2010	21	16	56	25	-94
EMILY	2011	5	9	111	26	-77
IRENE	2011	9	23	59	20	-44
MARIA	2011	14	9	39	14	-59
OPHELIA	2011	16	31	56	13	-32
ERNESTO	2012	5	8	93	29	-86
ISAAC	2012	9	10	74	27	-69
RAFAEL	2012	17	19	130	15	-28
GONZALO	2014	8	40	19	20	-43
ERIKA	2015	5	9	56	25	-90
MATTHEW	2016	14	20	93	25	-86
HARVEY	2017	9	8	111	31	-86
IRMA	2017	11	97	9	29	-67
JOSE	2017	12	68	54	25	-49
MARIA	2017	15	93	26	23	-62
ISAAC	2018	9	9	86	25	-81
DORIAN	2019	5	24	39	18	-35
JERRY	2019	10	18	113	25	-49
KAREN	2019	12	10	141	25	25
SEBASTIEN	2019	20	14	101	13	-65

Table A-3. Historical TCs with distance-adjusted atmospheric parameters for CRL 844.

Name	Year	NHC ID	Δp (hPa)	R_{max} (km)	V_t (km/h)	θ (deg)
UNNAMED	1938	2	20	67	24	-59
UNNAMED	1938	3	16	49	42	-66
UNNAMED	1938	5	13	142	16	-45
UNNAMED	1938	6	85	40	34	-71
UNNAMED	1939	5	33	69	11	-58
UNNAMED	1940	3	12	167	27	-80
UNNAMED	1940	5	18	123	22	-69
UNNAMED	1941	4	19	32	23	-83
UNNAMED	1941	5	16	104	31	-57
UNNAMED	1942	5	13	57	29	-74
UNNAMED	1943	2	13	108	26	-58
UNNAMED	1943	3	48	24	19	-41
UNNAMED	1943	9	40	35	21	-29
UNNAMED	1944	2	14	25	31	-72
UNNAMED	1944	4	46	34	22	-65
UNNAMED	1944	7	26	66	25	-69
UNNAMED	1944	11	13	144	16	0
UNNAMED	1945	3	16	56	26	-77
UNNAMED	1945	4	14	58	30	-75
UNNAMED	1945	8	16	102	31	-49
UNNAMED	1945	9	59	65	24	-71
UNNAMED	1947	4	63	51	27	-59
UNNAMED	1947	10	17	131	27	-69
UNNAMED	1948	3	24	63	24	-48
UNNAMED	1949	1	24	82	31	-66
UNNAMED	1949	2	19	126	30	-65
UNNAMED	1949	3	13	100	22	-74
UNNAMED	1949	4	22	124	18	-27
UNNAMED	1949	10	31	53	25	-60
UNNAMED	1949	15	12	103	33	-79
ABLE	1950	1	20	94	22	-54
BAKER	1950	2	12	99	20	-78
DOG	1950	4	58	46	11	-45
UNNAMED	1951	1	17	57	15	-88

Table A-3. (cont.) Historical TCs with distance-adjusted atmospheric parameters for CRL 844.

Name	Year	NHC ID	Δp (hPa)	Rmax (km)	Vt (km/h)	θ (deg)
CHARLIE	1951	4	26	63	36	-79
DOG	1951	5	28	60	26	-84
ABLE	1952	2	19	71	18	-71
BAKER	1952	4	25	65	23	-45
CAROL	1953	4	90	22	29	-45
DOLLY	1953	6	15	121	20	-62
EDNA	1953	7	18	156	28	-52
EDNA	1954	8	12	97	18	-64
ALICE	1954	16	24	55	11	-129
CONNIE	1955	2	62	59	26	-58
IONE	1955	8	26	86	29	-39
HILDA	1955	9	12	128	18	-69
JANET	1955	10	18	32	21	-73
KATIE	1955	13	54	37	24	23
BETSY	1956	3	38	34	28	-60
GRETA	1956	8	47	44	24	75
BECKY	1958	2	12	76	45	-71
ELLA	1958	5	27	78	29	-84
FIFI	1958	6	17	75	21	-58
GERDA	1958	7	13	103	22	-74
HELENE	1958	8	14	104	19	-61
ILSA	1958	9	63	51	10	-45
EDITH	1959	6	15	61	28	-67
ABBY	1960	2	18	30	20	-78
DONNA	1960	5	81	56	15	-60
FLORENCE	1960	7	13	115	19	-97
FRANCES	1961	7	12	85	22	-49
DAISY	1962	4	14	150	19	-21
EDITH	1963	6	26	67	20	-35
FLORA	1963	7	64	29	21	-59
HELENA	1963	9	16	114	10	17
CLEO	1964	5	84	22	28	-80
BETSY	1965	3	18	144	27	-33
ELLA	1966	5	13	60	17	-62

Table A-3. (cont.) Historical TCs with distance-adjusted atmospheric parameters for CRL 844.

Name	Year	NHC ID	Δp (hPa)	Rmax (km)	Vt (km/h)	θ (deg)
FAITH	1966	6	31	50	27	-62
GRETA	1966	7	15	109	16	-68
INEZ	1966	9	90	24	24	-79
BEULAH	1967	13	78	27	15	-50
EDITH	1967	18	12	58	15	-88
DOROTHY	1970	9	12	95	22	-79
UNNAMED	1970	15	12	49	15	-88
CHLOE	1971	8	20	32	23	-70
CARMEN	1974	10	16	58	41	-88
ELOISE	1975	13	15	124	15	-74
EMMY	1976	10	19	123	28	-47
UNNAMED	1976	19	12	55	18	-82
DAVID	1979	9	99	8	19	-71
FREDERIC	1979	11	13	181	18	-88
ALLEN	1980	4	113	9	31	-76
FLOYD	1981	14	17	104	18	-52
GERT	1981	15	13	45	30	-54
KLAUS	1984	18	19	102	14	23
UNNAMED	1985	7	13	76	25	-76
GLORIA	1985	9	64	76	24	-67
KATE	1985	13	34	50	11	-123
DANIELLE	1986	8	13	103	31	-76
EMILY	1987	12	48	41	28	-60
GILBERT	1988	8	36	36	22	-74
DEAN	1989	5	32	43	11	-45
HUGO	1989	11	76	32	16	-54
IRIS	1989	12	12	134	18	-64
ARTHUR	1990	2	15	44	28	-67
KLAUS	1990	13	13	141	20	-73
NANA	1990	16	22	30	11	-38
CHANTAL	1995	3	12	51	13	-39
IRIS	1995	10	33	87	16	-12
LUIS	1995	13	82	53	18	-45
MARILYN	1995	15	70	20	15	-50

Table A-3. (cont.) Historical TCs with distance-adjusted atmospheric parameters for CRL 844.

Name	Year	NHC ID	Δp (hPa)	Rmax (km)	Vt (km/h)	θ (deg)
SEBASTIEN	1995	20	12	71	14	-119
BERTHA	1996	2	49	51	25	-56
EDOUARD	1996	5	64	51	24	-72
FRAN	1996	6	38	51	14	-65
HORTENSE	1996	8	29	51	22	-42
ERIKA	1997	7	44	30	12	-32
GRACE	1997	9	18	92	25	68
BONNIE	1998	2	18	195	28	-59
DANIELLE	1998	4	29	44	21	-74
GEORGES	1998	7	51	43	23	-68
FLOYD	1999	8	60	113	19	-82
JOSE	1999	14	25	51	12	-51
LENNY	1999	16	89	30	18	37
DEBBY	2000	7	22	64	35	-71
CHANTAL	2001	4	13	93	31	-81
IRIS	2001	11	16	20	30	-81
OLGA	2001	17	13	113	10	-130
LILI	2002	13	13	55	22	-79
FABIAN	2003	10	76	30	12	-50
ISABEL	2003	13	83	40	23	-75
MINDY	2003	18	13	63	24	-42
ODETTE	2003	20	14	113	33	24
CHARLEY	2004	3	17	48	41	-62
FRANCES	2004	6	79	113	26	-77
IVAN	2004	9	84	8	24	-76
JEANNE	2004	11	27	45	13	-62
DENNIS	2005	4	17	48	24	-60
EMILY	2005	5	61	18	31	-76
ALPHA	2005	26	12	39	22	-55
GAMMA	2005	28	13	51	18	-82
CHRIS	2006	4	13	10	19	-56
ERNESTO	2006	6	15	45	22	-74
DEAN	2007	4	93	8	26	-84
NOEL	2007	16	12	84	22	-126

Table A-3. (cont.) Historical TCs with distance-adjusted atmospheric parameters for CRL 844.

Name	Year	NHC ID	Δp (hPa)	Rmax (km)	Vt (km/h)	θ (deg)
OLGA	2007	17	12	200	27	-84
GUSTAV	2008	7	21	96	21	-52
HANNA	2008	8	17	103	18	-82
IKE	2008	9	55	48	25	-107
KYLE	2008	11	15	96	15	46
OMAR	2008	15	62	10	34	29
EARL	2010	7	84	64	22	-60
FIONA	2010	8	17	100	34	-41
OTTO	2010	17	17	138	16	-45
TOMAS	2010	21	20	51	24	-91
EMILY	2011	5	13	113	25	-76
IRENE	2011	9	28	55	20	-46
MARIA	2011	14	13	32	15	-60
OPHELIA	2011	16	36	51	14	-35
ERNESTO	2012	5	12	93	28	-84
ISAAC	2012	9	14	71	26	-69
RAFAEL	2012	17	24	134	16	-31
GONZALO	2014	8	46	10	20	-45
ERIKA	2015	5	13	51	24	-88
MATTHEW	2016	14	25	93	24	-84
HARVEY	2017	9	12	113	30	-84
IRMA	2017	11	107	8	28	-67
JOSE	2017	12	76	49	24	-50
MARIA	2017	15	103	18	23	-62
ISAAC	2018	9	13	85	24	-79
DORIAN	2019	5	29	32	18	-38
JERRY	2019	10	22	115	24	-50
KAREN	2019	12	14	146	24	16
SEBASTIEN	2019	20	18	102	14	-65

Appendix B: CHS-PR Synthetic Tropical Cyclone Master Tracks

Table B-1 presents the 40 master tracks developed for the CHS-PR synthetic TCs. The atmospheric forcing parameters assigned to each synthetic TC are documented in Table B-2.

Table B-1. SACS master tracks selected for CHS-PR.

SACS Master Track ID	θ (deg)	Reference Lat (deg)	Reference Lon (deg)
1	-140	18.23	-65.59
2	-140	18.23	-65.59
3	-140	18.23	-65.59
4	-140	18.23	-65.59
5	-140	18.23	-65.59
6	-140	18.23	-65.59
7	-100	18.23	-65.59
8	-100	18.23	-65.59
9	-100	18.23	-65.59
10	-100	18.23	-65.59
11	-100	18.23	-65.59
12	-60	18.23	-65.59
13	-60	18.23	-65.59
14	-60	18.23	-65.59
15	-60	18.23	-65.59
16	-60	18.23	-65.59
17	-60	18.23	-65.59
18	-20	18.23	-65.59
19	-20	18.23	-65.59
20	-20	18.23	-65.59
21	-20	18.23	-65.59
22	-20	18.23	-65.59
23	-20	18.23	-65.59

Table B-1. (cont.) SACS master tracks selected for CHS-PR.

SACS Master Track ID	θ (deg)	Reference Lat (deg)	Reference Lon (deg)
24	-20	18.23	-65.59
25	-20	18.23	-65.59
26	-20	18.23	-65.59
27	-20	18.23	-65.59
28	-20	18.23	-65.59
29	-20	18.23	-65.59
30	-20	18.23	-65.59
31	-20	18.23	-65.59
32	-20	18.23	-65.59
33	-20	18.23	-65.59
34	-20	18.23	-65.59
35	60	18.23	-65.59
36	60	18.23	-65.59
37	60	18.23	-65.59
38	60	18.23	-65.59
39	60	18.23	-65.59
40	60	18.23	-65.59

Table B-2. Atmospheric-forcing parameters of the CHS-PR synthetic TC suite.

CHS-PR TC ID	SACS Master Track ID	θ (deg)	Δp (hPa)	R_{max} (km)	V_t (km/h)
1	1	-140	148	8.0	12.1
2	1	-140	128	29.2	15.0
3	1	-140	108	35.6	26.4
4	1	-140	88	48.2	11.1
5	1	-140	68	58.0	25.2
6	1	-140	48	40.1	14.6
7	1	-140	28	137.3	19.3
8	1	-140	8	18.0	35.0
9	2	-140	148	20.0	8.6
10	2	-140	128	27.2	21.0
11	2	-140	108	16.4	16.7
12	2	-140	88	44.6	9.6
13	2	-140	68	107.8	19.7
14	2	-140	48	36.4	21.9
15	2	-140	28	62.4	24.5
16	2	-140	8	60.6	13.8
17	3	-140	148	24.4	10.3
18	3	-140	128	20.5	17.6
19	3	-140	108	18.3	17.6
20	3	-140	88	35.2	28.1
21	3	-140	68	49.5	18.6
22	3	-140	48	52.3	11.1
23	3	-140	28	86.5	13.3
24	3	-140	8	22.0	27.4
25	4	-140	148	10.7	16.5
26	4	-140	128	31.4	19.7
27	4	-140	108	33.0	15.0
28	4	-140	88	61.6	8.9
29	4	-140	68	38.5	23.5
30	4	-140	48	29.1	12.0
31	4	-140	28	117.1	18.2
32	4	-140	8	25.9	40.0
33	5	-140	148	12.5	9.7
34	5	-140	128	13.4	18.6
35	5	-140	108	30.7	22.4

Table B-2. (cont.) Atmospheric-forcing parameters of the CHS-PR synthetic TC suite.

CHS-PR TC ID	SACS Master Track ID	θ (deg)	Δp (hPa)	Rmax (km)	Vt (km/h)
36	5	-140	88	88.6	20.9
37	5	-140	68	68.3	9.9
38	5	-140	48	15.1	12.8
39	5	-140	28	35.9	21.7
40	5	-140	8	99.2	19.0
41	6	-140	148	22.8	14.1
42	6	-140	128	33.8	14.2
43	6	-140	108	10.9	21.0
44	6	-140	88	38.2	10.3
45	6	-140	68	92.1	20.8
46	6	-140	48	44.0	13.7
47	6	-140	28	52.8	28.0
48	6	-140	8	42.3	29.4
49	7	-100	138	25.1	13.8
50	7	-100	118	23.3	14.6
51	7	-100	98	55.0	24.9
52	7	-100	78	13.0	21.5
53	7	-100	58	27.5	10.9
54	7	-100	38	131.7	15.8
55	7	-100	18	33.1	25.1
56	8	-100	138	20.5	9.3
57	8	-100	118	16.5	15.4
58	8	-100	98	50.5	27.3
59	8	-100	78	98.3	15.3
60	8	-100	58	14.4	22.7
61	8	-100	38	64.9	9.6
62	8	-100	18	75.6	14.5
63	9	-100	138	37.7	14.5
64	9	-100	118	18.1	29.0
65	9	-100	98	34.4	9.4
66	9	-100	78	18.4	14.5
67	9	-100	58	116.7	25.9
68	9	-100	38	23.2	23.9
69	9	-100	18	120.6	12.6
70	10	-100	138	10.9	8.1

Table B-2. (cont.) Atmospheric-forcing parameters of the CHS-PR synthetic TC suite.

CHS-PR TC ID	SACS Master Track ID	θ (deg)	Δp (hPa)	Rmax (km)	Vt (km/h)
71	10	-100	118	27.1	19.2
72	10	-100	98	46.7	10.8
73	10	-100	78	26.7	12.1
74	10	-100	58	99.6	16.1
75	10	-100	38	15.9	29.5
76	10	-100	18	82.0	26.7
77	11	-100	138	23.5	18.0
78	11	-100	118	21.5	20.3
79	11	-100	98	11.6	19.2
80	11	-100	78	45.4	13.6
81	11	-100	58	88.8	18.0
82	11	-100	38	50.7	12.2
83	11	-100	18	69.8	31.0
84	12	-60	148	28.6	17.4
85	12	-60	128	36.6	11.4
86	12	-60	108	26.2	12.0
87	12	-60	88	14.7	13.3
88	12	-60	68	25.7	27.2
89	12	-60	48	106.4	24.8
90	12	-60	28	67.7	15.2
91	12	-60	8	38.1	10.0
92	13	-60	148	15.5	10.9
93	13	-60	128	23.7	16.6
94	13	-60	108	24.2	30.0
95	13	-60	88	75.9	16.7
96	13	-60	68	62.8	10.7
97	13	-60	48	18.6	17.4
98	13	-60	28	39.9	11.5
99	13	-60	8	77.1	25.7
100	14	-60	148	31.6	23.0
101	14	-60	128	19.0	10.2
102	14	-60	108	14.5	18.6
103	14	-60	88	41.3	11.8
104	14	-60	68	42.0	34.0
105	14	-60	48	124.7	16.4

Table B-2. (cont.) Atmospheric-forcing parameters of the CHS-PR synthetic TC suite.

CHS-PR TC ID	SACS Master Track ID	θ (deg)	Δp (hPa)	Rmax (km)	Vt (km/h)
106	14	-60	28	44.1	16.2
107	14	-60	8	51.1	12.8
108	15	-60	148	26.3	15.6
109	15	-60	128	22.1	12.1
110	15	-60	108	12.7	19.7
111	15	-60	88	32.4	25.7
112	15	-60	68	22.7	22.1
113	15	-60	48	66.7	10.3
114	15	-60	28	104.3	14.2
115	15	-60	8	55.8	21.4
116	16	-60	148	8.9	18.4
117	16	-60	128	51.4	28.0
118	16	-60	108	22.2	9.9
119	16	-60	88	24.5	17.6
120	16	-60	68	82.1	11.5
121	16	-60	48	61.6	20.7
122	16	-60	28	48.4	38.0
123	16	-60	8	71.2	10.9
124	17	-60	148	11.6	9.1
125	17	-60	128	44.4	24.7
126	17	-60	108	59.5	13.5
127	17	-60	88	17.1	32.0
128	17	-60	68	53.6	14.8
129	17	-60	48	48.1	18.4
130	17	-60	28	16.6	12.4
131	17	-60	8	109.3	31.8
132	18	-20	138	19.2	17.0
133	18	-20	118	31.3	18.1
134	18	-20	98	13.7	13.0
135	18	-20	78	75.1	19.2
136	18	-20	58	37.8	9.3
137	18	-20	38	42.3	25.5
138	18	-20	18	97.4	23.6
139	19	-20	138	21.9	20.3
140	19	-20	118	33.6	9.7

Table B-2. (cont.) Atmospheric-forcing parameters of the CHS-PR synthetic TC suite.

CHS-PR TC ID	SACS Master Track ID	θ (deg)	Δp (hPa)	Rmax (km)	Vt (km/h)
141	19	-20	98	22.3	18.1
142	19	-20	78	84.1	18.1
143	19	-20	58	34.2	35.0
144	19	-20	38	46.4	16.8
145	19	-20	18	141.3	17.5
146	20	-20	138	9.8	11.8
147	20	-20	118	36.2	13.8
148	20	-20	98	31.8	31.0
149	20	-20	78	53.1	12.8
150	20	-20	58	80.5	24.2
151	20	-20	38	30.6	27.3
152	20	-20	18	25.1	22.2
153	21	-20	138	16.7	27.0
154	21	-20	118	25.1	8.4
155	21	-20	98	78.8	17.2
156	21	-20	78	35.5	17.1
157	21	-20	58	17.7	19.1
158	21	-20	38	76.3	11.3
159	21	-20	18	107.5	34.1
160	22	-20	138	26.9	21.8
161	22	-20	118	10.1	17.1
162	22	-20	98	67.6	10.1
163	22	-20	78	29.5	11.3
164	22	-20	58	30.8	11.7
165	22	-20	38	100.1	32.4
166	22	-20	18	89.2	28.7
167	23	-20	138	15.5	8.7
168	23	-20	118	46.4	21.7
169	23	-20	98	15.8	15.4
170	23	-20	78	32.5	24.5
171	23	-20	58	67.8	14.3
172	23	-20	38	59.9	17.8
173	23	-20	18	29.1	11.7
174	24	-20	138	31.2	10.5
175	24	-20	118	14.9	23.4

Table B-2. (cont.) Atmospheric-forcing parameters of the CHS-PR synthetic TC suite.

CHS-PR TC ID	SACS Master Track ID	θ (deg)	Δp (hPa)	Rmax (km)	Vt (km/h)
176	24	-20	98	40.0	16.3
177	24	-20	78	23.9	9.8
178	24	-20	58	45.2	30.7
179	24	-20	38	112.3	13.1
180	24	-20	18	21.2	13.6
181	25	-20	138	28.9	11.2
182	25	-20	118	39.1	12.4
183	25	-20	98	20.1	14.6
184	25	-20	78	38.7	29.0
185	25	-20	58	73.7	20.2
186	25	-20	38	38.3	22.5
187	25	-20	18	45.6	10.8
188	26	-20	138	34.0	9.9
189	26	-20	118	13.3	10.4
190	26	-20	98	37.1	12.3
191	26	-20	78	57.5	22.9
192	26	-20	58	62.5	15.1
193	26	-20	38	19.5	37.0
194	26	-20	18	37.1	9.9
195	27	20	148	18.8	13.4
196	27	20	128	17.6	10.8
197	27	20	108	48.6	11.3
198	27	20	88	22.0	22.3
199	27	20	68	13.7	12.3
200	27	20	48	78.7	26.6
201	27	20	28	24.2	23.0
202	27	20	8	65.7	14.8
203	28	20	148	17.6	21.1
204	28	20	128	25.4	22.6
205	28	20	108	28.4	12.7
206	28	20	88	52.1	12.6
207	28	20	68	19.7	17.6
208	28	20	48	94.8	28.7
209	28	20	28	31.9	30.3
210	28	20	8	83.6	15.8

Table B-2. (cont.) Atmospheric-forcing parameters of the CHS-PR synthetic TC suite.

CHS-PR TC ID	SACS Master Track ID	θ (deg)	Δp (hPa)	Rmax (km)	Vt (km/h)
211	29	20	148	36.4	14.8
212	29	20	128	9.4	13.5
213	29	20	108	41.3	14.2
214	29	20	88	19.5	19.7
215	29	20	68	16.7	13.1
216	29	20	48	72.3	9.4
217	29	20	28	94.6	20.5
218	29	20	8	34.0	17.9
219	30	20	148	9.8	12.7
220	30	20	128	40.0	15.8
221	30	20	108	38.3	8.6
222	30	20	88	56.5	18.7
223	30	20	68	35.2	16.6
224	30	20	48	32.7	36.0
225	30	20	28	28.0	9.7
226	30	20	8	143.6	16.8
227	31	20	148	16.5	11.5
228	31	20	128	16.2	8.9
229	31	20	108	44.7	24.1
230	31	20	88	12.3	15.0
231	31	20	68	31.9	29.8
232	31	20	48	86.0	19.5
233	31	20	28	57.5	10.6
234	31	20	8	29.9	24.1
235	32	20	148	21.3	26.0
236	32	20	128	10.8	8.3
237	32	20	108	20.2	10.6
238	32	20	88	67.8	14.1
239	32	20	68	74.5	14.0
240	32	20	48	22.1	31.6
241	32	20	28	73.3	26.1
242	32	20	8	46.7	20.2
243	33	20	148	14.5	19.6
244	33	20	128	14.8	9.5
245	33	20	108	69.2	15.8

Table B-2. (cont.) Atmospheric-forcing parameters of the CHS-PR synthetic TC suite.

CHS-PR TC ID	SACS Master Track ID	θ (deg)	Δp (hPa)	Rmax (km)	Vt (km/h)
246	33	20	88	27.1	23.8
247	33	20	68	45.6	15.7
248	33	20	48	25.6	23.3
249	33	20	28	79.6	33.3
250	33	20	8	90.8	11.9
251	34	20	148	13.5	8.0
252	34	20	128	12.1	12.8
253	34	20	108	53.3	9.2
254	34	20	88	29.7	15.8
255	34	20	68	28.8	9.1
256	34	20	48	56.8	15.5
257	34	20	28	20.4	17.2
258	34	20	8	122.7	22.7
259	35	60	138	12.0	16.1
260	35	60	118	42.4	11.0
261	35	60	98	43.2	23.1
262	35	60	78	62.5	9.0
263	35	60	58	20.9	12.6
264	35	60	38	83.0	18.9
265	35	60	18	50.0	16.5
266	36	60	138	43.5	13.1
267	36	60	118	11.7	16.2
268	36	60	98	26.9	8.7
269	36	60	78	49.1	26.4
270	36	60	58	53.3	13.4
271	36	60	38	70.3	21.2
272	36	60	18	17.3	15.5
273	37	60	138	8.7	23.8
274	37	60	118	29.1	11.7
275	37	60	98	60.5	13.8
276	37	60	78	42.0	33.0
277	37	60	58	24.1	21.4
278	37	60	38	26.9	10.4
279	37	60	18	59.4	19.7
280	38	60	138	13.1	12.4

Table B-2. (cont.) Atmospheric-forcing parameters of the CHS-PR synthetic TC suite.

CHS-PR TC ID	SACS Master Track ID	θ (deg)	Δp (hPa)	Rmax (km)	Vt (km/h)
281	38	60	118	60.1	13.1
282	38	60	98	29.3	20.3
283	38	60	78	15.7	16.2
284	38	60	58	49.1	17.0
285	38	60	38	55.1	14.0
286	38	60	18	41.3	39.0
287	39	60	138	17.9	15.3
288	39	60	118	19.8	25.6
289	39	60	98	18.0	11.5
290	39	60	78	68.2	20.3
291	39	60	58	41.4	10.1
292	39	60	38	34.4	20.0
293	39	60	18	54.6	20.9
294	40	60	138	14.3	19.1
295	40	60	118	51.7	9.1
296	40	60	98	24.6	21.6
297	40	60	78	21.1	10.5
298	40	60	58	57.7	28.0
299	40	60	38	90.7	14.9
300	40	60	18	64.4	18.6

Appendix C: List of Historical TCs Used by Ocean Weather, Inc. (OWI), in the Generation of Wind and Pressure Fields

Tables C-1, C-2, and C-3 document the historical storm parameters applied in the pre-landfall filling, closest approach, and landfall filling analyses documented in Section 5. Tables C-1 and C-2 report the parameters at the closest approach and 250 km prior for historical storms applied for analysis, and Table C-3 documents the parameters of storms making landfall in Puerto Rico.

Table C-1. TC set applied in closest approach analysis by OWI.

IBTracsName	Name	YYYYMM	DDHHMM	Closest Approach Latitude (deg)	Closest Approach Longitude (deg)	Closest Approach SLP (hPa)	Closest Approach Heading (deg)	Closest Approach Speed (kt)
1938220N18298	UNNAMED	193808	082110	19.01	-65.50	998	285	16
1939220N19296	UNNAMED	193908	080110	19.58	-64.74	1014	295	7
1940219N19295	UNNAMED	194008	052030	18.98	-65.47	1008	287	17
1943226N17300	UNNAMED	194308	140920	18.89	-65.11	1004	298	15
1943284N13300	UNNAMED	194310	141720	17.39	-67.44	976	336	12
1944195N20291	UNNAMED	194407	130600	19.60	-68.60	1016	319	13
1945214N14302	UNNAMED	194508	031650	16.84	-65.91	998	287	14
1945230N17307	UNNAMED	194508	191230	19.64	-65.14	1003	285	17
1945255N19302	UNNAMED	194509	130640	19.84	-65.04	962	283	12
1947290N19297	UNNAMED	194710	170730	19.62	-65.07	1003	294	15
1949235N18300	UNNAMED	194908	240310	19.37	-65.04	991	294	15
1949246N19295	UNNAMED	194909	030000	18.50	-65.40	1005	326	8
1949264N14299	UNNAMED	194909	211650	16.96	-66.35	988	295	12
1950231N12306	BAKER	195008	231000	17.67	-65.83	1004	289	11
1950243N15304	DOG	195009	021110	19.44	-64.24	961	327	6
1951224N12316	CHARLIE	195108	161000	15.80	-66.00	992	279	19
1953251N18295	DOLLY	195309	080800	18.43	-65.53	1009	292	12
1953258N19296	EDNA	195309	150250	19.37	-64.61	998	309	16
1954248N20295	EDNA	195409	050000	19.80	-65.30	1013	292	9

Table C-1. (cont.) TC set applied in closest approach analysis by OWI.

IBTracsName	Name	YYYYMM	DDHHMM	Closest Approach Latitude (deg)	Closest Approach Longitude (deg)	Closest Approach SLP (hPa)	Closest Approach Heading (deg)	Closest Approach Speed (kt)
1954364N22309	ALICE	195501	031010	16.98	-63.95	996	223	6
1955215N15320	CONNIE	195508	062030	19.93	-64.44	959	295	14
1955255N19294	HILDA	195509	120000	19.20	-66.10	1002	289	9
1956222N14313	BETSY	195608	121140	17.86	-65.82	981	302	16
1958242N13302	ELLA	195808	310650	15.91	-65.74	1002	284	17
1958257N17293	GERDA	195809	140600	17.40	-67.50	1009	279	15
1959230N14302	EDITH	195908	182350	16.68	-65.45	1013	289	18
1959264N20292	GRACIE	195909	201200	19.80	-68.30	1009	277	13
1960243N10337	DONNA	196009	051250	19.18	-64.94	958	298	12
1961273N16303	FRANCES	196110	021500	16.70	-66.60	1010	299	10
1963267N11308	EDITH	196309	270000	17.80	-67.50	989	318	10
1964234N13316	CLEO	196408	230910	16.41	-65.84	939	276	15
1966233N13340	FAITH	196608	262250	19.56	-64.83	985	298	14
1966265N10325	INEZ	196609	281230	16.82	-65.82	945	278	13
1967249N14303	BEULAH	196709	100000	16.80	-66.70	946	298	9
1971233N12313	DORIA	197108	240010	18.62	-65.44	1012	294	15
1973238N11346	CHRISTINE	197309	041400	18.60	-65.40	1012	298	13
1974241N17304	CARMEN	197408	300750	16.86	-65.73	1012	273	23
1974258N15295	FIFI	197409	141740	15.68	-66.42	1012	283	15
1975256N18306	ELOISE	197509	152310	18.99	-65.49	1007	280	9
1979197N13314	CLAUDETTE	197907	180640	18.31	-65.58	1011	275	15
1979238N12324	DAVID	197908	301740	16.58	-66.14	924	285	10
1979241N11335	FREDERIC	197909	041040	18.10	-65.58	1004	270	10
1981247N16300	FLOYD	198109	042320	19.44	-64.62	1002	310	9
1981250N15306	GERT	198109	081920	18.04	-65.73	1004	299	17
1984311N15291	KLAUS	198411	070820	18.19	-65.57	998	46	7
1984348N35300	LILI	198412	240240	20.23	-66.17	1009	250	21
1985280N18291	ISABEL	198510	070000	17.80	-69.20	1006	319	14
1985320N21296	KATE	198511	170600	20.40	-66.40	984	263	7
1987263N10309	EMILY	198709	221450	16.28	-68.36	965	305	16
1988235N15317	CHRIS	198808	241420	17.32	-65.78	1009	284	13
1988253N12306	GILBERT	198809	102040	15.79	-66.02	991	280	13
1989254N13340	HUGO	198909	181240	18.27	-65.57	946	316	9
1990277N16301	KLAUS	199010	071900	19.28	-65.10	1004	290	12
1993227N14301	CINDY	199308	160000	16.40	-66.90	1010	293	12

Table C-1. (cont.) TC set applied in closest approach analysis by OWI.

IBTracsName	Name	YYYYMM	DDHHMM	Closest Approach Latitude (deg)	Closest Approach Longitude (deg)	Closest Approach SLP (hPa)	Closest Approach Heading (deg)	Closest Approach Speed (kt)
1995240N11337	LUIS	199509	061220	19.44	-64.24	943	315	8
1995256N12309	MARILYN	199509	160650	18.57	-65.28	952	318	8
1995294N14306	SEBASTIEN	199510	242350	17.51	-64.49	1008	235	5
1996187N10326	BERTHA	199607	081920	18.78	-65.17	976	297	16
1996248N15319	HORTENSE	199609	100250	17.52	-66.48	989	308	8
1997288N20291	GRACE	199710	141200	20.00	-68.70	1002	304	4
1998232N15312	BONNIE	199808	211250	19.61	-64.69	1000	293	15
1998259N10335	GEORGES	199809	212120	18.05	-65.67	968	280	13
1999291N10309	JOSE	199910	211450	18.74	-65.04	995	309	8
1999318N17278	LENNY	199911	171800	17.40	-64.80	933	62	7
2000233N12316	DEBBY	200008	221800	18.80	-65.40	995	289	17
2000260N15308	HELENE	200009	171920	16.77	-65.93	1010	274	17
2001235N18296	DEAN	200108	221540	18.63	-65.28	1009	304	17
2003284N19291	MINDY	200310	101800	19.10	-68.80	1004	319	12
2004238N11325	FRANCES	200408	312010	20.41	-65.51	942	284	14
2004258N16300	JEANNE	200409	151500	17.90	-65.85	991	296	8
2005296N16293	ALPHA	200510	221510	16.17	-68.03	1006	305	12
2006213N16302	CHRIS	200608	030120	19.97	-65.02	1008	291	10
2007297N18300	NOEL	200710	260450	18.16	-65.53	1005	238	10
2007345N18298	OLGA	200712	110320	18.46	-65.59	1006	271	13
2008229N18293	FAY	200808	151200	18.40	-67.40	1011	275	13
2008287N15291	OMAR	200810	160300	17.45	-64.55	964	47	19
2009245N17303	ERIKA	200909	040220	16.88	-65.89	1009	280	10
2010236N12341	EARL	201008	302150	19.38	-64.90	944	298	12
2010244N12328	GASTON	201009	072210	16.94	-65.78	1010	276	17
2011214N15299	EMILY	201108	022340	15.98	-66.12	1004	283	13
2011233N15301	IRENE	201108	220420	18.06	-65.64	991	293	12
2011250N12324	MARIA	201109	111550	19.42	-64.48	1005	303	8
2012287N15297	RAFAEL	201210	140300	18.40	-63.55	1004	352	9
2013189N09319	CHANTAL	201307	100120	15.73	-66.22	1008	285	25
2013248N16294	GABRIELLE	201309	050140	16.81	-66.49	1008	309	7
2014210N10323	BERTHA	201408	021400	17.10	-66.47	1009	303	19
2014285N16305	GONZALO	201410	140810	19.39	-64.29	975	318	11
2015237N14315	ERIKA	201508	280220	17.32	-65.76	1006	279	16

Table C-2. TC data at closest approach and 250 km prior.

IBTracsName	Name	Closest Approach Pressure Deficit (hPa)	Closest Approach Forward Speed (kts)	Number of Points in Linear Fit	250 km Pressure Deficit (hPa)	Ratio of Closest Approach /250km Pressure Deficit
1938220N18298	NOTNAMED	15	16	7	19	1.24
1943226N17300	NOTNAMED	9	15	6	9	0.97
1943284N13300	NOTNAMED	37	12	12	34	0.91
1945214N14302	NOTNAMED	15	14	7	15	0.98
1945230N17307	NOTNAMED	10	17	7	13	1.34
1945255N19302	NOTNAMED	51	12	9	39	0.77
1947290N19297	NOTNAMED	10	15	4	4	0.42
1949235N18300	NOTNAMED	22	15	8	19	0.85
1949264N14299	NOTNAMED	25	12	8	17	0.69
1950231N12306	BAKER	9	11	9	14	1.53
1950243N15304	DOG	52	6	6	71	1.37
1951224N12316	CHARLIE	21	19	6	19	0.89
1954364N22309	ALICE	17	6	13	30	1.74
1955215N15320	CONNIE	54	14	7	52	0.96
1956222N14313	BETSY	32	16	7	35	1.10
1958242N13302	ELLA	11	17	6	5	0.46
1960243N10337	DONNA	55	12	4	63	1.14
1961273N16303	FRANCES	3	10	10	5	1.70
1963267N11308	EDITH	24	10	8	16	0.67
1964234N13316	CLEO	74	15	7	60	0.81
1966233N13340	FAITH	28	14	7	23	0.83
1966265N10325	INEZ	68	13	7	60	0.88
1967249N14303	BEULAH	67	9	11	46	0.68
1975256N18306	ELOISE	6	9	10	5	0.82
1979197N13314	CLAUDETTE	2	15	4	3	1.66
1979238N12324	DAVID	89	10	8	86	0.97
1979241N11335	FREDERIC	9	10	10	12	1.33
1981247N16300	FLOYD	11	9	5	5	0.47
1981250N15306	GERT	9	17	6	9	1.04
1984311N15291	KLAUS	15	7	13	12	0.78
1984348N35300	LILI	4	21	5	6	1.45
1985320N21296	KATE	29	7	13	19	0.65
1987263N10309	EMILY	48	16	6	34	0.70
1988235N15317	CHRIS	4	13	7	4	1.00
1988253N12306	GILBERT	22	13	8	17	0.77

Table C-2. (cont.) TC data at closest approach and 250 km prior.

IBTracsName	Name	Closest Approach Pressure Deficit (hPa)	Closest Approach Forward Speed (kts)	Number of Points in Linear Fit	250 km Pressure Deficit (hPa)	Ratio of Closest Approach /250km Pressure Deficit
1989254N13340	HUGO	67	9	3	81	1.21
1990277N16301	KLAUS	9	12	17	15	1.68
1993227N14301	CINDY	3	12	4	2	0.74
1995240N11337	LUIS	70	8	9	70	1.00
1995256N12309	MARILYN	61	8	12	42	0.69
1995294N14306	SEBASTIEN	5	5	14	8	1.56
1996187N10326	BERTHA	37	16	7	30	0.82
1996248N15319	HORTENSE	24	8	15	23	0.97
1998232N15312	BONNIE	13	15	7	10	0.77
1998259N10335	GEORGES	45	13	6	46	1.03
1999291N10309	JOSE	18	8	8	24	1.34
1999318N17278	LENNY	80	7	8	60	0.75
2000233N12316	DEBBY	18	17	4	20	1.09
2000260N15308	HELENE	3	17	6	3	1.00
2001235N18296	DEAN	4	17	3	2	0.61
2004238N11325	FRANCES	71	14	7	66	0.93
2004258N16300	JEANNE	22	8	11	15	0.68
2005296N16293	ALPHA	7	12	3	3	0.47
2006213N16302	CHRIS	5	10	11	10	1.94
2007297N18300	NOEL	8	10	14	6	0.76
2007345N18298	OLGA	7	13	5	5	0.70
2008287N15291	OMAR	49	19	7	37	0.76
2009245N17303	ERIKA	4	10	10	5	1.15
2010236N12341	EARL	69	12	9	51	0.75
2010244N12328	GASTON	3	17	6	3	1.00
2011214N15299	EMILY	9	13	8	7	0.80
2011233N15301	IRENE	22	12	6	13	0.60
2011250N12324	MARIA	8	8	9	8	1.03
2012287N15297	RAFAEL	9	9	12	8	0.87
2013189N09319	CHANTAL	5	27	4	6	1.24
2013248N16294	GABRIELLE	5	7	4	0	-0.08
2014210N10323	BERTHA	4	19	6	5	1.21
2014285N16305	GONZALO	38	11	4	26	0.69
2015237N14315	ERIKA	7	16	7	8	1.15

Table C-3. Storms with landfall on Puerto Rico 1928-2016.

IBTracsName	Name	Landfall Sea Level Pressure (hPa)	Landfall Forward Speed (kts)	Landfall Central Pressure Deficit (hPa)	Post-landfall Sea Level Pressure (hPa)	Intensity Change (hPa)
1928250N1434	NOTNAMED	931	11.1	82	941	-10
1979241N11335	FREDERIC	1004	9.5	9	1006	-2
1981250N15306	GERT	1004	17.1	9	1006	-2
1989254N13340	HUGO	946	9.1	67	958	-12
1996248N15319	HORTENSE	989	8.4	24	989	0
1998259N10335	GEORGES	968	13	45	972	-4
2004258N16300	JEANNE	991	8.4	22	992	-1
2007345N18298	OLGA	1005	12.8	8	1004	1
2011233N15301	IRENE	990	12	23	989	1

Appendix D: CHS-PR Geospatial Bias and Uncertainty

As described in Section 6.2, Figures D-1 through D-8 illustrate the geospatial bias and uncertainty computed for the study area. The absolute and relative forms of both bias and uncertainty were computed on a VG basis as shown below.

D.1 Bias and uncertainty of ADCIRC simulations

Figure D-1. Absolute form of ADCIRC bias for the CHS-PR study area.

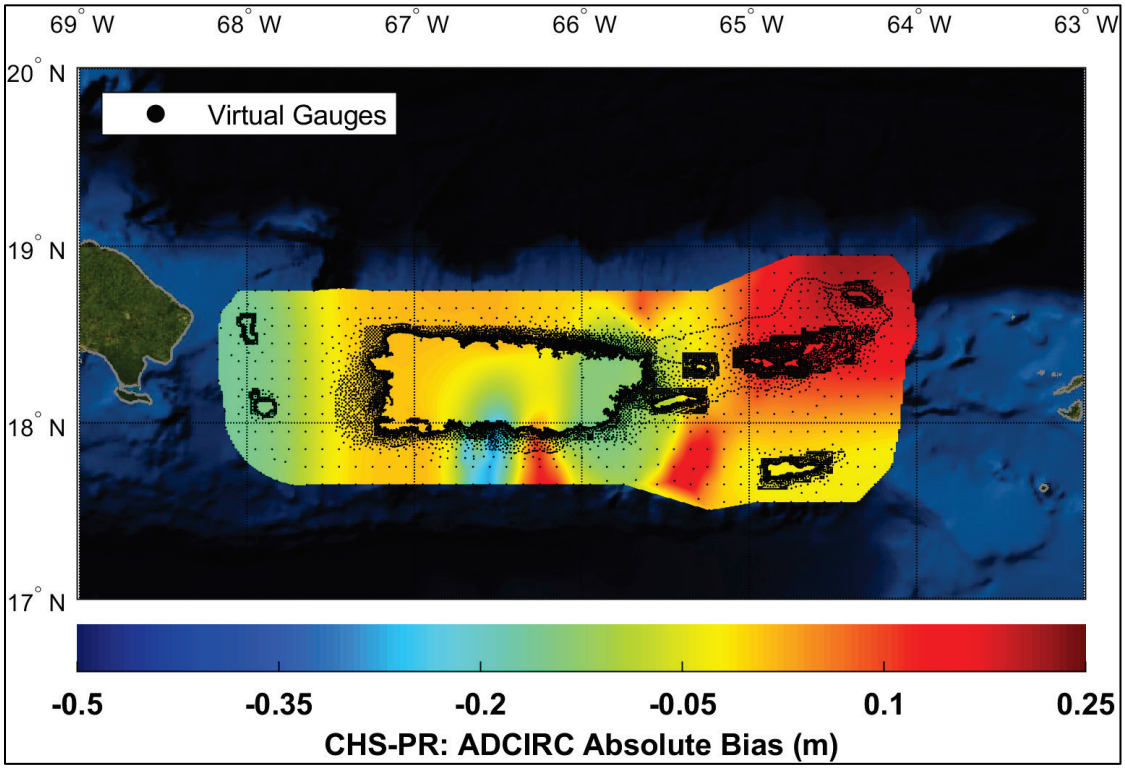

Figure D-2. Relative form of ADCIRC bias for the CHS-PR study area.

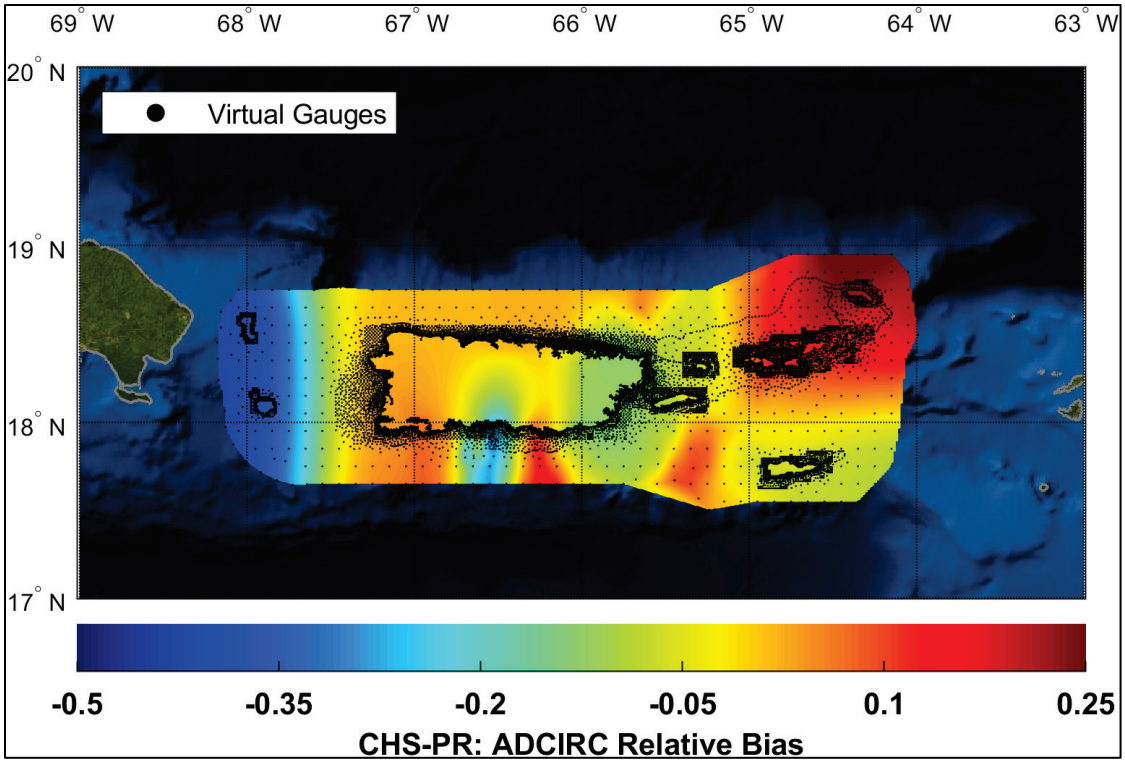

Figure D-3. Absolute form of ADCIRC uncertainty for the CHS-PR study area.

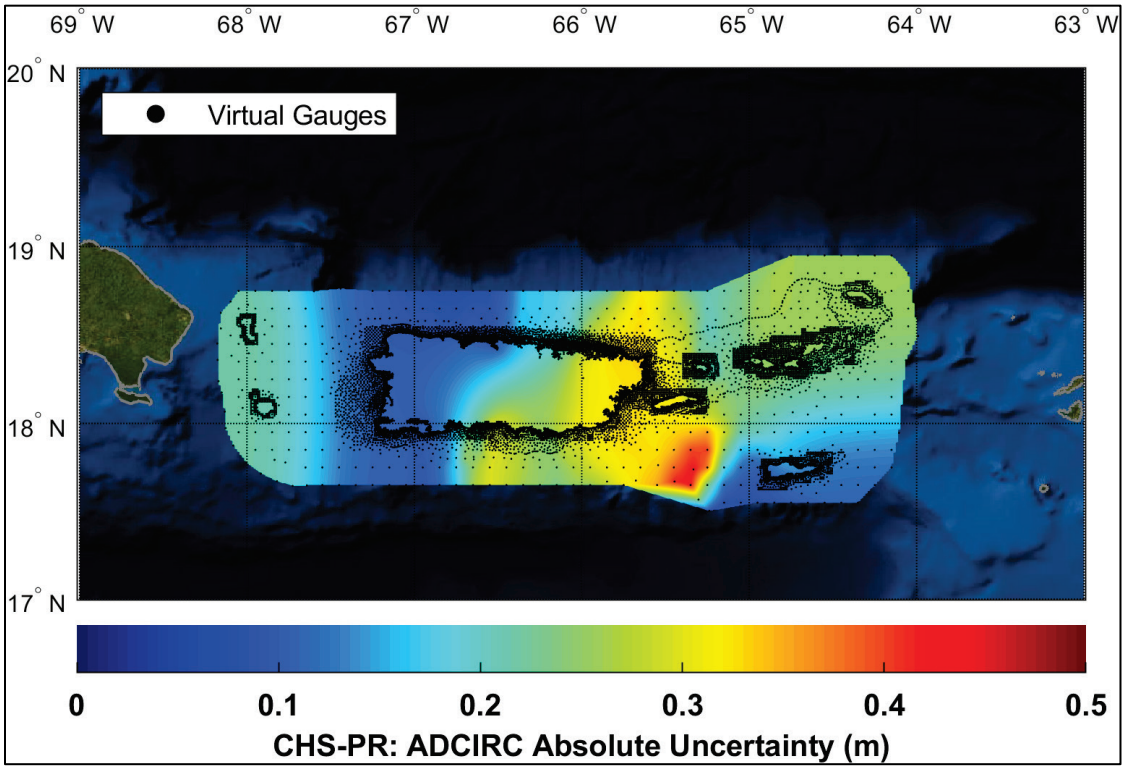

Figure D-4. Relative form of ADCIRC uncertainty for the CHS-PR study area.

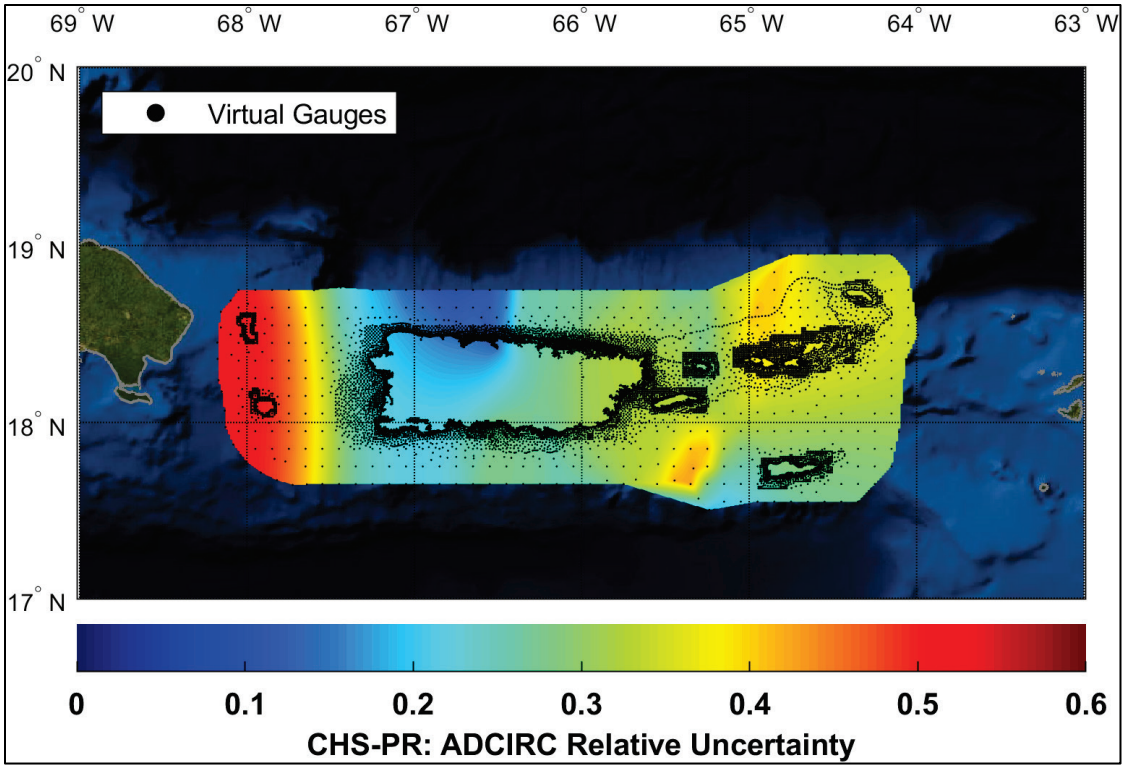

D.2 Bias and uncertainty of PBL simulations

Figure D-5. Absolute form of PBL bias for the CHS-PR study area.

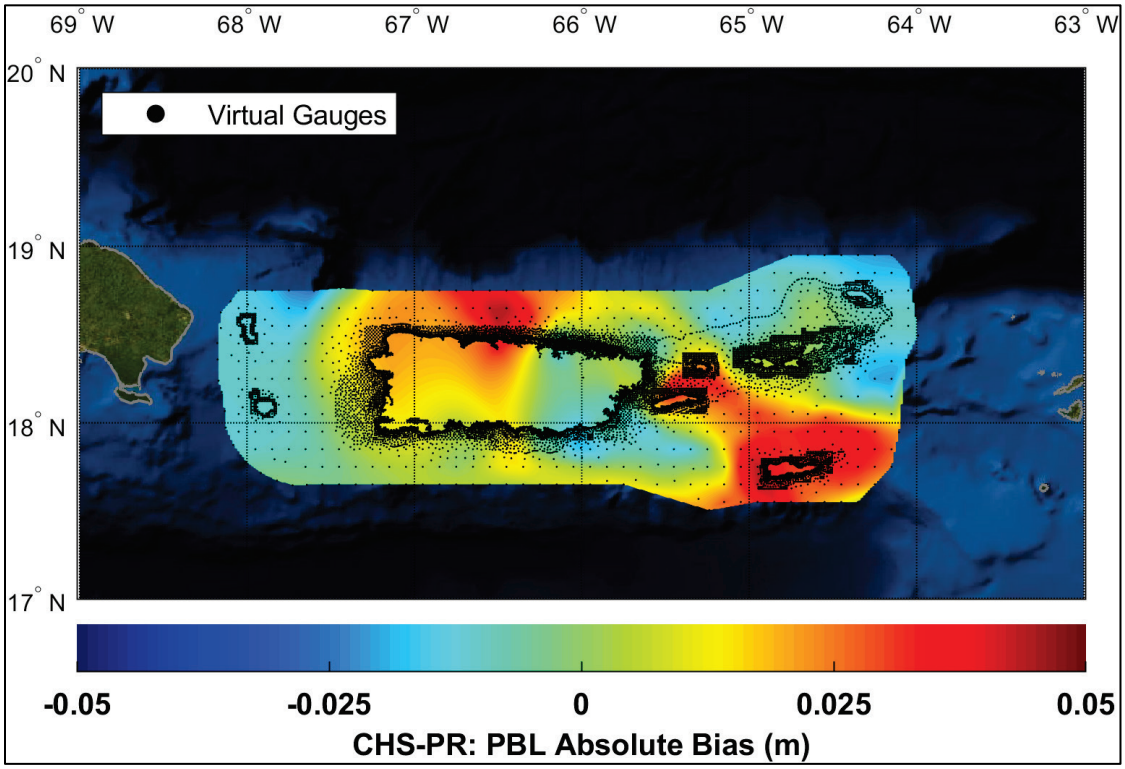

Figure D-6. Relative form of PBL bias for the CHS-PR study area.

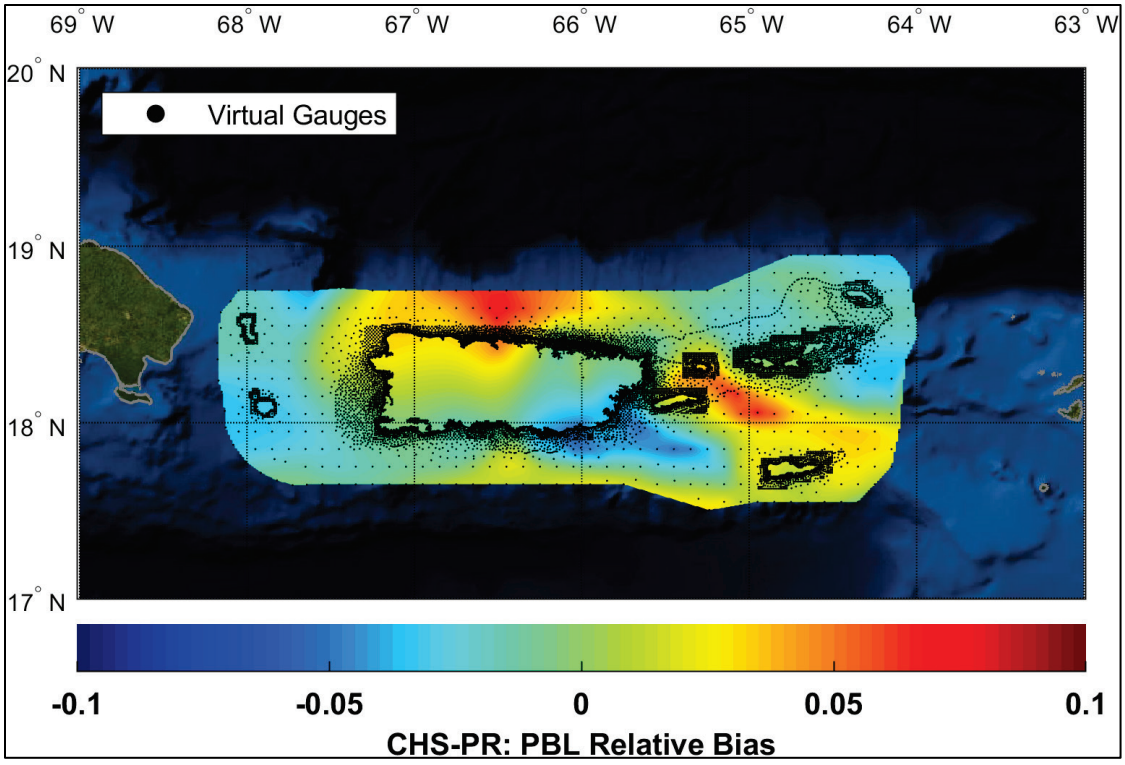

Figure D-7. Absolute form of PBL uncertainty for the CHS-PR study area.

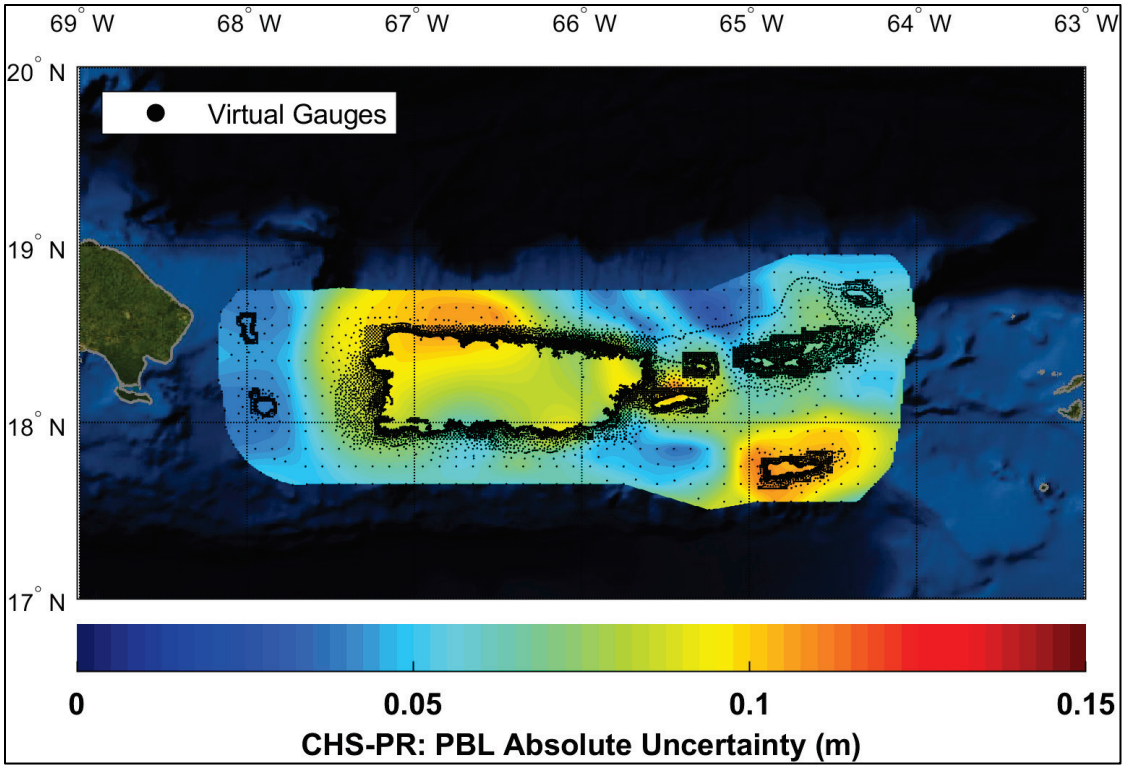

Figure D-8. Relative form of PBL uncertainty for the CHS-PR study area.

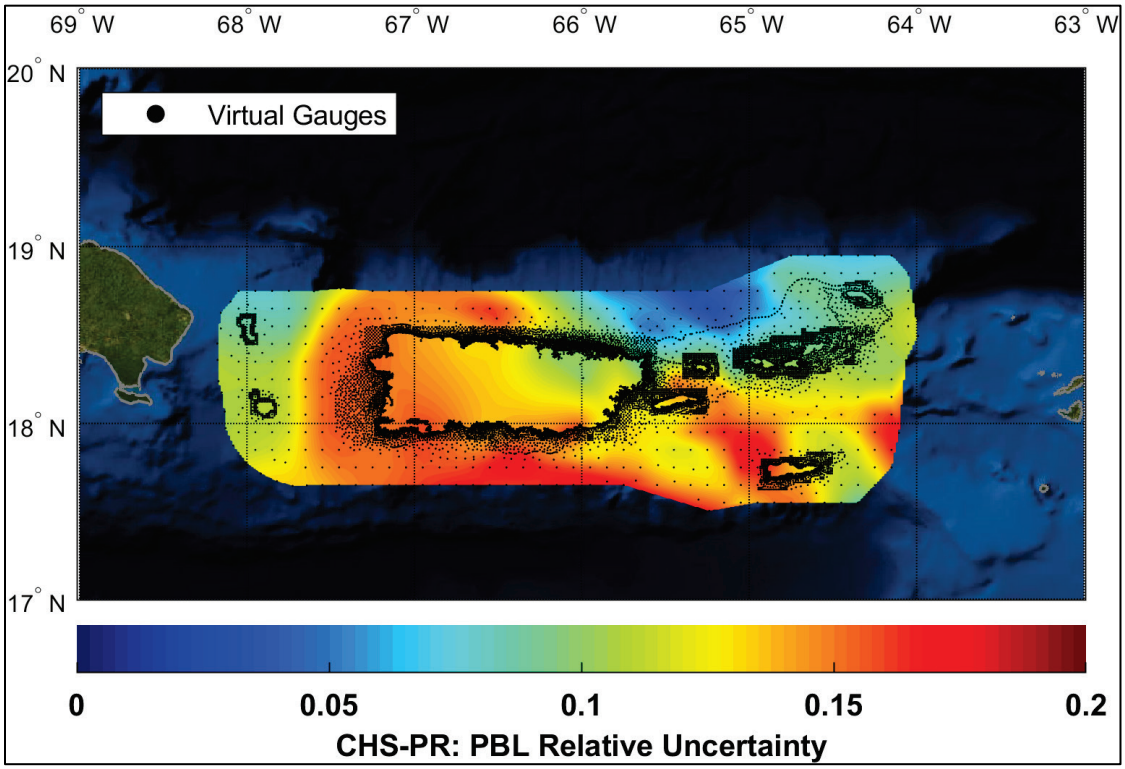

Abbreviations

2D	Two-dimensional
ADCIRC	ADvanced CIRCulation
AEF	Annual exceedance frequency
AEP	Annual exceedance probability
ARI	Average recurrence interval
ATCS	Augmented tropical cyclone suite
BND	Bivariate normal distribution
BQ	Bayesian quadrature
CDF	Cumulative distribution function
CHS	Coastal Hazards System
CHS-LA	Coastal Hazards System–Louisiana
CHS-PR	Coastal Hazards System–Puerto Rico and US Virgin Islands
CL	Confidence limit
CRL	Coastal reference location
CSR	Coastal structure reliability
CTXS	Coastal Texas Protection and Restoration Study
DNC	Dry-node correction
DSRR	Directional storm recurrence rate
DSW	Discrete storm weight
DTWD	Doubly-truncated Weibull distribution
EBTRK	Extended best track

EKF	Epanechnikov kernel function
FEMA	Federal Emergency Management Agency
FIS	Flood Insurance Study
GKF	Gaussian kernel function
GKS	Gaussian kernel surface
GoM	Gulf of Mexico
GPM	Gaussian process metamodeling
HI	High intensity
HURDAT2	Hurricane database
HWM	High-water mark
IBTrACS	International Best Track Archive for Climate Stewardship
ITCS	Initial tropical cyclone suite
JPM	Joint probability method
JPM-OS	Joint probability method with optimal sampling
JPM-OS-BQ	JPM-OS by Bayesian quadrature
JPM-OS-RS	JPM-OS by response surface
LACPR	Louisiana Coastal Protection and Restoration Authority
LI	Low intensity
MCAP	Mississippi Coastal Analysis Project
MCS	Monte Carlo simulation
MGC	Meta-Gaussian copula
MI	Medium intensity
MORPHOS	Modeling of Relevant Physics of Sedimentation

MSL	Mean-sea-level
NACCS	North Atlantic Coast Comprehensive Study
NHC	National Hurricane Center
NOAA	National Oceanic and Atmospheric Administration
ODGP	Ocean Data Gathering Program
ORP	Offshore reference point
OS	Optimal sampling
OS-BQ	Optimal sampling by Bayesian quadrature
OS-RS	Optimal sampling by response surface
OWI	Oceanweather, Inc.
PBL	Planetary boundary layer
PCHA	Probabilistic Coastal Hazard Analysis
PDF	Probability distribution function
PROS	Peaks, Runup, Overtopping, and Stone Sizing
RS	Response surface
SACS	South Atlantic Coastal Study
SAD	South Atlantic Division
SLC	Sea level change
SLR	Sea level rise
SRR	Storm recurrence rate
SSHWS	Saffir-Simpson Hurricane Wind Scale
SST	Stochastic Simulation Technique
StormSim	Stochastic Storm Simulation System

STWAVE	STeady-state spectral WAVE
SWL	Still water level
TC	Tropical cyclone
UKF	Uniform kernel function
USACE	US Army Corps of Engineers
VG	Virtual gauge
XC	Extratropical cyclone

REPORT DOCUMENTATION PAGE

Form Approved
OMB No. 0704-0188

1. REPORT DATE	2. REPORT TYPE	3. DATES COVERED *(From - To)*
December 2022	Final Report	FY19–FY21

4. TITLE AND SUBTITLE
Coastal Hazards System–Puerto Rico and US Virgin Islands (CHS-PR)

5a. CONTRACT NUMBER

5b. GRANT NUMBER

5c. PROGRAM ELEMENT NUMBER

6. AUTHOR(S)
Norberto C. Nadal-Caraballo, Madison C. Yawn, Luke A. Aucoin, Meredith L. Carr, Jeffrey A. Melby, Efrain Ramos-Santiago, Fabian A. Garcia-Moreno, Victor M. Gonzalez, Thomas C. Massey, Margaret B. Owensby, Alexandros A. Taflanidis, Aikaterini P. Kyprioti, Andrew T. Cox, and Juan Gonzalez-Lopez

5d. PROJECT NUMBER

5e. TASK NUMBER

5f. WORK UNIT NUMBER

7. PERFORMING ORGANIZATION NAME(S) AND ADDRESS(ES) (see reverse)

8. PERFORMING ORGANIZATION REPORT NUMBER
ERDC/CHL TR-22-23

9. SPONSORING/MONITORING AGENCY NAME(S) AND ADDRESS(ES)
US Army Corps of Engineers, South Atlantic Division (SAD)
60 Forsyth St. SW
Atlanta GA, 30303-8001

10. SPONSOR/MONITOR'S ACRONYM(S)
USACE SAD

11. SPONSOR/MONITOR'S REPORT NUMBER(S)

12. DISTRIBUTION/AVAILABILITY STATEMENT
Approved for public release; distribution is unlimited.

13. SUPPLEMENTARY NOTES
US Army Corps of Engineers, Labor Charge Code

14. ABSTRACT

The South Atlantic Coastal Study (SACS) was completed by the US Army Corps of Engineers to quantify storm surge and wave hazards allowing for the expansion of the Coastal Hazards System (CHS) to the South Atlantic Division (SAD) domain. The goal of the CHS-SACS was to quantify coastal storm hazards for present conditions and future sea level rise (SLR) scenarios to aid in reducing flooding risk and increasing resiliency in coastal environments. CHS-SACS was completed for three regions within the SAD domain, and this report focuses on the Coastal Hazards System–Puerto Rico and US Virgin Islands (CHS-PR). This study applied the CHS Probabilistic Coastal Hazard Analysis (PCHA) framework for quantifying tropical cyclone (TC) responses, leveraging new atmospheric and hydrodynamic numerical model simulations of synthetic TCs developed explicitly for the CHS-PR region. This report focuses on documenting the PCHA conducted for CHS-PR, including the characterization of storm climate, storm sampling, storm recurrence rate estimation, marginal distributions, correlation and dependence structure of TC atmospheric-forcing parameters, development of augmented storm suites, and assignment of discrete storm weights to the synthetic TCs. As part of CHS-PR, coastal hazards were estimated for annual exceedance frequencies over the range of 10 yr^{-1} to 10^{-4} yr^{-1}.

15. SUBJECT TERMS
Floods, Puerto Rico—Coasts, Risk assessment, Risk management, Storm surges, Tides, United States Virgin Islands--Coasts

16. SECURITY CLASSIFICATION OF:			17. LIMITATION OF ABSTRACT	18. NUMBER OF PAGES	19a. NAME OF RESPONSIBLE PERSON
a. REPORT	b. ABSTRACT	c. THIS PAGE			Norberto C. Nadal-Caraballo
Unclassified	Unclassified	Unclassified	SAR	169	19b. TELEPHONE NUMBER *(Include area code)* 601-634-2008

7. PERFORMING ORGANIZATION NAME(S) AND ADDRESS(ES) (continued)

Coastal and Hydraulics Laboratory
US Army Engineer Research and Development Center
3909 Halls Ferry Road
Vicksburg, MS 39180-6199

University of Notre Dame
Fitzpatrick Hall
Notre Dame, IN 46556

Oceanweather, Inc.
5 River Road, Suite 1
Cos Cob, CT 06807

Wood Environment & Infrastructure Solutions, Inc.
50 Troop Ave #300
Dartmouth, NS B3B 1Z1, Canada